New Routes to Nitride Materials:
Oxide Precursors and Nitrogen Plasmas
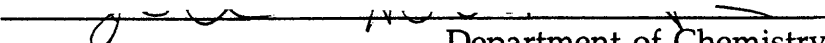
by

Joel David Houmes

B.A., Northwestern University, Evanston, Illinois
(1992)

SUBMITTED TO THE DEPARTMENT OF CHEMISTRY
IN PARTIAL FULFILLMENT OF THE REQUIREMENTS
FOR THE DEGREE OF DOCTOR OF PHILOSOPHY

at the
MASSACHUSETTS INSTITUTE OF TECHNOLOGY

August 15, 1996

Signature of Author _____
Department of Chemistry
August 15, 1996

Certified by _____
Hans-Conrad zur Loye
Thesis Supervisor

Accepted by _____
Dietmar Seyferth
Chairman, Departmental Committee on Graduate Students

This doctoral thesis has been examined by a Committee of the Department of Chemistry as follows:

Professor Dietmar Seyferth_____

Chairman

Professor Hans-Conrad zur Loye_____

Thesis Supervisor

Professor Christopher Cummins_____

New Routes to Nitride Materials: Oxide Precursors and Nitrogen Plasmas

by
Joel David Houmes

SUBMITTED TO THE DEPARTMENT OF CHEMISTRY IN
PARTIAL FULFILLMENT OF THE REQUIREMENTS FOR THE DEGREE OF
DOCTOR OF PHILOSOPHY

ABSTRACT

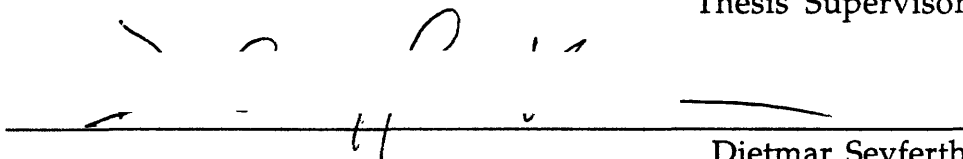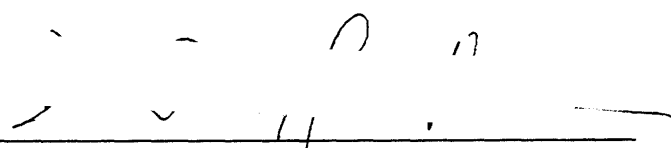For years, the synthesis of nitride materials has proven to be a synthetic challenge to solid state chemists, due primarily to the thermodynamic stability of N_2, which yields them unstable with respect to disproportionation. In addition, the formation of nitride coatings on the surfaces of reactant particles pose large kinetic barriers to the diffusion of nitrogen and other metal reactants. In this thesis, two new routes for the synthesis of nitride materials are presented, ammonolysis of oxide precursors and plasma nitridation of metal powders and metal oxides. In oxide precursors, the atomic level mixing of the reactant metal atoms, should shorten the diffusion distance and allow the reaction to take place at a lower temperature in a reasonable amount of time. These lower temperature reactions should allow for the formation of new phases due to the lowered risk of disproportionation. The synthesis of several new oxynitride materials, some with technologically important applications, are presented here. In addition, the synthesis of several fully nitride materials is described.

The kinetically active nitrogen species present in a microwave generated nitrogen plasma allow for the formation of nitride materials in reduced reaction times. The formation of nitride coatings on the surface of the reactant particles is disrupted by the constant bombardment of energetic electrons and ionized plasma particles, which eases the diffusion constraints into the interior of the reactant particle. By using microwave plasma

nitridation techniques, several binary nitride materials can be synthesized in under 24 hours. In addition, complete conversion of several oxide materials (i.e. Al_2O_3, Ga_2O_3 and TiO_2) in nitrides can be accomplished. Equivalent ammonolysis reactions have significant thermodynamic and kinetic limitations. Also, the synthesis of several ternary lithium metal nitride compounds was accomplished by taking advantage of the ability of conducting powders to be heated in a microwave field.

Thesis Supervisor: Dr. Hans-Conrad zur Loye
Title: Paul Cook Career Development Professor of Chemistry

ACKNOWLEDGMENTS

I would like to thank my advisor, Hanno zur Loye, for financial support, helpful suggestions and the freedom to pursue chemistry I found interesting. I would also like to thank the past and present members of the zur Loye group, particularly Kurt Kendall, Carlos Navas and Jennifer Pell, who made my time at MIT enjoyable and sometimes interesting. In addition, I thank David Bem, who taught me most of what I know about nitrides, and Sandhya Deo and Hans Olsen, who put up with my almost non-existent managerial style.

I would also like to thank those outside the zur Loye group who contributed significantly to my research: Ross Plovnick (3M), who was very helpful in the selection and design of our microwave plasma setup; Jim Sommers (Teledyne); who was kind enough to run some combustion oxygen measurements for me; Newell Washburn (UC-Berkeley), who performed a number of diffuse reflectance measurements; and Tom Mallouk (Penn. State) who performed some catalysis measurement.

Special thanks to my friends and roommates Matt "Chuckles" Reding, Steve "Elvis" Reid and Shane "Mr. Krispy" Krska. These have been four very difficult years and without friends like these, I do not know if I would have made it through. I would like to thank my family, Mom, Dad and Jori. You have stood by me no matter what, always honored my decisions, and given me the freedom and means to do anything I desire. Most of all, I would like to thank Catherine Brescia, a bright light in four years of darkness. In nine short months, you taught me a lifetime's worth of knowledge about life, love and death.

TABLE OF CONTENTS

LIST OF FIGURES

LIST OF TABLES

1. Introduction to Nitride Chemistry

1.1 INTRODUCTION

Nitride materials, as a relatively unexplored class of materials, are full of untapped potential to provide useful new materials. Binary nitrides (nitrides which contain one metal and nitrogen only) are the most extensively studied nitrides and display properties that have been exploited in numerous technological applications including abrasives, refractories, electronic packaging materials and magnetic recording media. However, unlike oxide materials, the number of ternary and higher nitride materials is very small, owing to the various synthetic challenges these materials present to the solid state chemist.

Of the problems associated with the synthesis of ternary and higher nitride compounds, those stemming from the thermodynamic trap of dinitrogen formation, are the most significant. Due to dinitrogen's large bond energy (941 kJ/mol), high temperatures are required to activate the diatomic gas for reaction with a substrate material. However, at high temperatures, all nitrides become unstable with respect to the metal and N_2, leading to the formation of materials with low nitrogen contents in which metal-metal interactions predominate. The loss of nitrogen is exacerbated by entropic effects, which favor lower nitrogen-to-metal ratios with increasing temperature. For example, in the binary tantalum nitride system, Ta_3N_5 decomposes successively to Ta_4N_5, Ta_5N_6, ϵ-TaN and Ta_2N with increasing temperature.[1] Therefore, high temperature synthetic routes often result in the formation of intermetallic sub-nitrides or simple binary nitrides.

A second difficulty in the synthesis of ternary and higher nitrides results from the stability of the binary phases. As with most solid-state syntheses, the reaction proceeds from the exterior of the reactant particles to the interior and, is dramatically limited by the slow diffusion rates present in the solid state. For the synthesis of nitride materials, the rate of gas diffusion into metals particles is much slower than the equivalent diffusion rates

found in related oxide materials. Most materials, when reacted with nitrogen or ammonia, will form a binary nitride coating through which diffusion of a solid or a gas is notoriously slow. To overcome the limit of this rate of diffusion, the experimentalist usually turns to higher reaction temperatures to force the reaction to go to completion in a reasonable amount of time, which again can limit nitrogen content and result in phase separation to lower nitrides.

Over the past 10 years, a significant amount of work has been carried out in an attempt to find new routes for synthesizing nitride phases in an efficient and cost effective manner. Work has focused both on methods which attempt to lower the reaction temperature, which could allow the formation of new phases, and on ways to achieve more active nitrogen species, which will shorten the reaction time. The purpose of this chapter is to provide a summary of the methods used over the past 10 years for synthesizing nitride materials, with particular emphasis on the structures (and corresponding properties) of the resulting materials. This chapter introduces nitride chemistry and covers background information relevant to the work presented in this thesis.

Although the main thrust of the nitride research in this group has been the synthesis of "Ionic/Covalent" type nitrides, some work has been done toward the synthesis of intermetallic type nitrides, particularly binary intermetallic nitrides which have demonstrated commercially useful properties (i.e. AlN, BN, TiN, Fe_4N). Therefore, some background information on the chemistry of intermetallic nitrides is presented before covering the ionic/covalent type nitrides.

1.2 INTERMETALLIC NITRIDES

Intermetallic nitrides are a class of materials in which metal-metal interactions are dominant and where the nitrogen atoms are interstitially located within the metal array.[2] These phases are stabilized by metal-metal

interactions and, consequently, their structures and physical properties are similar to those found in many other systems with high metal contents, such as alloys, metals, and intermetallic carbides.[3] The dominance of the metal-metal interactions in the intermetallic phases is evidenced by the existence of a wide range of stoichiometries (a trait also exhibited in carbides) and by the fact that many intermetallic nitrides are refractories. Because of the extensive number of known intermetallic nitrides, this chapter will not comprehensively review their synthesis, structure and properties, but rather will only cover background information pertinent to this work. The reader is referred to reviews by Stadelmaier, Johansen, Toth and Goldschmidt in which intermetallic nitrides have been thoroughly covered.[2-5]

1.2.1 Synthesis

Standard powder metallurgy techniques, which utilize very high temperatures (>1200°C), can be used to synthesize many intermetallic nitrides because of their appreciable thermodynamic stability. However, the high synthesis temperature leads, in many cases, to low nitrogen content, which results in greater metal-metal interactions and physical behavior similar to that found in elemental metals and alloys. Most interstitial nitrides have been synthesized either by 1) the reaction of a metal or metal hydride powder with nitrogen or ammonia or 2) the nitriding of a metal oxide powder in the presence of carbon.[3] The use of a carborizing agent to reduce the metal oxide powder often results in carbon contamination, since carbides and nitrides readily form solid solutions as a consequence of the similarities in their structures and bonding interactions.[2] Intermetallic nitrides, just like carbides, often require high temperatures for formation (> 1000 °C), which is in part due to the refractory nature of many of these materials. Other methods of intermetallic nitride synthesis include the ammonolysis of metal chlorides, and the decomposition of ionic/covalent type nitrides.[3]

1.2.2 Structures

Intermetallic nitrides form structures similar to those found for carbides. A set of empirical rules formulated by Hägg in 1931 was developed to predict the structures of transition metal carbides and nitrides. The rules state that the structure of the intermetallic phase will depend upon the radius ratio of X (X = N, C) relative to the radius of the transition metals.[6] The Hägg rules predict whether an interstitial compound will form in a simple or in a complicated structure type. For example, it correctly predicts that TiN will form the simple NaCl structure type.[3] Although the Hägg rules can be used to predict many of the known structures of intermetallic nitrides, the technique is not universal and several known complex binary and ternary intermetallic nitrides cannot be described as Hägg phases.[2] One class of such materials, the η-carbide type nitrides, Fe_3Mo_3N and Co_3Mo_3N, exhibit a complex 3-dimensional arrangement of iron-centered $[Mo_6M_6]$ dodecahedra and corner shared NMo_6 octahedra.[7,8]

1.2.3 Properties

Intermetallic nitrides exhibit several properties that make them technologically important. Intermetallic nitrides are, in general, extremely hard, with microhardness values falling between those of Al_2O_3 and diamond.[3] As a result, intermetallic nitrides are often used as abrasive materials and as wear-resistant coatings. More recently, the electronic, magnetic, and optical properties of these nitrides have been explored. For example, niobium nitride (NbN) has one of the highest reported superconducting transition temperature, T_C, for a binary compound of any heteroatom (T_C = 17.3 K) and intermetallic iron nitrides are used as magnetic recording media.[3] Other intermetallic nitrides have interesting catalytic properties which are thought to be due to the similarity between the electronic structures of these nitrides and the noble metals.[9-12] Many intermetallic nitrides exhibit extreme stability and inertness to high

temperatures and corrosive environments, which have allowed the use of these compounds in applications where other materials would fail.[2]

Despite their many technological applications, our knowledge of the electronic and magnetic properties of intermetallic nitrides is very incomplete. Most experiments have been conducted on poorly characterized materials. The presence of small amounts of impurities (usually oxygen or carbon) can lead to variations in structure and can also drastically affect the properties.[3] The impurity content and precise stoichiometry is often not reported or is unknown in many compounds, which makes it difficult to critically evaluate much of the nitride literature.

1.3 IONIC/COVALENT NITRIDES

Ionic/covalent type nitrides are compounds in which metal-nitrogen bonding is dominant and where metal atoms are interstitial in a nitrogen array. In contrast to the structures of the intermetallic nitrides, these phases consist of metal atoms with predominately covalent bonds to a nitrogen framework, resulting in octahedral, trigonal prismatic, tetrahedral, trigonal planar, and linear[13,14] metal-anion coordination environments, similar to those encountered in molecular compounds. Also, ionic/covalent nitrides often are often more closely related structurally to oxides or sulfides rather than to carbide type materials; further emphasizing differences in the bonding schemes. The packing of the metal-anion polyhedra can lead to low-dimensional structures and corresponding unusual low-dimensional behavior which is not commonly found in intermetallic type materials. Several extensive reviews on the crystal chemistry of inorganic nitrides, including ionic/covalent type nitrides, have been published.[15,16]

Until recently, the synthesis of ionic/covalent nitrides was relatively unexplored except for the pioneering work of Juza on ternary lithium nitrides.[17] However, many of Juza's materials exhibit predominately ionic type bonding and result in simple repulsion minimization structures, which

obey the radius ratio rules. Because of the lack of covalent bonding interactions in these materials, many of the desirable properties of intermetallic nitrides (hardness and inertness) are lost. In fact, many of these materials are readily attacked by water, decomposing to an oxide with the release of ammonia.

However, within the last decade, several groups have begun to explore new methods for the synthesis of ternary ionic/covalent nitride systems, many of which have relied on the inductive effect. The inductive effect is based on the donation of electron density from an electropositive element to an adjacent metal-nitrogen bond, thereby increasing the bond covalency and product stability. Successful utilization of the inductive effect is illustrated by the fact that almost all of the known ionic/covalent ternary nitrides contain electropositive elements (i.e. alkali, alkaline earth or rare earth metal). However, although methods which utilize the inductive effect have led to the synthesis of a large number of materials, the scope of compounds which can be synthesized by this technique is limited to materials which contain electropositive elements (alkali metals, alkaline earths and rare earths). Fortunately, several methodologies have been or are being explored which promise to widen the range of known ternary ionic/covalent nitride materials.

The remainder of this chapter will focus on the recent progress that has taken place in the synthesis and characterization of ionic/covalent type ternary nitrides. This survey will include several typical synthetic strategies for the preparation of ternary nitrides, as well as a review of recent ionic/covalent type nitrides containing alkali, alkaline earth, rare earth and transition metals. The reader is referred to several helpful tables which have been included at the end of this chapter. Table 1.1 includes a list of most of the ionic/covalent type nitride materials synthesized in the last 11 years. Selected transition metal-nitrogen bond distances are reported in Table 1.2. Table 1.3 contains a list of bond valance parameters which can be useful for evaluating the validity of the structures listed here as well as other new

structures yet to be found, as well as theoretical M-N bond distances which were reported in a review by Brese *et al.*[15] These parameters can also be used to qualitatively determine oxidation states for new materials.

1.4 SYNTHESIS OF TERNARY AND QUATERNARY IONIC/COVALENT NITRIDES

The number of techniques used for the synthesis of ternary and quaternary nitride phases can be divided into a surprisingly small number of classes. Table 1.4, located at the end of this chapter, lists five general reaction methodologies into which most synthetic strategies for ternary nitride materials can be placed. However, the vast majority of nitride materials have been synthesized using only two methods: 1) the reaction of a metal nitride with a metal or another metal nitride and 2) the reaction of two metal powders with nitrogen gas or ammonia.

The most common approach has been the reaction of a binary nitride with a metal or second binary nitride (Table 4, **Reaction 1**). In order to overcome diffusion barriers during the reaction pathway, high reaction temperatures (800 - 1800 °C) are usually required. However, at these high temperatures, decomposition of nitride materials into the component elements becomes thermodynamically favorable. Therefore, the inductive effect is used to stabilize product formation. Li_3N is a favored starting material due to its stability and relatively low melting temperature (mp = 813 °C), which can help speed the reaction kinetics through flux or flux-assisted synthesis. As a result, more ionic/covalent ternary nitrides containing lithium are known than with any other element. Stable binary nitrides of all other alkali metals are unknown, which precludes the use of this technique to synthesize other alkali ternary systems. However, since the binary nitrides of all the alkaline earths are known, ternary nitrides containing these elements have been synthesized by a similar method. Apart from lithium, the alkaline earth ternary nitrides make up the second largest

group of known phases, which is a testament to the success of this synthetic method.

To a lesser extent, the reaction of two metal powders under nitrogen or ammonia (Table 4, **Reaction 2**) has been employed in the synthesis of ternary nitrides (Table 1.1). Because the energetics of formation of many binary metal nitrides are highly favorable, many metals will form nitrides at reasonably low temperatures (i.e. iron metal reacts with ammonia at room temperature to form iron nitride). As a result, binary nitrides are often formed *in situ* and **Reaction 1** is often more appropriate for describing ternary nitride formation. As expected, many ternary nitrides made by heating two metal powders under nitrogen or ammonia may also be synthesized through the reaction of the corresponding binary nitrides. In some cases, i.e. Ba_3FeN_3,[18] materials may only be made by first heating the metal powders in an inert atmosphere (e.g. Ar) and exposing the reactants to nitrogen or ammonia only after the reaction temperature has been reached. The reaction of two metals under ammonia or nitrogen has been especially successful when one of the metals is an alkali metal, since they have low melting points and can act as a reactive flux, which also facilitates single crystal formation. The greatest disadvantage of the direct reaction of two metals under nitrogen or ammonia is due to the stability of the binary nitrides themselves at relatively low temperatures. The metal reactants will form a nitride skin, which slows diffusion of both nitrogen and the other metal reactant into the center of the metal particle. As a result, times for the reaction of two metal powders can be quite long.

To form new ternary nitride phases and structure types, there has been an effort to explore synthetic routes which utilize lower reaction temperatures (<900°C). One such approach is the synthesis of ternary nitrides from metal amides, especially the amides of the alkali and alkaline earth metals (Table 1.4, **Reaction 3**). Using this technique, polycrystalline materials often can be synthesized under flowing ammonia or nitrogen. Another method uses high pressures in autoclaves containing supercritical ammonia and sometimes results in the formation of single crystals. The use of these

heterogeneous reactions have resulted in a number of interesting phases. For example, $NaTaN_2$ has been synthesized by the reaction of $NaNH_2$ with Ta_3N_5 either under flowing ammonia at 500°C[19] or under high pressure ammonia at 400°C.[20] One limitation of this method is that stable amides are not known for many metals. Therefore, the technique is primarily limited to the synthesis of alkaline earth and alkali metal ternary nitrides, for which stable amides are known.

Recently, an interesting variation of **Reaction 3** has surfaced. Schnick and co-workers have utilized the ability of silicon diimide to be heated and melted in a high-frequency induction furnace to synthesize a number of silicon containing nitrides. These reactions, unlike those with alkali imides, are carried out at very high temperatures. For example, the reaction between barium metal and silicon diimide is carried out at temperatures between 1550 and 1600 °C under a nitrogen atmosphere. Single crystals of a number of materials ($Sr_2Si_5N_8$[21], $Ba_2Si_5N_8$[21], $Ca_2Si_5N_8$[22] and $Ce_3Si_6N_{11}$[23]) have been grown through slow cooling of the reaction mixture.

Reaction 4 is another low temperature technique involving the ammonolysis of ternary metal oxides. For example, $LiMO_4$ (M = Mo, W) has been reacted with flowing ammonia to yield $LiMN_2$.[24,25] The use of oxide precursors offers the advantage of atomic-level mixing of the metals, which decreases the diffusion distances of the cations and may lower the temperature necessary for reaction. Also, the structure of the precursor may act as a template for product formation[26] and yield phases unattainable by other synthetic routes. Thermodynamic studies of ammonolysis syntheses have indicated that the formation and subsequent removal of water under flow-through conditions drives the reaction to completion.[27] By using the out of equilibrium reaction conditions of a flow-through reactor, it is sometimes possible to make ternary nitrides which are less stable than the oxide precursor. For example, work in this group over the last several years has focused on the synthesis of ternary transition metal nitrides by the ammonolysis of a ternary metal oxide precursor. This work represents the

first reported synthesis of a ternary ionic/covalent nitride in the absence of the inductive effect. A large number of ternary transition metal nitrides have been synthesized by this route including $FeWN_2$[28], $MnMoN_2$[28], $(Fe_{0.8}Mo_{0.2})MoN_2$[29], and α- and β-$MnWN_2$[8]. The utility of this technique for the synthesis of binary and ternary nitrides will be discussed in detail in Chapters 2 and 3.

Most of the known quaternary nitrides contain lithium and are synthesized by reacting a lithium-containing ternary nitride with a metal or metal nitride (Table 1.1, **Reaction 5**). Most of these compounds may also be synthesized by the reaction of the elements using either N_2 or Li_3N as a source of nitrogen. Because of the infancy of the field of ternary and higher nitride synthesis, very few true quaternary compounds have been synthesized. Instead, workers have chosen to focus ternary systems which are compositionally and structurally simpler in order to obtain an understanding of the synthesis of ionic/covalent type nitride compounds. Further studies and understanding of ternary systems are needed before advances in the synthesis of quaternary systems can be realized.

Several other unique routes to ternary nitrides have been developed. One such method is the synthesis of $LiMoN_2$ from thermal decomposition of the molecular precursor, $Li_2Mo(N^tBu)_4$, under NH_3.[24] Although this is an effective preparative route, no advantages were reported over the ammonolysis of the oxide precursor, Li_2MoO_4. However, it is likely that the large volume of knowledge and understanding of coordination materials, when coupled with an understanding of the solid-state energetics, could lead to other ternary nitride syntheses through the decomposition of molecular precursors. Another unique approach is the metathesis reaction of CuI with the ternary nitride $NaTaN_2$ to produce $CuTaN_2$.[30] Because the alkali metals can be deintercalated from many parent ternary nitrides,[19,24,31] it may be possible to apply the metathesis route to create other new phases. However, the air and moisture sensitivity of many alkali ternary nitrides could make

this a difficult synthetic technique at best. Thermal decomposition reactions of one nitride into another, such as the transformation of $Li_2Ta_3N_5$ into the structurally related phase, $Li_{2-x}Ta_{2+x}N_4$, represents an approach that, in theory, could be applied to many other metal-nitride systems. Other novel synthetic approaches will undoubtedly make their appearance over the next few years as groups work on achieving lower reaction temperatures and/or more active nitrogen species.

1.5 STRUCTURES OF REPORTED TERNARY NITRIDES

1.5.1 Lithium-Containing Ternary and Quaternary Nitrides

Lithium-containing ternary nitrides have been found which exhibit a wide range of metal coordination. In this quick survey of the structures of these lithium containing nitrides, several common structural types will be focused upon, moving from a low coordination number (4) to higher ones. The structures of several quaternary materials also will be described.

1.5.1.1 Four-Fold Coordination

Lithium-containing ternary nitrides ($Li_{2y-x}M_xN_y$) most commonly form anti-fluorite related structures (anti-CaF_2)[15] In this structure, nitrogen atoms occupy the 8-coordinate calcium sites of the anti-fluorite structure and form a FCC array, while the Li/M occupy the tetrahedral fluoride sites. While some compounds do exist where the Li/M site is disordered, many exhibit ordered metal positions, which leads to supercells of the basic anti-fluorite structure. For example, in Li_7MN_4 (M = Nb or Ta),[32,33] the lithium and M are ordered and form Li_7M cubes. Eight of these cubes make up one unit cell, doubling the anti-fluorite unit cell in all three dimensions. In addition, the Li_7M cubes are slightly distorted due to the positive charge repulsion and size difference of Li^+ and M^{5+}.[33] Other nitrides that form in the fluorite or anti-fluorite
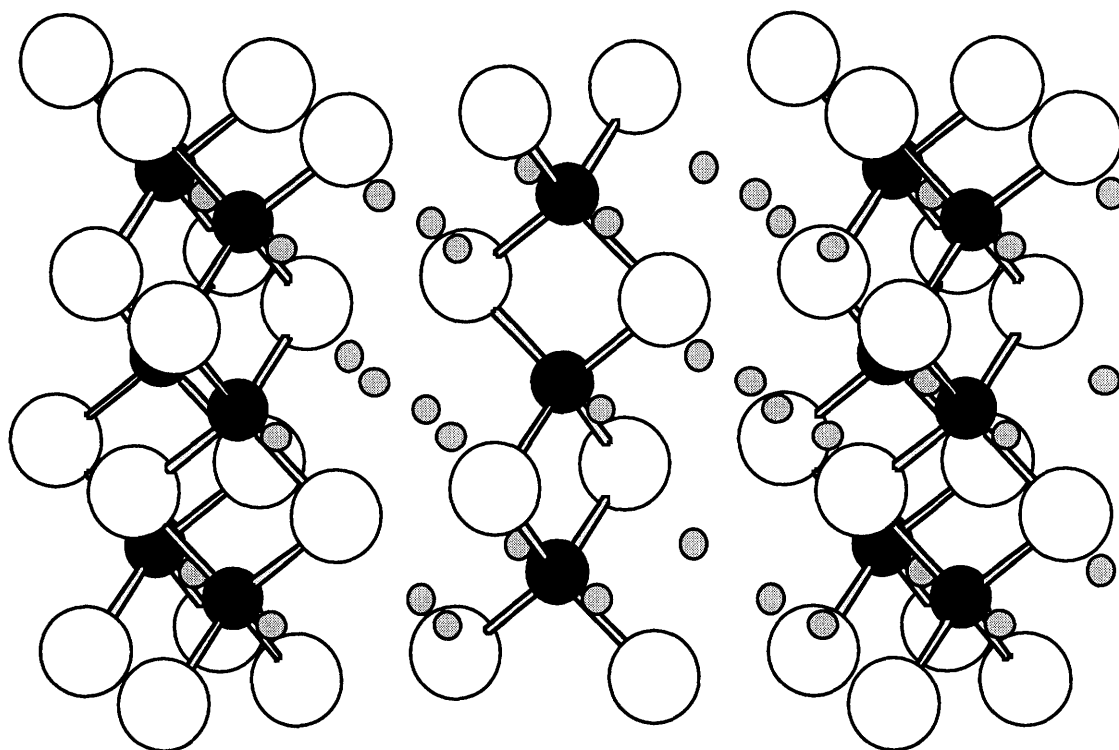
Figure 1.5.1: Structure of Li$_{3-x}$FeN$_2$.
An example of a lithium-containing ternary nitride with FeN$_2$
Chains. Gray = Lithium, Black = Iron, White = Nitrogen.

related structures[15-17] include the recently synthesized Li_3FeN_2 (Figure 1.5.1),[34] Li_6MoN_4, Li_6WN_4, and $Li_{15}Cr_2N_9$.[35]

1.5.1.2 Six-Fold Coordination

Lithium containing ternary nitrides are also known in which the metal atom is in six-fold coordination. For example, a high pressure phase, $Li_2Ta_3N_5$, has been synthesized and found to crystallize with a sodium chloride type structure.[36] Like the anti-fluorite type compounds, the nitrogen atoms form a FCC array. However, high pressure usually favors higher coordination numbers and, in this case, causes an increase in the metal coordination over the anti-fluorite type structures from tetrahedral to octahedral. A structurally related phase, $Li_{2-x}Ta_{2+x}N_4$, can be synthesized from the high temperature decomposition of $Li_2Ta_3N_5$, and can be described as a disordered high temperature phase of $Li_2Ta_3N_5$.[37]

Six coordinate metals are also found in the isostructural phases $LiMoN_2$[24] and $LiWN_2$ (Figure 1.5.2).[25] In these materials, the nitrogen atoms form hexagonal close-packed layers with alternating interstitial layers of lithium and M (M = Mo, W) atoms. The structure may also be thought of as having layers of LiN_6 octahedra and layers of MN_6 trigonal prisms that are stacked along the c-axis in an $A_{oct}A_{tp}B_{oct}B_{tp}C_{oct}C_{tp}$ fashion (Figure 1.5.2).

$LiTa_3N_4$ is closely related to the $LiMoN_2$ structure.[37] The nitrogen atoms form hexagonally closed packed layers with the metals occupying both octahedral and trigonal prismatic sites. Alternating layers of TaN_6 trigonal prisms and LiN_6/TaN_6 octahedra are stacked in an $A_{oct}B_{tp}A_{oct}C_{tp}$ fashion.

A   TP (M'-N)

A   Oct (M-N)

B   TP (M'-N)

B   Oct (M-N)

C   TP (M'-N)

C   Oct (M-N)
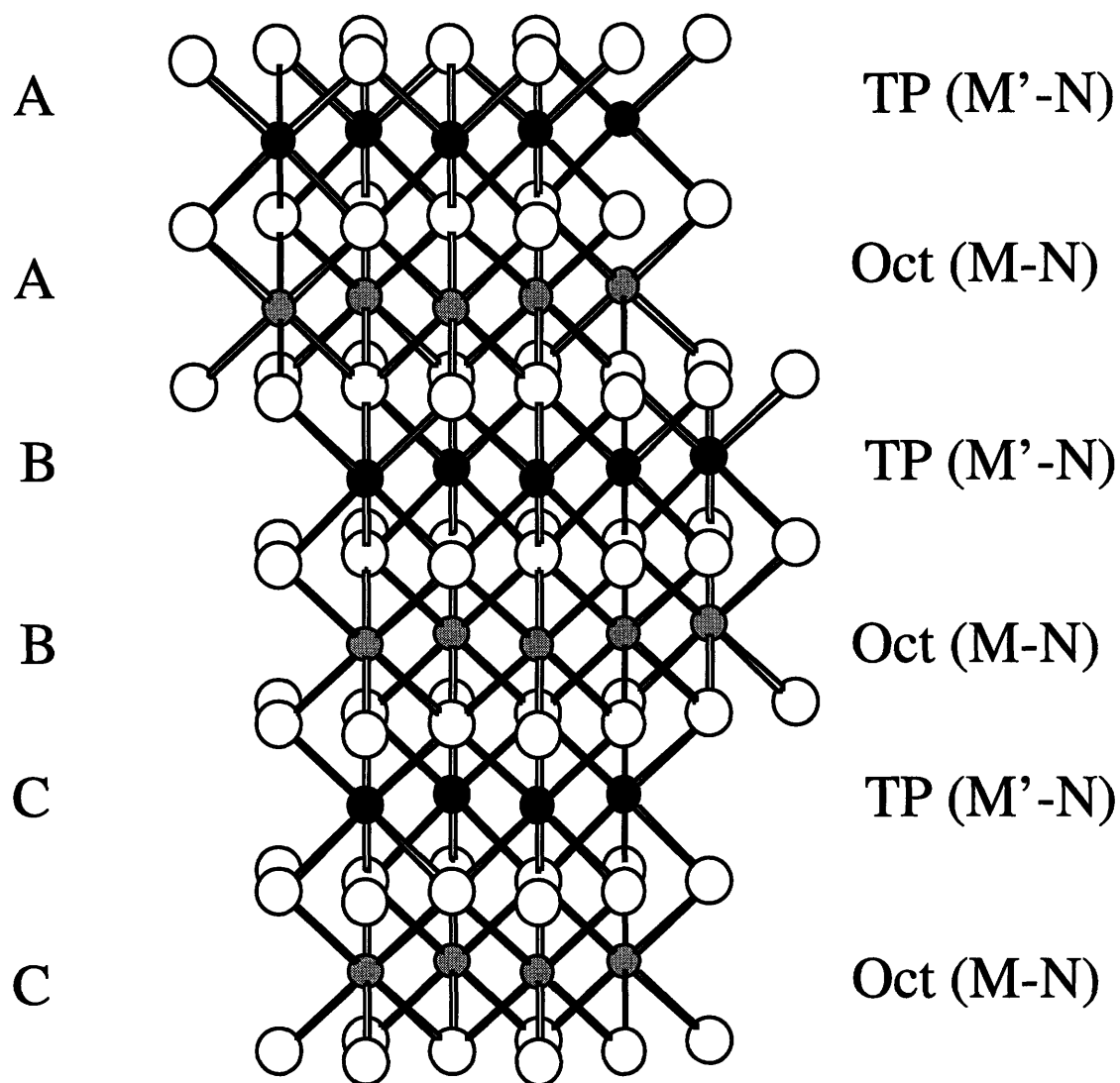
Figure 1.5.2: Structure of LiMN$_2$ (M = Mo, W).
Examples of a ternary nitride containing lithium octahedra and M (M = Mo, W) trigonal prisms. Gray = Lithium, Black = Molybdenum/Tungsten, White = Nitrogen

1.5.1.3 Lithium Nitride Related Structures

Some ternary nitrides of lithium form Li_3N type structures, which can be classified into two groups: **1)** solid solutions of Li_3N and **2)** structures containing fragments of Li_3N. The reaction of many of the first row transition metals with Li_3N results in solid solutions having the Li_3N structure. An exception is Li_2FeN_2, in which half the sites linking the Li_2N layers of the Li_3N structure are filled by two-coordinate Fe atoms.[15,38] The crystal chemistry of these compounds has been covered in reviews by Brese and Gudat.[15,34]

1.5.1.4 Quaternary systems

Most known quaternary nitride systems contain lithium and are formed in reaction where lithium or lithium nitride are used as a reactive flux. The quaternary lithium nitride, $Li_3Ba_2MN_4$ (M = Ta, Nb) has been synthesized by the reaction of elemental lithium, barium, and M (M = Ta, Nb) under N_2 at 850 °C.[39] The structure was determined by single crystal X-ray diffraction to have the space group C2/c. As in the anti-fluorite structure, the M^{5+} (M = Ta, Nb) and Li^+ are tetrahedrally coordinated to nitrogen. Alternating M (M = Ta, Nb) and Li tetrahedra are edge-shared forming parallel chains along the b-axis. These chains are then linked together by distorted LiN_4 tetrahedra to form a three dimensional network. The Ba coordination is 8-fold with nitrogen atoms and forms distorted dodecahedrons. No other quaternaries with this structure have been reported. $LiCa_4B_3N_6$[40] exhibits unusual low-coordination coordination, which is reminiscent of that found in molecular species. Figure 1.5.3 shows the structure of this unusual material which contains linear 2-fold coordinate BN_2^{3-} units, which are isoelectronic with CO_2.
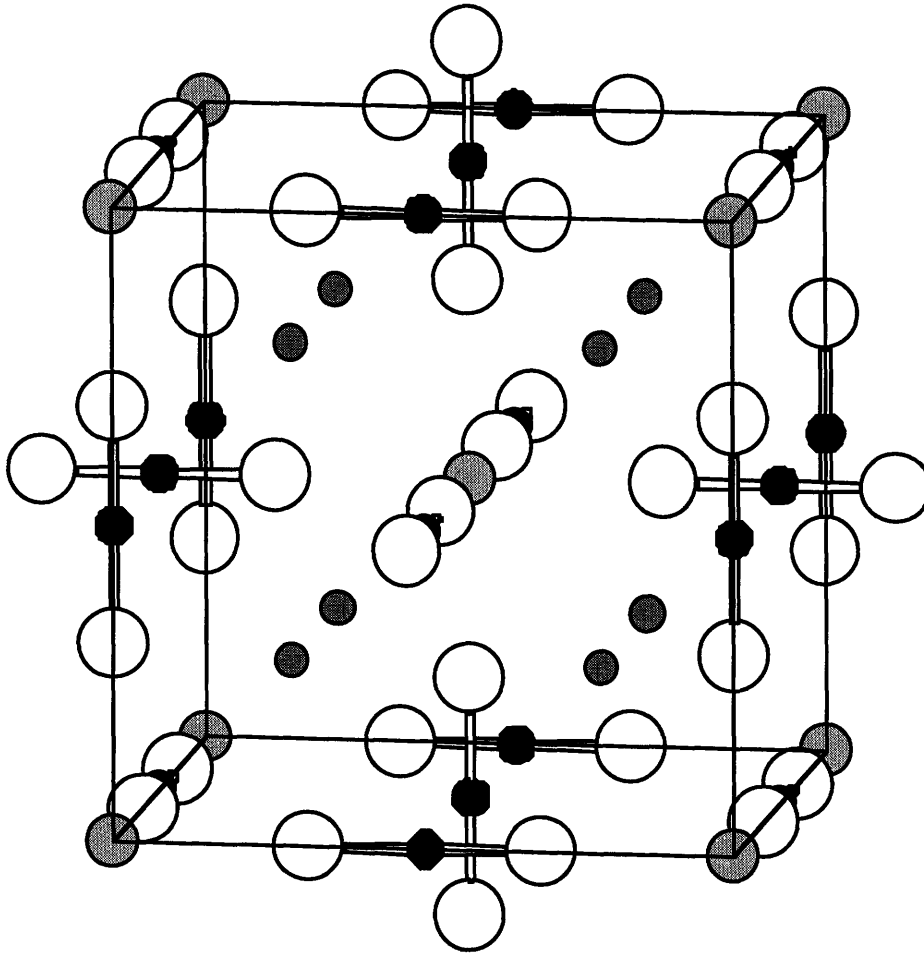
Figure 1.5.3: Structure of LiCa₄B₃N₆.
Large gray = Li, Small gray = Ca, Black = B, White = Nitrogen.

1.5.2 Other Alkali Metal-Containing Ternary Nitrides

Since the alkali metals can be difficult to handle and only lithium has a stable binary nitride, most Group I ternary nitrides are lithium compounds. However, recently several groups have used alkali metal amides to synthesize ternary nitrides which contain other alkali metals. For example, $MM'N_2$ (M = Ta, Nb and M' = Na, Cs)[19,20,41,42] and $MTaN_2$ (M = K, Rb)[20] have been synthesized by reaction of the alkali metal amide with Ta_3N_5 or NbN in a high-pressure autoclave at 400 - 800 °C. $MTaN_2$[19] (M = Na or K) and $MNbN_2$[19] (M = Na, K) also may be synthesized from Ta_3N_5 or NbN using an excess of the alkali amide under 1 atm of flowing ammonia at 500 °C.

The structure of $NaTaN_2$ and $NaNbN_2$ (Figure 1.5.4), which crystallize in the hexagonal α-$NaFeO_2$ structure, consists of alternating NaN_6 and TaN_6/NbN_6 octahedra that are stacked in an ABCABC fashion. Both sets of octahedra are distorted with the MN_6 octahedra (M = Ta, Nb) shortened and the NaN_6 octahedra elongated along the c-axis, a phenomenon usually associated with increased M-N bond covalency. As is observed for many layered sulfide and oxide materials, the sodium in $NaTaN_2$ can be extracted to nearly one full equivalent. The resulting compound, "TaN_2", is a poorly crystalline material and was indexed with an hexagonal unit cell, similar to the parent nitride, $NaTaN_2$. The removal of sodium caused a decrease in the c-axis from c = 16.902(3) Å in $NaTaN_2$ to c = 14.84 Å in TaN_2.[19] However, the structure of the final product could not be determined due to the poor crystallinity of the material after deintercalation. Sodium re-intercalation was not successful, which suggests the formation of a highly-disordered material.[19]
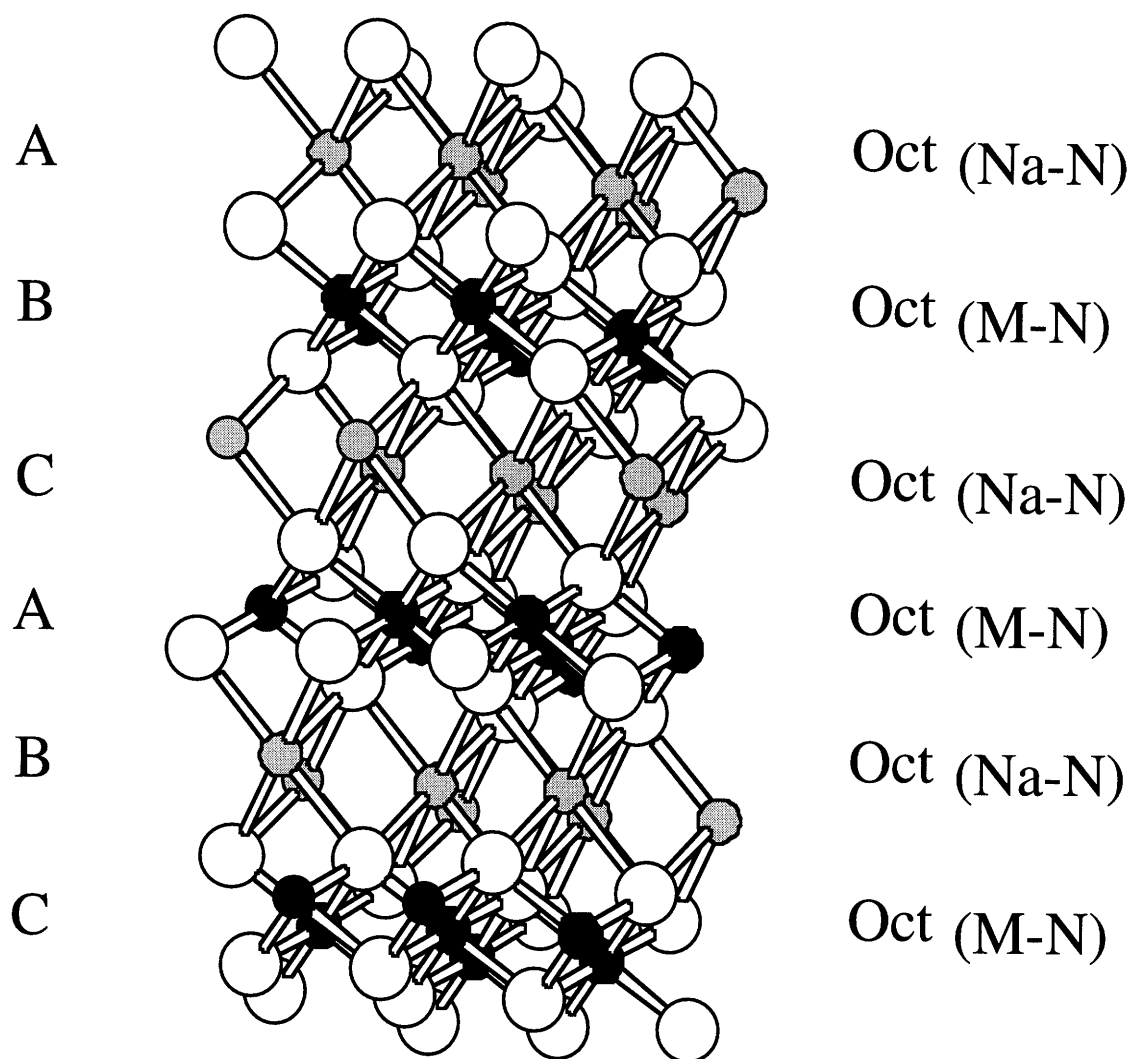
Figure 1.5.4: Structure of NaTaN$_2$ and NaNbN$_2$.

Examples of a ternary nitrides containing sodium and niobium/tantalum octahedra. Gray = Lithium, Black = M (M = Nb, Ta), White = Nitrogen.
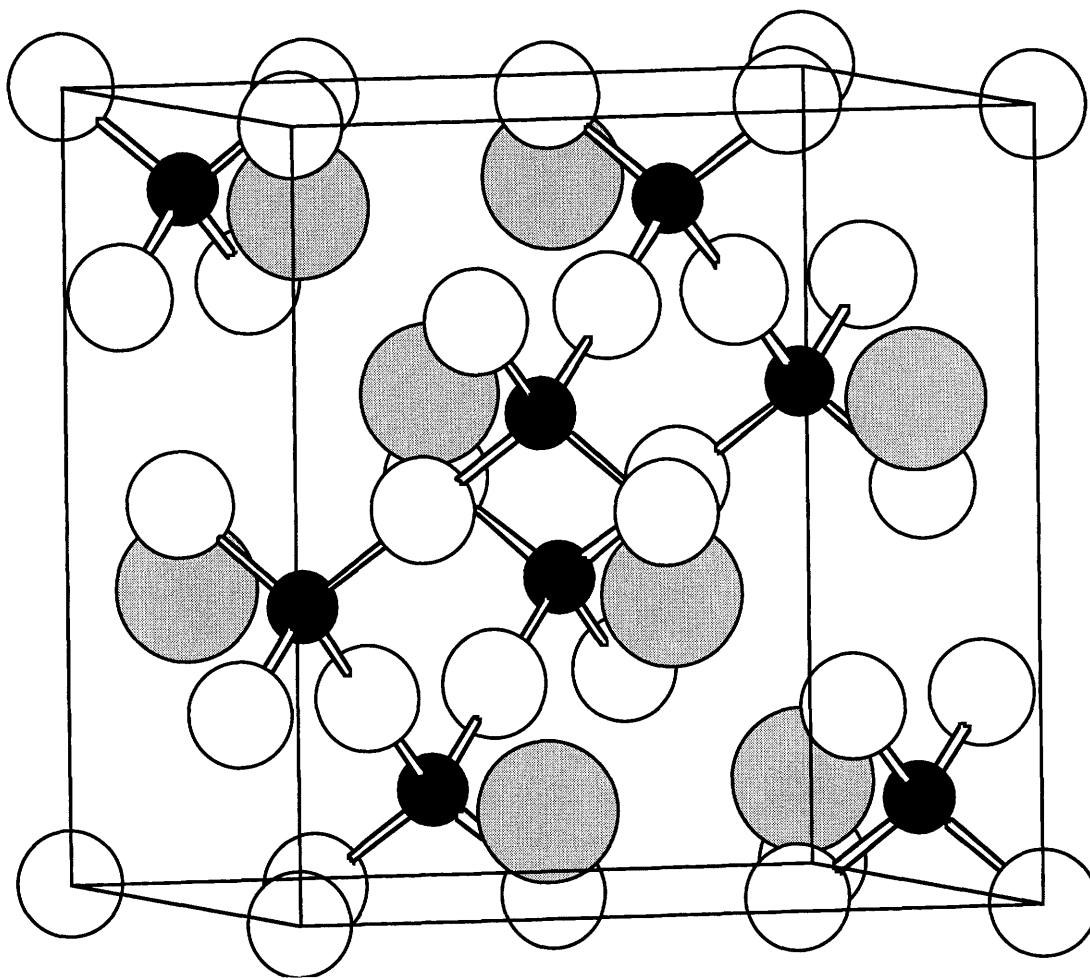
Figure 1.5.5: Structure of CsTaN$_2$ and CsNbN$_2$.

Examples of a ternary nitride in the β-cristobalite structure.
Gray = Cesium, Black = Tungsten/Niobium, White = Nitrogen.

$KTaN_2$,[20] $RbTaN_2$,[20] $CsTaN_2$,[20] and $CsNbN_2$[41] form structurally related phases. $CsTaN_2$ (Figure 1.5.5) is cubic, with a filled β-cristobalite type structure, and consists of corner shared TaN_4 tetrahedra and 12 coordinate cesium. $KTaN_2$ and $KNbN_2$ are also cubic and are isostructural with $CsNbN_2$ when synthesized as polycrystalline powders at ambient pressure.[19] However, single crystals of $KTaN_2$, synthesized in a high pressure autoclave, form in a related lower symmetry orthorhombic structure, which is isostructural with $RbTaN_2$.[20]

The isostructural compounds Na_3WN_3 and Na_3MoN_3 can be synthesized from the metal nitride and sodium amide either at 400 °C under high-pressure ammonia[43] or from the metal nitride and sodium amide under flowing ammonia gas at 500 °C.[44] Na_3MN_3 (M = Mo, W) is monoclinic and is composed of MN_4 tetrahedra which are corner shared to form chains. The sodium atoms are located between the chains and are 4- and 5-coordinate.[14,44] This structure type can be expanded to include partial substitution of sodium for one of the higher alkali metals, Na_2KWN_3[45] and $Na_{11}Rb[(WN_3)_4]$ [45], while maintaining the linked MN_4 tetrahedral chains. As is apparent from the large number of nitrides synthesized in the last several years, the amide synthesis route has been quite successful in leading to nitride materials with new structure types. Future work using metal amides promises to lead to the synthesis of many new alkali metal ternary nitrides.

1.5.3 Alkaline Earth Containing Ternary Nitrides

Alkaline earth containing ternary nitrides make up the second largest group of ternary phases after lithium containing nitrides. Because the alkaline earth metals form stable binary nitrides, most group 2 ternary nitrides have been synthesized by the reaction of a binary nitride with a metal or by the reaction of two binary nitrides (**Reaction 1**). This synthesis method has resulted in a number of new ternary nitrides with a variety of structures. A systematic review of the structure types exhibited by the alkaline earth

containing ternary nitrides will start with low coordination number (2) for the metal and proceed to progressively higher coordination.

1.5.3.1 Two-Fold Coordination

Several alkaline earth ternary nitrides with transition metals in unusual solid-state coordinations have been discovered. Linear 2-coordinate transition metals are known for several the alkaline earth containing nitrides. For example, Ca_2ZnN_2 contains Zn atoms which are linearly coordinated between layers of CaN_5 centered square pyramids.[46] The analogous compounds of the higher alkaline earths also exist (Sr_2ZnN_2[47] and Ba_2ZnN_2[47]). The structurally related phase, CaNiN (Figure 1.5.6) contains linear Ni-N-Ni-N chains which run in the **ab** plane. The calcium atoms are located between these nickel-nitrogen planes and form CaN_4 tetrahedra. The structure may also be described with anion centered polyhedra as containing NCa_4Ni_2 octahedra.[15] The compound is metallic and paramagnetic[13]. It is also interesting to note that some evidence exists for the presence of M-N (and perhaps N-N) covalent interactions in these compounds.

MCN_2 (M = Mg, Sr, Ba) is an interesting class of compounds for several reasons, both of which involve the presence of CN_2^{2-} anionic units within the structure (Figure 1.5.7). $MgCN_2$ forms in the delafossite structure and contains carbon in a linear coordination with two nitrogen atoms. These units are contained in close-packed layers, with the N-C-N axis parallel to the c-axis. The alkaline earth is located in octahedral coordination between the CN_2^{2-} layers. This structure is identical to the $NaTaN_2$ structure discussed earlier and is related to the $LiMN_2$ structure.
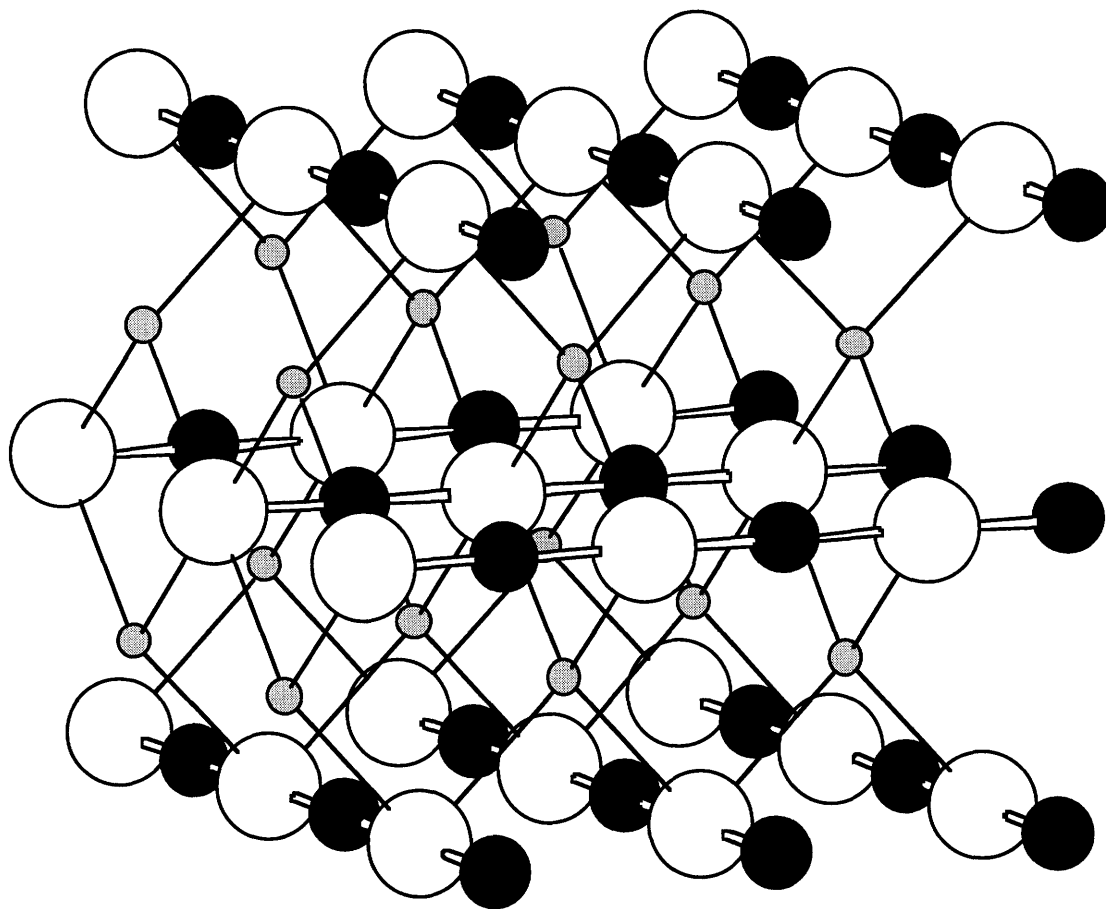
Figure 1.5.6: Structure of CaNiN.
An example of a calcium ternary nitride containing ternary nitride containing linear Ni-N Chains. Gray = Calcium, Black = Nickel, White = Nitrogen.
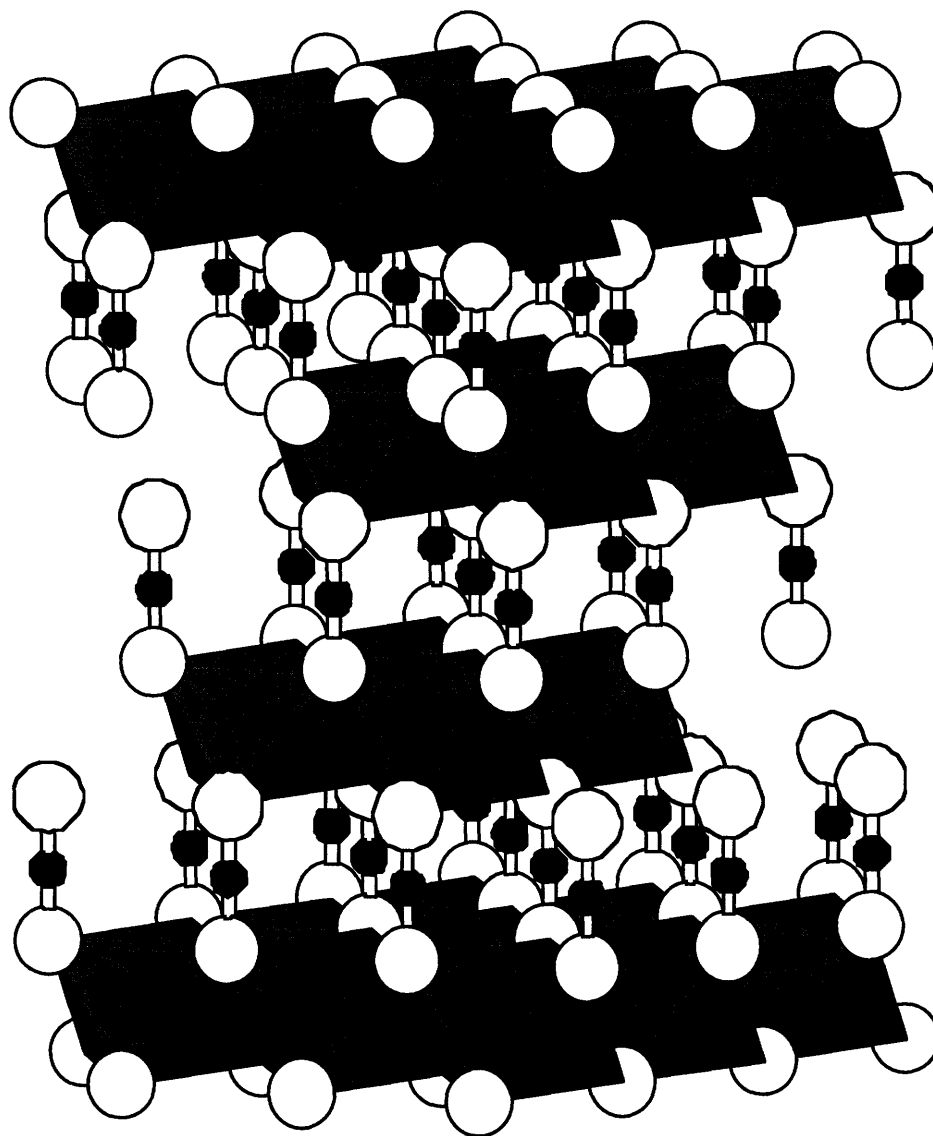
Figure 1.5.7: Structure of MgCN$_2$
Black = C; White = N; Octahedra = MgN$_6$

1.5.3.2 Three-Fold Coordination

A number of alkaline earth ternary nitrides which contain a metal in three-fold coordination have been synthesized. One group of structurally related phases (Figure 1.5.8) contains trigonal planar MN_3 units (M = transition metal). Such phases include Ca_3VN_3,[48,49] Ca_3CrN_3,[50] Ca_3CoN_3,[51] Ba_3FeN_3,[18] Sr_3FeN_3,[18] Ca_6GaN_5,[52] Ca_6FeN_5,[52] and Ca_6MnN_5[53] (Table 1.1). Ca_3MN_3 (M =V, Cr, Co) is orthorhombic in the space group $Cmcm$ and consists of eclipsed trigonal planar MN_3 units, stacked along the c axis.[48] Neighboring $[MN_3]^{6-}$ anions are displaced by 1/2 in the c direction, with the orientation of the trigonal planar unit reversed. The calcium atoms are in CaN_5 square pyramids. The structurally related phases M_3FeN_3 (M = Ba, Sr)[18] also contain trigonal planar MN_3 units, but differ in the coordination of the alkaline earth. In M_3FeN_3 (M = Ba, Sr), the alkaline earth has MN_5 trigonal bipyramidal layers and crystallizes with a hexagonal structure. Although Ca_6MN_5 (M' = Fe, Ga) is also hexagonal, the calcium is in square pyramidal coordination similar to the calcium coordination in Ca_3MN_3 (M =V, Cr, Co).
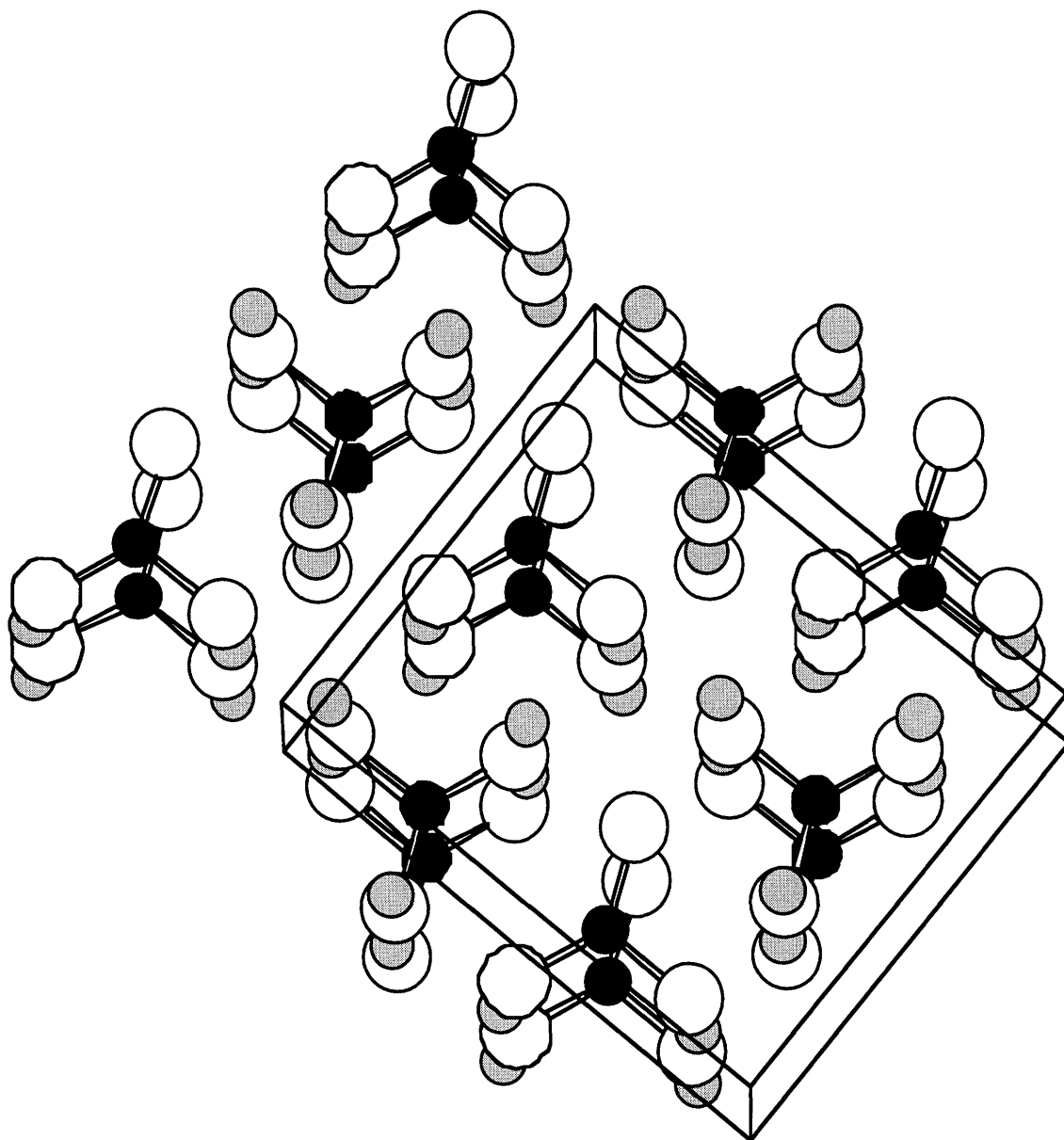
Figure 1.5.8: Structure of Ca$_3$MN$_2$ (M = V, Cr, Co).

An example of a calcium ternary nitride containing MN$_3{}^{6-}$ anionic units. Gray = Calcium, Black = M (M = V, Cr, Co), White = Nitrogen.

1.5.3.3 Four-Fold Coordination

A number of ternary nitride materials are known which contain MN_4 units, which are often corner shared to form chains and other low dimensional structures within the material. Several examples exist of materials which contain isolated MN_4 anionic units. In Ba_5CrN_5[54], nearly ideal CrN_4^{7-} tetrahedra are contained at the center of Ba_6 octahedra. Also, in Ca_2SrWN_4,[55] isolated WN_4 tetrahedra are hexagonally close packed with the alkaline earth cations interstitial. This material is related to a low temperature modification of Ba_3MN_4 (M = Mo, W),[56] which also consists of hexagonally closed packed MoN_4 tetrahedra. M_2VN_3 (M = Sr and Ba) and Ba_2NbN_3 form in related structure types in which distorted corner-shared VN_4 tetrahedra form one-dimensional chain along the c axis. The distortion of the tetrahedra in Sr_2VN_3 is greater than in the barium analogue, which results in a drop in symmetry from orthorhombic to monoclinic. Similar chains are seen in $Sr_3Al_2N_4$.[57] However, the AlN_4 tetrahedra in this material are edge shared, forming chains parallel to the b axis. MN_4 tetrahedra can also be corner shared to form 2-dimensional sheets as is the case in $BaZrN_2$. Corner-shared ZrN_4 tetrahedra form 2-dimensional sheets in the ab plane with the barium atoms located between the sheets. Three dimensional networks of MN_4 units are the common structural motif for silicon containing alkaline earth nitrides (i.e. $Sr_2Si_5N_8$,[21] $Ba_2Si_5N_8$,[21] and $Ca_2Si_5N_8$[22]). These materials contain three dimensional corner-shared covalent networks of corner and/or edge shared SiN_4 tetrahedra. Perhaps the most interesting arrangement of MN_4 tetrahedra is found in $Ba_{10}Ti_4N_{12}$[58], in which four TiN_4 tetrahedra are each connected by two corners to form centrosymmetrical rings, which are stacked along [100] forming tubes.

1.5.3.4 Six-Fold Coordination

The reaction of calcium nitride with group IV or group V metals/metalloids forms a series of structurally related ternary nitrides with

anti-perovskite type structures. In Ca_3MN (M = P, As, Sb, Bi, Ge, Sn, Pb) (Figure 1.5.9), the anionic metal/metalloid and N^{3-} anions occupy the A and B sites of the perovskite structure (ABX_3) and the X sites are occupied by the Ca^{2+} site.[59,60] An interesting variation from the cubic perovskite structure is the orthorhombic distortion observed in Ca_3AsN, which is produced by a tilting the Ca_6N octahedra.[60] Some evidence exists for a high temperature undistorted cubic phase, however it has not yet been fully characterized.

1.5.4 Rare Earth Ternary Nitrides

Despite the potentially interesting electronic properties, rare earth (RE) containing ternary nitrides with high nitrogen contents were an unexplored class of materials until the last couple of years. The majority of these materials are synthesized at high temperatures and contain 3-dimensional arrays of REN_x polyhedra. $TaThN_3$, synthesized from the reaction of the binary metal nitrides, has the perovskite structure.[61] Ce_2CrN_3 contains square planar chromium and has a structure related to K_2NiF_4.[62] A number of silicon containing rare earth nitrides have been made ($Ln_3Si_6N_{11}$ (Ln = La, Ce, Pr, Nd, Sm),[63] $LnSi_3N_5$ (Ln = Se, Pr, Nd)[63] and $Ce_3Si_6N_{11}$[23]) all of which contain 3-dimensional arrays of SiN_4 tetrahedra.
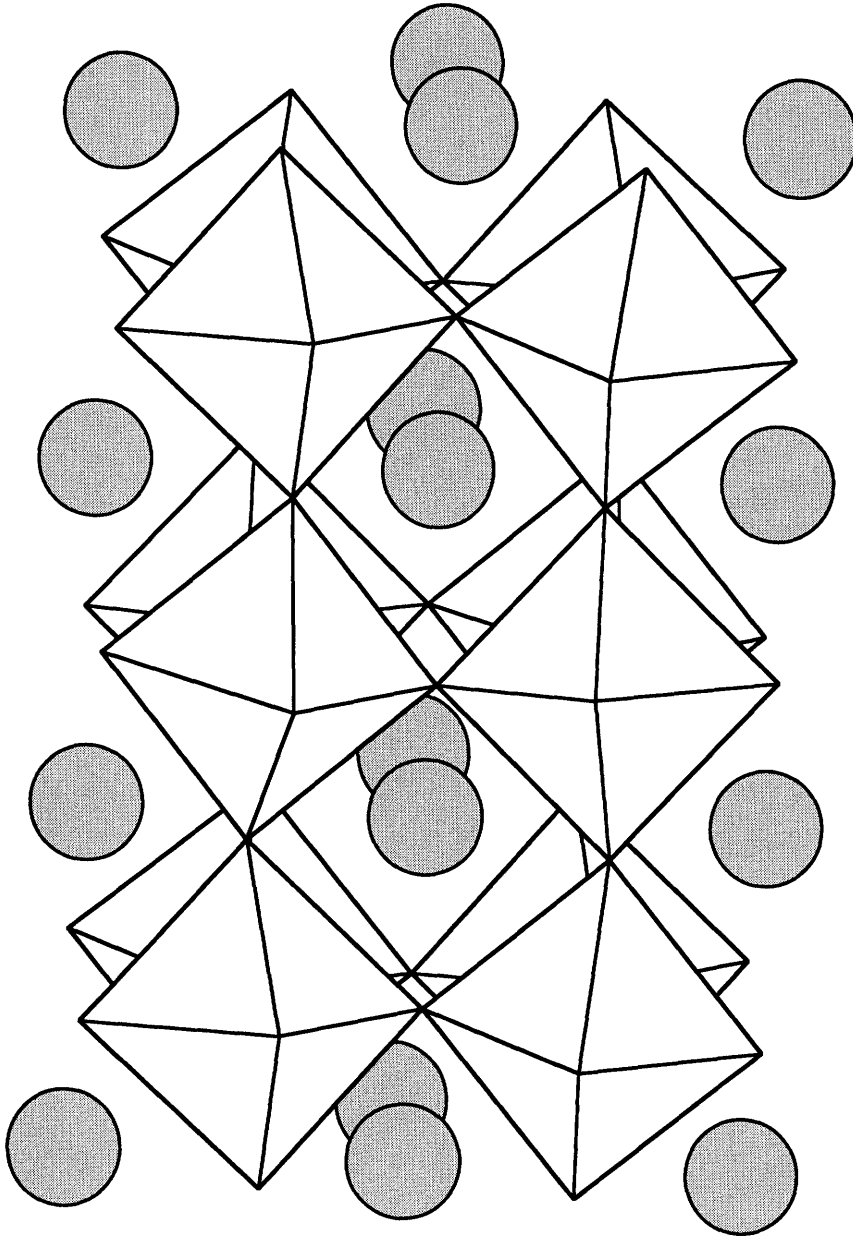
Figure 1.5.9: Structure of Ca_3AsN.

An example of a calcium ternary nitride containing ternary nitride in the anti-perovskite structure. Gray = Arsenic, White = Ca_6N octahedra.

1.5.5 Transition Metal Ternary Nitrides

The synthesis of ternary transition metal nitrides through the reaction of two binary nitrides (Table 1.4, **Reaction 1**) or by nitriding two metals (Table 1.4, **Reaction 2**) has been relatively unsuccessful. As a result, until recently, the number of reports of the synthesis of ternary transition metal nitrides was very small and all of dubious quality. However, several new techniques have allowed the synthesis of a number of new compounds in this interesting class. The ternary transition metal nitride $CuTaN_2$[30] was synthesized by the low temperature metathesis reaction of CuI and $NaTaN_2$. The structure of the parent nitride, $NaTaN_2$, is not maintained, and $CuTaN_2$ crystallizes in the delafossite structure with layers of corner shared TaN_6 octahedra with linearly coordinated Cu between each layer.

In the past few years, several ternary transition metal nitrides have been synthesized in this group, using an ammonolysis technique. In this technique, an oxide precursor, synthesized either through a solid state technique or through an aqueous precipitation method, is heated under flowing ammonia at temperatures between 600 and 800 °C. The resulting materials are air and water stable and have structures which closely resemble those found for the alkali-transition metal nitrides and the transition metal dichalcogenides. A representative structure of these compounds ($FeWN_2$) is shown in Figure 1.5.10 and consists of alternating layers of face- or edge-shared MN_6 trigonal prisms and octahedra. The structure and properties of these compounds, as well as several other more recent ternary nitrides and structurally related binary oxynitrides will be discussed in more detail in Chapter 2 and 3.

A   (W-N)$_{TP}$

A   (Fe-N)$_{OCT}$

A   (W-N)$_{TP}$

A   (Fe-N)$_{OCT}$

A   (W-N)$_{TP}$
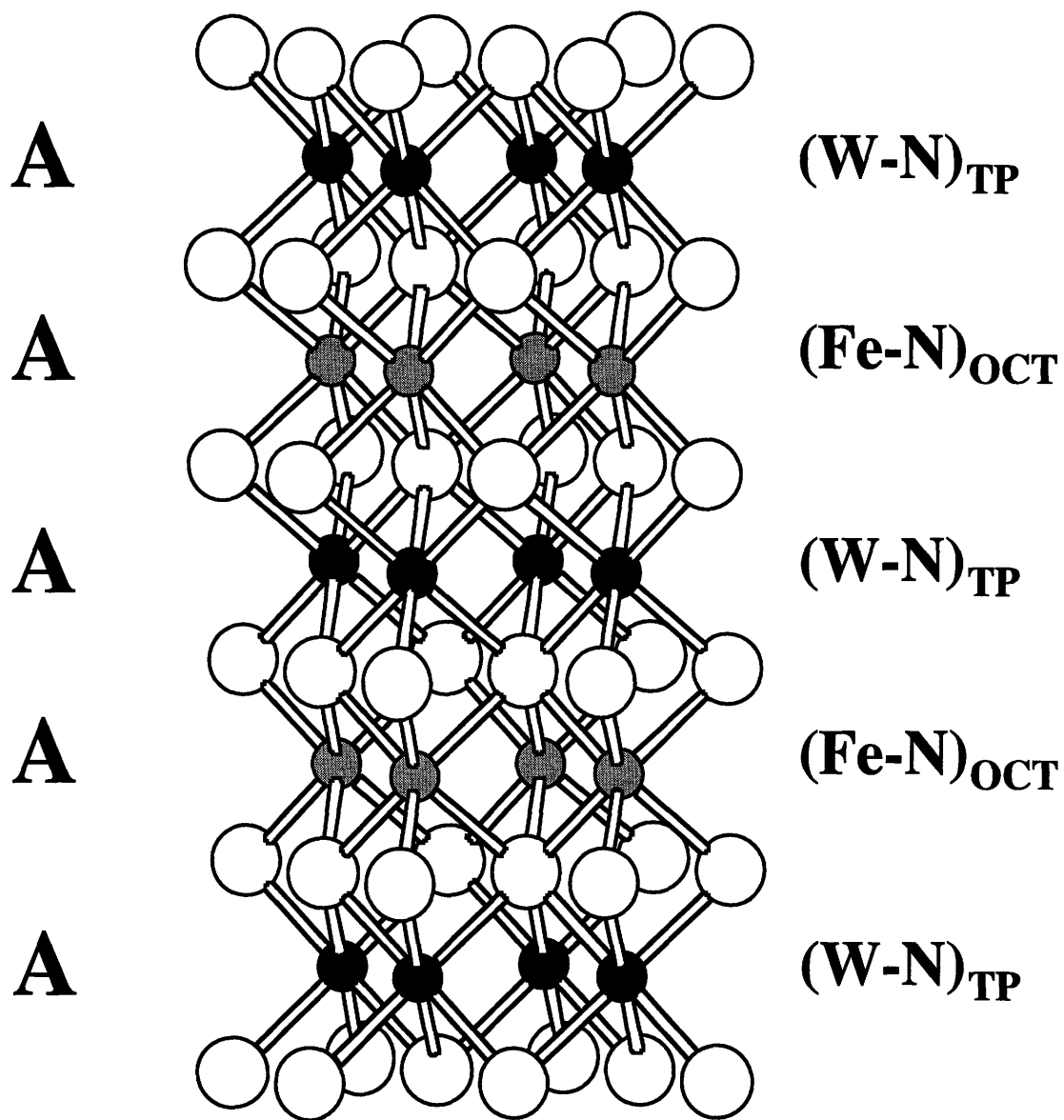
Figure 1.5.10: **Proposed structure of FeWN$_2$.**
Gray = Fe, Black = W, and White = N. Metal stacking
A$_{oct}$A$_{tp}$A$_{oct}$A$_{tp}$

1.6 PROPERTIES OF IONIC/COVALENT TERNARY NITRIDES

As is true for any new class of materials, ternary nitrides have been found to exhibit many unusual characteristics. For example, the ternary nitride CaNiN combines one-dimensional Ni-N chains in an unusual three-dimensional arrangement.[13] Despite the formal d^9 configuration of Ni and the linear chains (which could be a possible candidate for a Peierls instability) this compound is found to exhibit metallic conductivity $(2.5 \times 10^4 \, S/cm)$ and paramagnetic susceptibility down to very low temperatures.[64] Band structure calculations show that the metallic properties are a result of coupling of the Ni-N chains through weak N-N interactions.[64] These calculations also suggest a possible tendency toward buckling of the nickel nitrogen chains, which is not observed in CaNiN, but is observed in the structurally related nitride BaNiN.[65]

Nitrogen-nitrogen interactions may also be present in the $LiMN_2$ phases (M = Mo, W) as well as the ternary transition metal nitrides $FeWN_2$, α,β-$MnWN_2$, $MnMoN_2$ and $(Fe_{0.8}Mo_{0.2})MoN_2$. All these compounds are structurally related, consisting of two dimensional layers of MN_6 (M = Fe, Mn, Li) octahedra and $M'N_6$ (M' = Mo, W) trigonal prisms (Figure 1.5.1.2). Band structure calculations, performed on $LiMoN_2$, found strongly covalent MoN_2 sheets with unusually pronounced N-N interactions between the interplanar nitrogen atoms of the MoN_6 trigonal prisms.[66] These interactions result in unusually short interplanar nitrogen-nitrogen distances across the trigonal prisms $(d_{N-N}(LiMoN_2) = 2.56 \, Å)$[24] as compared to an N-N single bond[15] or the sum of the N^{3-} radii (2.8-3.4Å).

Magnetic ordering is not observed in $LiMoN_2$ and $LiWN_2$ which exhibit temperature independent Pauli paramagnetism and temperature independent conductivity,[24,25] similar to that exhibited by intermetallic binary nitrides.[3] However, in the iron containing systems, some anti-ferromagnetic ordering is observed at ~17 K. The reported values of the

electronic conductivity for all the ternary transition metal nitride materials (0.2-25 S/cm) are low for metal-like systems. However, all measurements were performed on pressed pellets of polycrystalline powders in which the conductivity can be dominated by grain boundary resistance. Therefore, these values represent lower limits of the conductivity. The metallic properties are consistent with band structure calculations which predict metallic, three-dimensional bands.[66]

The unusual structure of ternary nitrides of the formula Ca_3MN_3 (M = V, Co, Cr) and Ca_6MN_5 (M = Fe, Ga) also result in interesting properties. The nitrides, Ca_3MN_3 (M = V, Co, Cr), exhibit semiconducting behavior, consistent with the presence of isolated MN_3 groups, and measurements of the magnetic susceptibilities are consistent with low spin ions.[48,50,67] Extended Hückel calculations of the MN_3^{6-} (M = V, Cr, Fe) ion suggest that all MN_3^{6-} compounds contain low spin ions and that the chromium and iron containing species will undergo Jahn-Teller distortions in which one bond of the trigonal prism lengthens to stabilize the spin pairing.[68] Ca_3CrN_3 contains the first example of a low spin three-coordinate Cr^{3+} compound and exhibits low-dimensional antiferromagnetic ordering at low temperature.[50]

Another example of an unexpected low-spin transition metal was found in $Li_{3-x}FeN_2$ which contains low-spin tetrahedral Fe^{3+} and exhibits Curie-Weiss paramagnetism consistent with a moment of $1.7\mu_B$ (one unpaired electron).[34] $Li_{3-x}FeN_2$[31,34,69] exhibits significant lithium ion conduction, which is not unexpected for a compound composed of one-dimensional chains. The intercalation chemistry of lithium in $Li_{3-x}FeN_2$ is extensive, with smooth extraction and reversible insertion of lithium up to x = 1. $Li_{3-x}FeN_2$ shows a large constant OCV potential window (the potential only increases by 30 mV from x = 0 to 0.6), which makes this material suitable for application as a lithium battery electrode.[31] The Mössbauer spectrum after extraction of one equivalent of lithium is consistent with the presence of low spin tetrahedral Fe(IV) and the oxidation of Fe(III) to Fe(IV). The room

temperature electronic conductivity is 0.5 S/cm for x = 0 and 0.1 S/cm for x = 1. Li_4SrN_2,[70] Li_3AlN_2,[71] and Li_3BN_2[72] have also been reported to be lithium ion conductors. The lithium conductivity of these materials can be quite high (~$2x10^{-3}$ at 200 °C) and with activation energies between 0.5 and 1.0 eV.

Deintercalation of the alkali metal also is observed in $LiMoN_2$. Lithium can be reversibly deintercalated up to 0.64 equivalents,[24] however the lithium ion conduction was not measured. Similar deintercalation experiments were not performed on $LiWN_2$ but it is likely, given the similarity of the structures and properties, that it will exhibit similar behavior. Deintercalation of sodium in the alkaline earth nitride $NaTaN_2$ also has been reported.[19] The alkali metal can be extracted up to one full equivalent from $NaTaN_2$. However, the resulting compound (TaN_2) has very poor crystallinity and has not been well characterized. No other alkali metal ternary nitrides are reported to show deintercalation or ionic conductivity.

1.7 CONCLUSIONS

Several trends regarding the structure property relationship between nitride phases and their synthesis temperature can be drawn from the data presented in this chapter. As mentioned earlier, lower reaction temperatures (<800°C) tend to result in increasing metal-nitrogen bond covalency. Also, lower temperatures tend to result in lower metal-nitrogen coordination number. These trends can be summarized by drawing comparisons to other classes of materials based on the synthesis temperature of the nitride. In general, nitrides which are synthesized at low temperatures (<750°C) have structures and properties resembling those of the chalcogenides. Most notably, several alkali metal and transition metal ternary nitrides form in structures similar to the transition metal dichalcogenide structures. Low temperature nitrides materials are often structurally and electronically low-dimensional, often exhibiting low-dimensional properties resembling

those found in chalcogenide materials. They typically have short M-N and N-N distances, indicative of the high degree of M-N and N-N covalency, and can exhibit metallic type conductivity. As is found in low-dimensional chalcogenide and oxide materials, the alkali metals in many ternary nitrides can be removed through deintercalation reactions, though usually not completely. In all these respects, the similarity to transition metal chalcogenides can been seen. Perhaps, as new synthetic methods are explored, the number of known nitride materials will grow as rapidly as the number of chalcogenide materials have in recent years.

Nitrides synthesized at moderate temperature (800-1400°C) have structures and properties which more closely resemble those found in oxide materials. In general, materials synthesized in this temperature range have salt like structures, which can be predicted using the radius ratio rules. Such structure types as the perovskite and anti-fluorite structures, both common among oxide materials, are found in materials synthesized in this temperature range. As expected, the metal-metal and metal-nitrogen distances in these compounds are fairly uniform and conform more closely to the distances obtained as a sum of ionic radii. While many of these materials exhibit appreciable ion conduction (especially lithium ion conduction), most are electronic insulators. Ternary nitrides containing silicon made in this temperature range often contain corner-shared SiN_4 tetrahedra, which form networks reminiscent of the SiO_4 network found in many silicates. However, in several systems, low-dimensional behavior is seen, particularly in silicon containing ternary nitride materials.

Nitrides synthesized at high temperatures (>1400C°C) have structures and properties similar to carbide type materials. Materials synthesized at these temperatures tend to have lower nitrogen contents, due to the entropic disproportionation of ternary materials into lower binary nitrides or metals and nitrogen, which increases with increasing temperature. Some materials with reasonably high nitrogen contents can be synthesized, particularly those containing silicon, but all rely heavily on the inductive effect. Materials

made in this temperature range tend to be refractory and exhibit metallic type electronic conductivity due to larger metal-metal interactions and broader valance and conduction bands. The metals coordinations tend to be higher than in nitrides synthesized at lower temperatures. In an interesting and perhaps counterintuitive trend, reaction times for nitride synthesis tend to increase with increasing temperature, a fact due primarily to the use of diffusion aids at low temperatures (i.e. fluxes). While exceptions to these rules exist, they can be used as a tool for tailoring synthetic conditions to yield desirable properties for a particular application.

Although many advances in the synthesis of ternary nitrides have been made in the last decade, the number of fully characterized phases is still relatively small. The compounds recently synthesized demonstrate that a large number of possible materials remain undiscovered. New approaches have been developed using alternative nitrogen sources (such as amide synthesis) and have resulted in the synthesis of new ternary phases. In order to broaden the number of ternary nitride phases and structure types known, novel synthetic approaches involving lower reaction temperatures and/or more active nitrogen species will be needed. The former will aid in the formation of new structure types which could exhibit new and interesting properties. The later could result in speeding reaction times or lowering the reaction temperature of high temperature reactions. More importantly, a broad data base of fully characterized compounds is needed to help understand the properties and synthetic pathways of the ternary nitrides.

The work presented in the remainder of this thesis addresses the investigation of two new routes to the synthesis of nitride materials, which yield either lower reaction temperatures or highly active nitrogen species or both. In Chapter 2, the synthesis of the ionic/covalent nitrides $Ta_5N_{6-\delta}O_x$ and $Nb_5N_{6-\delta}O_x$ from ternary iron-containing oxide precursors are described, as well as the role of iron in the synthesis of these compounds at reduced temperature. Chapter 3 deals with the synthesis of other nitride

$((Fe_{0.8}W_{0.2})WN_2)$ and oxynitride $(LiTaO_{3-3x}N_{2x})$ materials. Their structures and characterization of electronic and magnetic properties are also discussed. Chapter 3 is concluded by a critical analysis of the oxide precursor route to nitride materials, including the limitations and possible avenues of further research. In the second half of this thesis, the use of microwaves as a heating source toward the synthesis of nitride materials is presented. Chapter 4 begins the discussion with a brief review of the theory of microwave heating and plasma physics, as well as with a review of the recent literature on synthetic chemistry performed in a microwave oven. In Chapter 5, the use of microwaves and microwave plasmas as synthetic tools for the synthesis of binary and ternary nitrides will be presented. Finally, in Chapter 6, the success of these two routes in overcoming current limitations on nitride synthesis will be evaluated and several other possible routes to the synthesis of both binary and ternary nitride presented.

Table 1.1: Synthetic conditions of ternary and quaternary nitrides

Compound	Method	Synthesis Conditions	Structure Characterization	Space Group	Reference
$Li_{0.98}Ta_{3.02}N_4$	1,3	1200-1500 °C, 24 hrs, 1 atm Ar	Single Crystal XRD, Powder XRD, and Neutron Diffraction	$P6_3/mcm$	37
LiCaN	1	850 °C, 12 hrs, 1 atm N_2	Single Crystal XRD	Pnma	70
$LiMoN_2$	4*	650 °C 18 hrs. flowing NH_3, ~ 1 atm	Powder XRD and Neutron Diffraction	R3	24
$LiWN_2$	4	700 °C, 12 hrs under flowing NH_3, ~ 1 atm	Powder XRD	R3	25
$Li_2Ta_3N_5$	1, 2, 3	550 °C, 5 days, 0.6 GPa NH_3	Powder XRD and Neutron Diffraction	C2/m	36
Li_3FeN_2	1,2	800 °C 100-800 mbar incremental increase in pressure	Single Crystal XRD	Ibam	31,34,69
Li_4SrN_2	1	700 °C, 12 hrs, 1 atm N_2	Powder XRD	$I4_1/amd$	70
Li_4FeN_2	2	900 °C, 100-800 mbar incremental increase in pressure	Single Crystal XRD	Cmmm	38
Li_6MN_4 (M = Cr, Mo, W)	1	830-870 °C, 550-950 mbar N_2	Single Crystal XRD	$P4_2/nmc$	35
Li_7TaN_4	1	800-950 °C, 60 hrs in 1 atm N_2	Single Crystal XRD	Pa-3	32
Li_7NbN_4	†	1000 °C, 10 hrs, cooled to 500 °C over 30 hrs †	Single Crystal XRD	Pa3	33
$Li_{15}Cr_2N_9$	1	1 hrs at 550 °C, 45 min at 730 °C, 560 mbar N_2	Single Crystal XRD	P4/nnc	35
$LiSr_2CoN_2$	2	850 °C, 48 hrs, cooled at 100 °C/hrs, 1 atm N_2	Single Crystal XRD	$P4_2/mnm$	73
$LiBa_2Fe_2N_3$	5	750 °C, 36 hrs, 1 atm N_2	Single Crystal XRD	C2/c	74
$LiSr_2Fe_2N_3$	5	750 °C, 36 hrs, 1 atm N_2	Single Crystal XRD	C2/c	74
$LiBa_4Mo_2N_7$	1	1050 °C, 18 hrs, 1 atm N_2	Single Crystal XRD	P2/n	75
$LiBa_4W_2N_7$	1	1050 °C, 18 hrs, 1 atm N_2	Single Crystal XRD	P2/n	75
$LiCa_4B_3N_6$	1	1025 °C in a sealed Nb ampule	Single Crystal XRD	I m -3 m	40
$Li_3Sr_3Ni_4N_4$	1,5	800 °C, 20 hrs, 1 atm N_2	Single Crystal XRD	Immm	76,77

$Li_3Ba_2TaN_4$	3	Heated to 860° C under Ar, at 860 °C N_2 introduced 34 hrs, 1 atm N_2	Single Crystal XRD	C2/c	39
$NaTaN_2$	3	400-800 °C in an autoclave under NH_3 or 700 °C, 12 hrs, flowing ammonia	Single Crystal and Powder XRD	R-3m	19,20
$NaNbN_2$	3	400-800 °C in an autoclave under NH_3 or 700 °C, 12 hrs, flowing ammonia	Single Crystal and Powder XRD	R-3m	19,42
Na_3MoN	3	900 °C in an autoclave under NH_3 or 500 °C, flowing NH_3	Single Crystal XRD and Neutron Diffraction	Cc	43,44
Na_3WN_3	3	900 °C in an autoclave under NH_3 or 500 °C, flowing ammonia	Single Crystal XRD and Neutron Diffraction	Cc	14,44
Na_2KWN_3	3	700 °C, 5days, in autoclave	Single Crystal XRD	Pbcm	45
$Na_{11}RbW_4N_{12}$	3	700 °C, 5days, in autoclave	Single Crystal XRD	Pbcm	45
$NaBa_4B_3N_6$	1	1050 °C, under vacuum	Single Crystal XRD	Im-3m	78
$KTaN_2$	3	400-800 °C in an autoclave under NH_3 or 700 °C 12 hrs, flowing ammonia	Single Crystal and Powder XRD	Pbca	19,20
$KNbN_2$	3	700 °C, 12 hrs, flowing ammonia	Powder XRD	Pbca	19
$RbTaN_2$	3	400-800 °C in an autoclave under NH_3	Single Crystal XRD	Pbca	20
$CsTaN_2$	3	400-800 °C in an autoclave under NH_3	Single Crystal XRD	Fd3m	20
$CsNbN_2$	3	400-800 °C in an autoclave under NH_3	Single Crystal XRD	Fd3m	41
$MgTa_3N_4$	1,3	1200 °C, 24 hrs	Powder XRD and Neutron Diffraction	P6₃/mcm	37
$MgCN_2$	3	750°C, 2 days, Ar	Powder XRD	R-3m	79
CaNiN	1	1000 °C, 2 days, 1 atm N_2	Powder XRD	P4₂/mmc	13
$Ca_2Si_5N_8$	3	1600 °C slow cooled to 1200 °C in 72 hrs. 1 atm N_2	Single Crystal XRD	Cc	22

Compound	Prep	Synthesis conditions	Characterization	Space group	Ref
Ca_3VN_3	Pwder 1 Xtals 2	Xtals: 950 °C 18.5hrs, cooled 22.5 °C/hrs to 500 °C, 1 atm Ar, slow into N_2 Pwder: 1350 °C, 30hrs, vac.	Single Crystal XRD	Cmcm	48,49
Ca_3CoN_3	1	1000 °C 20-36 hrs, 1 atm N_2	Powder XRD	-	51
Ca_3CrN_3	1	1350 °C, 4 days, 1 atm Ar	Single Crystal XRD	Cmcm	50
Ca_3AsN	1	1000 °C, 2 days, 1 atm N_2	Powder XRD and Neutron Diffraction	Pbnm	60
Ca_3MN M = P, As, Sb, Bi, Ge, Sn, Pb	1	P, As, Sb, Bi: 1000 °C, 2 days, 1 atm N_2 Ge, Sn, Pb: 1300 °C, 1 atm N_2	Powder XRD	Pbnm	59
Ca_6GaN_5	2	850 °C, 1 atm N_2	Single Crystal XRD	P63/mcm	52
Ca_6FeN_5	2	950-1100 °C, 1 atm N_2	Single Crystal XRD	P63/mcm	52
Ca_6MnN_5	1	1030 °C, 5 days, flowing Ar	Powder XRD	P63/mcm	53
Ca_2SrWN_4	1	1200 °C, 1 atm N_2	Single Crystal XRD	Pbca	55
$SrNiN$	1	1000 °C, 2 days, 1 atm N_2	Powder XRD	Pnma	80
$SrCN_2$	3	850 °C, 2 days, Ar	Single Crystal XRD	Pnma	79
Sr_2VN_3	1	1030 °C, 5 days, flowing Ar	Powder XRD	C2/c	81
Sr_2ZnN_2	#	750 °C, under vacuum with slow cooling	Single Crystal XRD	I4/mmm	47
$Sr_2Si_5N_8$	3	1500 °C with slow cooling, N_2	Single Crystal XRD	Pmn2$_1$	21
Sr_3FeN_3	2	1000 °C, 24 hrs, 1 atm Ar, introduce N_2 slowly	Single Crystal XRD	P63/m	18
$Sr_3Al_2N_4$	2	1100°C, 24hrs, 1 atm N_2	Single Crystal XRD	Pnma	57
$BaNiN$	2	1000 °C, 15 hrs, 1 atm N_2	Single Crystal XRD	Pnma	65
$BaZrN_2$	2	950 °C, 1 atm N_2	Single Crystal XRD and Neutron	P4/nmm	82
$BaCN_2$	3	740 °C, 2 days, Ar	Single Crystal XRD	R-3c	79
Ba_2VN_3	1	1030 °C, 5 days, flowing Ar	Powder XRD	Cmca	81
Ba_2NbN_3	1, 2	1000 °C, 1 atm N_2	Single Crystal XRD	C2/c	82
Ba_2ZnN_2	#	750 °C, under vacuum with slow cooling	Single Crystal XRD	I4/mmm	47
$Ba_8Ni_6N_7$	1	800 °C	Single Crystal XRD	C2/c	83
$Ba_2Si_5N_8$	3	1500 °C with slow cooling, N_2	Single Crystal XRD	Pmn2$_1$	21

Ba_3FeN_3	2	1000 °C, 24 hrs, 1 atm Ar, introduce N_2 slowly	Single Crystal XRD	P63/m	18
Ba_3MoN_4	1	900 °C, 20 hrs, 1 atm N_2	Single Crystal XRD	Pbca	84
Ba_3WN_4	1	950 °C, 20 hrs, 1 atm N_2	Single Crystal XRD	Pbca	84
Ba_5CrN_5	1	700 °C, 2 days, 1 atm N_2	Single Crystal XRD	C2/m	54
$Ba_{10}Ti_4N_{12}$	1	980 °C, 12 hrs. flowing Ar	Single Crystal XRD	P-1	58
$TaThN_3$	1	1400 °C under vacuum	Powder XRD	Pm3m	61
$LnSi_3N_5$ (Ln=Ce, Pr, Nd)	2	1500 °C, 1 week under N_2	-	-	63
Ce_2CrN_3	1	900°C, 1 week under vacuum	Single Crystal XRD	Immm	62
$Ln_3Cr_{10-x}N_{11}$ (Ln = La, Ce,Pr)	1	1160 °C, 1week under vacuum	Single Crystal XRD	Fm-3m	62
$Ce_3Si_6N_{11}$	3	1660 °C, 12 hrs. under N_2 slow cooled to 500 °C	Single Crystal XRD	P4bm	23
$Ln_3Si_6N_{11}$ (Ln=La, Ce, Pr, Nd)	2	1500 °C, 1 week under N_2	Single Crystal XRD	P4bm	63
$CuTaN_2$	††	400 °C, 24 hrs.	Powder XRD	R-3m	30

* $LiMoN_2$ has also been synthesized from $Li_2Mo(N^tBu)_4$ 650 °C 18hrs. under flowing NH_3

† Synthesized by Li_3N in an Nb tube using Ca_3N_2 or Zn_3N_2 as nitrogen source.

†† Synthesized through ion exchange of CuI and $NaTaN_2$.

Synthesized by reaction of the metals in a Na/NaN_3 flux.

Table 1.2: Transition metal-nitrogen bond distances of selected transition metal nitrides.

Compound	Space group	Bond	d(M-N) (Å)
ε-Ti$_2$N	P4$_2$/mnm	Ti-N	3 x 2.08
δ-Ti$_2$N	I4$_1$/amd	Ti-N	6 x 2.12
Li$_5$TiN$_3$	I$a\bar{3}$	Ti-N	4 x 2.02
Li$_2$ZrN$_2$	P$\bar{3}m$1	Zr-N	6 x 2.27
Zr$_3$AlN	Cmcm	Zr-N	1 x 1.52
			4 x 2.84
ε-Hf$_3$N$_2$	R$\bar{3}m$	Hf-N	6 x 2.26
ζ-Hf$_4$N$_2$	R$\bar{3}m$	Hf-N	6 x 2.06
			3 x 2.26
β-V$_2$N	P$\bar{3}1m$	V-N	3 x 1.98
Li$_7$VN$_4$	P$\bar{4}3n$	V-N	4 x 2.00
			4 x 2.08
β-Nb$_2$N	P$\bar{3}1m$	Nb-N	3 x 2.15
γ–Nb$_4$N$_3$	I4/mmm	Nb-N	6 x 2.19
β-Ta$_2$N	P$\bar{3}1m$	Ta-N	3 x 2.15
Ta$_3$N$_5$	Cmcm	Ta-N	6 x 2.08
			6 x 2.09
NaTaN$_2$	R$\bar{3}m$	Ta-N	6 x 2.11
CsTaN$_2$	Fd$\bar{3}m$	Ta-N	4 x 1.93
Li$_{15}$Cr$_2$N$_9$	P4/ncc	Cr-N	4 x 1.77
La$_6$Cr$_{21}$N$_{23}$	F$m\bar{3}m$	Cr-N	6 x 2.16
			6 x 2.16
			6 x 2.16

Compound	Space group	Bond	d(M-N) (Å)
Ca_3CrN_3	$Cmcm$	Cr-N	3 x 1.80
Li_6MoN_4	$P4_2/nmc$	Mo-N	4 x 1.88
WN_2	$R\bar{3}m$	W-N	8 x 3.01
Li_6WN_4	$P4_2/nmc$	W-N	4 x 1.91
Li_7MnN_4	$P\bar{4}3n$	Mn-N	4 x 1.91
			4 x 2.07
ε-Mn_4N	$Pm\bar{3}m$	Mn-N	6 x 3.34
			2 x 1.93
Mn_3N_2	$I4/mmm$	Mn-N	2 x 1.93
			5 x 2.11
ε-Fe_2N-Fe_3N	$P312$	Fe-N	2 x 1.90
Fe_4N	$Pm\bar{3}m$	Fe-N	2 x 1.90
Li_3FeN_3	$Ibam$	Fe-N	4 x 1.96
Co_3N	$P6_322$	Co-N	6 x 1.54
Co_4N	$Pm\bar{3}m$	Co-N	2 x 1.87
Ni_3N	$P6_322$	Ni-N	4 x 1.39
Ni_4N	$Pm\bar{3}m$	Ni-N	8 x 3.22
			2 x 3.22
CaNiN	$P4_2/mmc$	Ni-N	2 x 1.79
BaNiN	$Pnma$	Ni-N	4 x 2.86
$Ba_8Ni_6N_7$	$C2/c$	Ni-N	2 x1.81
			2 x 1.76
			2 x 1.80
Cu_3N	$Pm\bar{3}m$	Cu-N	2 x 1.91
LiZnN	$F\bar{4}3m$	Zn-N	4 x 2.11
Ca_3ZnN_2	$I4/mmm$	Zn-N	2 x 1.84

Table 1.3: Bond valence parameters for transition metal nitrides.
V is the valence and "4", "6", and "8" refer to the coordination
number. R_{iN} = Ionic radius of nitride ion.

Atom	V	R_{iN}	4	6	8
Sc	3	1.98	2.08	2.23	2.34
Ti	4	1.93	1.93	2.08	2.19
V	5	1.86	1.77	1.92	2.03
Cr	3	1.85	1.95	2.10	2.21
Mn	2	1.87	2.12	2.27	2.38
Fe	2	1.86	2.11	2.26	2.37
Co	2	1.84	2.09	2.24	2.35
Ni	2	1.75	2.00	2.15	2.26
Cu	1	1.61	2.12	2.27	2.38
Zn	2	1.77	2.02	2.17	2.28
Y	3	2.17	2.27	2.42	2.53
Zr	4	2.11	2.11	2.26	2.37
Nb	5	2.06	1.97	2.12	2.23
Mo	6	2.04	1.89	2.04	2.15
Cd	2	1.96	2.21	2.36	2.47
La	3	2.34	2.44	2.59	2.70
Hf	4	2.09	2.09	2.24	2.35
Ta	5	2.01	1.92	2.07	2.18
W	6	2.06	1.91	2.06	2.17

Table 1.4: Reactions commonly used in ternary nitride synthesis

(1) $MN + M'/M'_yN_z$ $\rightarrow$ M-M'-N

(2) $M + M' + N_2(NH_3)$ $\rightarrow$ M-M'-N (+ H_2)

(3) $MNH_2 + M'/M'_yN_z$ $\rightarrow$ M-M'-N (+ H_2)

(4) $MM'O_x + NH_3$ $\rightarrow$ M-M'-N + H_2O + N_2

(5) M-M'-N + M''/M''_yN_z $\rightarrow$ M-M'-M''-N
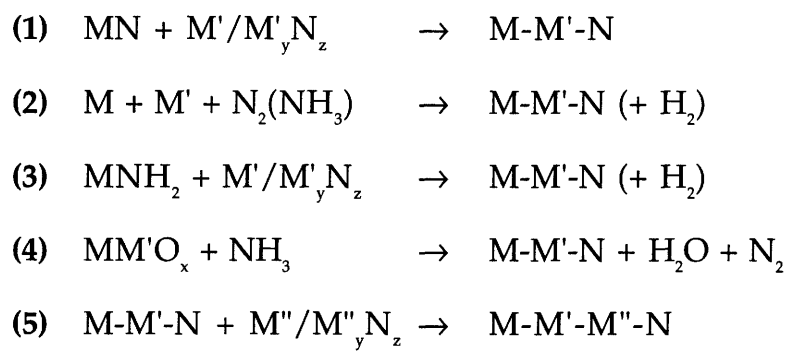
1.8 REFERENCES

(1) Terao, N. *Jap. J. Appl. Phys.* **1971**, *10*, 248-59.

(2) Goldschmidt, H. J. In *Interstitial Alloys*Plenum Press: New York, 1967; pp 214-244.

(3) Toth, L. E. *Transition Metal Carbides and Nitrides*; Academic Press: New York, 1971.

(4) Stadelmaier, H. H. In *Developments in the Structural Chemistry of Alloy Phases*; B. C. Giessen, Ed.; Plenum Press: New York, 1969; pp 141-180.

(5) Johansen, H. A. In *Survey of Progress in Chemistry*; A. F. Scott, Ed.; Academic Press, Inc.: New York, 1977; Vol. 8; pp 57-81.

(6) Hägg, G. Z. *Phys. Rev. B* **1931**, *12*, 33.

(7) Bem, D. S.; Gibson, C. P.; zur Loye, H.-C. *Chem. Mater.* **1993**, *5*, 397-399.

(8) Houmes, J.; Bem, D.; zur Loye, H. *Mat. Res. Soc. Symp. Proc. Vol. 327* **1994**, 153-64.

(9) Levy, R. B.; Boudart, M. *Science* **1973**, *181*, 547-549.

(10) Kugler, E. L.; McCandlish, L. E.; Jacobson, A. J.; Chianelli, R. R. In United States Patent, #5,138,111, 1992.

(11) Volpe, L.; Boudart, M. *J. Solid State Chem.* **1985**, *59*, 332-347.

(12) Volpe, L.; Boudart, M. *Catal. Rev.-Sci. Eng.* **1985**, *27*, 515-538.

(13) Chern, M. Y.; DiSalvo, F. J. *J. Solid State Chem.* **1990**, *88*, 459-464.

(14) Jacobs, H.; Niewa, R. *Eur. J. Solid State Inorg. Chem.* **1994**, *31*, 105-113.

(15) Brese, N. E.; O'Keefe, M. *Struct. Bonding* **1992**, *79*, 307-78.

(16) Marchand, R.; Laurent, Y.; Guyader, J.; L'Haridon, P.; Verdier, P. *J. Eur. Ceram. Soc.* **1991**, *8*, 197-213.

(17) Juza, R.; Langer, K.; Von Benda, K. *Angew. Chem.* **1968**, *80*, 373-384.

(18) Höhn, P.; Kniep, R.; Rabenau, A. *Z. Kristallogr.* **1991**, *196*, 153-158.

(19) Rauch, P. E.; DiSalvo, F. J. *J. Solid State Chem.* **1992**, *100*, 160-165.

(20) Jacobs, H.; Von Pinkowski, E. *J. Less-Common Met.* **1989**, *146*, 147-60.

(21) Schlieper, T.; Milius, W.; Schnick, W. *Z. anorg. allg. Chem.* **1995**, *621*, 1380-1384.

(22) Schlieper, T.; Schnick, W. *Z. anorg. allg. Chem.* **1995**, *621*, 1037-1041.

(23) Schlieper, T.; Schnick, W. *Z. anorg. allg. Chem.* **1995**, *621*, 1535-1538.

(24) Elder, S. H.; DiSalvo, F. J.; Doerrer, L. H. *Chem. Mater.* **1992**, *4*, 928-937.

(25) Subramanya Herle, P.; Hegde, M. S.; Vasanthacharya, N. Y.; Gopalakrishnan, J.; Subbanna, G. N. *J. Solid State Chem.* **1994**, *112*, 208-10.

(26) Banaszak, M. M.; Wolczanski, P. T.; Van Duyne, G. D. *JACS* **1990**, *112*, 7989-7994.

(27) Elder, S. H.; Disalvo, F. J.; Topor, L.; Navrotsky, A. *Chem. Mater.* **1993**, *5*, 1545-53.

(28) Bem, D. S.; Lampe-Önnerud, C. M.; H.P., O.; zur Loye, H. C. *Inorg. Chem.* **1996**, *35*, 581-585.

(29) Bem, D. S.; Olsen, H. P.; zur Loye, H. C. *Chem. Mater.* **1995**, *7*, 1824-1828.

(30) Zachwieja, U.; Jacobs, H. *Eur. J. Solid State Inorg. Chem.* **1991**, *28*, 1055-1062.

(31) Nishijima, M.; Takeda, Y.; Imanishi, N.; Yamamoto, O.; Takano, M. *J. Solid State Chem.* **1994**, *113*, 205-210.

(32) Wachsmann, C.; Jacobs, H. *J. Alloys Compd.* **1992**, *190*, 113-6.

(33) Vennos, D. A.; DiSalvo, F. J. *Acta Cryst.* **1992**, *C48*, 610-612.

(34) Gudat, A.; Kniep, R.; Rabenau, A.; Bronger, W.; Ruschewitz, U. *J. Less-Common Met.* **1990**, *161*, 31-36.

(35) Gudat, A.; Haag, S.; Kniep, R.; Rabenau, A. *Z. Naturforsch.* **1990**, *45b*, 111-120.

(36) Brokamp, T.; Jacobs, H. *J. Alloys Compd.* **1991**, *176*, 47-60.

(37) Brokamp, T.; Jacobs, H. *J. Alloys Compd* **1992**, *183*, 325-44.

(38) Gudat, A.; Kniep, R.; Rabenau, A. *Angew. Chem. Int. Ed. Engl.* **1991**, *30*, 199-200.

(39) Chen, X. Z.; Ward, D. L.; Eick, H. A. *J. Alloys Compds.* **1994**, *206*, 129-32.

(40) Somer, M.; Herterich, U.; Curda, J.; Peters, K.; von Schnering, H. G. *Z. Kristall.* **1994**, *209*, 182.

(41) Jacobs, H.; Hellmann, B. *J Alloys Compd* **1993**, *191*, 277-8.

(42) Jacobs, H.; Hellmann, B. *J. Alloys Compd.* **1993**, *191*, 51-52.

(43) Ostermann, D.; Zachwieja, U.; Jacobs, H. *J. Alloys Compd.* **1992**, *190*, 137-140.

(44) Rauch, P. E.; Disalvo, F. J.; Brese, N. E.; Partin, D. E.; O'Keefe, M. O. *J. Solid State Chem.* **1994**, *110*, 162-6.

(45) Niewa, R.; Jacobs, H. *J. Alloy Comp.* **1996**, *233*, 61-68.

(46) Chern, M. Y.; DiSalvo, F. J. *J. Solid State Chem.* **1990**, *88*, 528-533.

(47) Yamane, H.; DiSalvo, F. J. *J. Solid State Chem.* **1995**, *119*, 375-379.

(48) Vennos, D. A.; DiSalvo, F. J. *J. of Solid State Chem.* **1992**, *98*, 318-322.

(49) Vennos, D. A.; DiSalvo, F. J. *J. Solid State Chem.* **1992**, *100*, 401.

(50) Vennos, D. A.; Badding, M. E.; DiSalvo, F. J. *Inorg. Chem.* **1990**, *29*, 4059-4062.

(51) Yamamoto, T.; Kikkawa, S.; Kanamaru, F. *J. Solid State Chem.* **1995**, *119*, 161-163.

(52) Cordier, G.; Höhn, P.; Kniep, R.; Rabenau, A. *Z. anorg. allg. Chem.* **1990**, *591*, 58-66.

(53) Gregory, D. H.; Barker, M. G.; Edwards, P. P.; Siddons, D. J. *Inorg. Chem.* **1995**, *34*, 5195-5198.

(54) Tennstedt, A.; Kniep, R.; Hüber, M.; Haase, W. *Z. anorg. allg. Chem.* **1995**, *621*, 511-515.

(55) Berger, U.; Schultz-Coulon, V.; Schnick, W. *Z. Naturforsch.* **1995**, *50b*, 213-216.

(56) Gudat, A.; Höhn, P.; Kniep, R.; Rabenau, A. *Z. Naturforsch.* **1991**, *46b*, 566-572.

(57) Blase, W.; Cordier, G.; Ludwig, M.; Kniep, R. *Z. Naturforsch.* **1994**, *49b*, 501-505.

(58) Seeger, O.; Strähle, J. *Z. anorg. allg. Chem.* **1995,** *621,* 761-764.

(59) Chern, M. Y.; Vennos, D. A.; DiSalvo, F. J. *J. Solid State Chem.* **1992,** *96,* 415-425.

(60) Chern, M. Y.; DiSalvo, F. J.; Parise, J. B.; Goldstone, J. A. *J. Solid State Chem.* **1992,** *96,* 426-435.

(61) Brese, N. E.; DiSalvo, F. J. *J. Solid State Chem.* **1995,** *120,* 378-380.

(62) Broll, S.; Jeitschko, W. *Z. Naturforsch.* **1995,** *50b,* 905-912.

(63) Woike, M.; Jeitschko, W. *Inorg. Chem.* **1995,** *34,* 5105-5108.

(64) Massidda, S.; Pickett, W. E.; Posternak, M. *Phys. Rev. B* **1991,** *44,* 1258-1265.

(65) Gudat, A.; Haag, S.; Kniep, R.; Rabenau, A. *J. Less-Common Met.* **1990,** *159,* L29-L31.

(66) Singh, D. J. *Phys. Rev. B* **1992,** *46,* 9332-9335.

(67) Yamamoto, T.; Kikkawa, S.; Takahashi, M.; Miyamoto, Y.; Kanamaru, F. *Physica C* **1991,** *185-189,* 2719-2720.

(68) Yee, K. A.; Hughbanks, T. *Inorg. Chem.* **1992,** *31,* 1921-1925.

(69) Frankenburger, W.; Andrussow, L.; Dürr-Ludwigshafen, F. *Z. Electrochem.* **1928,** *34,* 632-635.

(70) Cordier, G.; Gudat, A.; Kniep, R.; Rabenau, A. *Angew. Chem.* **1989,** *101,* 1689-1690.

(71) Yamane, H.; Kikkawa, S.; Koizumi, M. *Solid State Ionics* **1985,** *15,* 51-54.

(72) Yamane, H.; Kikkawa, S.; Koizumi, M. *J. Solid State Chem.* **1987,** *71,* 1-11.

(73) Höhn, P.; Kniep, R. *Z. Naturforsch.* **1992,** *47b,* 434-436.

(74) Höhn, P.; Sabine, H.; Wolfgang, M.; Kniep, R. *Angew. Chem. Int. Ed. Engl.* **1991,** *30,* 831-832.

(75) Höhn, P.; Kniep, R.; Maier, J. *Z. Naturforsch.* **1994,** *49b,* 5-8.

(76) Gudat, A.; Kniep, R.; Rabenau, A. *Z. anorg. allg. Chem.* **1991,** *597,* 61-67.

(77) Gudat, A.; Kniep, R.; Rabenau, A. *Thermochim. Acta* **1990,** *160,* 49-56.

(78) Somer, M.; Herterich, U.; Curda, J.; Peters, K.; von Schnering, H. G. *Z. Krist.* **1995**, *210*, 529.

(79) Berger, U.; Schnick, W. *J. Alloys Comp.* **1994**, *206*, 179-184.

(80) Yamamoto, T.; Kikkawa, S.; Kanamaru, F. *Solid State Ionics* **1993**, *63-65*, 148-53.

(81) Gregory, D. H.; Barker, M. G.; Edwards, P. P.; Siddons, D. J. *Inorg. Chem.* **1995**, *34*, 3912-3916.

(82) Seeger, O.; Hofmann, M.; Strähle, J.; Laval, J. P.; Frit, B. *Z. anorg. allg. Chem.* **1994**, *620*, 2008-2013.

(83) Gudat, A.; Milius, W.; Haag, S.; Kniep, R.; Rabenau, A. *J. Less-Common Met.* **1991**, *168*, 305-312.

(84) Gudat, A.; Milius, W.; Haag, S.; Kniep, R.; Rabenau, A. *J. Less-Common Met.* **1991**, *168*, 305-312.

2. Iron Assisted Synthesis of Tantalum and Niobium Oxynitride

2.1 INTRODUCTION

The use of oxide precursors has been well documented as an experimentally simple and inexpensive method for the synthesis of a wide variety of nitride and oxynitride products. Of particular note are the recent syntheses of ternary nitrides containing two transition metals starting from the appropriate ternary oxide, demonstrating that complete conversion to a nitride product is possible.[1-6] In addition, numerous examples of ammonolysis reactions of ternary oxides, including those containing rare earth elements[7-9] vanadium[10] or alkaline earth elements[11] are known to yield distinct, stoichiometric oxynitride products.

Synthesis routes starting from precursors offer several advantages over normal solid state reaction techniques. The reactants in solid state syntheses are usually mixed together manually or mechanically. Consequently, the reaction rate is dependent on: 1) the particle size of the reactants, 2) the degree of homogenization achieved on mixing, 3) the intimacy of contact between these grains, and 4) the temperature at which the reaction is carried out.[12] On the other hand, precursors can achieve a high degree of homogenization together with intimate contact of the reactants, which result in much higher reaction rates and lower reaction temperatures. In addition, the structure of the precursor may affect product formation[13] and yield phases unattainable by other synthetic routes.

In an attempt to synthesize iron tantalum and iron niobium nitride analogues of $FeWN_2$[1] via ammonolysis of the respective ternary metal oxide precursors, we found that no iron is incorporated in the product. Instead, oxynitride products, $Ta_5N_{6-\delta}O_y$ and $Nb_5N_{6-\delta}O_y$, are formed. We have established that the presence of iron in the precursor is crucial to the formation of these oxynitride phases. In the literature, compounds of the stoichiometry Ta_5N_6 and Nb_5N_6 synthesized by a variety of techniques have been reported. However, oxygen analysis of these compounds was not

reported, and the complete absence of oxygen from the nitride product is unlikely. The most straightforward method reported for the synthesis of Ta_5N_6 is the ammonolysis of Ta_2O_5 at 975°C.[14] However, lower synthesis temperatures lead to a mixed phase product containing Ta_5N_6 and Ta_3N_5. A mixed phase product containing Ta_5N_6 and Ta_3N_5 can also be obtained by decomposing Ta_3N_5 under ammonia at 950°C[14,15] and the appearance of Ta_5N_6 as an impurity after the decomposition of Ta_3N_5 at higher temperatures has been reported[16]. Nitridation of Ta powder at 1200°C under a nitrogen pressure of 300 bar yields phase-pure Ta_5N_6,[17] while lower pressure nitridation of tantalum metal yields a mixture of phases.[18] There have also been several reports of the synthesis of Ta_5N_6 in thin film form through the nitridation of Ta films[19,20] or by using nitrogen implantation;[21] however, all lead to the formation of mixed phase products and in no case do the authors report on the oxygen content of the final products nor do they provide a structure solution or refinement.

The formation of Nb_5N_6 is much less extensively discussed in the literature. Nb_5N_6 has been reported as a minor product of both the ammonolysis of niobium thin films[22] and as a mixed-phase product in the chemical vapor deposition of films of niobium nitride from $NbCl_5$ in ammonia.[23] However, as was the case for tantalum nitride, no oxygen analyses or structure solutions for Nb_5N_6 have been reported.

In this chapter, we discuss the preparation of $Ta_5N_{6-\delta}O_y$ and $Nb_5N_{6-\delta}O_y$ by the ammonolysis reactions of iron-containing ternary oxide precursors at 900 °C and 700 °C respectively. These syntheses represent the lowest reported temperatures for the preparation of $Ta_5N_{6-\delta}O_y$ and $Nb_5N_{6-\delta}O_y$. In addition, the structures of $Ta_5N_{6-\delta}O_y$ and $Nb_5N_{6-\delta}O_y$, as determined by powder X-ray Rietveld refinement, are reported. The apparent catalytic role of iron in affecting nitride formation is also discussed.

2.2 EXPERIMENTAL

2.2.1 Synthesis:

2.2.1.1 Precursor Preparation:

The ternary transition metal oxides used as precursors in this study, $FeNbO_4$, $FeNb_2O_6$, $FeTaO_4$, and $FeTa_2O_6$, were prepared by solid state reactions of the oxides using the method of Koenitzer.[24] All starting materials were used as purchased (Fe_2O_3(Cerac, 99.99%), Fe(Aldrich, 99.9%), Ta_2O_5(Johnson-Matthey, 99.9%), Nb_2O_5(Aldrich, 99.9%)). $FeMO_4$ (M=Ta and Nb) was synthesized by heating an equimolar mixture of Fe_2O_3 and M_2O_5 at 1000 °C in air for 48 hours. FeM_2O_6 was synthesized by heating a 1:1:3 molar mixture of Fe_2O_3, Fe and M_2O_5 in an evacuated quartz tube at 900°C for 48 hours. The phase purity of all precursors was confirmed by powder X-ray diffraction.

2.2.1.2 Ammonolysis Reactions:

Ammonolysis of $FeNbO_4$, $FeNb_2O_6$, $FeTaO_4$, $FeTa_2O_6$, Nb_2O_5 and Ta_2O_5, as well as of FeTa and FeNb alloys, and intimate mixtures of Fe_2O_3/Nb_2O_5 and Fe_2O_3/Ta_2O_5 were carried out in alumina boats which were placed in a quartz flow-through reactor located in a hinged tube furnace (Figure 2.2.1). Each sample was heated in flowing ammonia (Airco, Anhydrous 99.99%, 160 cm³/min. used without further purification) at 5 °C/minute to 700 °C for the niobium-containing precursors and to 900 °C for the tantalum-containing precursors. The samples were held at their respective temperatures for ~3.5 days and then rapidly cooled to room temperature by turning off and opening the furnace. Residual iron from the precursor was removed by washing the samples with 5 ml concentrated HCl followed by 5 ml water. Attempts to dissolve the oxynitride products in acids or bases (HCl, HNO_3, aqua regia, H_2SO_4, HF, NaOH) as well as in organic solvents (methanol, ethanol and acetone) were unsuccessful.
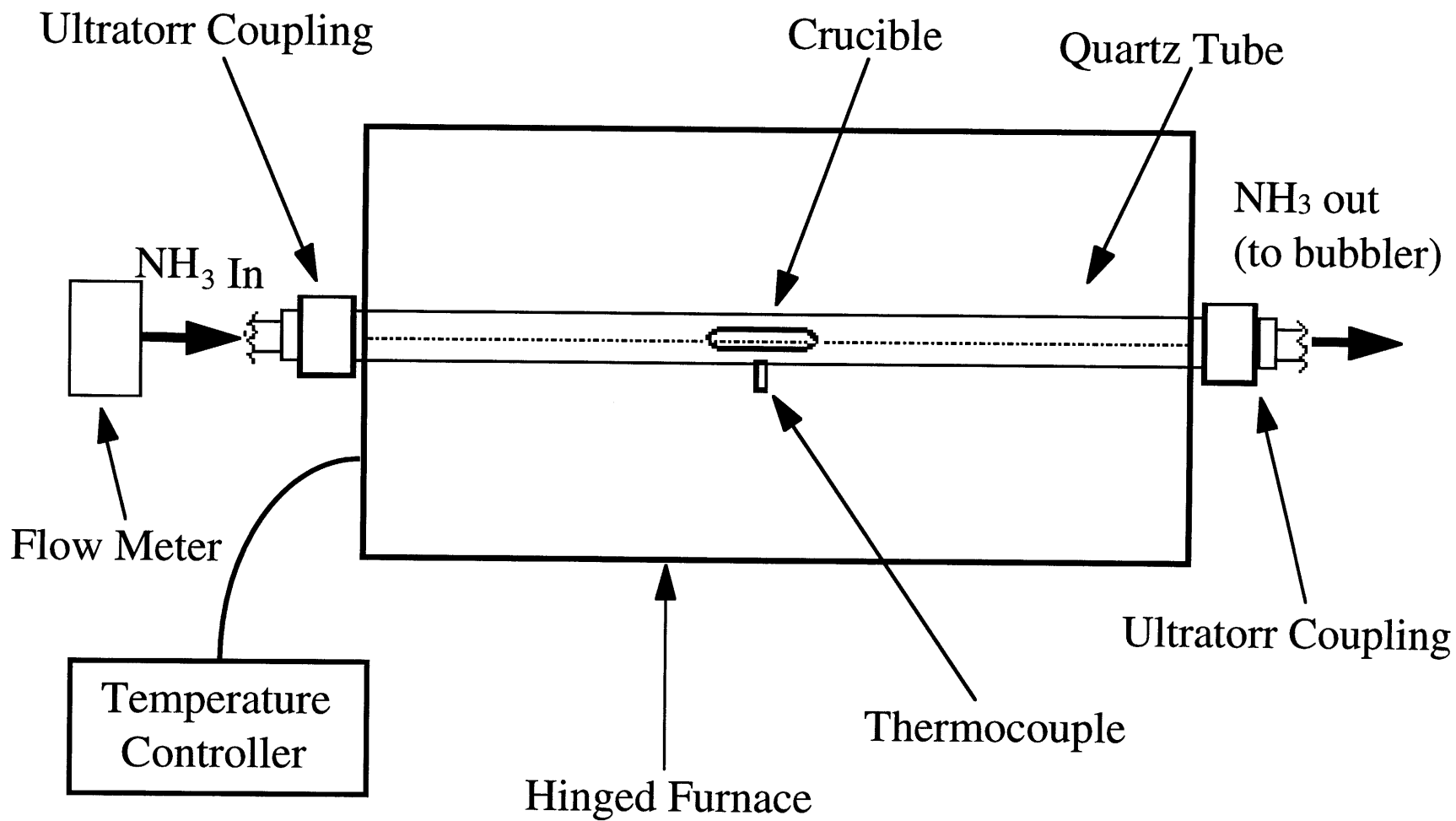
Figure 2.2.1: Schematic diagram of ammonia flow-through furnace.

Table 2.1: Reactions to investigate the affect of iron on product formation

Reactants	Ammonolysis Conditions		Products
$FeTaO_4$	900°C	4500min.	$Ta_5N_{5.99}O_{0.01}$ + Fe_2N + FeO
$FeTa_2O_6$	900°C	4500min.	$Ta_5N_{5.99}O_{0.01}$ + Fe_2N + FeO
$FeTaO_4$	900°C	2186min.	$Ta_5N_{5.99}O_{0.01}$ + TaON + Fe_2N + FeO
$FeTaO_4$	900°C	900min.	$Ta_5N_{5.99}O_{0.01}$ + TaON + Fe_2N + FeO
$FeTaO_4$	900°C	5 min.	$FeTa_2O_6$ + Fe_2N
Fe_2O_3 + Ta_2O_5	900°C	4500min.	$Ta_5N_{5.99}O_{0.01}$ + Fe_2N + FeO
FeTa	900°C	4500min.	$Ta_5N_{5.99}O_{0.01}$ + Fe_2N + FeO
Ta_2O_5	900°C	4500min.	Ta_3N_5
Ta_2O_5	900°C	1000min.	Ta_3N_5
Ta_2O_5	900°C	5min.	Ta_2O_5 + TaON + Ta_3N_5
$FeNbO_4$	700°C	4500min.	$Nb_5N_{5.31}O_{0.50}$ + Fe_2N + FeO
$FeNbO_4$	700°C	800min.	$Nb_5N_{5.31}O_{0.50}$ + $NbN_{0.6}O_{0.3}$ + Fe_2N + FeO
$FeNbO_4$	700°C	5 min.	$FeNb_2O_6$ + $FeNb_{11}O_{29}$ + Fe_2N
$FeNb_2O_6$	700°C	4500min.	$Nb_5N_{5.31}O_{0.50}$ + Fe_2N + FeO
Fe_2O_3 + Nb_2O_5	700°C	4500min.	$Nb_5N_{5.31}O_{0.50}$ + Fe_2N + FeO
Nb_2O_5	700°C	4500min.	$NbN_{0.6}O_{0.2}$ + Nb_4N_3
Nb_2O_5	700°C	1000min.	$NbN_{0.6}O_{0.3}$
Nb_2O_5	700°C	5min.	Nb_2O_5 + $NbN_{0.6}O_{0.3}$

2.2.2 Characterization:

2.2.2.1 Elemental Analysis:

The nitrogen content of $Ta_5N_{6-8}O_y$ and $Nb_5N_{6-8}O_y$ was established by C,H,N combustion analysis (Oneida Research Services, Inc.). Metal compositions were determined by Energy Dispersive Spectroscopy (EDS) on a Jeol JSM 6400 scanning electron microscope collected by a Noran Z-max windowless detector with quantification performed using virtual standards on the associated Voyager software. Oxygen content determinations were made by combustion oxygen analysis (Massachusetts Materials Research and Teledyne).

2.2.2.2 Structural Analysis:

The polycrystalline samples were structurally characterized using either a Siemens D5000 or a Rigaku RU300 powder X-ray diffractometer operated with Cu $K\alpha$ radiation. Because of the slight air and water sensitivity of $Ta_5N_{6-8}O_y$ still containing residual iron, the powdered samples were pressed into the sample holder in an argon-filled glove box and covered with Kaptan film (Du Pont) to limit exposure to air. A powder X-ray diffraction step scan of the iron-containing (unwashed) sample was collected from $14°-118°$ 2θ $(0.04° \ 2\theta$ steps) using the Siemens diffractometer. Due to the poor crystallinity of the unwashed $Nb_5N_{6-8}O_y$, the powder sample diffracted only marginally better than the Kaptan film used to limit exposure to air. As a result, the background could not be adequately fit using GSAS[25] and further refinement proved futile. Diffraction data for acid-washed samples were collected from $16-118°$ 2θ $(0.04 \ °2\theta$ steps) for $Ta_5N_{6-8}O_y$ and $5-140°$ 2θ $(0.04 \ °2\theta$ steps) for $Nb_5N_{6-8}O_y$ using the Rigaku RU300 and Siemens D5000 instruments, respectively. Rietveld refinements of the powder X-ray diffraction data were performed using the General Structure Analysis System (GSAS) refinement

package.[25] The suggested crystal structure information from the literature was used as a starting model.[15]

2.3 RESULTS:

$Ta_5N_{6-\delta}O_y$ and $Nb_5N_{6-\delta}O_y$ are dark-gray polycrystalline materials. As synthesized from the iron-containing oxide precursors, both samples contained Fe_2N and FeO impurities, which can be removed by washing with concentrated HCl. $Ta_5N_{6-\delta}O_y$ and $Nb_5N_{6-\delta}O_y$ are insoluble in water, polar organic solvents (i.e. methanol, ethanol and acetone), strong acids and 6N NaOH. However, exposure to strong acid does result in the incorporation of additional oxygen into the final product. Whether this incorporation takes the form of bulk or of surface oxidation is unclear.

2.3.1 Precursor Experiments

The ammonolysis reactions of the iron-containing ternary oxide precursors lead to the formation of the oxynitrides $Ta_5N_{6-\delta}O_y$ and $Nb_5N_{6-\delta}O_y$ plus the impurities Fe_2N and FeO. None of the iron in the precursor is incorporated into the product, as shown by EDS, which indicates less than 1 atomic percent iron in the acid-washed samples. Interestingly, the presence of iron in the reaction mixture is essential for the formation of these oxynitride phases. While the iron does not have to be part of the precursor structure, it must be present in the reaction mixture if formation of $Ta_5N_{6-\delta}O_y$ and $Nb_5N_{6-\delta}O_y$ is to be achieved at these temperatures. For example, iron may be added to the reaction mixture by grinding together M_2O_5 (M=Ta or Nb) and Fe_2O_3. In the absence of iron, the formation of other binary nitrides, Ta_3N_5 and Nb_4N_3, is favored.

To test the dependence of the ammonolysis reaction on the starting materials, several different precursor compositions were prepared and reacted under identical conditions (Table 2.1). In addition to $FeMO_4$ (M = Ta, Nb), FeM_2O_6 was prepared, as were mixtures of $M_2O_5/FeMO_4$ and 1:1 and 1:2 molar

mixtures of Fe_2O_3/M_2O_5. In every case, the ammonolysis products were Fe_2N and $M_5N_{6-8}O_y$. The ammonolysis of pure Ta_2O_5 or Nb_2O_5, under reaction conditions identical to those used for the iron metallates, yields only Ta_3N_5 and $Nb_4N_3/NbN_{0.6}O_{0.2}$ respectively, as determined by powder X-ray diffraction and visual inspection (Ta_3N_5 is brick red). If Fe_2O_3 is present in the reaction chamber but is separated from M_2O_5 by a small distance, the only observed products are again Ta_3N_5 or $Nb_4N_3/NbN_{0.6}O_{0.2}$, which are the expected products for the ammonolysis of Ta_2O_5 and Nb_2O_5 at these temperatures.[22,26] Since several precursors having varying metal ratios and structures were tried, these factors can be eliminated as causes of the unusual formation of $M_5N_{6-8}O_y$ under our reported reaction conditions. One common factor between all the successful reactions was the presence of iron in the reaction mixture.

In order to elucidate the role of iron in influencing the reaction pathway, a series of quenching experiments were carried out (Table 2.1). From these experiments it is found that the formation of Ta_3N_5 during the ammonolysis of Ta_2O_5 is quite rapid, with detectable product formation after only 5 min. at 900 °C and going to completion in approximately 12 hours (Table 2.1). When the ammonolysis reaction was stopped early, TaON was found to be an intermediate on the reaction pathway, However, it is completely converted to Ta_3N_5 in under 12 hours. Early stoppage of the reaction by quenching of the ammonolysis reaction of $FeTaO_4$, on the other hand, results in the formation of $FeTa_2O_6$ and Fe_2N after 5 min. at 900°C. After slightly longer reaction times (900 min.) TaON, Fe_2N and $Ta_5N_{6-8}O_y$ are formed. Likewise, early stoppage of the ammonolysis reaction of $FeNbO_4$ results in the formation of $FeNb_2O_6$, $FeNb_{11}O_{29}$ and Fe_2N (Table 2.1) after 5 min. at 700°C. After slightly longer reaction times (800 min.) $NbN_{0.6}O_{0.3}$, Fe_2N and $Nb_5N_{6-8}O_y$ are formed. NbON was not detected in quenching experiments of $FeNbO_4$. However, since TaON demonstrates greater thermal stability and robustness than NbON, the absence of NbON in the quenching is perhaps not

surprising. Instead, $NbN_{0.6}O_{0.3}$ is found to be the intermediate. Similarly, when the ammonolysis reaction of Nb_2O_5 is quenched early, the oxynitride $NbN_{0.6}O_{0.3}$ is observed. As the reaction is allowed to proceed further, the oxynitrides are gradually replaced by $M_5N_{6-\delta}O_y$, which suggests that the formation of the binary $M_5N_{6-\delta}O_y$ oxynitrides proceeds via these lower oxynitride intermediates. Since Fe_2N, which is present in the product mixture, decomposes above 300 °C and iron oxide reduces to the metal at about 450°C in an ammonia atmosphere, it is reasonable to assume that metallic iron is present under the reaction conditions. Only when the sample is cooled to below 300°C, can Fe_2N begin to form. From these experiments, we hypothesize that the presence of metallic iron in the reaction mixture helps to promote the formation of the $M_5N_{6-\delta}O_y$ phases.

2.3.2 Elemental Analysis of $Ta_5N_{6-\delta}O_y$ and $Nb_5N_{6-\delta}O_y$

2.3.2.1 $Ta_5N_{6-\delta}O_y$:

After washing the nitride product in concentrated HCl, no iron is detected in the product by EDS. Nitrogen analysis of the unwashed product mixture yields N_{Ta}=8.86 wt. %, which compares reasonably well with the calculated nitrogen content for Ta_5N_6 (8.5 wt. %). The nitrogen content of the acid-washed product drops significantly (N_{Ta}=8.21 wt. %), presumably due to surface oxidation of the particles or incorporation of oxygen into the oxynitride structure or both. In addition, the removal of iron nitride from the product mixture further lower the total nitrogen content. Combustion oxygen analysis of the unwashed product mixture indicates total oxygen impurities as 0.795 wt. %, whereas the single-phase acid-washed tantalum oxynitride phase, as expected, contains a larger amount of oxygen ($O_{Ta-washed}$ = 2.9 wt. %). The quantity of FeO and Fe_2N present in the unwashed product mixture was extracted as a weight percent from a three-phase Rietveld refinement of the powder X-ray diffraction data. Once these values are

known, a modified theoretical nitrogen content may be calculated taking into account the amount of nitrogen and oxygen present in Fe_2N and FeO respectively. The modified nitrogen content (8.86 wt. %) compares very well with the nitrogen content measured by elemental analysis (8.86 wt. %). Given the uncertainty of the phase fraction analysis results using Rietveld refinement, the agreement of the nitrogen analysis with the calculated results is probably not as clear cut as the numbers indicate. However, the exact $Ta_5N_{6-\delta}O_y$ stoichiometry is undoubtedly close to ideal Ta_5N_6 in the unwashed tantalum nitride. With the oxygen and nitrogen present as FeO and Fe_2N subtracted, these results yield an overall composition for the unwashed tantalum oxynitride of $Ta_5N_{5.99}O_{0.01}$ (very nearly the idealized composition of Ta_5N_6). After the sample is washed with strong acid, the overall composition becomes $Ta_5N_{4.79}O_{1.81}$.

2.3.2.2 $Nb_5N_{6-\delta}O_y$:

After washing the nitride product in concentrated HCl, no iron is detected in the product by EDS. Nitrogen analysis of the unwashed product mixture (N_{Nb}=12.09 wt. %) is somewhat lower than the calculated values of N_{Nb}= 13.34 wt. % for Nb_5N_6. The nitrogen content of the single-phase acid-washed niobium oxynitride drops significantly (N_{Nb}=6.4 wt. %), presumably due to surface oxidation of the particles or incorporation of oxygen into the oxynitride structure or both. Combustion oxygen analysis of the unwashed product mixture indicates a small oxygen impurity (O_{Nb} 2.85 wt. %), while the single-phase acid-washed niobium oxynitride, as expected, contain a larger amount of oxygen (O_{Nb} 6.7 wt. %). Since a Rietveld refinement of the powder X-ray diffraction data was not possible due to sample decomposition, the quantity of FeO and Fe_2N present in the unwashed products was assumed to be identical to that found for $Ta_5N_{6-\delta}O_y$. With the oxygen and nitrogen present as FeO and Fe_2N subtracted, these results yield an estimated overall composition for unwashed niobium

oxynitride of $Nb_5N_{5.3}O_{0.5}$. When the samples is washed with strong acid, the overall composition becomes $Nb_5N_{2.45}O_{2.25}$.

2.3.3 Structure Refinements

The powder X-ray diffraction patterns of both $Ta_5N_{6-\delta}O_y$ and $Nb_5N_{6-\delta}O_y$ were indexed to a hexagonal cell. The structure of $Ta_5N_{6-\delta}O_y$ has been suggested to be in the space group $P6_3/mcm$ and to consist of alternating layers of trigonal prismatically and octahedrally-coordinated tantalum atoms with 1/3 of the octahedral sites vacant.[14] More recently, Brokamp and Jacobs[27] have reported a new nitride, $MgTa_2N_3$, which appears to be structurally similar to $Ta_5N_{6-\delta}O_y$ and which is in the space group $P6_3/mcm$ with $a=5.205$Å and $c = 10.425$Å. The reported lattice parameters of $MgTa_2N_3$ and the isostructural $FeTa_2N_3$,[28] and the general shape of the diffraction pattern, compare well with those observed for both $Ta_5N_{6-\delta}O_y$ (a=5.1817(2)Å and c=10.3610(3)Å) and $Nb_5N_{6-\delta}O_y$ (a=5.2026(2)Å and c=10.3667(4)). This model was therefore used as a starting point for structural refinements.

2.3.3.1 Unwashed $Ta_5N_{6-\delta}O_y$.

The powder X-ray diffraction data of $Ta_5N_{6-\delta}O_y$ can be indexed with an hexagonal cell (a = 5.1817(2)Å, c = 10.3610(3)Å). On the basis of systematic absences and the similarity of the data to that exhibited by the compounds listed above, space group $P6_3/mcm$ (No. 193) was chosen. Powder X-ray diffraction patterns calculated for $Ta_5N_{6-\delta}O_y$ in space group $P6_3/mcm$ (using the program DISPOW, part of the NRCVAX crystal structure system[29]) agree well with the observed patterns. The data was refined using the computer program GSAS.[25] Structural models for the iron impurity phases (FeO[30] and Fe_2N[31]) were obtained from Structure Reports. The unusual background, due to the presence of the Kaptan film, was described by refining 15 coefficients of a power series. Two parameters were used to refine the unit cell of $Ta_5N_{6-\delta}O_y$ as well as two for Fe_2N and one for FeO. One parameter was included to

refine the zero point in 2θ. Three terms were used to refine the phase fractions. A pseudo-voigt function[32] was used to describe the peak shapes with the following parameters: one Gaussian half-width (W), a Lorentzian half-width and a Lorentzian strain broadening. The structure refinement of $Ta_5N_{6-\delta}O_y$ included two positional coordinates for the nitrogen atoms as well as one for one of the tantalum atoms, and isotropic thermal displacement factors for each atom. The fractional coordinates and the isotropic thermal parameters for the iron phases were not refined. The refinement converged with Rwp = 6.45%, Rp = 4.92%, and χ^2 = 2.889. Figure 2.3.1 shows the observed and calculated powder X-ray diffraction patterns along with the residuals for unwashed $Ta_5N_{6-\delta}O_y$ in space group $P6_3/mcm$. The refined lattice parameters and residual values are shown in Table 2.2; atomic positions and thermal parameters are listed in Table 2.3a.

2.3.3.2 Acid-washed $Ta_5N_{6-\delta}O_y$

The powder X-ray diffraction data of acid-washed $Ta_5N_{6-\delta}O_y$ can be indexed with an hexagonal cell (a = 5.1817(2)Å, c = 10.3610(3)Å). On the basis of systematic absences and the similarity of the data to that exhibited by the compounds listed above, space group $P6_3/mcm$ (No. 193) was chosen. Powder X-ray diffraction patterns calculated for $Ta_5N_{6-\delta}O_y$ in space group $P6_3/mcm$ (using the program DISPOW, part of the NRCVAX crystal structure system[29]) agree well with the observed patterns. The data was refined using the computer program GSAS.[25] The background was described by refining 6 coefficients of a power series. Two parameters were used to refine the unit cell. One parameter was included to refine the zero point in 2θ. A pseudo-voigt function[32] was used to describe the peak shapes with the following parameters: a Lorentzian half-width and strain broadening. The structure refinement of $Ta_5N_{6-\delta}O_y$ included two positional coordinates for the nitrogen atoms as well as one for one of the tantalum atoms, and isotropic thermal displacement factors for each atom. The refinement converged with Rwp =

6.56%, Rp = 5.03%, and χ^2 = 2.91. Figure 2.3.2 shows the observed and calculated patterns as well as the residuals for acid-washed $Ta_5N_{6-\delta}O_y$ in space group $P6_3/mcm$. Table 2.3b lists the atomic positions and thermal parameters for $Ta_5N_{6-\delta}O_y$. Little difference is found in the atomic positions between the acid washed and unwashed $Ta_5N_{6-\delta}O_y$.

2.3.3.3 Acid-washed $Nb_5N_{6-\delta}O_y$.

The powder X-ray diffraction data of $Nb_5N_{6-\delta}O_y$ can be indexed with an hexagonal cell (a = 5.2026(2)Å, c = 10.3667(4)Å). On the basis of systematic absences and the similarity of the data to that exhibited by the compounds listed above, space group $P6_3/mcm$ (No. 193) was chosen. Powder X-ray diffraction patterns calculated for $Nb_5N_{6-\delta}O_y$ in space group $P6_3/mcm$ (using the program DISPOW, part of the NRCVAX crystal structure system[29]) agree well with the observed patterns. The data was refined using the computer program GSAS.[25] The background was described by refining 6 coefficients of a power series. Two parameters were used to refine the unit cell. One parameter was included to refine the zero point in 2θ. A pseudo-voigt function[32] was used to describe the peak shapes with the following parameters: a Lorentzian half-width and an asymmetric broadening. The structure refinement of $Nb_5N_{6-\delta}O_y$ included two positional coordinates for the nitrogen atoms as well as one for one of the niobium atoms, and isotropic thermal displacement factors for each atom. The refinement converged with Rwp = 10.84%, Rp = 8.47, and χ^2 = 7.006. It should be noted that several impurity phases are present in the powder X-ray diffraction pattern of $Nb_5N_{6-\delta}O_y$. The small peak at 42° arises from the presence of $NbN_{0.6}O_{0.3}$, apparently an intermediate on the reaction pathway. This phase can be eliminated through longer reaction times. However, longer reaction times lead to the formation of hexagonal δ-NbN and ε-NbN, which result from a collapse of the $Nb_5N_{6-\delta}O_y$ structure and occupancy of all the metal sites. All of these impurity phases have diffraction peaks which overlap with those from

$Nb_5N_{6-\delta}O_y$. Because of the structural similarity to the product and the very small amount of the impurities, multiple phase refinements to include the presence of the impurity phases failed. The presence of the impurity phases in the Rietveld refinement presented undoubtedly lead to inflated values of R_{wp}, R_p and χ^2. Figure 2.3.3 shows the observed and calculated diffraction patterns along with the residuals for acid-washed $Nb_5N_{6-\delta}O_y$ in space group $P6_3/mcm$. Table 2.3c lists the atomic positions and thermal parameters for $Nb_5N_{6-\delta}O_y$.
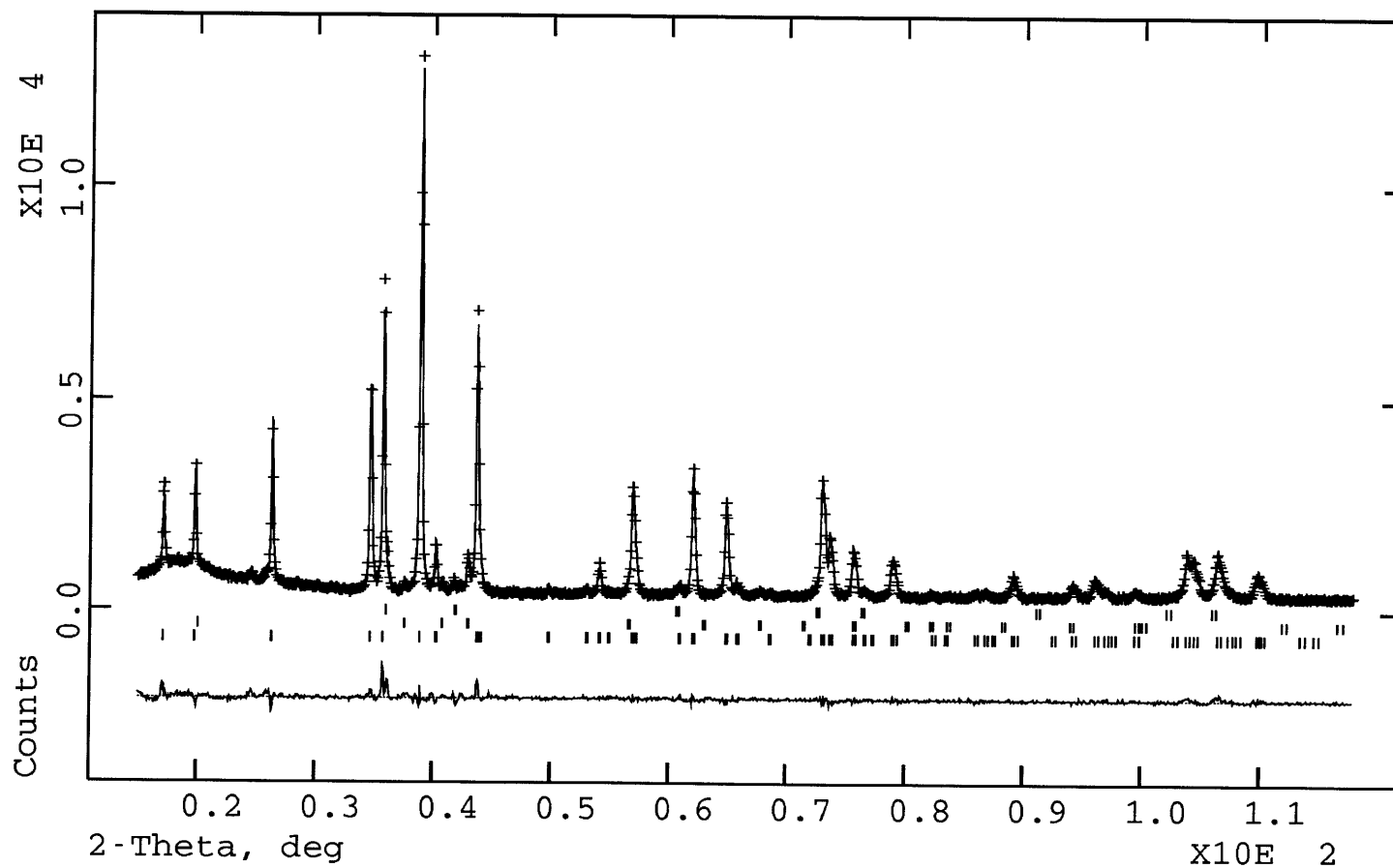
Figure 2.3.1: Observed (dotted) and calculated (solid line) X-ray profile for $Ta_5N_{6-\delta}O_y$.
Tic-marks below the diffractogram represent allowed Bragg reflections. The difference line, observed minus calculated, is located at the bottom of the figure.
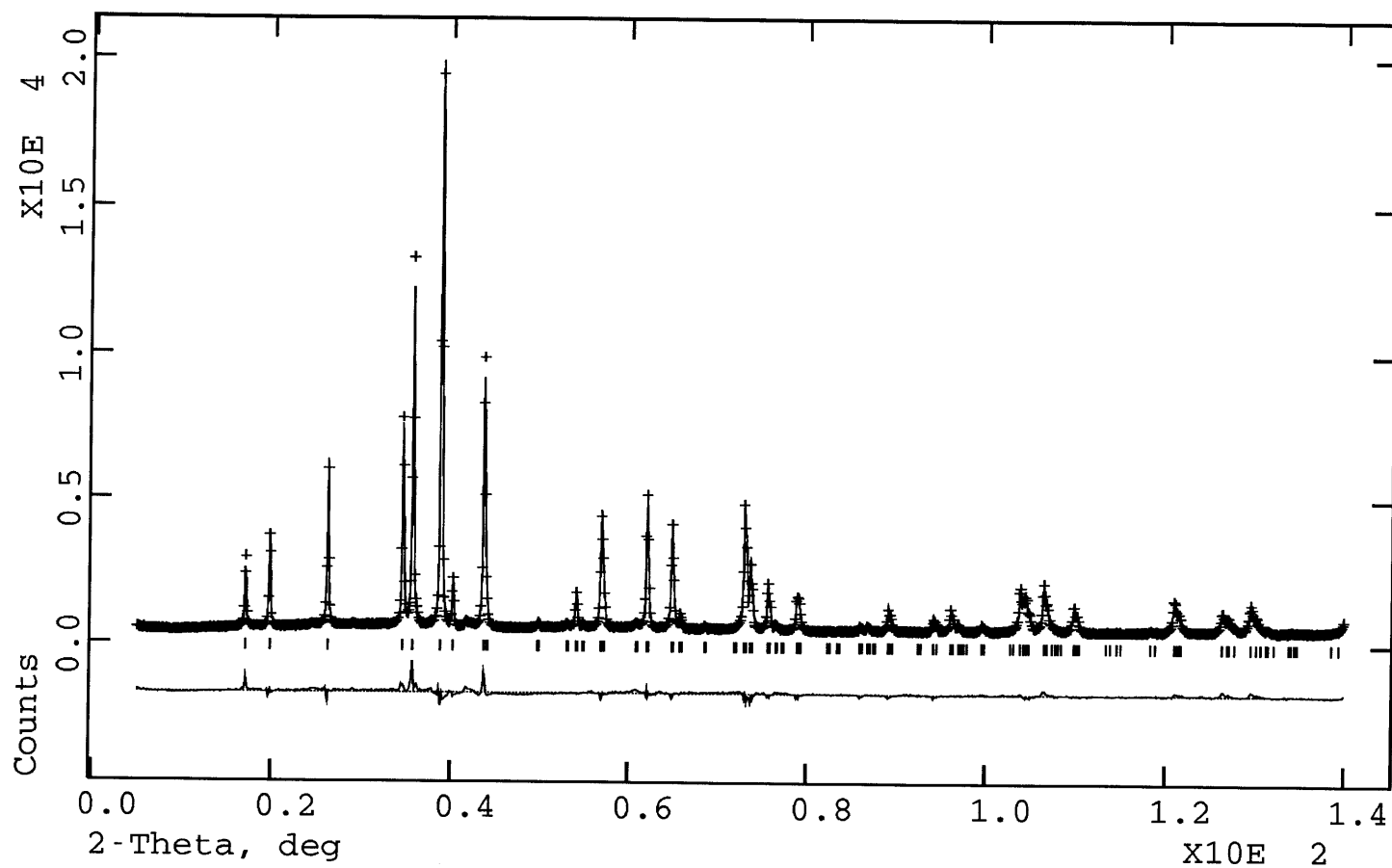
Figure 2.3.2: Observed (dotted) and calculated (solid line) X-ray profile for acid washed Ta$_5$N$_{6-\delta}$O$_y$.
Tic-marks below the diffractogram represent allowed Bragg reflections. The difference line, observed minus calculated, is located at the bottom of the figure.
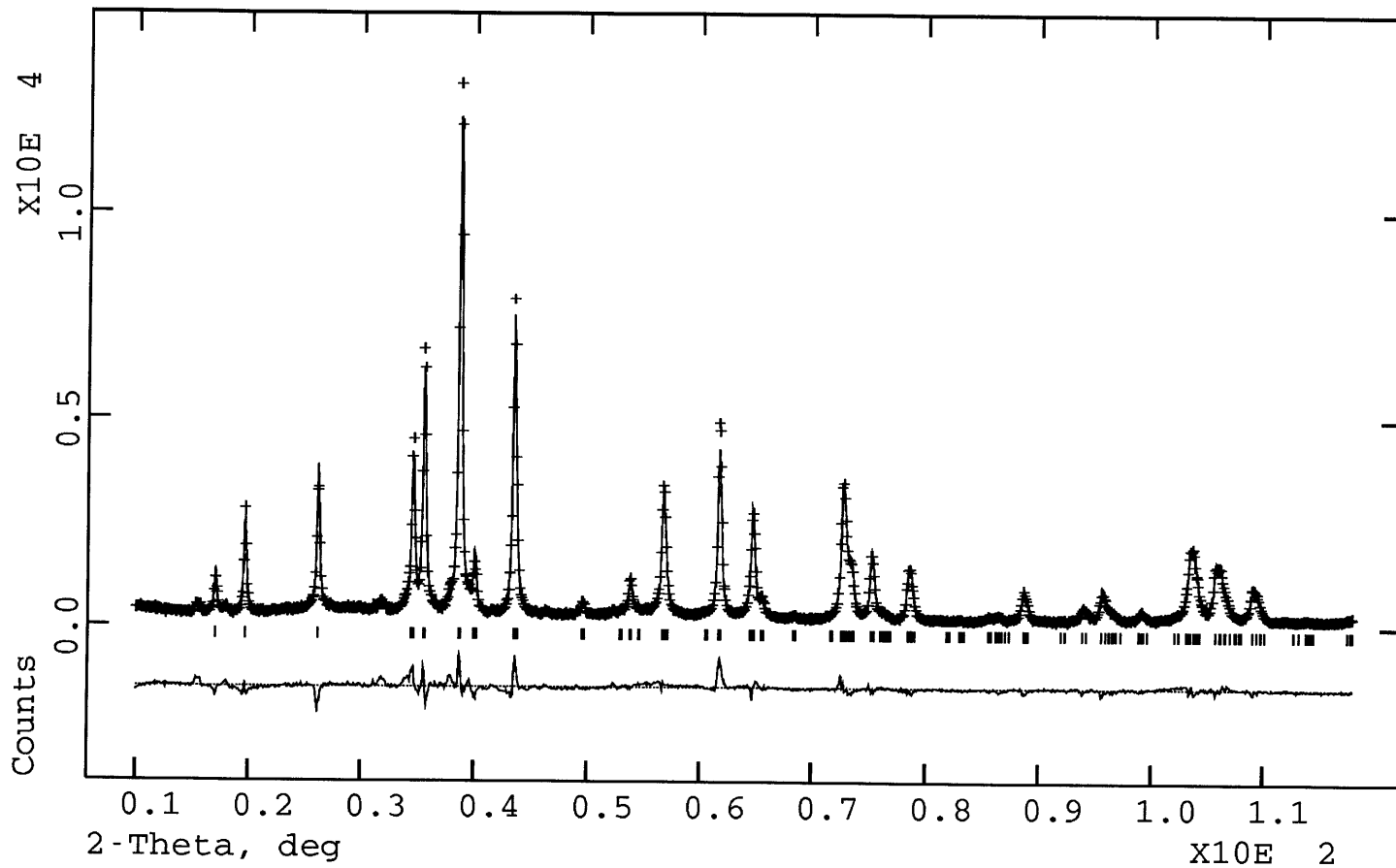
Figure 2.3.3: Observed (dotted) and calculated (solid line) X-ray profile for acid washed $Nb_5N_{6-\delta}O_y$.
Tic-marks below the diffractogram represent allowed Bragg reflections. The difference line, observed minus calculated, is located at the bottom of the figure.

Table 2.2: Rietveld refinement data

	Washed $Ta_5N_{6-\delta}O_y$	Unwashed $Ta_5N_{6-\delta}O_y$	Washed $Nb_5N_{6-\delta}O_y$
Powder color	Dark Gray	Dark Gray	Dark Gray
Formula	$Ta_5N_{4.79}O_{1.81}$	$Ta_5N_{5.99}O_{0.01}$	$Nb_5N_{2.45}O_{2.25}$
Formula weight	1000.796	988.805	534.847
Space group	$P6_3/mcm$	$P6_3/mcm$	$P6_3/mcm$
a, Å	5.1803(1)	5.1818(1)	5.2038(3)
c, Å	10.3603(2)	10.3611(3)	10.3714(7)
V, Å	241.077(7)	240.93(1)	243.23(4)
Z	2	2	2
D_{calc}, g/cm^3	13.785	13.629	7.490
2Θ scan range (°)	5-140	15-118	3-118
R_{wp}	6.56%	6.20%	10.84%
R_p	5.03%	4.75%	8.47%
R_{exp}	3.55%	3.82%	4.11%
χ^2	2.910	2.676	7.006

Refinement Rietveld using GSAS with pseudo-Voigt peak shape function.

Table 2.3: Atomic positions of oxynitride materials

a) Unwashed $Ta_5N_{6-\delta}O_y$

Metal	Wyckoff	x	y	z	100*Uiso
Ta(1)	4(d)	1/3	2/3	0	2.36(6)
Ta(2)	6(f)	0.3255(4)	0	1/4	0.67(4)
N	12(k)	0.667(3)	0.667(3)	0.6214(10)	0.7(3)

a) Acid washed $Ta_5N_{6-\delta}O_y$

Metal	Wyckoff	x	y	z	100*Uiso
Ta(1)	4(d)	1/3	2/3	0	2.33(4)
Ta(2)	6(f)	0.3236(2)	0	1/4	0.53(2)
N	12(k)	0.667(2)	0.667(2)	0.6230(5)	1.3(2)

c) $Nb_5N_{6-\delta}O_y$

Metal	Wyckoff	x	y	z	100*Uiso
Nb(1)	4(d)	1/3	2/3	0	0.48(6)
Nb(2)	6(f)	0.3254(4)	0	1/4	0.11(4)
N	12(k)	0.676(2)	0.676(2)	0.6189(7)	1.3(3)

2.4 DISCUSSION:

2.4.1 Structure of $M_5N_{6-\delta}O_y$ (M=Ta and Nb)

The structure of $M_5N_{6-\delta}O_y$ (M=Ta and Nb) is quite similar to structures exhibited by many ternary molybdenum and tungsten nitride materials[1-6] as well as by some intercalated dichalcogenide materials[33-35] and the recently reported carbide, $ScCrC_2$.[36] It consists of close-packed nitrogen/oxygen layers with the metal in alternating layers of octahedral and trigonal prismatic coordination as shown in Figure 2.4.1. Tantalum occupies all of the trigonal prismatic sites and 2/3 of the octahedral sites, with the remaining octahedral sites vacant. The atom stacking can be denoted **AbAcBaBcA** (capital letters denote anion stacking, lower case letters denote metal stacking). Inter-atomic distances are reported in Table 2.4. The metal-nitrogen distances found in both $Ta_5N_{6-\delta}O_y$ and $Nb_5N_{6-\delta}O_y$ (unwashed Ta-N: 2.162(8), 2.140(8), 2.224(12)Å; Nb-N: 2.170(6), 2.276(9), 2.148(6)Å) are comparable to the metal-nitrogen distance found in binary nitrides and in other oxynitrides of tantalum and niobium (e.g., β-Ta_2N, 2.08Å;[37] Ta_3N_5, 2.09Å;[37] TaON, 2.09Å;[37] β-Nb_2N, 2.15Å;[37] γ-Nb_4N_3, 2.19Å;[37] NbON, 2.09Å[37]). The M-N distance comparisons are more reliable in the case of $Ta_5N_{6-\delta}O_y$ because the Nb-N (and Ta-N distances for the acid washed $Ta_5N_{6-\delta}O_y$) are presumably affected by oxygen introduced in the acid-washing step.

It is particularly interesting to note the structural relationships between these oxynitrides and several ternary nitrides which have recently been synthesized, $FeWN_2$, α,β-$MnWN_2$, $(Fe_{0.8}Mo_{0.2})MoN_2$ and $LiMoN_2$. The similarity between the ternary transition metal nitride and the oxynitride compounds can be emphasized by utilizing the notation $(M_{0.67}\square_{0.33})MN_{2-\delta}O_y$ (M = Ta or Nb; $\square$ = vacancy), a similarity which is particularly striking for the unwashed tantalum oxynitride, which, if the small degree (<0.01 equivalents)

of oxygen "contamination" is ignored, may be written as $(Ta_{0.67}\square_{0.33})TaN_{2-\delta}$. The presence of this vacancy in the octahedral layer can be understood by examining some ternary transition metal nitrides which have similar structures. Mössbauer spectroscopy measurements performed on $FeWN_2$ indicate that the iron in the octahedral site has a valence of +2.[38] Thus, formally, $FeWN_2$ has WN_2^{-2} trigonal prismatic layers which are isoelectronic with the WS_2 layers present in tungsten disulfide. If similar TaN_2^{-2} layers in $(Ta_{0.67}\square_{0.33})TaN_{2-\delta}$ are assumed to be isoelectronic with TaS_2, one +2 cation must be incorporated for every trigonal prismatic tantalum to maintain charge balance. In $(Ta_{0.67}\square_{0.33})TaN_{2-\delta}$, the unit cell has three octahedral sites and 3 trigonal prismatic tantalum sites per layer. Given the preference for Ta(III) over Ta(II), one third of the octahedral sites in this structure must remain vacant in order to maintain charge balance with Ta(III).

Nitrogen analysis, oxygen analysis and Rietveld refinement indicated that a phase of nearly Ta_5N_6 composition is present before the tantalum oxide ammonolysis product is washed with HCl. However, the analogous Nb_5N_6 apparently does not form. Instead, a structurally similar oxynitride forms, presumably due to the lower reaction temperature used in the ammonolysis of the niobium precursor. Attempts to run the ammonolysis of the niobium precursors at temperatures above 700°C result in the formation of lower binary nitrides (NbN and Nb_4N_3).

Electrical conductivity measurements performed on $Nb_5N_{6-\delta}O_y$ (Figure 2.4.2)and $Ta_5N_{6-\delta}O_y$ (Figure 2.4.3) demonstrate semiconducting behavior for both materials, with very little temperature dependence. While these conductivities are not exceptionally high when compared with those found in the structurally related transition metal nitrides, the measurements were performed on pressed pellets and, therefore, represent only a lower limit to the conductivity. Also, both conductivity measurements were performed on acid-washed samples of the oxynitrides as the presence of the iron nitride impurity would interfere with the conductivity measurement. The

incorporation of oxygen into the product undoubtedly affects the total conductivity measurement.

Both oxynitride materials exhibit paramagnetic susceptibility (Figure 2.4.4 and Figure 2.4.5). However, once again, these measurements were carried out on the acid-washed products because the presence of the ferromagnetic iron nitride impurity would obscure the magnetic behavior of the oxynitride material. Despite the presence of oxygen in the sample, some conclusions can be drawn about the electronic structure of the materials. Both materials demonstrate approximately 1.2 unpaired electrons, a high total magnetization and only a slight temperature dependence. Such behavior is also seen in the transition metal ternary nitrides as well as both $LiWN_2$ and $LiMoN_2$. In these materials, the presence of this unusual magnetization is ascribed to a Pauli-paramagnetic contribution, which is also the most likely explanation for the magnetism in the oxynitride materials.
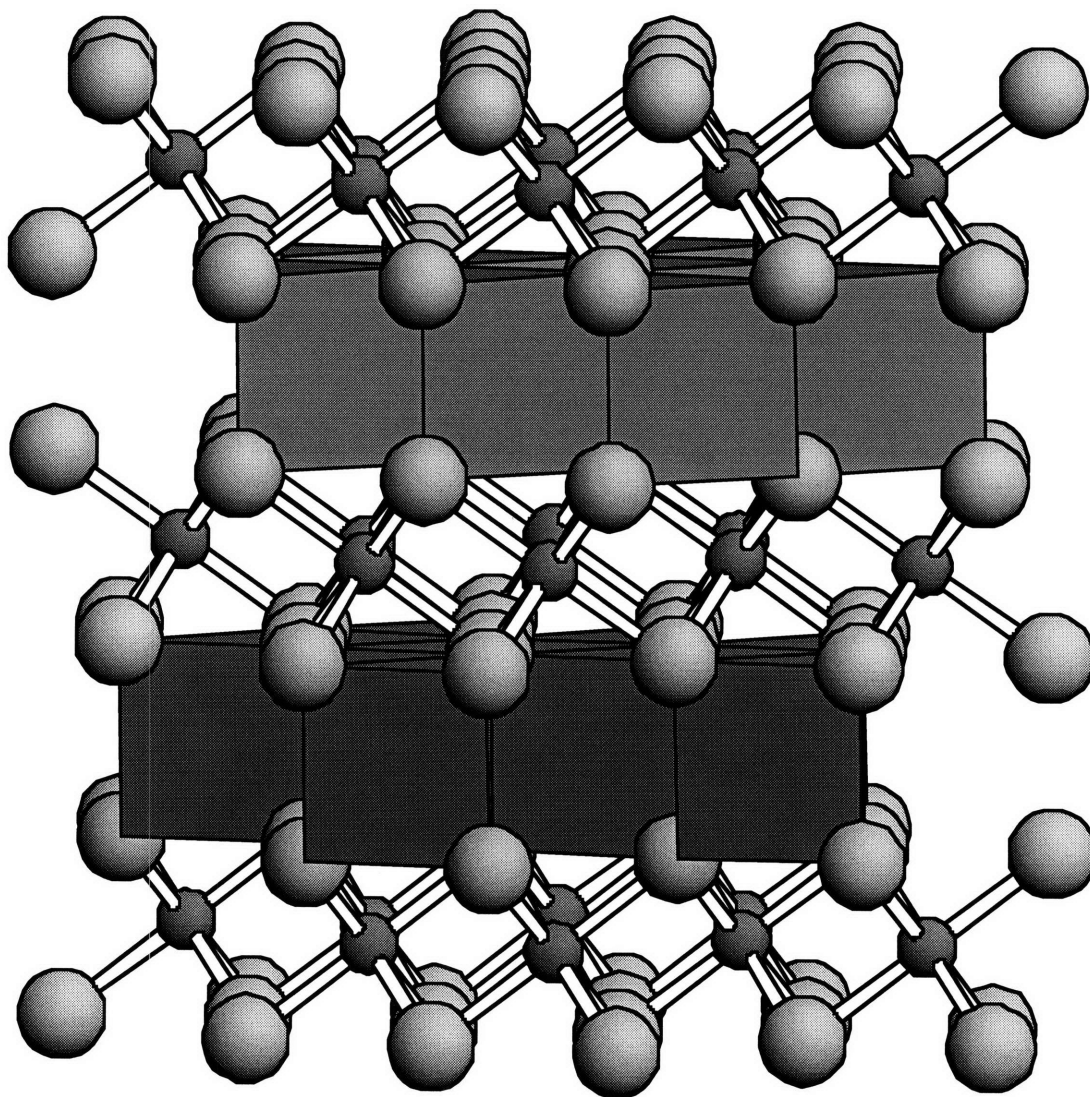
Figure 2.4.1: **Proposed structure for $Ta_5N_{6-\delta}O_y$ and $Nb_5N_{6-\delta}O_y$.**
Trigonal prismatic tantalum/niobium is shown as filled polyhedra. The octahedral tantalum/niobium and all the nitrogen/oxygen positions are indicated by a ball and stick representation. The small dark gray spheres represent tantalum/niobium atoms and large light gray spheres represent nitrogen/oxygen atoms.

2.4.2 Role of Iron in Product Formation

Table 2.1 lists a series of reactions undertaken to elucidate the role of iron in product formation. In the absence of iron, the oxynitride intermediates are observed only fleetingly, suggesting that the role of the iron is to stabilize these species. In fact, the apparent necessity of the presence of iron in the formation of $Ta_5N_{6-\delta}O_y$ and $Nb_5N_{6-\delta}O_y$ suggests a possible catalytic role for iron. In the quenching experiments of the iron containing precursors, iron nitride (Fe_2N) is found in the product after only 5 minutes at the reaction temperature (Table 2.1), indicating a loss of iron/iron oxide from the precursor. Since both Fe_2N and Fe_2O_3 are unstable above ~450 °C, the reduction of iron in the precursor to iron metal at the reaction dwelling temperature is suggested. The iron can agglomerate in the reaction mixture to form finely divided particles, whose presence is demonstrated by the strongly exothermic reaction which results if the sample is exposed to air without sufficient soak time under 300°C to allow the formation of a protective Fe_2N coating. Iron has been reported to affect the ammonolysis of other materials. For example, Glasson reports that iron impurities appear to accelerate the nitridation of Si, W, Mo and other elements.[39] In the experiments reported in this paper, it appears to slow the formation of the oxynitride intermediate and affect the formation of $M_5N_{6-\delta}O_y$ from the oxynitride intermediate.

The role of intermediate oxynitrides in affecting the formation of specific products has been observed in other instances. Jaggers *et al.* studied the ammonolysis reaction of ammonium molybdates and found that the reaction product, MoN or Mo_2N, was dependent on the type of molybdate precursor employed and on the temperature at which the oxynitride intermediate was formed.[13] In this study, not only is the formation of TaON much slower than in the ammonolysis of Ta_2O_5, but the conversion of the TaON intermediate to the nitride product takes much longer, with complete

conversion taking ~3.5 days (Table 2.1). Likewise, in the ammonolysis of iron-containing precursors to form $Nb_5N_{6-\delta}O_y$ the formation of the oxynitride intermediate is also slower than in the ammonolysis of Nb_2O_5. However, some oxynitride remains in the product mixture even after 4500 min. at 700°C. The persistence of a lower niobium oxynitride in the ammonolysis of niobium oxide could be explained by the lower reaction temperature relative to the ammonolysis of tantalum oxide, which could slow the exchange of nitrogen into the material. Also, very few binary nitride or oxynitride materials are known which contain niobium with a formal oxidation state of greater than 3, which could also explain the persistence of the lower oxynitride in the ammonolysis of Nb_2O_5. Regardless, the presence of iron in the reaction mixture dramatically effects the synthetic pathway in these ammonolysis reactions, a fact which warrants further investigation in the future.
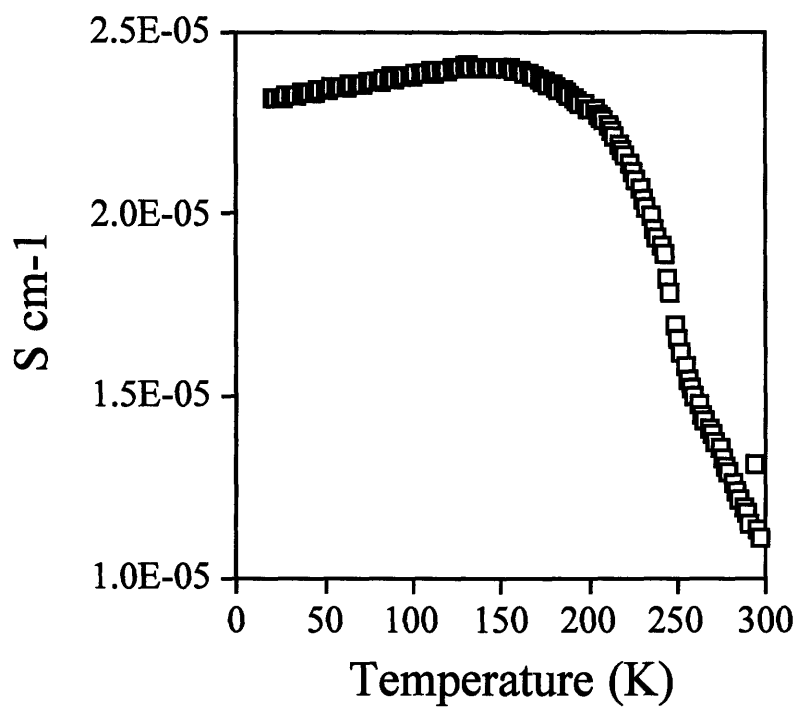
Figure 2.4.2: Electrical conductivity of $Nb_5N_{6-\delta}O_y$.
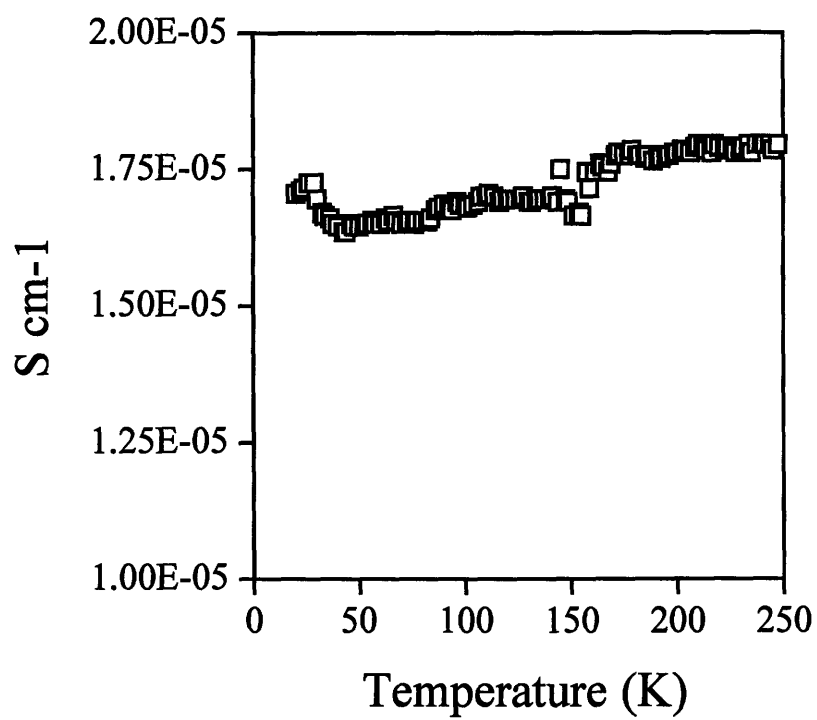
Figure 2.4.3: Electrical conductivity of $Ta_5N_{6-\delta}O_y$.
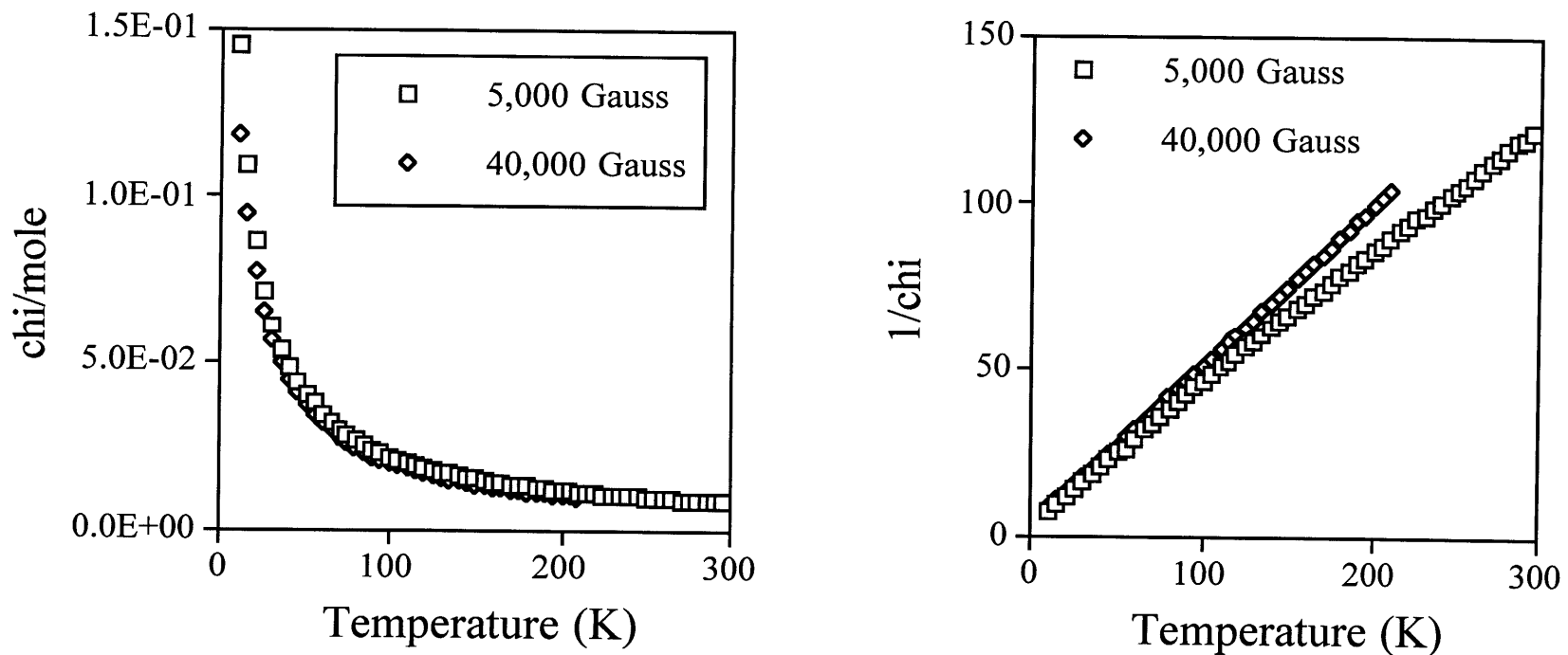
Figure 2.4.4: Magnetic Susceptibility of $Nb_5N_{6-\delta}N_y$.
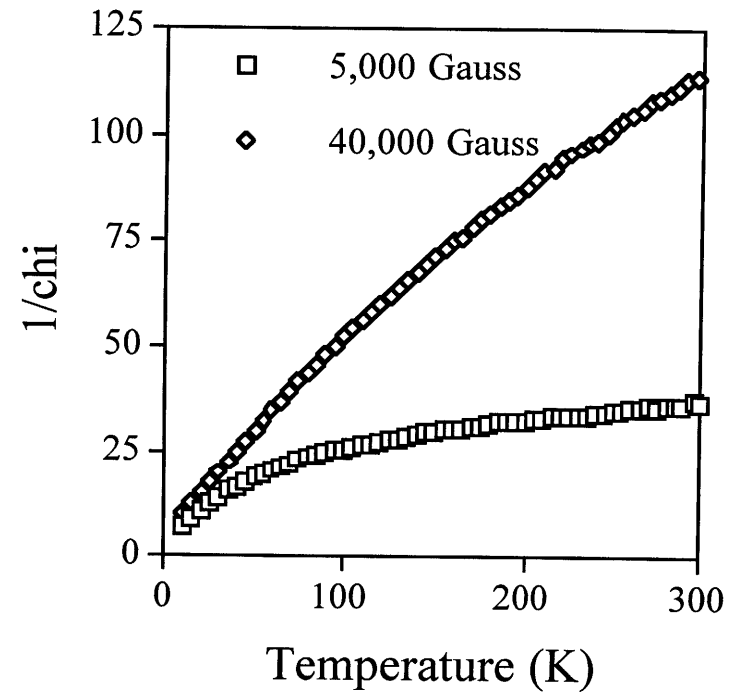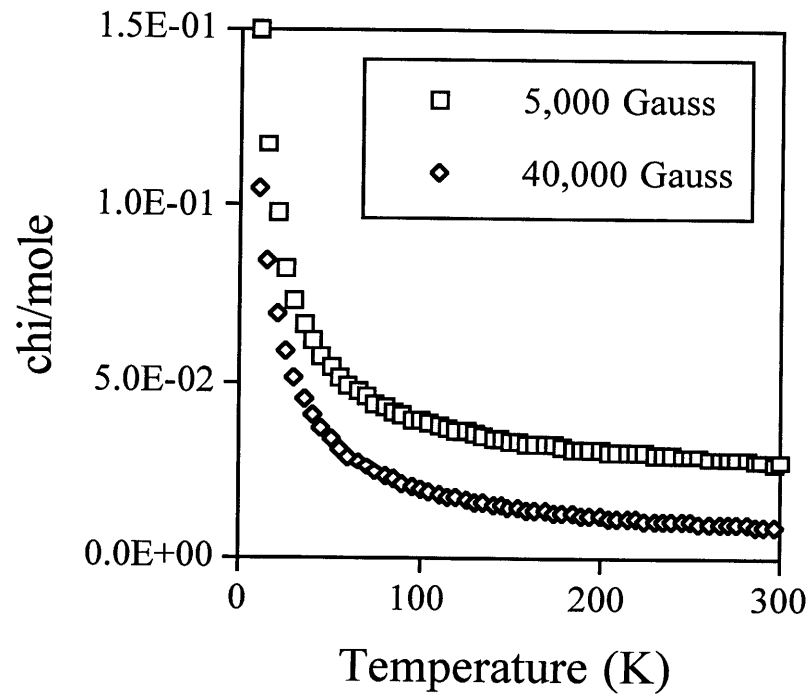
At 40 KG: C = 0.490
            μ = 1.988
            # unpaired e⁻ = 1.226

Figure 2.4.5: Magnetic Susceptibility of $Ta_5N_{6-\delta}O_y$.

Table 2.4: Inter-atomic distances of $M_5N_{6-\delta}O_y$

	Unwashed $Ta_5N_{6-\delta}Oy$ $P6_3/mcm$	Washed $Ta_5N_{6-\delta}Oy$ $P6_3/mcm$	$Nb_5N_{6-\delta}Oy$ $P6_3/mcm$
M(1)-M(1)	2.99172(7)Å	2.99081(2)Å	3.0044(2)Å
M(1)-M(2)	3.1249(5)Å	3.1274(3)Å	3.1333(7)Å
M(2)-M(2)	3.028(2), 2.921(3)Å	3.036(1), 2.903(2)Å	3.047(2), 2.921(4)Å
M(1)-N	2.141(8)Å	2.145(5)Å	2.141(7)Å
M(2)-N	2.161(8), 2.225(12)Å	2.152(5), 2.232(8)Å	2.174(7), 2.290(10)Å
N-N	3.00(1), 2.97(2), 2.67(2)Å	3.004(7), 2.96(1), 2.66(1)Å	3.05(1), 2.92(2), 2.75(2)Å

2.5 REFERENCES

(1) Bem, D. S.; Lampe-Önnerud, C. M.; H.P., O.; zur Loye, H. C. *Inorg. Chem.* **1996**, *35*, 581-585.

(2) Bem, D. S.; Olsen, H. P.; zur Loye, H. C. *Chem. Mater.* **1995**, *7*, 1824-1828.

(3) Bem, D. S.; zur Loye, H.-C. *J. Solid State Chem.* **1993**, *104*, 467.

(4) Houmes, J.; Bem, D.; zur Loye, H. *Mat. Res. Soc. Symp. Proc. Vol. 327* **1994**, 153-64.

(5) Elder, S. H.; DiSalvo, F. J.; Doerrer, L. H. *Chem. Mater.* **1992**, *4*, 928-937.

(6) Subramanya Herle, P.; Hegde, M. S.; Vasanthacharya, N. Y.; Gopalakrishnan, J.; Subbanna, G. N. *J. Solid State Chem.* **1994**, *112*, 208-10.

(7) Marchand, R.; Antoine, P.; Laurent, Y. *J. Solid State Chem.* **1993**, *107*, 34-8.

(8) Pors, F.; Marchand, R.; Laurent, Y. *J. Solid State Chem.* **1993**, *107*, 39-42.

(9) Bacher, P.; Antoine, P.; Marchand, R.; L'Haridon, P.; Laurent, Y.; Roult, G. *J. Solid State Chem.* **1988**, *77*, 67-71.

(10) Yu, C. C.; Oyama, S. T. *J. Solid State Chem.* **1995**, *116*, 205-207.

(11) Grins, J.; Svensson, G. *Mat. Res. Bull.* **1994**, *29*, 801-9.

(12) West, A. R. *Solid State Chemistry and its Applications*; John Wiley and Sons: New York, 1984, pp 734.

(13) Jaggers, C. H.; James, N. M.; Stacy, A. M. *Chem. of Materials* **1990**, *2*, 150-157.

(14) Fontbonne, A.; Gilles, J.-C. *Rev. Int. Hautes Temper. et Refract.* **1969**, *6*, 181-92.

(15) Gilles, J.-C. *C. R. Acad. Sc. Paris, Ser. C.* **1968**, *266*, 546-7.

(16) Yajima, A.; Matsuzaki, R.; Saeki, Y. *Denki Kagaku Oyobi Kogyo Botsuri Kagaku* **1983**, *51*, 676-80.

(17) Vendl, A. *Monatsh. Chem.* **1978**, *109*, 1009-12.

(18) Brauer, G.; Mohr-Rosenbaum, E. *Monatsh. Chem.* **1971**, *102*, 1311-1316.

(19) Terao, N. *Jap. J. Appl. Phys.* **1971**, *10*, 248-59.

(20) Dawson, P. T.; Stazyk, S. A. J. *J. Vac. Sci. Technol.* **1992**, *20*, 966-7.

(21) Raole, P. M.; Narsale, A. M.; Kothari, D. C.; Gogawale, W. V.; Guzman, L.; Dapor, M. *Mater. Sci. Eng., A* **1989**, *A115*, 73-7.

(22) Terao, N. *J. Less-Common Metals* **1971**, *23*, 159-69.

(23) Oya, G.; Onodera, Y. *J. Appl. Phys.* **1974**, *45*, 1389-97.

(24) Koenitzer, J.; Khazai, B.; Hormadaly, J.; Kershaw, R.; Dwight, K.; Wold, A. J. *Solid State Chem.* **1980**, *35*, 128-32.

(25) Larson, A. C.; von Dreele, R. B. In *GSAS:*Los Alamos National Laboratry: Los Alamos, NM, 1990.

(26) Brauer, V. G.; Weidlein, J.; Strahle, J. *Z. Anorg. Allge. Chem.* **1966**, *348*, 298-308.

(27) Brokamp, T.; Jacobs, H. *J. Alloys Compd* **1992**, *183*, 325-44.

(28) Schonberg, N. *Acta Chem. Scan.* **1954**, *8*, 213-20.

(29) Larson, A. C.; Lee, F. L.; Le Page, Y.; Webster, M.; Charland, J. P.; Gabe, E. J. In Chemistry Division, NRC, Ottawa, Canada, K1A 0R6, pp .

(30) Werner, P. E.; Eriksson, L.; Westdahl, M. *J. Appl. Crystallogr.* **1985**, *18*, 367.

(31) Harris, W. F. In *Determination of Gaseous Elements in Metals*; L. M. Melnick, L. L. Lewis and B. D. Holt, Ed.; John—Wiley and Sons: New York, 1974; Vol. 40; pp 113.

(32) Thompson, P.; Cox, D. E.; Hastings, J. B. *J. Appl. Cryst.* **1987**, *20*, 79-83.

(33) Di Salvo, F. J.; Bagley, B. G.; Voorhoeve, J. M.; Waszczak, J. V. *Phys. Chem. Solids* **1973**, *34*, 1357-1362.

(34) Whittingham, M. S. *Prog. Solid St. Chem.* **1978**, *12*, 41-99.

(35) Rouxel, J. In *Intercalated Layered Materials*; 1st ed.; F. Levy, Ed.; D. Reidel Publishing Co.: Hingham, MA, 1979; Vol. 6; pp 201-250.

(36) Pöttgen, R.; Witte, A. M.; Jeitschko, W.; Ebel, T. *J. Solid State Chem.* **1995**, *119*, 324-330.

(37) Brese, N. E.; O'Keefe, M. *Struct. Bonding* **1992**, *79*, 307-78.

(38) Bem, D. S.; Houmes, J. D.; zur Loye, H.-C. In *MRS Covalent Ceramics II: Non Oxides*; Boston, Massachusetts, 1993.

(39) Glasson, D. R.; Jayaweera, S. A. A. *J. Appl. Chem.* **1968**, *18*, 65-77.

3. Review of the Oxide Precursor Method

3.1 INTRODUCTION

The ammonolysis of oxide precursors has proven to be a fruitful area of research toward the synthesis of new ternary nitride materials and toward some structurally related oxynitrides. The chemistry of these materials is discussed in the previous chapter, with careful attention paid to the elemental composition and structure. Several precursor systems, most notably the molybdates and tungstates of iron and manganese, yield single phase ternary nitride products. However, attempts to broaden the applicability of the oxide precursor technique to include other oxide precursor systems were met with widely varying degrees of success. In this chapter, two additional systems (($Fe_{0.8}W_{0.2}$)WN$_2$ and $LiTaO_{3-3x}N_{2x}$) will be examined in some detail. These systems demonstrate several of the experimental problems and limitations of working with oxide precursors for the synthesis of nitride materials. Using these two materials as examples, a brief review of nitrides and oxynitrides synthesized through an oxide precursor route will be presented. From the data generated in this and other groups, an attempt will be made to extract trends in the oxide precursor data. Using these trends, some predictions will be made with respect to future reactions involving oxide precursors.

3.2 SUCCESSES OF THE OXIDE PRECURSOR METHOD

3.2.1 Ternary Transition Metal Nitrides and Related Binary Oxynitrides

To understand the success of the oxide precursor method, it is useful to review the work carried out in this group over the last several years. Our work has opened a new area of nitride chemistry and has created an interesting class of structurally related compounds. All of our ternary transition metal nitride materials, as well as several oxynitride materials, have been made by an ammonolysis route employing a ternary transition

metal oxide precursor (Table 3.1). The use of oxide precursors has been well documented as an experimentally simple and inexpensive method for the synthesis of a wide variety of nitride and oxynitride products.[1-5] In addition to fully nitrided materials, ammonolysis reactions of ternary oxides containing rare earths[6-8] or vanadium[9] yield distinct stoichiometric oxynitride products. Our recent syntheses of ternary nitrides containing two transition metals starting from the appropriate ternary oxide has demonstrated that complete conversion to a nitride product is possible and indeed favorable under certain reaction conditions. In addition, the ammonolysis of lithium molybdate and tungstate precursors has been shown to yield ternary nitride materials with structures related to the ternary metal nitrides containing two transition metals.

Interestingly, while the precursors used in the ammonolysis reactions carried out in this group vary both in structure and composition, the nitrides and oxynitrides which result demonstrate remarkable structural similarity. We have prepared several new ionic/covalent nitrides and oxynitrides, $FeWN_2$[4], $(Fe_{0.8}W_{0.2})WN_2$, $(Fe_{0.8}Mo_{0.2})MoN_2$[1], $MnMoN_2$[10], $MnWN_2$[10], $M(M_{0.67}\square_{0.33})N_{2-\delta}O_y$ (M = Ta or Nb; $\square$ = vacancy)[11], using transition metal molybdate, tungstate, tantalate and niobate solid state precursors. The structures of all the nitride/oxynitride compounds contain as the common structural motif layers of trigonal prismatically and octahedrally coordinated transition metals. All these materials demonstrate remarkable structural similarity to lithium intercalated molybdenum and tungsten dichalcogenides, which has important ramifications in the electronic and bonding characteristics of the materials. In the following sections, the syntheses of these nitrides and their structural relationships are presented.

3.2.1.1 Synthesis

The synthesis of all the molybdenum and tungsten containing materials is carried out using an ammonolysis technique similar to that used in Chapter 2 for the synthesis of $M(M_{0.67}\square_{0.33})N_{2-\delta}O_y$ (M = Ta or Nb; $\square$ =

vacancy). The transition metal tungstates (FeWO$_4$, MnWO$_4$, Fe$_2$W$_3$O$_{12}$) and molybdates (Fe$_2$Mo$_3$O$_{12}$, MnMoO$_4$) were used respectively as precursors for the transition metal nitrides FeWN$_2$, α,β-MnWN$_2$, (Fe$_{0.8}$Mo$_{0.2}$)MoN$_2$ and MnMoN$_2$. Hydrated tungstate and molybdate precursors were prepared by the drop-wise addition of iron or manganese chloride to aqueous solutions of the sodium metallates under careful pH control. The ammonolysis of the oxide precursors was carried out in a quartz flow-through reactor located in a hinged tube furnace (**Figure 2.2.1**). Approximately 0.4 g of the precursor was placed into an alumina boat which was placed inside the reactor. The samples were heated under flowing ammonia gas (150cc/min.) at temperatures ranging between 650-750°C and times ranging from 12-96 hours. At the end of the ammonolysis reaction, the samples were rapidly (10 min.) cooled to <100°C by turning off and opening the furnace. Structural characterization and phase purity analysis was carried out via powder X-ray diffraction.

3.2.1.2 Structure

Ammonolysis reactions of the metallate precursors yield a family of structurally related nitrides and oxynitrides with the general formulation MM′N$_2$. The structure consists of close packed nitrogen layers with the metals located in alternating layers of octahedral and trigonal prismatic coordination. In the case of the oxynitrides, oxygen atoms randomly occupy the nitrogen site(s). This structure type is similar to those exhibited by several other compounds, including the well known molybdenum and tungsten dichalcogenides, LiMoO$_2$[12], LiNbO$_2$[13] and ScCrC$_2$[14]. The ammonolysis of both Li$_2$MoO$_4$ and Li$_2$WO$_4$ yield products of similar stoichiometry and structure, LiMoN$_2$[2] and LiWN$_2$[3].

The structure of FeWN$_2$ was obtained from Rietveld refinement of the powder X-ray diffraction data. The powder X-ray pattern for FeWN$_2$ was indexed as hexagonal, a = 2.87618(9)Å, c = 10.9317(4)Å. The pattern was

refined in space group $P6_3/mmc$ (Rwp = 8.73%, Rp = 6.66%). In this material, iron is octahedrally coordinated and tungsten is trigonal prismatically coordinated layers between nitrogen sheets as is shown in Figure 1.5.10. The metal layer stacking of $FeWN_2$ is **AcAcBcBcA** (lower case letter indicate metals stacking and capital letters indicate nitrogen stacking), with the unit cell defined by the shifting of the nitrogen stacking.

Several other ternary transition metal nitrides form with this structure. For example, $(Fe_{0.8}Mo_{0.2})MoN_2$ exhibits an identical structure with occupation of 20% of the iron sites by molybdenum (Figure 3.2.1). The stacking of the metal layers is also **AcAcBcBcA**, the same as that found for $FeWN_2$. The lattice parameters for $(Fe_{0.8}Mo_{0.2})MoN_2$, as expected, are similar to those observed in $FeWN_2$, with a = 2.8562(1) and c = 10.9997(4). One notable omission from this family is $FeMoN_2$, which has not yet been synthesized. We have observed that the ammonolysis of molybdate and tungstate precursors is greatly affected by the structure of the precursor itself. Since the exact structure and composition of molybdate and tungstate species formed by aqueous precipitation routes can be greatly affect by synthesis conditions (i.e. pH and metal salt), $FeMoN_2$ might be synthesized if a precursor with the appropriate structure is used.

Manganese containing precursors yield nitrides with a slightly different structure. For example, in $MnMoN_2$, the structure still consists of close packed layers of nitrogen, between which the metals are in octahedral and trigonal prismatic coordination. However, the layer stacking in this material is **BaCbCaBcB**, maintaining a unit cell similar (a = 2.92260(9), c = 10.8550(4)) to that found in $FeWN_2$. In $MnWN_2$, two different metal stackings are observed resulting in two phases: α-$MnWN_2$ and β-$MnWN_2$. β-$MnWN_2$ forms with a metal stacking identical to that found in $MnMoN_2$ and subsequently has nearly identical lattice parameters, a = 2.9390(4) and c = 11.022(2). However, in α-$MnWN_2$, the metal layer stacking is **BaCaCbAbAcBcB**, which results in an

increase in the c lattice parameter ($a = 2.9126(1)$ and $c = 16.556(1)$). α-MnWN$_2$ appears to be isostructural with the previously reported LiMoN$_2$.[2]

The structural similarity and the fact that the alpha phase is synthesized at a temperature 100°C lower than the beta phase suggests that it might be possible to thermally convert one form of MnWN$_2$ into the other. It was found that by heating the alpha phase to 800°C under ammonia it is possible to convert it into the beta phase. However, it does not appear possible to convert the beta phase into the alpha phase by annealing it at 700°C, suggesting that the activation energy (in terms of kT) for the conversion between the two phases lies between 700 and 800°C and that the thermodynamic stability of the two phases is roughly comparable.

Ta$_5$N$_{6-\delta}$O$_y$ and Nb$_5$N$_{6-\delta}$O$_y$, two isostructural binary oxynitrides, were prepared by ammonolysis of FeTaO$_4$ and FeNbO$_4$ at 900°C and 700°C respectively, as explained in detail in Chapter 2. The ammonolysis product contains, in addition to the tantalum or niobium nitride, Fe$_2$N, which can be removed by washing in HCl. The structure of Ta$_5$N$_{6-\delta}$O$_y$ and Nb$_5$N$_{6-\delta}$O$_y$ consist of close packed layers of nitrogen/oxygen with metals in alternating trigonal prismatic and octahedral coordination between the layers. All of the trigonal prismatic sites are occupied, but 1/3 of the octahedral sites are vacant. As such, these compounds can be thought of as $M(M_{0.67}\square_{0.33})N_{2-\delta}O_y$ (M = Ta/Nb; $\square$ = vacancy), in order to be consistent with the formula notation for this family of compounds. The similarity between these compounds and the MM'N$_2$ family is most striking for Ta$_5$N$_{5.99}$O$_{0.01}$, which contains only a very small amount of oxygen. The compound may be expressed as $(Ta_{0.67}\square_{0.33})TaN_{2.00}O_{0.003}$. The layer stacking of these materials, **BaCbCaBcB**, is identical to that found in MnMoN$_2$ and β-MnWN$_2$.

All of these nitrides and oxynitrides are related by a complex series of structural rearrangements involving sliding of the metal and nitrogen layers relative to each other. Figure 3.2.5 and Figure 3.2.6 demonstrate two possible stacking faults which could occur in all the compounds mentioned in this

section. In Figure 3.2.5, the octahedrally coordinated metal atoms shift by [1/3 1/3 0] to yield a new metal stacking without changing the nitrogen stacking sequence. In Figure 3.2.6, one MN_6 sheet is shifted by [1/3 1/3 0] to yield both a new metal and a new nitrogen stacking sequence. Even materials which are considered phase pure demonstrate broad peak shapes, particularly in [h k l] l ≠ 0, which is indicative of stacking faults along the c-axis of the material. If these stacking faults occur with sufficient regularity, new phases are formed, as evidenced by the polytypism of $MnWN_2$. In the following section, the presence of these stacking faults in $(Fe_{0.8}W_{0.2})WN_2$ will be discussed along with the associated difficulties they create for the structure solution of this material.

Structural similarities between this family of compounds and the transition metal dichalcogenides may be drawn. In the lithium intercalated phases of MoS_2, which have structures identical or strongly related to the ternary nitride and oxynitride materials described in this section, the MoS_6 trigonal prisms are compressed along the c-axis (S-S in ab-plane 3.16Å, S-S parallel to c-axis 2.98Å). Band structure calculations have indicated that this distortion of the trigonal prismatic sites results from an increased Mo-S bond covalency and the formation of discrete S-S dimers along the edges of the trigonal prisms parallel to the c-axis.[15] Together these result in a highly covalently bonded material which exhibits metallic type conductivity.

Similar structural distortions are observed in the ternary transition metal nitride and binary oxynitride materials synthesized in this lab. The trigonal prismatic MN_6 units in the ternary transition metal nitrides are contracted along the c-axis (Figure 3.2.7 , Table 3.2) as a result of increased metal-nitrogen bond covalency as suggested by band structure calculations performed on the structurally similar ternary nitride $LiMoN_2$[16]. These calculations also provide some evidence for the presence of N-N interactions along the c-axis. The argument is strengthened by the fact that the N-N distances in all these materials are shorter than the N-N distances in CaNiN (3.58Å), in which N-N interactions have been found.[17] Indeed, the N-N

distances in all these materials are among the shortest reported. All the interplanar N-N distances are significantly shorter than the sum of the N^{3-} ionic radii (2.8-3.4Å), though still longer than a true N-N single bond (N-N in hydrazine is 1.40Å).

Further similarities to the transition metal dichalcogenides are observed in the phase transitions present in both the dichalcogenides and in the nitride materials. As mentioned earlier, two phases are observed for $MnWN_2$. The lower temperature kinetic phase undergoes an irreversible phase transition at 800°C to yield the higher temperature kinetic phase (Figure 3.2.8). A similar phase transition is observed in the transition metal dichalcogenides. For example, the 3R phase of TaS_2 (structurally similar to α-$MnWN_2$ with a vacancy on the Mn site and with similar lattice parameters; R-3m; a=3.32Å, c=17.90Å) undergoes an irreversible phase transition at 800°C to yield the 2H form (structurally similar to β-$MnWN_2$ and with similar lattice parameters; $P6_3/mmc$; a=3.314, c=12.10).[18]

Mössbauer experiments conducted on $FeWN_2$ are indicative of the presence of highly localized Fe(II) centers. Since all the ternary nitride materials exhibit poor metallic conductivity, the presence of highly covalent MN_2 layers (M = Mo and W) is again implied and would be responsible for the metallic type conductivity observed. Between these layers, an ionic metal species is located for charge balance. Again, the similarity is seen between these materials and the intercalated transition metal dichalcogenides, in which a highly ionic alkali metal species is located between covalent MS_2 layers.

Perhaps the most interesting property of all the ternary transition metal nitrides is their chemical inertness. Many of the previously known ternary nitride materials, particularly those which contain alkali metals, are readily attacked by water to give oxide decomposition products with the release of ammonia. However, all the ternary transition metal nitrides discussed here are stable not only to atmospheric water, but also to more

extreme environments such as concentrated hydrochloric, sulfuric or hydrofluoric acid. Although the thermal stability of these materials is not great (all the materials listed in this thesis decompose under ammonia ~50°C above their synthesis temperatures), the chemical stability again demonstrates the covalent nature of the bonding in these materials.

One property of the transition metal dichalcogenides which has received considerable attention is the mobility of the metal ions in the van der Waals gap between the MS_2 layers. If the similarity between these materials and the ternary transition metal nitrides is extended, one could envision the deintercalation of the ionic octahedrally coordinated species. The end member of this intercalation would be MN_2 (M = Mo or W). Such deintercalation experiments have been attempted with $LiMoN_2$.[2] However, only 0.64 equivalents of Li could be extracted before the onset of sample decomposition. Also, the deintercalation process was found to be extremely slow and electrochemically irreversible (though it was reversible for chemical extraction of lithium), limiting the potential application of these nitrides as battery materials. The deintercalation experiment, in the case of the ternary transition metal nitrides and binary oxynitrides, can not be brought into reality due to the difficulty associated with moving a doubly charged cations through a crystal lattice. However, partial substitution of the trigonal prismatically coordinated atom into octahedral sites can be accomplished. By effecting this substitution, a partial intergrowth structure between octahedrally coordinated MN_2 and trigonal prismatically coordinated MN_2 can be accomplished. In the next section, the synthesis and characterization of such a compound is discussed.

A $(Mo\text{-}N)_{TP}$

A $(Fe/Mo\text{-}N)_{OCT}$

A $(Mo\text{-}N)_{TP}$

A $(Fe/Mo\text{-}N)_{OCT}$

A $(Mo\text{-}N)_{TP}$
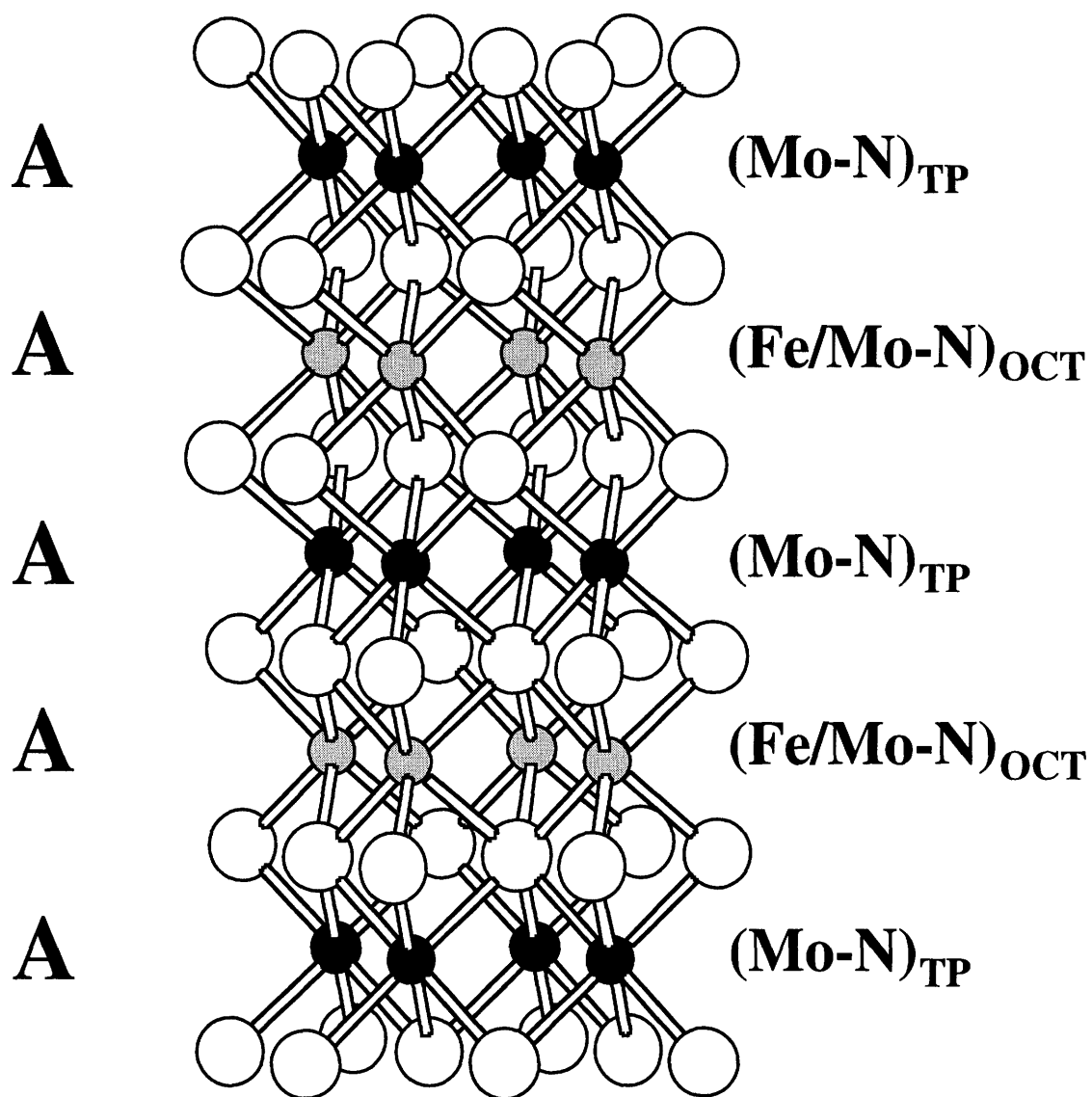
Figure 3.2.1: Proposed structure of $(Fe_{0.8}Mo_{0.2})MoN_2$.
Gray = Fe, Black = Mo, and White = N.
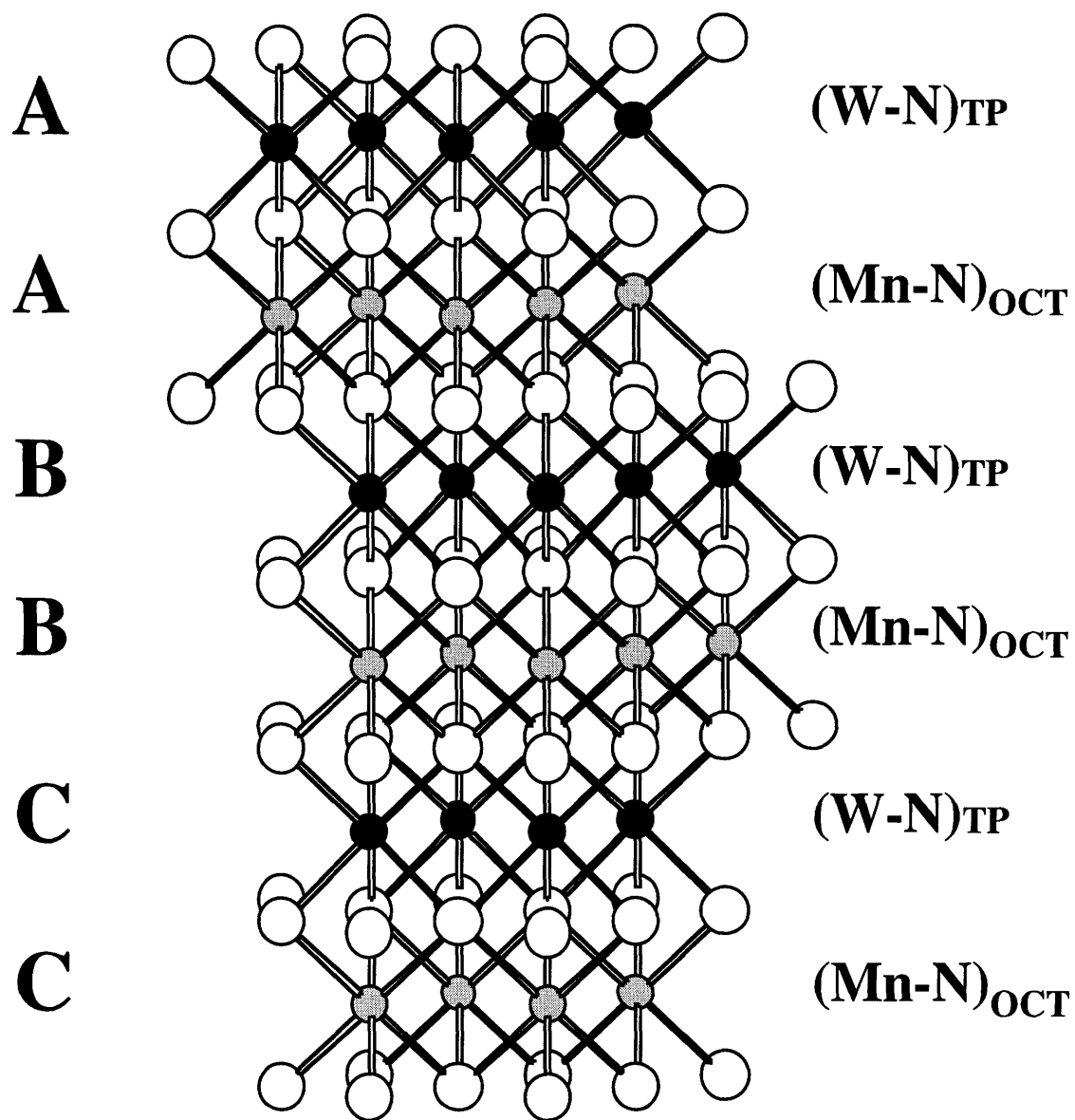
Figure 3.2.2: Proposed structure for α-MnWN₂
Gray = Mn, Black = W and White = N.
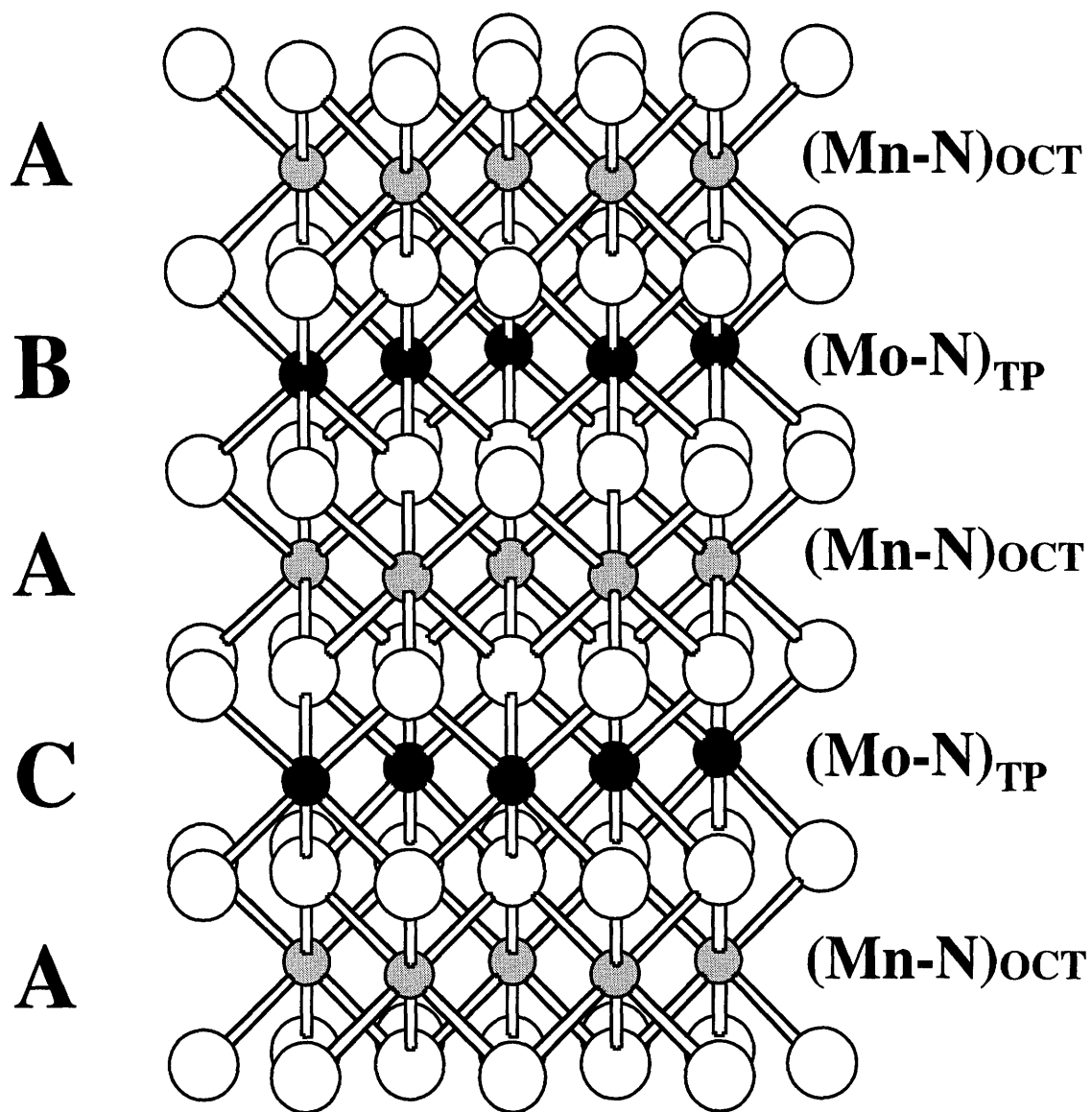
Figure 3.2.3: Proposed structure for MnMoN$_2$.
Gray = Mn, Black = Mo, and White = N.
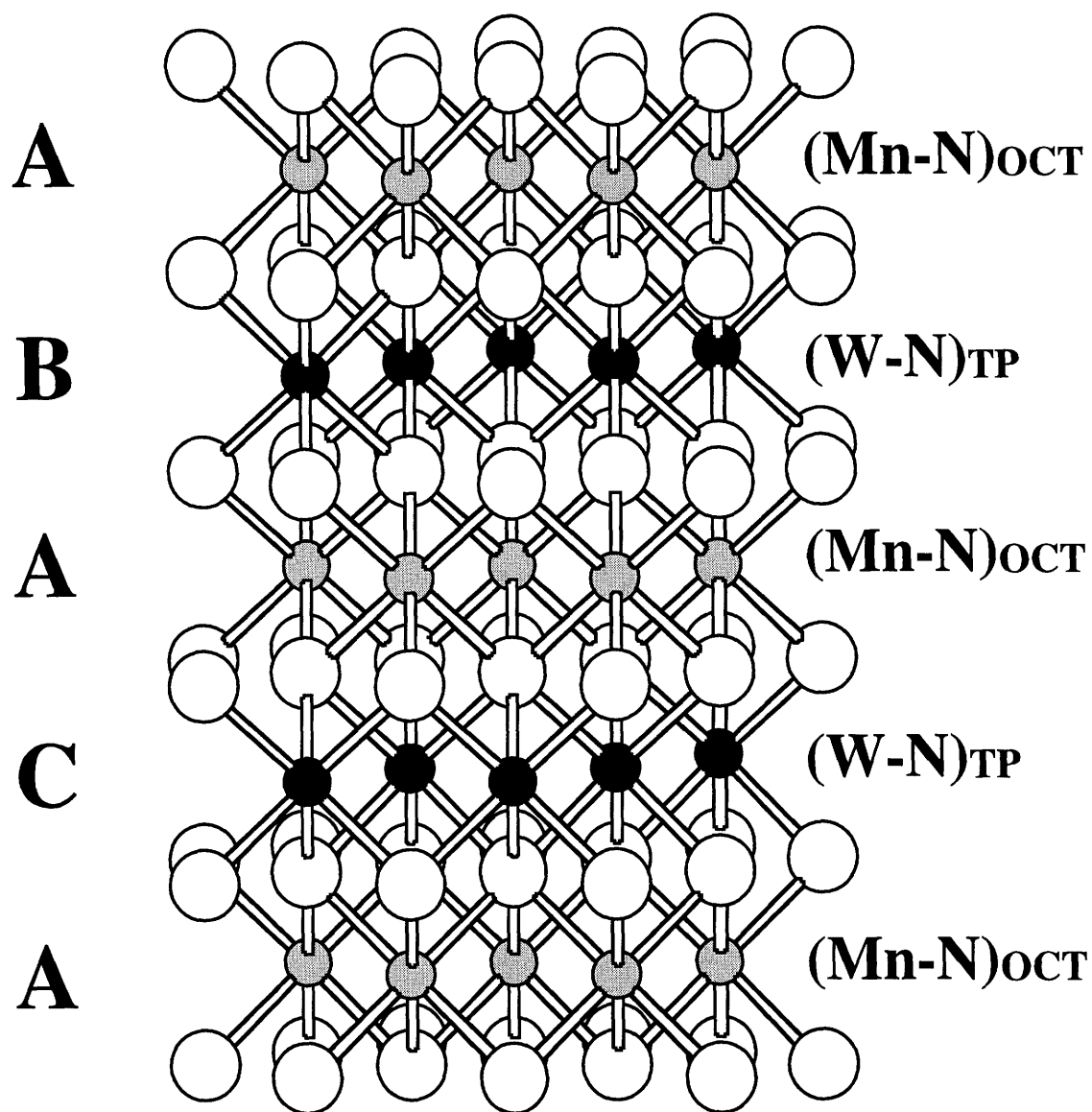
Figure 3.2.4: Proposed structure for β-MnWN₂.
Gray = Mn, Black = W, and White = N.
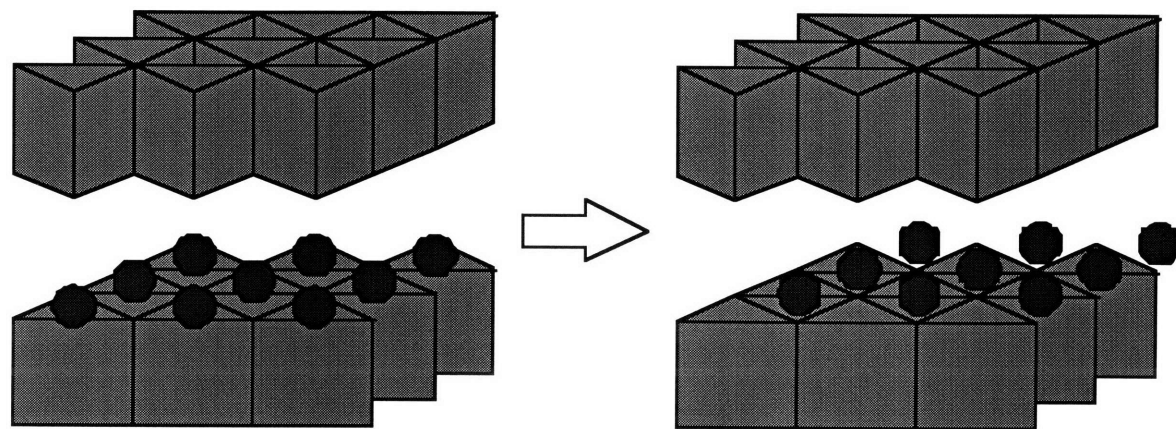
Figure 3.2.5: Stacking fault resulting from a shift of interstitial atoms.
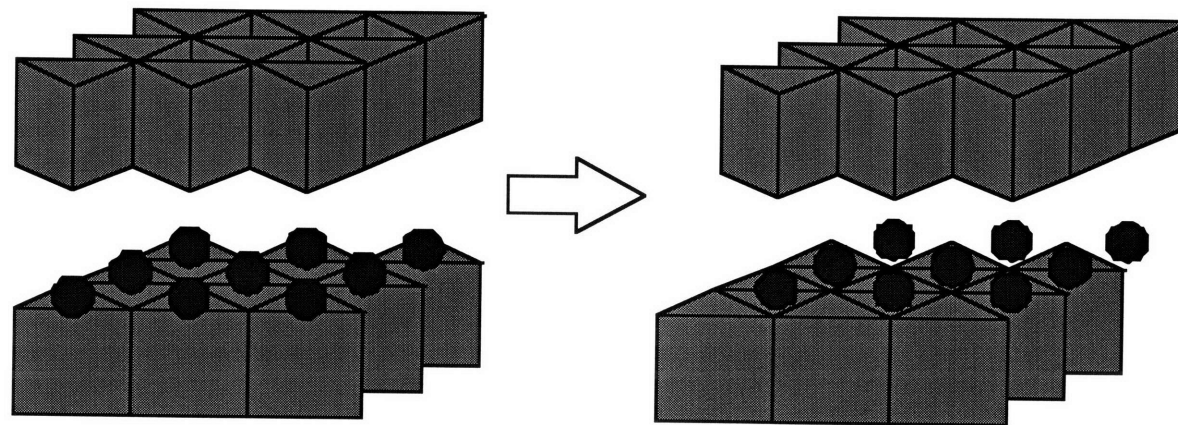
Figure 3.2.6: Stacking fault resulting from a shift of MN$_6$ sheets.

Table 3.1: Ternary nitrides and binary oxynitrides with the nickel arsenide-like structure.

Precursor	Reaction Temp. °C	Product
$MnWO_4$	700	$\alpha\text{-}MnWN_2$
$MnWO_4$	800	$\beta\text{-}MnWN_2$
$FeWO_4$	700	$FeWN_2$
$Fe_2(WO_4)_3$	675	$(Fe_{0.8}W_{0.2})WN_2$
$Fe_2(MoO_4)_3$	700	$(Fe_{0.8}Mo_{0.2})MoN_2$
$MnMoO_4$	625	$MnMoN_2$
$FeNbO_4$	700	$(Nb_{2/3}\square_{1/3})NbN_{2\text{-}d/3}O_{y/3}$
$FeTaO_4$	900	$(Ta_{2/3}\square_{1/3})TaN_2$

$\square$ = vacancy
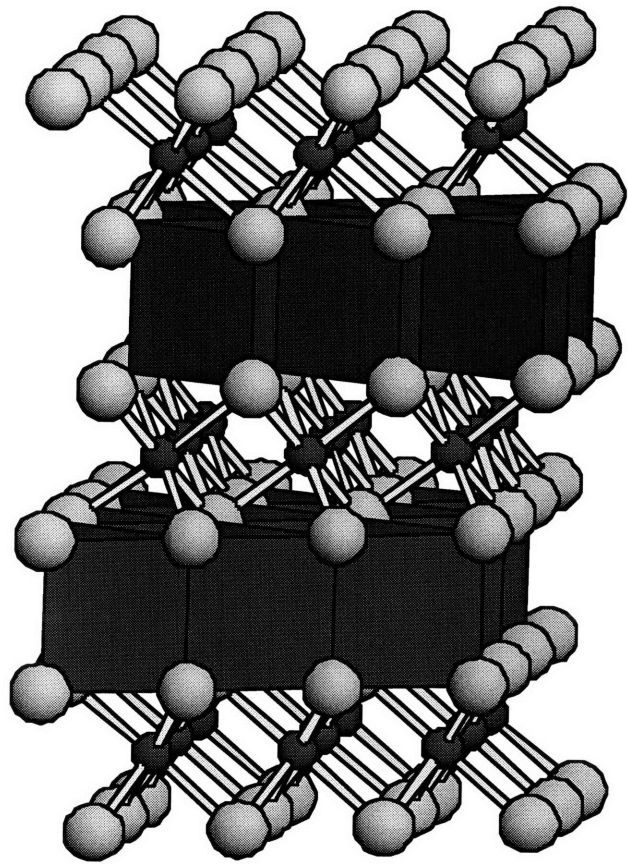
LiMoS$_2$
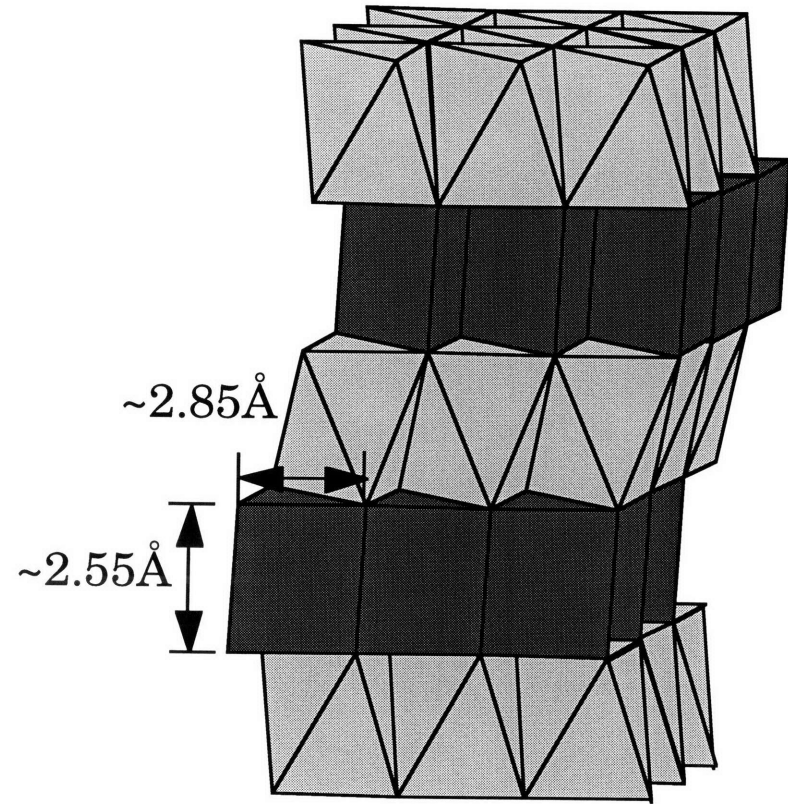
MnMoN$_2$, β-MnWN$_2$, (M$_{2/3}$□$_{1/3}$)NbN$_{2-\delta/3}$O$_{y/3}$
(M=Nb, Ta)

~2.85Å

~2.55Å

Figure 3.2.7: Comparison of lithium intercalated molybdenum disulfide and ternary nitride materials.

α–**MnWN**$_2$

β–**MnWN**$_2$

800 °C

C

C

c = 16.556

c =11.022
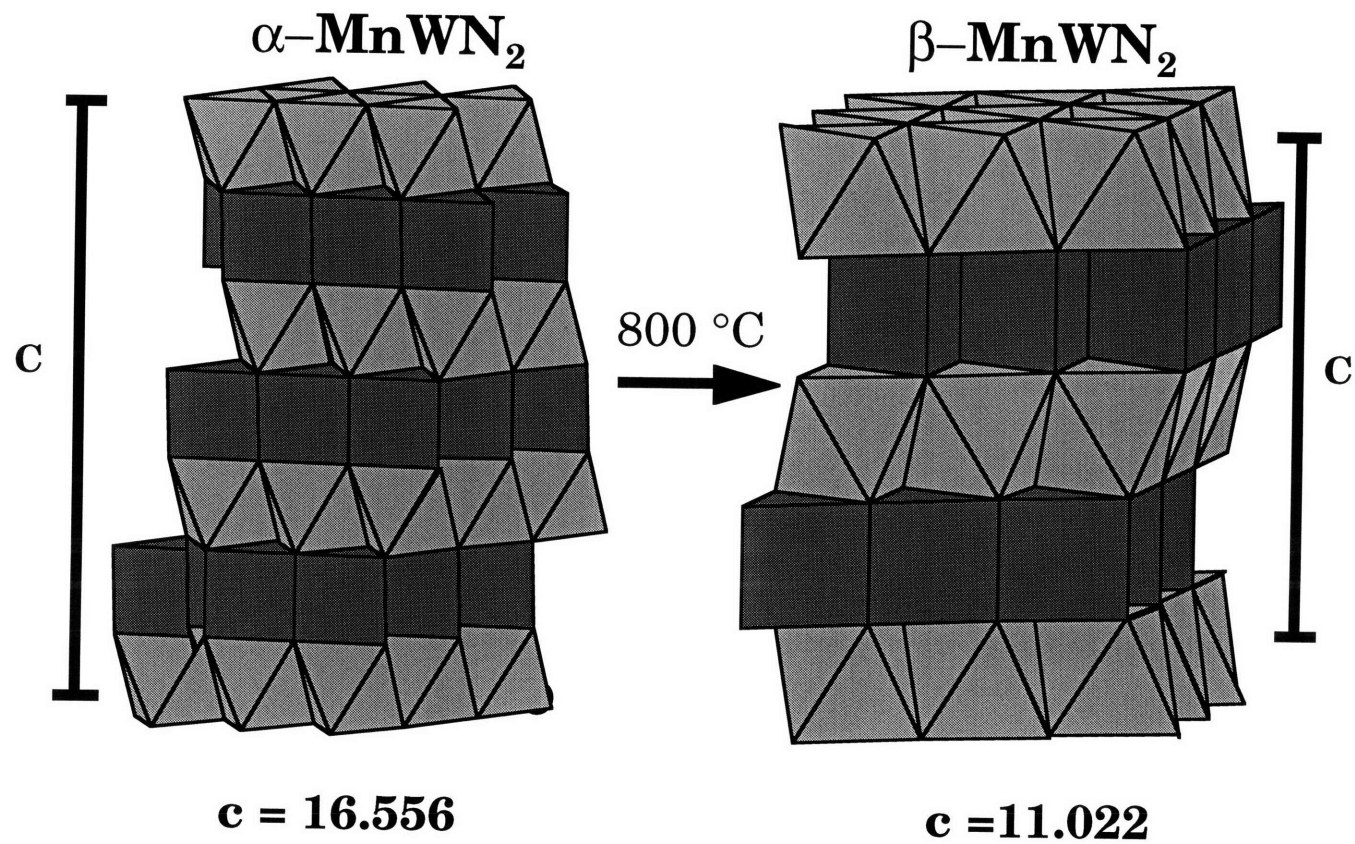
Figure 3.2.8: Structural change observed in MnWN$_2$.

Table 3.2: N-N distances in nitrides and oxynitrides synthesized by ammonolysis.
Distances parallel to c axis are across one edge of the MN_6 trigonal prism.
□ = vacancy.

Material	N-N distance in ab-plane (Å)	N-N distance parallel to c axis (Å)
$FeWN_2$	2.87630(5)	2.75(2)
$MnMoN_2$	2.92262(8)	2.566(8)
$(Fe_{0.8}Mo_{0.2})MoN_2$	2.8562(1)	2.69(1)
$(Ta_{0.67}□_{0.33})TaN_2$	2.97(2)	2.67(2)
$(Nb_{0.67}□_{0.33})TaN_2$	2.92(2)	2.75(2)

3.2.2 $(Fe_{0.8}W_{0.2})WN_2$

The formation of $(Fe_{0.8}Mo_{0.2})MoN_2$, as demonstrated in the previous section, has demonstrated that nitride materials with metal stoichiometries other than 1:1 can be synthesized such that either tungsten or molybdenum is found on the iron site. An iron deficient iron-tungsten material, $(Fe_{0.8}W_{0.2})WN_2$, can be synthesized from an iron tungstate precursor having a 2:3 iron:tungsten ratio. By making a material which is iron deficient, a partial intergrowth between octahedrally coordinated WN_2 and trigonal prismatically coordinated WN_2 can be accomplished. The synthesis of this material demonstrates not only the difficulty associated with the synthesis of a single phase nitride material, but also some of the difficulty associated with product characterization in a material with extensive structural disorder. The synthesis and chemistry of $(Fe_{0.8}W_{0.2})WN_2$ will be presented in the following sections.

3.2.2.1 Synthesis of $(Fe_{0.8}W_{0.2})WN_2$

$(Fe_{0.8}W_{0.2})WN_2$ is synthesized using techniques similar to those used in the synthesis of the ternary transition metal nitrides discussed in the previous section. The iron tungstate precursor, $Fe_2W_3O_{12}$ is synthesized by dropwise addition of a 50 ml aqueous solution of iron chloride (Aldrich, 97%, 0.023 mol) to a 500 ml solution of sodium tungstate (Cerac, 99.9%, 0.034 mol). The solution was acidified to pH 3.6 by the addition of acetic acid. After addition, the solution was stirred for 1 hr. and the yellow precipitate isolated by vacuum filtration. The solid was dried overnight and was found to be amorphous by powder X-ray diffraction.

The nitride, $(Fe_{0.8}W_{0.2})WN_2$, was synthesized by heating ~0.5 g of $Fe_2W_3O_{12}$ under flowing ammonia at 700°C for 96 hrs. with one intermediate grinding. The oxide powder, $Fe_2W_3O_{12}$, was placed into an alumina boat, which was then inserted into a flow through reactor (Figure 2.2.1). The sample was heated at 5°C/min. to 700°C and soaked for 48 hours under

flowing ammonia gas (Airco, anhydrous 99.99%, 150 cm^3/min.) After 48 hrs., the sample was cooled by turning off the furnace and opening it to the air. Once the sample had cooled to room temperature, it was removed from the system, ground, and reheated using the identical heating cycle. A pure product was obtained only over a narrow temperature range for a given flow rate. By trial and error, 700 °C was found to be the reaction temperature that gave the cleanest, most crystalline product.

3.2.2.2 Characterization

Powder X-ray diffraction patterns were collected using a Siemens D5000 diffractometer operating at 40 kV and 45 mA with Cu Kα radiation. Qualitative phase analysis of the oxide precursor and the nitride product was performed using a continuous scan. Pattern indexing was carried out using the indexing program TREOR.[19] The lattice parameters and theoretical powder patterns were calculated using the NRCVAX crystal structure system.[20] A step-scanned diffraction pattern of $(Fe_{0.8}W_{0.2})WN_2$ (5° ≤ 2θ ≤ 118°, 0.05° steps) was used for Rietveld refinement, which were performed using the General Structure Analysis System, GSAS.[21]

The nitrogen content of the nitride was determined by nitrogen combustion analysis (Galbraith Laboratories Inc.) (N 9.95 wt. %). The oxygen impurity was determined by vacuum fusion analysis[22] (LECO O 2.26 wt. %, Mass Materials Research). The metal ratio of the amorphous powder was determined by ICP (Galbraith Laboratories Inc.). The ratio (Fe weight %)$_{obs}$/(W weight %)$_{obs}$ = 0.22 agrees with the expected ratio (Fe weight %)$_{theor}$/(W weight %)$_{theor}$ = 0.20. Together, these yield an overall composition of $(Fe_{0.8}W_{0.2})WN_{2.15}O_{0.4}$. We were unable to determine whether the oxygen impurity is due to unreacted starting material or surface oxidation.

Magnetic data were collected using a Quantum Design MPMS SQUID magnetometer at temperatures ranging from 5 to 400 K in an applied field of 5 kG. A total of three 6 cm scans were averaged with 32 measurements for each scan length. Temperature-dependent two- and four-probe resistance

measurements were performed on pressed pellets using a Keithly 236 source measure unit and a Janis closed-cycle refrigerator (Model ccs-200) by measuring the voltage at a constant current of 1 mA. Pellets where pressed at 5000 psi in air.

3.2.2.3 Results and Discussion

The product of the ammonolysis of $Fe_2W_3O_{12}$, $Fe_{0.8}W_{1.2}N_2$, is a black crystalline powder which is stable to air and moisture. The nitride was decomposed by heating in oxygen at 900 °C to yield Fe_2O_3 and WO_3. The observed mass gain 12.40 wt. % (Figure 3.2.9) was smaller than the theoretical mass gain of 14.26% for the oxidation of $Fe_{0.8}W_{1.2}N_2$ to $0.4Fe_2O_3$ and 1.2 WO_3, which indicates the presence of residual oxygen in the nitride. The mass gain corresponds to a starting composition of $Fe_{0.8}W_{1.2}N_2$ with 2.1 wt. % residual oxygen, which is close to the value for the oxygen content obtained from oxygen analysis (2.26 wt. %).

Indexing of the powder X-ray diffraction data for $Fe_{0.8}W_{1.2}N_2$ gave a hexagonal unit cell of approximately $a = 2.87Å$, $c = 10.96Å$. Based on systematic absences and experience with other ternary transition metal nitrides of similar composition, the space group $P6_3/mmc$ was chosen. A powder pattern was calculated using this space group and found to be in agreement with the observed data. Given the similarities in elemental composition and diffraction pattern, the structure of $Fe_{0.8}Mo_{1.2}N_2$[1] was used as a starting point for a Rietveld refinement of the data.

Despite success using Rietveld refinement as a structural characterization tool for nitrides of similar composition and structure, refinements of $Fe_{0.8}W_{1.2}N_2$ failed to converge with acceptable goodness of fit values. Close inspection of the powder X-ray diffraction data (Figure 3.2.10) reveals the difficulty in refining this structure. The diffraction peaks of $Fe_{0.8}W_{1.2}N_2$ can be divided into two groups. The peaks at 36° and 65° 2-theta exhibit peak shapes which are significantly narrower than the remainder of the diffraction peaks. For these two peaks [hkl] l = 0, while for all other peaks

$l{\neq}0$. This variation in peak FWHM is indicative of significant structural disorder along the c-axis, which could take the form of a shifting of the WN_6 trigonal prismatic slabs, a disorder of the metal positions or a shifting of the nitrogen positions.

The presence of two disparate peak shapes makes refinement of the powder X-ray diffraction data problematic. The GSAS structure refinement package does not handle two peak shapes within the same phase well. In addition, no good model for stacking faults exists. Several unsuccessful attempts were made to account for the peak width disparity. Refinement of only anisotropic profile values resulted in slight improvement of the goodness of fit values. However, neither set of peaks was fit well. Also, an attempt was made to refine the phase as two histograms, one of which contain only the narrow peaks and the other containing the wider. However, this approach did not yield any significant improvement in the fit.

Despite the difficulties in refining the structure of $Fe_{0.8}W_{1.2}N_2$, we propose that the structure is identical or closely related to that of $Fe_{0.8}Mo_{1.2}N_2$. The proposed atomic position for $Fe_{0.8}W_{1.2}N_2$ are listed in Table 3.3. The structure (Figure 3.2.1) consists of alternating layers of edge-shared octahedra and trigonal prisms, where the octahedra and trigonal prisms are face-shared in the c direction. The arrangement of the nitrogen and metal atoms can be represented by **AcAcBcBcA**, where **A** and **B** represent the close-packed nitrogen atoms with significant disorder between the two positions and c represents the metal atoms. The trigonal prismatic layer is occupied exclusively by tungsten, while the octahedral layer contains iron and molybdenum randomly distributed in an approximately 4:1 ratio. The composition can be more accurately written as $(Fe_{0.8}W_{0.2})WN_2$.

Patterson maps constructed from the powder X-ray diffraction step-scan data in space group P1 provide some insight in the cause of the peak broadening. Figure 3.2.11 shows the electron density in the [0 0 5/8] plane, which contains the nitrogen atoms. The electron density form a pseudo-6-fold symmetry axis around the c-axis, with almost identical electron

density at each site. The even distribution of electron density is repeated in every plane [0 0 n/8] (n = 1-8). This is in contrast to other ternary transition metal nitrides which exhibit much more ordered nitrogen positions with 3-fold symmetry around the c-axis. The distance between sites in the Patterson diffraction map is too small to allow for total occupation of all the sites. The partial occupancy therefore required could reasonably arise through severe disorder of the nitrogen planes caused by stacking faults along the c-axis.

The presence of 6-fold symmetry of nitrogen electron density around the c-axis indicate an almost complete disorder along the c-axis between the A and B positions of the nitrogen close packed planes. Such disorder could be affected while still maintaining the integrity of the highly covalent WN_2 sheets and without significantly affecting the unit cell by translation of one or more nitrogen close-packed planes by [1/3 1/3 0]. Such translation could be easily rationalized by the presence of tungsten in the iron layer of the structure. Tungsten(II) is significantly larger than iron(II) and would prefer trigonal prismatic coordination over octahedral. If the concentration of tungsten in the octahedral layer is sufficiently large, this preference could be accommodated by translation of one of the adjacent nitrogen planes [1/3 1/3 0], creating the necessary structural disorder, which could be responsible for the broadening of the peaks with [hkl] $l{\neq}0$. Additional heating of up to 96 hrs. does not result in any significant sharpening of the [hkl] $l{\neq}1$ peaks.

Despite the difficulty in satisfactorily refining the structure of $(Fe_{0.8}W_{0.2})WN_2$, the magnetic and electronic properties exhibited by the material are consistent with other members of this family of compounds. $(Fe_{0.8}W_{0.2})WN_2$ exhibits poor metallic conductivity (Figure 3.2.12), though the measurements are not well behaved and exhibit multiple discontinuities. It is entirely likely that the iron tungsten material is slightly unstable to the silver paint used to mount the material. In any case, the variations in the

data are most likely due to faulty electrode contacts and the conductivity of the bulk material is undoubtedly higher.

As with many other ternary transition metal nitrides, $(Fe_{0.8}W_{0.2})WN_2$ exhibits paramagnetic behavior with little temperature dependence. However, unlike the other known iron containing ternary transition metal nitrides ($FeWN_2$ and $(Fe_{0.8}W_{0.2})WN_2$), this materials does not exhibit anti-ferromagnetic behavior at low temperatures. There is a slight deviation in the susceptibility at approximately 50 K, but a satisfactory explanation for this deviation has not been obtained.
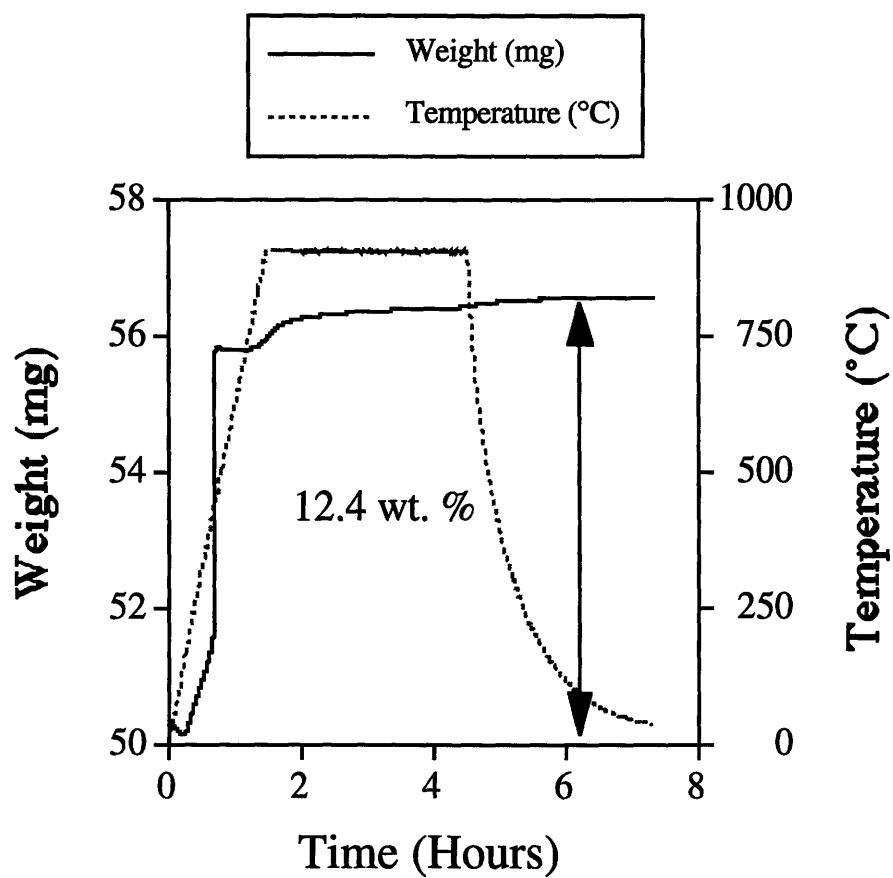
Figure 3.2.9: Thermogravametric data for $(Fe_{0.8}W_{0.2})WN_2$.
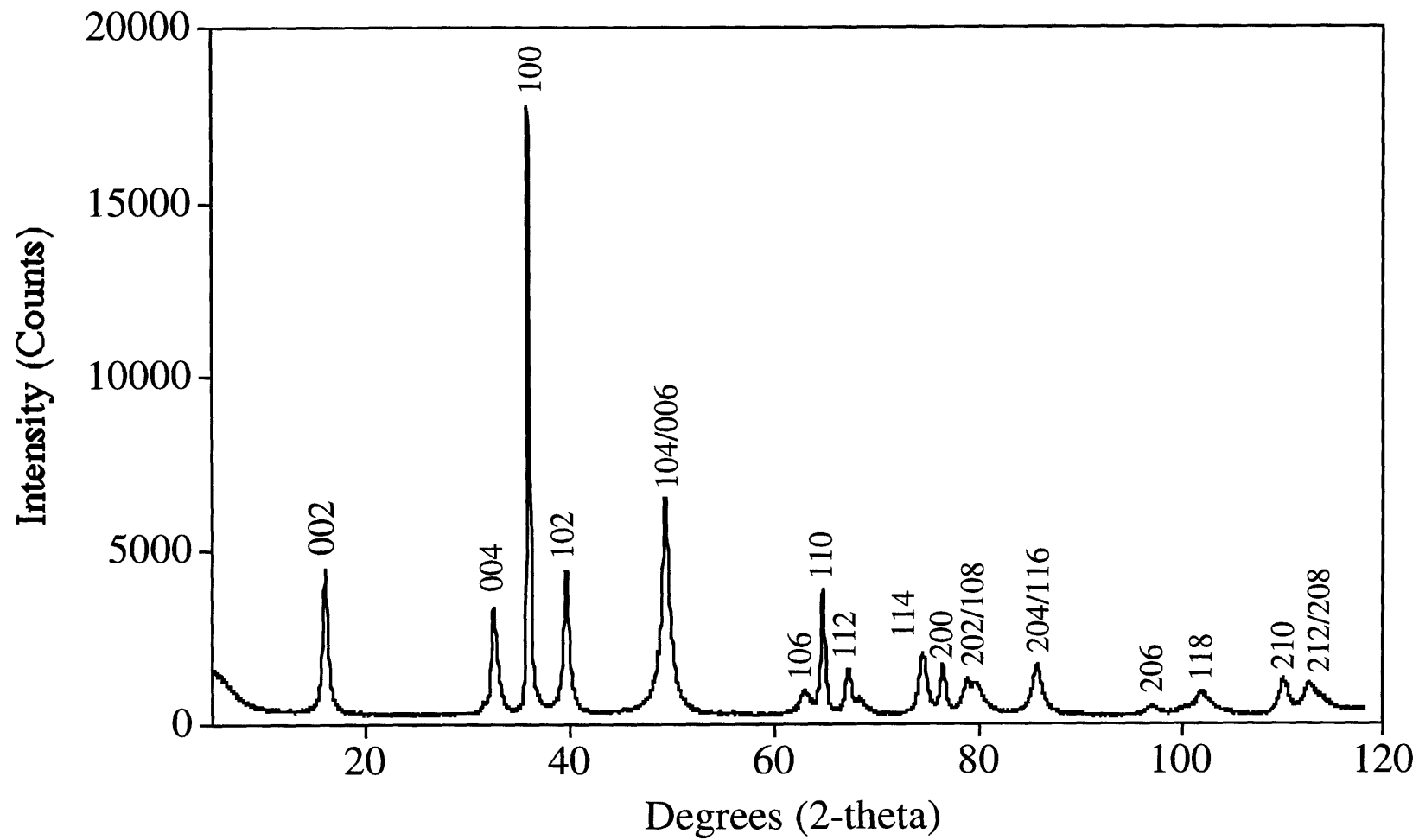
Figure 3.2.10: Powder X-ray diffraction pattern of $(Fe_{0.8}W_{0.2})WN_2$.
Numbers over peaks indicate hkl values.
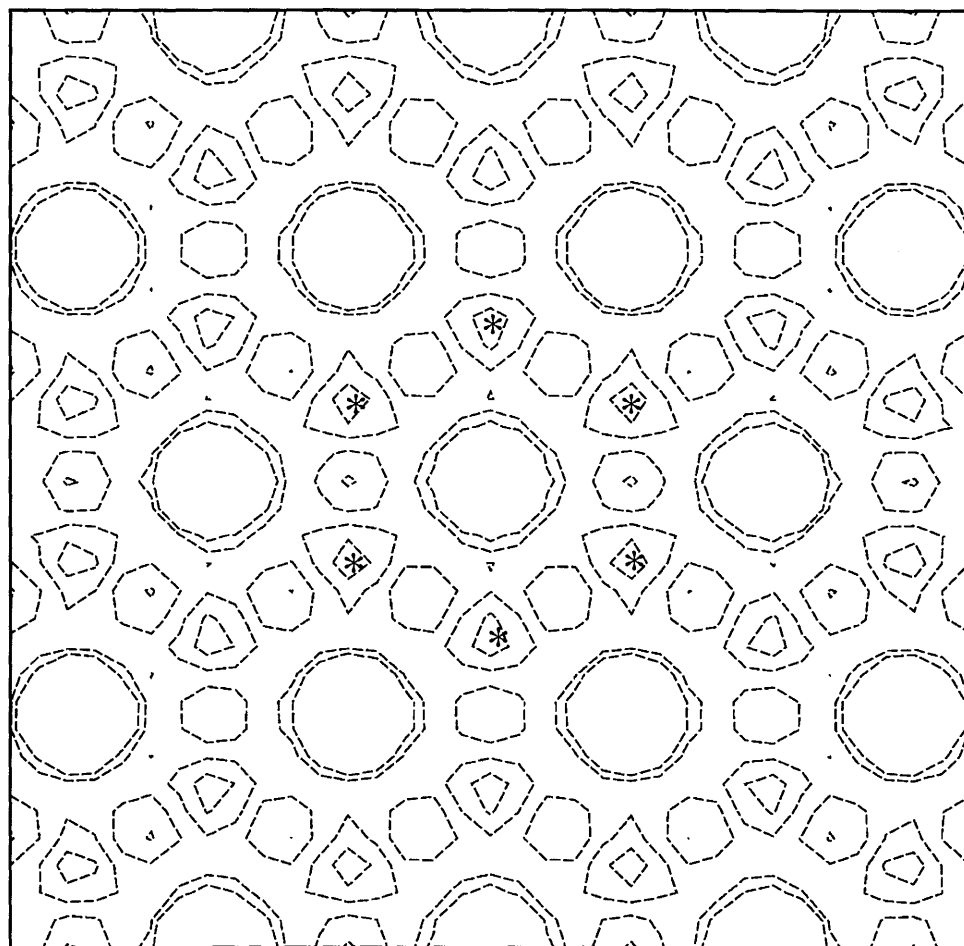
Center of reference
   0.000 0.000 0.625
Height above center
     0.000 A
Map size   10.000 A
Orientation matrix
     U   V   UXV
  0.3477 0.2007 0.0000
  0.0000 0.4015 0.0000
  0.0000 0.0000 0.0912
Contours are drawn at
  -0.30   -0.20   -0.10
   0.00
Times   0.1E+0

Figure 3.2.11: Patterson map of $(Fe_{0.8}W_{0.2})WN_2$ in 0 0 5/8 plane.
* - indicate possible positions for N.

Table 3.3: Proposed atomic positions for $(Fe_{0.8}W_{0.2})WN_2$.

Atom	Wyckoff	x	y	z	Occupancy
Fe	2b	0	0	1/4	0.8
W	2b	0	0	1/4	0.2
W	2a	0	0	0	1
N	4f	1/3	2/3	1/8	1
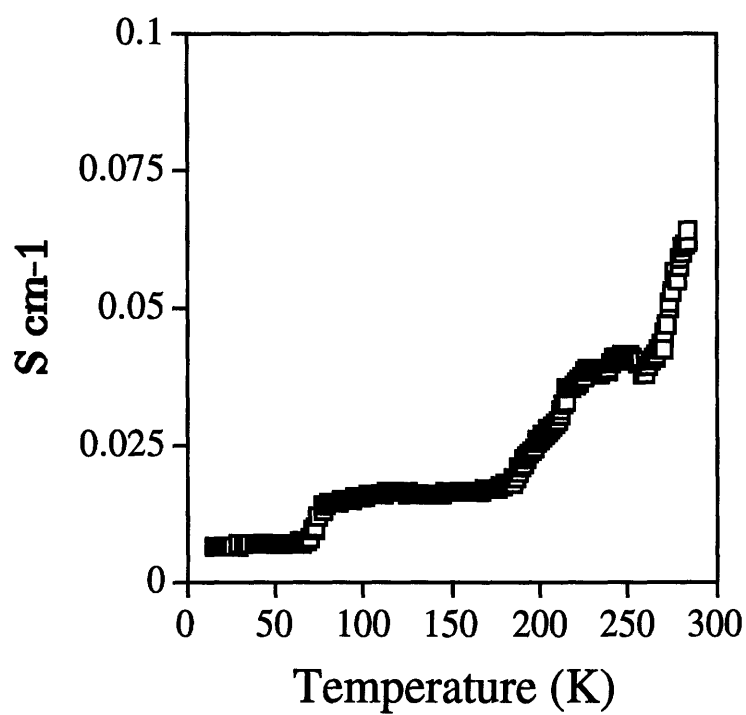
Figure 3.2.12: Electrical conductivity of (Fe$_{0.8}$W$_{0.2}$)WN$_2$.
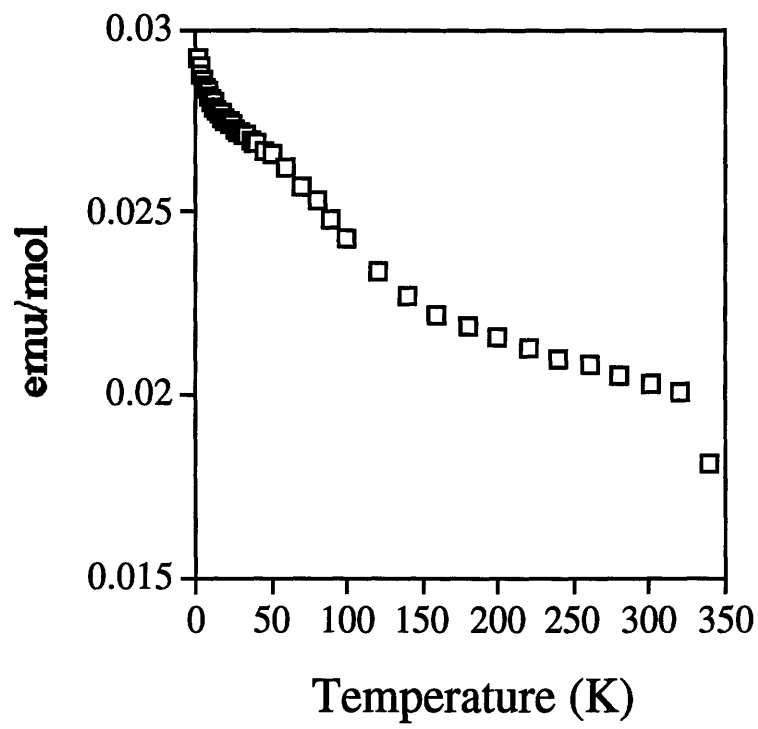
Figure 3.2.13: Magnetic susceptibility of $(Fe_{0.8}W_{0.2})WN_2$ at 5 kG.

3.3 LIMITATIONS OF THE OXIDE PRECURSOR METHOD

3.3.1 Introduction

As work in our group and others has progressed, the limitations of oxides as precursors for the synthesis of nitride materials are beginning to become clear. Some of these limitations, such as the structural disorder found during the characterization of $(Fe_{0.8}W_{0.2})WN_2$, are more a consequence of the nitride formed than of the use of oxide precursor. However, other limitations are fundamentally tied to the use of oxide precursors. Foremost among these is the incomplete removal of oxygen from the product. Even in the ternary nitride species discussed in Section 3.2, trace amounts are always present. If the oxygen content of the product is high, it becomes more useful to discuss the material as an oxynitride than as a nitride with oxygen impurities. While the incomplete formation of nitride materials from oxide precursors can be frustrating, the oxynitrides which are formed can have interesting and useful properties. In the following section, the formation of one family of oxynitride materials will be discussed in detail, along with potential technological applications of this material. In further sections the ammonolysis reactions of numerous systems, both those tried in this group and in others will be explored. From these experiments, trends will be drawn in order to determine possible future avenues for research involving oxide precursors.

3.3.2 $LiTaO_{3-3x}N_{2x}$

3.3.2.1 The Chemistry of Oxynitrides

The ammonolysis of oxide precursors, has led to the synthesis of a large number of new nitride and oxynitride materials, the latter being the result of the incomplete ammonolysis of the oxide starting material[5,7,8,23-25]. For some

elements, such as tantalum, there exists a rich oxynitride chemistry, which can be accessed by incomplete nitridation of metal oxides.[26] While many nitride structures are unique and different from those of oxides, some oxynitrides take on structures commonly found in oxides. For example, when $La_2W_2O_9$ is reacted with ammonia, the resulting product $(LaW(O,N)_3)$ has the perovskite structure[8,23]. In fact, the substitution of only small amounts of nitrogen (< 5 wt. %) for oxygen could occur with retention of the oxide structure. While the structural effects of such small doping levels can be almost insignificant, the effect of nitrogen substitution on the electronic properties can be quite large. For example, the magnetism of the nitrogen-doped rare-earth iron magnets is greatly enhanced over that of the metal alloys. [27]

As was presented in Chapter 2, we have been exploring the use of tantalum oxides as precursors to ternary tantalum nitrides. $LiTaO_3$ is an attractive starting material for nitride synthesis through oxide ammonolysis, because it is readily available and relatively inexpensive. Furthermore, Li_2MoO_4 and Li_2WO_4 have been reacted successfully with flowing ammonia to form the ternary nitrides $LiMoN_2$[2] and $LiWN_2$[3]. Also, the theoretical ammonolysis in which $2N^{3-}$ are substituted for $3O^{2-}$ (Eq. 3.1), would maintain the highly-stable +5 oxidation state for tantalum and would be expected to be favorable.

$$\text{Eq. 3.1} \qquad LiTaO_3 \xrightarrow{\ NH_3\ } LiTaN_2 + 3H_2O \uparrow$$
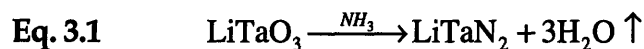
However, complete ammonolysis of the precursor could not be achieved. In this section, the synthesis of a new highly colored lithium tantalum oxynitride material, formed by a slight substitution of nitrogen for oxygen with retention of the oxide precursor structure, is discussed.

3.3.2.2 Synthesis and Characterization of $LiTaO_{3-3x}N_x$

$LiTaO_{3-3x}N_{2x}$ was synthesized by reacting $LiTaO_3$ (Johnson-Matthey Specialty Products, 99.998%) with anhydrous ammonia (160 cc/min.) in a gas

flow-through system (**Figure 2.2.1**) between 500°C and 900°C for 12 hours and was then quenched by turning off and opening the furnace. The ammonia was used as received and not dried further. X-ray diffraction analysis of all the lithium tantalum oxynitride products was performed on a Siemens D5000 diffractometer with Cu Kα radiation (λ = 1.54184 Å). Nitrogen analysis was performed by two methods, C,H,N combustion analysis (Oneida) and thermogravimetric (TGA) measurements on a Cahn thermogravimetric analyzer. Magnetic measurements were carried out on a Quantum Design SQUID magnetometer at temperatures ranging from 5 to 300 K in an applied field of 40 kG. Four-probe electrical conductivity measurements were performed on a pressed pellet using a Keithley 238 source measure unit, a Lake Shore 330 autotuning temperature controller and a Leybold RW3 cryo-refrigerator. Diffuse reflectance measurements were performed on a Lambda 9 diffuse reflectance spectrometer.

3.3.2.3 Results and Discussion

All reaction temperatures, ranging from 500°C to 900°C, resulted in a highly colored, free-flowing powder.[28] The color of the product, which depends critically on the reaction temperature and consequently the nitrogen content, ranges from tan at 500°C to bright orange at 700°C to red at 850°C (Table 3.4 and Figure 3.3.1). A dependence of product color on nitrogen content has been reported previously in other tantalum nitrides. For example, during the ammonolysis of Ta_2O_5 to form Ta_3N_5, color changes of the reaction product are observed as a function of the nitrogen content of the intermediates.[29] In this ammonolysis, the color changes from white to green to yellow-brown to red-brown to, finally, the red color of Ta_3N_5.

The investigation of the $LiTaO_3$ ammonolysis by powder X-ray diffraction analysis reveals that at temperatures of less than 700°C, the diffraction pattern of the product is unchanged from that of the $LiTaO_3$ starting material. At 700°C, small amounts of Ta_3N_5 begin to appear in the

diffraction pattern (Figure 3.3.2), eventually becoming the dominant phase at 800°C. By 900°C, the only phase present by X-ray diffraction is the blue-black cubic TaN. The products prepared at all temperatures appear to be quite stable to both air and water. Samples show no detectable decomposition even after exposure to air and sunlight for more than one year. Interestingly, the orange color of the 700°C product is retained even after a 400°C heat treatment in air for several hours.

Nitrogen analysis of the orange product (700°C) was performed by two methods, C,H,N combustion analysis and thermogravimetric (TGA) measurements. Combustion analysis (Oneida) indicates 1.15 weight percent nitrogen in the orange product, which corresponds to an elemental composition of $LiTaO_{2.712}N_{0.192}$. TGA experiments performed under oxygen show a weight gain of 0.724 weight percent to yield a white product ($LiTaO_3$ by powder X-ray diffraction). Assuming a 2:3 nitrogen for oxygen exchange, this weight gain corresponds to an initial nitrogen content of 1.23 weight percent ($LiTaO_{2.743}N_{0.171}$), which is consistent with the nitrogen content established by combustion analysis. The reversibility of the nitrogen substitution reaction at temperatures less than 700°C indicates the facility of nitrogen for oxygen exchange in this material.

Magnetic susceptibility measurements reveal that the orange 700°C product is diamagnetic (Figure 3.3.3). The diamagnetism demonstrates that the striking color of the product cannot be the result of a reduced metal center, and further supports the substitution of nitrogen for oxygen with maintenance of the overall structure. In addition, conductivity measurements demonstrate that the orange tantalum oxynitride (700°C) is a highly insulating material with a conductivity near the detection limit of the measurement apparatus (10^{-12} S/cm, Figure 3.3.4).

While the magnetic susceptibility, conductivity and nitrogen content do not rule out the possibility of a mixed phase product, the diffuse reflectance measurements strongly indicate the presence of a single oxynitride

product at temperatures less than 700°C (Figure 3.3.5). At 600°C, a strong transition in the visible at 2.36 eV (525nm), which is significantly lower in energy than the absorption band in $LiTaO_3$ (400nm or 3.10 eV)[30], is observed. Importantly, at this temperature, no other phases are evident in the powder X-ray diffraction pattern and the absorption band of Ta_3N_5 is not detected in the reflectance measurements. The presence of significant amounts of nitrogen in the product suggests that the 2.36 eV absorbance arises from the doping of nitrogen states into the band gap of $LiTaO_3$. With increasing reaction temperature, the peak of this absorption is shifted increasingly to higher wavelength and a shoulder appears, which presumably is due to the presence of Ta_3N_5 in the final product. Such a shift in the position would be expected with increasing nitrogen doping creating additional states within the $LiTaO_3$ bandgap. In addition, the strength of the 2.36 eV transition is consistent with a symmetry allowed charge transfer from localized nitrogen p states to a band of predominately metal d character.

Below 700°C, incorporation of small amounts of nitrogen into $LiTaO_3$ results in a significant change in the absorption band edge, as evidenced by the diffuse reflectance spectrum, without any significant concomitant structural changes. The extremely low electrical conductivity, the diamagnetism and the shift in the absorption peaks are all consistent with the presence of a few nitrogen centers that generate the intense absorbance at 2.36 eV, while retaining the highly insulating nature of the starting material. The presence of increasing amounts of Ta_3N_5 above 700°C results in a shoulder in the absorbance spectrum and changes the color from tan to an extremely bright orange color and, at higher temperatures, to the dark red color of Ta_3N_5. During the higher temperature ammonolysis reaction, excess lithium is removed from the final product through evaporation as Li_2O.

$LiTaO_3$ is, depending on the method of preparation and the handling, either white or light yellow, which is consistent with its absorption transition on the edge of the visible spectrum. It appears that the substitution of the

softer, less electronegative N^{3-} for O^{2-}, introduces localized states into the structure, which results in the lowering of the band gap from the edge of the visible to 600 nm. This substitution of N^{3-} for O^{2-}, when taken to extreme, can result in the formation of Ta_3N_5, with an even smaller band gap and a deep reddish-purple color[31].

The study of oxynitride materials is by no means new. The oxynitride material discussed in this section only serves to underscore the difficulty in obtaining phase-pure and oxygen-free nitride materials from oxide precursors. The difficulty in obtaining a fully nitrided material from $LiTaO_3$ is perhaps not surprising since the free energy of reaction for the formation of Li_3N from Li_2O is prohibitively high (+640 kJ/mol at 1000 K[32]). Indeed, it is perhaps surprising that some lithium containing ternary oxides (Li_2WO_4 and Li_2MoO_4) can be completely converted into ternary nitride materials. A closer examination of trends in nitride and oxynitride synthesis from oxide precursors is warranted.
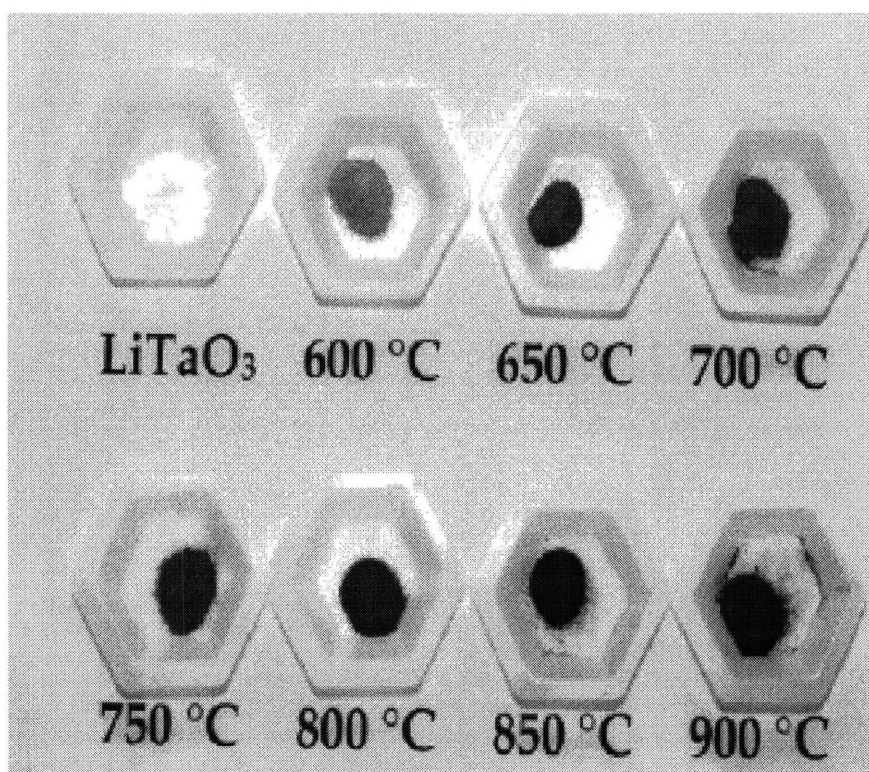
Figure 3.3.1: Color change of LiTaO$_3$ ammonolysis product with temperature.
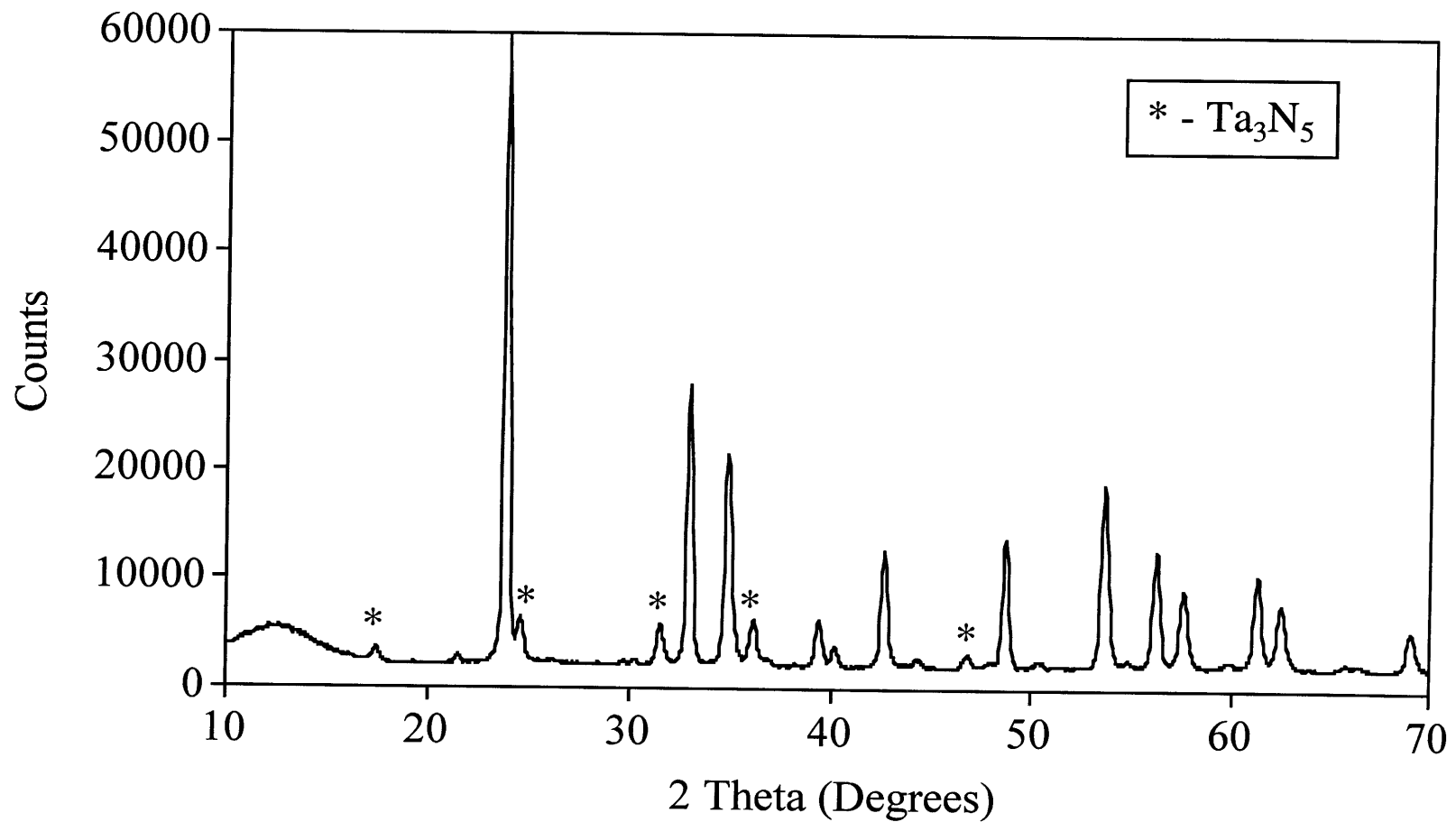
Figure 3.3.2: Powder X-ray diffraction pattern of the 700°C ammonolysis product of LiTaO$_3$.
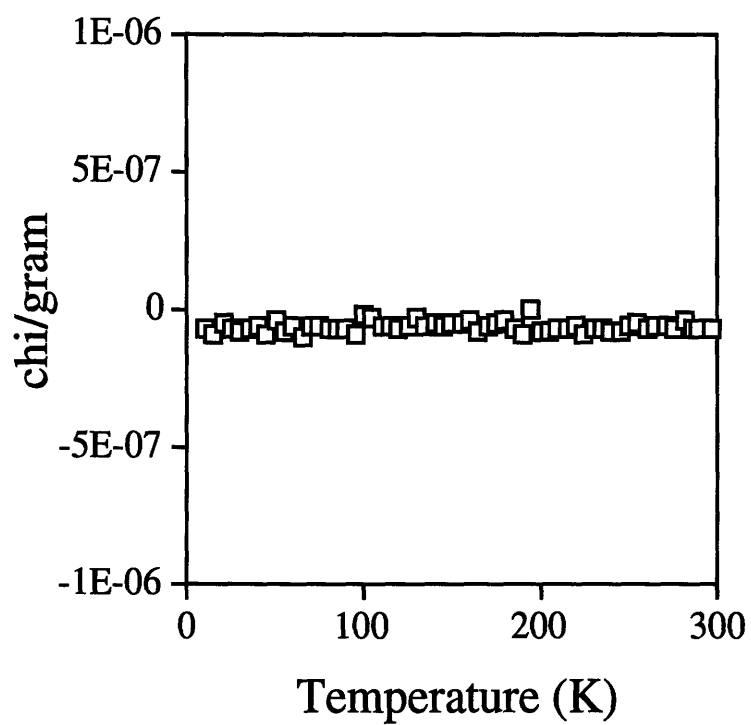
Figure 3.3.3: Temperature dependent magnetic susceptibility of the 700°C ammonolysis product of LiTaO$_3$.
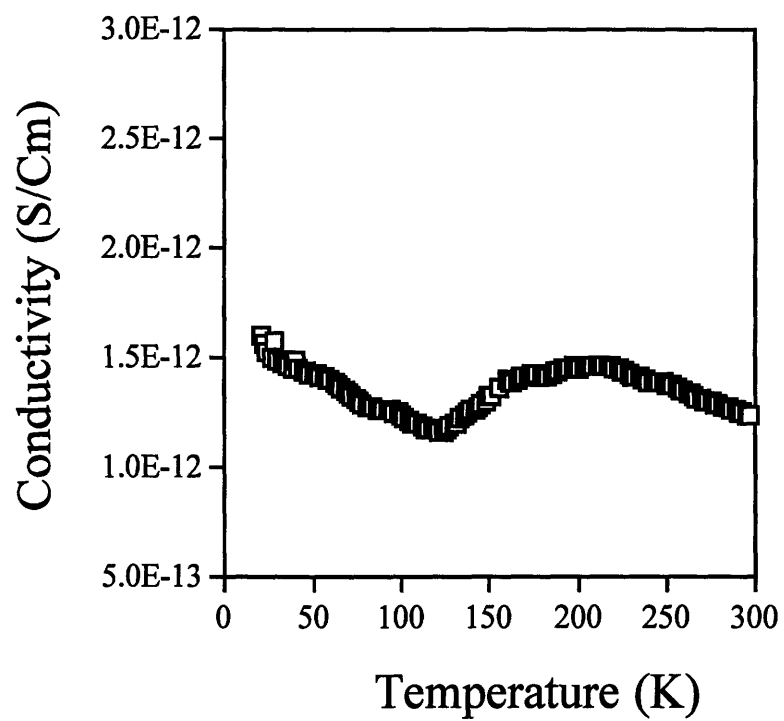
Figure 3.3.4: Electrical conductivity of the 700°C ammonolysis product of LiTaO₃.
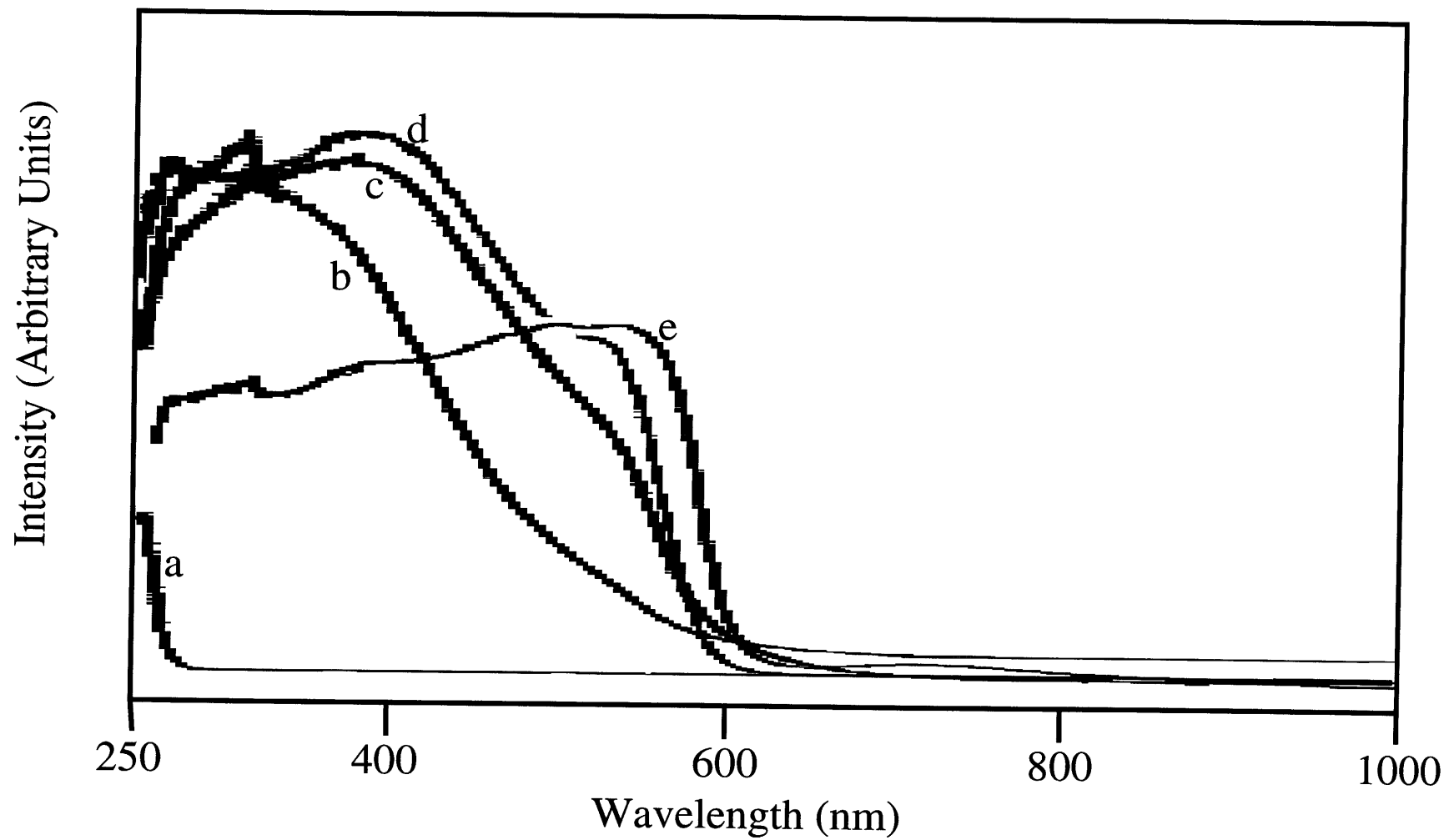
Figure 3.3.5: Diffuse reflectance spectra of colored products.
(a) LiTaO$_3$, (b) 600°C ammonolysis product, (c) 650°C ammonolysis product, (d) 700°C ammonolysis product, (e) Ta$_3$N$_5$.

Table 3.4: Color change of ammonolysis product of $LiTaO_3$ with synthesis
temperature.
A = oxynitride product.

Ammonolysis Temperature (°C)	Product Color	Product Composition	Nitrogen Weight Percent
600	Tan	A	0.98%
650	Light Orange	$A+Ta_3N_5$	0.65%
700	Orange	$A+Ta_3N_5$	1.15%
750	Orange	$A+Ta_3N_5$	2.49%
800	Red-Orange	$A+Ta_3N_5$	6.57%
850	Red	Ta_3N_5	-
900	Blue-Black	TaN	-

3.4 THE FUTURE OF OXIDE PRECURSORS

3.4.1 Introduction

In recent years, a number of oxynitride materials have been made from ammonolysis reactions of ternary oxide materials. Some of these materials such as $LaWO_{0.6}N_{2.4}$[8] (Perovskite), $Ln_2Ta_2O_5N_2$[7] (Pyrochlore), $BaTaO_2N$[33] (Perovskite), $Na_4MO_2N_2$ (M = W and Mo)[34] (Na_4CoO_4-type), and $KOsO_3N$[35] (Scheelite) form in specific stoichiometries due to the stability of the simple salt-like structures. Others, such as the lithium tantalum oxide discussed in the previous section, can form with a range of stoichiometries (i.e. $Li_{2-x}Nb_{2+x}O_yN_{4-y}$ ($0 \le x \le 0.31$ - $0.46 \le y \le 1.46$)[36] and $AZr_xTa_{1-x}O_{2+x}N_{1-x}$ (A = Ca, Sr, Ba and $0 \le x \le 1$)[25]). From these experiments, as well as additional experiments performed in this group, trends can be drawn about the ammonolysis reaction of oxide precursors.

3.4.2 Ammonolysis Experiments

Ammonolysis experiments of a number of ternary oxide precursors were carried out in a manner similar to that described in previous sections and are listed in Table 3.5. None of these experiments produced either single phase nitride or oxynitride materials. However, taken together with the inability to convert tantalate and niobate precursors into ternary nitride materials in an analogous fashion to that seen for molybdate and tungstate precursors, some insight into the limitations of the oxide precursor method is obtained. Successful ammonolysis reactions to form ternary nitride materials parallel the ease with which binary nitrides can be made through ammonolysis. In Figure 3.4.1, the periodic table is broken down according to the ability of the metal oxide to be converted to a metal nitride through reaction with ammonia. As can be seen from the table, elements which form ternary transition metal nitrides, namely combinations of Mo/W with

Mn/Fe, also have binary oxides which can be easily converted into binary nitrides. Niobium and tantalum form the boundary between those elements which will form ternary nitride materials and those which do not. The binary oxides of both elements can be converted into binary nitrides, but only at relatively high temperatures, approaching or exceeding 1000 °C. Also, both elements exhibit extensive oxynitride chemistry, which is indicative of the difficulty in affecting full nitridation. As evidenced in our experiments, the ammonolysis reactions of ternary oxides containing niobium and tantalum proceed only with difficulty, requiring high temperatures and long reaction times. However, even under these harsh conditions an oxygen-free product cannot be obtained and phase separation can occur.

Ammonolysis reactions of the group III and group IV elements are even more complex. At sufficiently high reaction temperatures (> 1000 °C), the ammonolysis reactions of MO_2 (M = Ti, Zr, Hf) become thermodynamically favorable. However, the kinetic barrier to the reaction is so large as to make ammonolysis impossible except on exceptionally fine oxide particles.[37] For elements in group I-III, the ammonolysis reaction is thermodynamically unfavorable and no nitride products can be formed from the binary oxides. As expected based on these trends, ammonolysis reactions of ternary oxide precursors (with the exception of ternary oxides containing lithium) which contain group I-IV elements result either in oxynitride formation or binary decomposition products.

The binary nitrides of the later transition metal elements exhibit progressively less thermodynamic stability going to the right and down the periodic table. The instability of the late transition metal nitrides has been attributed to the greater cohesive energy of the metallic elements (the heat of sublimation of Mg at 0 K is 145 kJ mol^{-1}, while for Ni it is 428 kJ mol^{-1}),[38] which results in progressively lower decomposition temperatures. In particular, the 4d and 5d elements of groups VIII-X have no known binary nitride, with the possible exception of silver. However, the reported binary nitride of silver is extremely unstable and decomposes explosively when

dried. In addition, nitrogen can donate electrons which fill the anti-bonding d-states and destabilize the nitride structure, a problem which is more severe for later transition metals with higher valance electron counts.

For the synthesis of ternary nitrides, a similar trend is observed. As is seen in Table 3.1, iron and manganese tungstates are readily converted into ternary nitrides under ammonia. However, for the tungstates of the later transition metal elements, precursor decomposition into the late transition metal and tungsten nitride is observed. The most notable example of the ammonolysis of late transition metal containing oxide precursors is the reported formation of $CoWN_2$ and $NiWN_2$ from $CoWO_4$ and $NiWO_4$.[39] In both these experiments, a poorly crystalline phase is obtained which can be indexed to a cell similar to that found for $FeWN_2$. However, the products contain a significant amount of metallic Co and Ni respectively. From the powder X-ray diffraction data, the nickel tungsten nitride contains more metal impurity than the cobalt sample as would be expected from the decrease in the thermal stability of the nitrides going to the right across the transition metals.

Similar trends are observed in the group XIII and XIV elements. Oxides of the 2p and 3p elements exhibit significant thermodynamic and kinetic stability. Conversion of their oxides into nitride materials is extremely difficult both thermodynamically and kinetically, often requiring high reaction temperatures. For the 5p and 6p elements, the nitrides become thermodynamically unstable with respect to disproportionation to the metal and nitrogen. When ternary oxides containing group XIII and XIV elements are used as precursors, they exhibit similar behavior (Table 3.5). Precursors which contain 2p and 3p elements are prone to decomposition to give the 2p/3p oxide (Eq. 3.2), while the 5p/6p elements reduce to the metal (Eq. 3.3). For example, $SnWO_4$ reacts very readily with ammonia to yield metallic tin and tungsten oxide.

$$\text{Eq. 3.2} \qquad Al_2W_3O_{12} \xrightarrow{\ NH_3\ } W_2N + Al_2O_3$$

Eq. 3.3 $\qquad SnWO_4 \xrightarrow{\quad NH_3 \quad} Sn + W_2N$
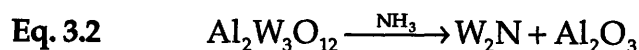
These trends suggest several possible avenues for further research in the synthesis of nitrides using oxide precursors. The first, an avenue which was explored briefly, is to try to extend the currently known systems of ternary nitride materials to include cobalt and nickel containing systems. As successively later transition metals are placed into this family of compounds, the Fermi level is raised by the additional electron. Work presented in this thesis as well as elsewhere demonstrates the ability of other ternary transition metal nitrides with nickel arsenide related structures to be made with a metal stoichiometry other than 1:1 through substitution of tungsten or molybdenum onto the octahedral site. These facts suggest the possibility that ternary transition metal nitrides containing cobalt and nickel can be made with partial occupancy of the octahedral sites by molybdenum or tungsten, which would lower the total valence electron count and stabilize the structure. Indeed, some evidence for the existence of these systems is present in the literature. As mentioned earlier, the reaction of $CoWO_4$ with ammonia yields a poorly crystalline phase[39] which bears some resemblance to $FeWN_2$. In addition, a significant amount of cobalt metal impurity is found in the diffraction pattern indicating the non-stoichiometric nature of the product. A similar nickel phase has been made, with an even larger amount of nickel impurity, as would be expected from a structure which is destabilized by the additional electrons on Ni. If suitable precursors could be prepared, clean cobalt and nickel tungsten/molybdenum nitrides might be prepared where the ratio of M:M' (M = molybdenum or tungsten, M' = cobalt or nickel) is greater than one.

A second avenue which could be followed is to prepare high surface area oxide precursors to help overcome some of the kinetic limitations present in ammonolysis reactions of the Group IV and V elements. Perhaps the most convenient method would be the synthesis of a xerogel or some analogous high surface area precursor containing two transition metals. Flash ammonolysis experiments should then be run in order to maintain the

benefits of high surface area. Such precursors could also help alleviate several of the problems which are observed in the ammonolysis reactions of ternary metal oxides containing group V elements. Most notably, the kinetic barriers which often result in long reaction times, incomplete removal of oxygen from the product and phase separation could be overcome by decreasing the ammonia diffusion distance using high surface area precursors.

Finally, the synthesis of fully nitrided materials could be abandoned in favor of oxynitride materials. The formation of oxynitride materials could probably be obtained at temperatures comparable to or lower than the moderate temperatures listed earlier for ternary nitride formation. However, product characterization, as is evidence by this thesis, can be enormously complex due to the similarities between nitrogen and oxygen, especially to X-ray diffraction, and the lack of accurate methods for detection of large amounts of oxygen in a product. The experimental difficulties associated with the characterization of oxynitride products has limited the work done in the field and many interesting materials are yet to be discovered.

The strategy for the synthesis of oxynitride materials would differ slightly from that used for the synthesis of fully nitrided materials. To synthesize oxynitride materials, a group I-IV element should be grouped in the precursor with an element that is easily nitrided. Indeed, this approach has yielded such materials as $BaTaO_2N$[33] and $Na_4MO_2N_2$ (M = W and Mo),[34] which also could be written as $(BaO)(TaON)$ and $(Na_2O)_2(MN_2)$. When written in this fashion, the composition can seen to consist of groups of oxides which cannot be converted into nitrides under ammonolysis conditions (BaO and Na_2O), those which are converted with difficulty ($Ta_2O_5 + 2NH_3 \rightarrow 2TaON + 3H_2O$) and those which can be converted easily to nitride materials ($MO_3 + 2NH_3 \rightarrow MN_2 + 3H_2O$, M = W and Mo). Many other systems could be used as precursors to oxynitride formation. For example, a precursor such as $LaW_2O_{7.5}$ might yield a fluorite-type nitride ($LaW_2N_3O_3$). Many similar systems could be imagined. Indeed, in work

carried out in this lab, the ammonolysis reactions of $BaWO_4$ and $BaMoO_4$ appear to yield at least one new phase. Figure 3.4.2 shows the powder X-ray diffraction pattern $BaWO_4$ after 12 hours of heating under flowing ammonia at 700°C. Clearly this powder pattern consists primarily of one phase which can be indexed as orthorhombic (a=9.889(3), b=2.992(1), c=2.1201(6)). However, the product decomposes at higher temperatures and longer reaction times, as is seen in Figure 3.4.3. Although several reaction temperatures and dwell times were tried, none of the phases were obtained cleanly and subsequent work on these materials was abandoned.

Table 3.5: Summary of ammonolysis experiments.

Reactants	Temperature	Products
$FeSiO_3$	700°C	$Fe + SiO_2$
$CoSiO_3$	700°C	$Co + SiO_2$
$MnSiO_3$	700°C	$MnO + SiO_2$
$NaVO_3$	700°C	$Na_3VO_4 + VN$
$LiNbO_3$	700°C	$LiNbO_3 + Nb4N_3$
$MnTa_2O_6$	900°C	$MnO + MnTa_2O_6 + Ta_3N_5$
$TiTa_2O_7$	900°C	$TiN + Ta_3N_5$
$CuTa_2O_6$	700°C	$Cu + Ta_3N_5$
$ScTaO_4$	900°C	$Sc_2O_3 + Ta_3N_5$
$MgMoO_4$	800°C	$MgO + Mo_2N$
$ZnWO_4$	700°C	$Zn + W_2N$
$SnWO_4$	700°C	$Sn + W_2N$
$Al_2W_3O_{12}$	700°C	$Al_2O_3 + W_2N$
$La_2W_3O_{12}$	900°C	$La_2O_3 + W_2N$
$MgWO_4$	800°C	$MgO + W_2N$
$MnRe_2O_8$	700°C	$MnO + Re$
$FeRe_2O_8$	900°C	$Fe_3N + Re$
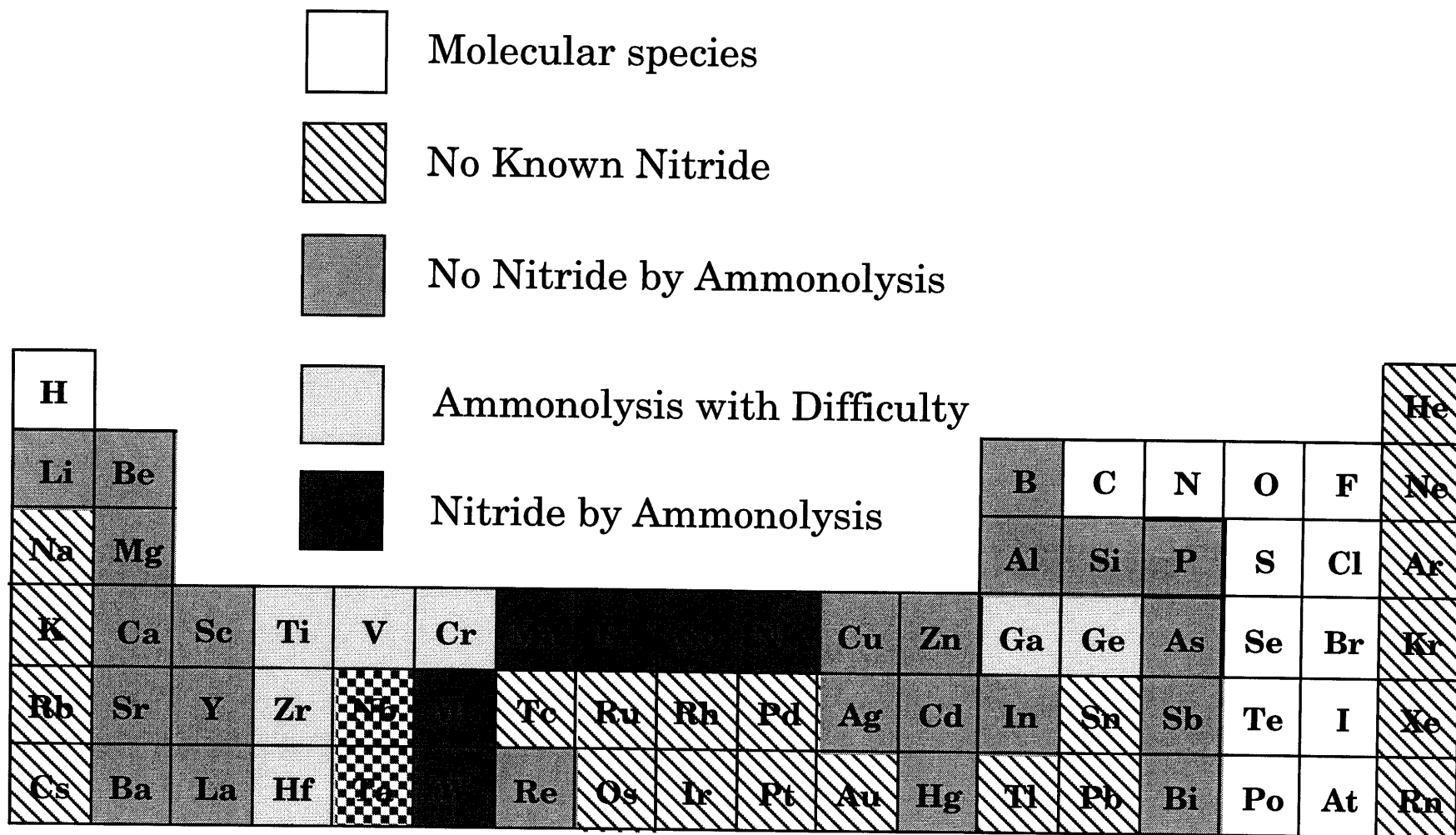
Figure 3.4.1: Periodic table indicate ease of ammonolysis reaction of binary metal oxides.
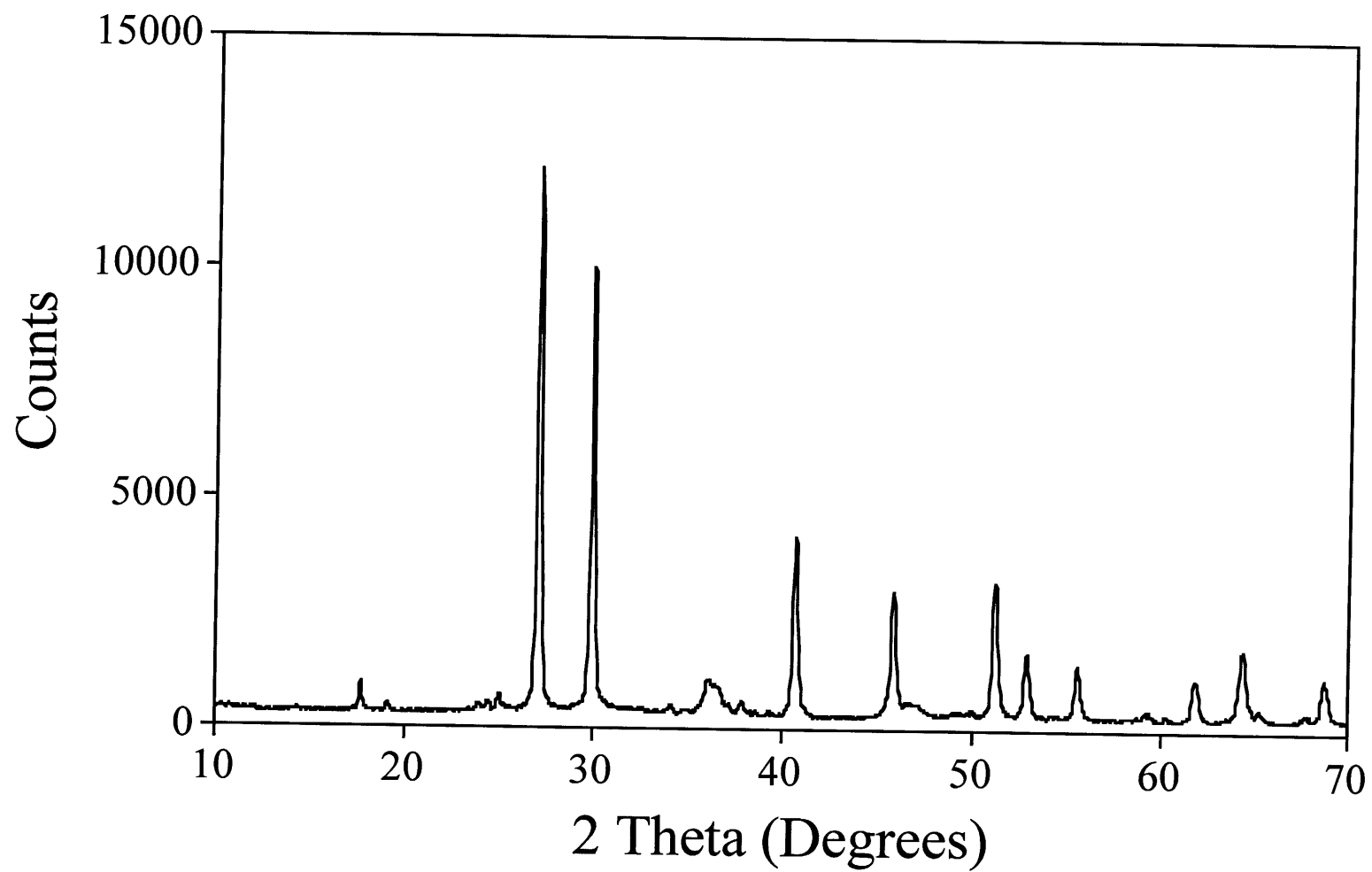
Figure 3.4.2: Ammonolysis Product of BaWO$_4$ for 12hours at 700°C.
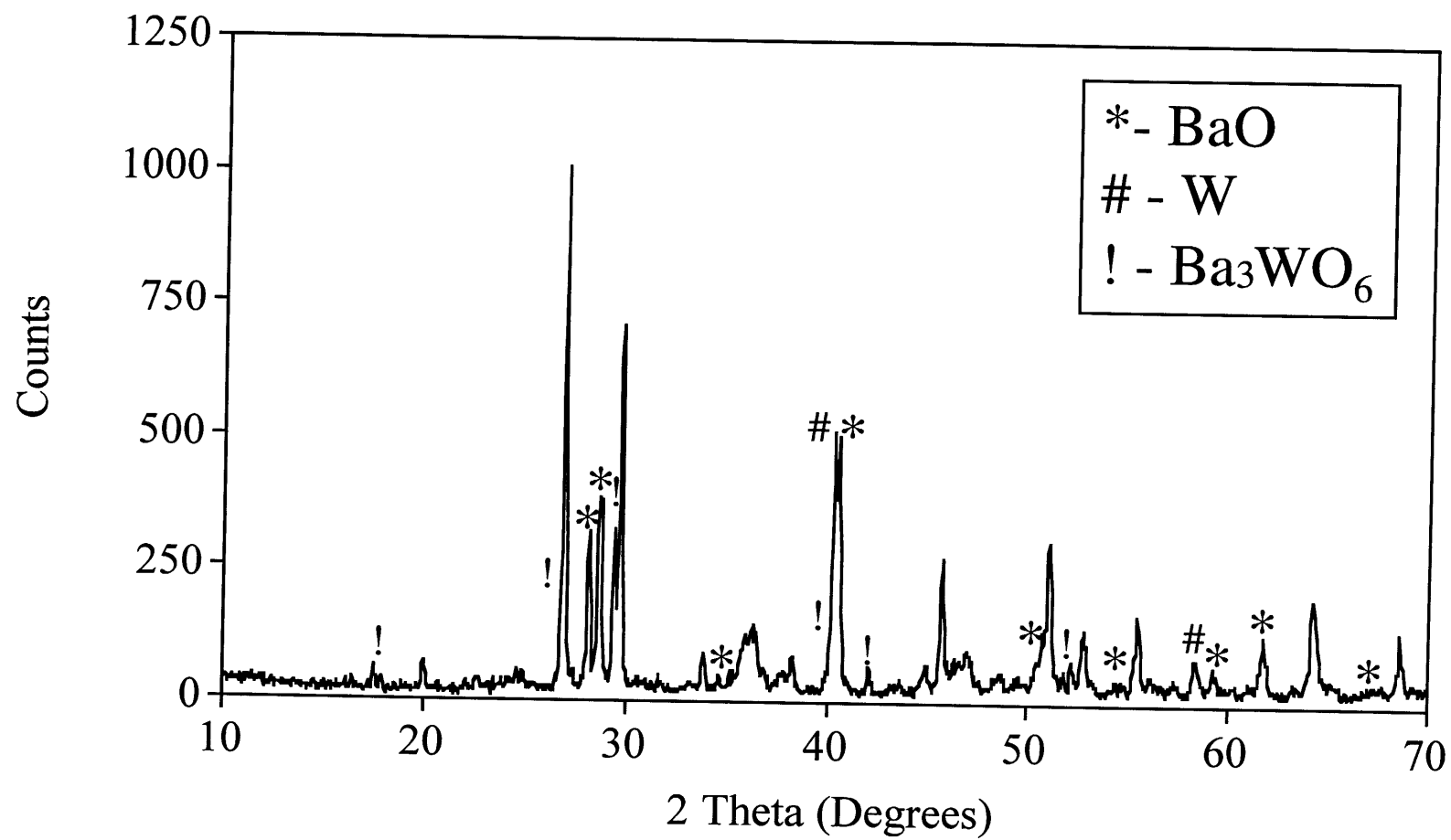
Figure 3.4.3: Ammonolysis product of BaWO$_4$ after 5 days at 900°C.

3.5 CONCLUSIONS

Clearly our understanding of oxides as precursors for the synthesis of nitride materials has progressed greatly. In addition to the synthesis of several new nitride and oxynitrides materials, limits and expectations can now be placed on future synthetic schemes. However, the possibilities for quick and easy syntheses of fully nitrided ternary materials from oxide precursors has been almost completely exhausted. It now becomes necessary to explore precursors which offer less probability for successful synthesis of fully nitrided materials or other synthesis methods.

With the limitations of the oxide precursor method now known, new methods for the synthesis of nitride materials need to be explored. In particular, an effort needs to be made to overcome some or all of the limitations present using oxide precursors, namely incorporation of oxygen, limited number of reactant elements and, in some cases, long reaction times. The remainder of this thesis will focus on one alternative technique for the synthesis of nitride materials which could overcome some of these limitations, namely the use of microwave generated nitrogen plasmas. In order to lower reaction times and raise the number of elements available for reaction, more active nitrogen species are needed. Microwave generated plasmas offer several advantages over conventional ammonolysis or nitridation reactions using ammonia. Because a plasma is composed of highly ionized particles in an electromagnetic field, individual particles (ions and electrons) are accelerated to extremely rapid speeds. These kinetically active particles have high effective temperatures and become extremely active toward nitride formation. In addition, as the surface of the reactant metal is bombarded with electrons and ions, the formation of nitride skins on the surface of the individual particles is disrupted, aiding the diffusion of nitrogen into the interior of the particles. Together, these characteristics of microwave generated nitrogen plasmas provides a source of exceptionally

active nitrogen which could be used as a synthetic tool for the synthesis of binary and ternary nitride materials.

3.6 REFERENCES

(1) Bem, D. S.; Olsen, H. P.; zur Loye, H. C. *Chem. Mater.* **1995**, *7*, 1824-1828.

(2) Elder, S. H.; DiSalvo, F. J.; Doerrer, L. H. *Chem. Mater.* **1992**, *4*, 928-937.

(3) Subramanya Herle, P.; Hegde, M. S.; Vasanthacharya, N. Y.; Gopalakrishnan, J.; Subbanna, G. N. *J. Solid State Chem.* **1994**, *112*, 208-10.

(4) Bem, D. S.; Lampe-Önnerud, C. M.; H.P., O.; zur Loye, H. C. *Inorg. Chem.* **1996**, *35*, 581-585.

(5) Marchand, R.; Laurent, Y.; Guyader, J.; L'Haridon, P.; Verdier, P. *J. Eur. Ceram. Soc.* **1991**, *8*, 197-213.

(6) Marchand, R.; Antoine, P.; Laurent, Y. *J. Solid State Chem.* **1993**, *107*, 34-8.

(7) Pors, F.; Marchand, R.; Laurent, Y. *J. Solid State Chem.* **1993**, *107*, 39-42.

(8) Bacher, P.; Antoine, P.; Marchand, R.; L'Haridon, P.; Laurent, Y.; Roult, G. *J. Solid State Chem.* **1988**, *77*, 67-71.

(9) Yu, C. C.; Oyama, S. T. *J. Solid State Chem.* **1995**, *116*, 205-207.

(10) Houmes, J.; Bem, D.; zur Loye, H. *Mat. Res. Soc. Symp. Proc. Vol. 327* **1994**, 153-64.

(11) Houmes, J. D.; zur Loye, H. C. *J. Solid State Chem.* **1996**, *Submitted,*

(12) Hibble, S. J.; Fawcett, I. D. *Inorg. Chem.* **1995**, *34*, 500-508.

(13) Meyer, G.; Hoppe, R. *J. Less-Common Met.* **1976**, *46*, 55.

(14) Pöttgen, R.; Witte, A. M.; Jeitschko, W.; Ebel, T. *J. Solid State Chem.* **1995**, *119*, 324-330.

(15) Friend, R. H.; Yoffe, A. D. *Adv. Phys.* **1987**, *36*, 1-94.

(16) Singh, D. J. *Phys. Rev. B* **1992**, *46*, 9332-9335.

(17) Massidda, S.; Pickett, W. E.; Posternak, M. *Phys. Rev. B* **1991**, *44*, 1258-1265.

(18) Jellinek, F. *J. Less-Common Metals* **1962**, *4*, 9-15.

(19) Werner, P. E.; Eriksson, L.; Westdahl, M. *J. Appl. Crystallogr.* **1985**, *18*, 367.

(20) Larson, A. C.; Lee, F. L.; Le Page, Y.; Webster, M.; Charland, J. P.; Gabe, E. J. In Chemistry Division, NRC, Ottawa, Canada, K1A 0R6.

(21) Larson, A. C.; von Dreele, R. B. In *GSAS:*Los Alamos National Laboratry: Los Alamos, NM, 1990.

(22) Harris, W. F. In *Determination of Gaseous Elements in Metals*; L. M. Melnick, L. L. Lewis and B. D. Holt, Ed.; John—Wiley and Sons: New York, 1974; Vol. 40; pp 113.

(23) Antoine, P.; Marchand, R.; Laurent, Y.; Michel, C.; Raveau, B. *Mat. Res. Bull.* **1988**, *23*, 953-7.

(24) Grins, J.; Käll, P.; Svensson, G. *J. Mater. Chem.* **1994**, *4*, 1293-301.

(25) Grins, J.; Svensson, G. *Mat. Res. Bull.* **1994**, *29*, 801-9.

(26) Brauer, V. G.; Weidlein, J.; Strahle, J. Z. *Anorg. Allge. Chem.* **1966**, *348*, 298-308.

(27) Sun, H.; Coey, J. M. D. *J. Phys.-Condens. Matt.* **1990**, *2*, 6465.

(28) Houmes, J. D.; zur Loye, H.-C. *U.S. Patent Pending*

(29) Brauer, G.; Weidlein, J. R. *Angew. Chem. inter. Ed. Engl.* **1965**, *4*, 241-2.

(30) Rez, I. S. *Bull. Acad. Sci. USSR Phys. Ser.* **1969**, *33*, 266-72.

(31) Strähle, J. *Z. anorg. allg. Chem.* **1973**, *402*, 47-57.

(32) Elder, S. H.; Disalvo, F. J.; Topor, L.; Navrotsky, A. *Chem. Mater.* **1993**, *5*, 1545-53.

(33) Pors, F.; Marchand, R.; Laurent, Y.; Bacher, P.; Roult, G. *Mat. Res. Bull.* **1988**, *23*, 1447-1450.

(34) Ostermann, D.; Zachwieja, U.; Jacobs, H. *Journal ofAlloys and Compounds* **1992**, *190*, 137-40.

(35) Laurent, Y.; Pastuszak, R.; L'Haridon, P.; Marchand, R. *Acta Cryst.* **1982**, *B32*, 914-6.

(36) Assabaa-Boultif, R.; Marchand, R.; Laurent, Y. *Ann. Chim. Fr.* **1994**, *19*, 39-44.

(37) Lengauer, W.; Wiesenberger, H.; Joguet, M.; Rafaja, D.; Ettmayer, P. In *The Chemistry of Transition Metal Carbides and Nitrides*; 1st ed.; S. T. Oyama, Ed.; Chapman & Hall: New York, 1996; pp 91-106.

(38) Brese, N. E.; O'Keefe, M. *Struct. Bonding* **1992**, *79*, 307-78.

(39) Subramanya Herle, P.; Vasanthacharya, N. Y.; Hegde, M. S.; Gopalakrishnan, J. *J. Alloy Cmpds.* **1995**, *217*, 22-24.

4. Introduction to Microwave Heating

4.1 INTRODUCTION

The microwave region of the electromagnetic spectrum (Figure 4.1.1) ranges from 1 cm to 1 m (30 GHz and 300 MHz respectively). Many of these frequencies are used for such everyday applications as telecommunications and RADAR. Of these frequencies, 2.45 GHz (12.2 cm) and 900 MHz (33.3 cm) have been set aside internationally for domestic and research use, in order to limit interference on other applications. Other frequencies may be obtained for research purposes by applying for an FCC license. Despite the limitations on frequencies available, microwaves can be effectively used to heat a wide range of materials in both the solid and liquid state and, indeed, have been used to do so since the discovery of efficient ways to produce microwaves during W.W.II. Microwaves are generated in a magnetron. In this device, electrons are accelerated from a cathode to an anode, which acts as a series of circuits tuned to oscillate at a specific frequency or its overtones. Conversion of electrical line power into electromagnetic energy using a magnetron is quite efficient, approaching 50%. In order to understand how microwaves could be used as a viable heating source for the synthesis of solid state materials and nitrides in particular, it is necessary to first understand why and how microwaves heat a substrate. Therefore, the theory of simple dielectric heating will be explained followed by the extension of this theory to include heating resulting from electrically conducting materials. Using these principles, we will examine how microwaves have been used recently to synthesize a number of solid state materials. We will then discuss, briefly, some of the basic tenets of plasma generation and how these affect the generation of nitrogen plasmas.

Frequency (Hz)
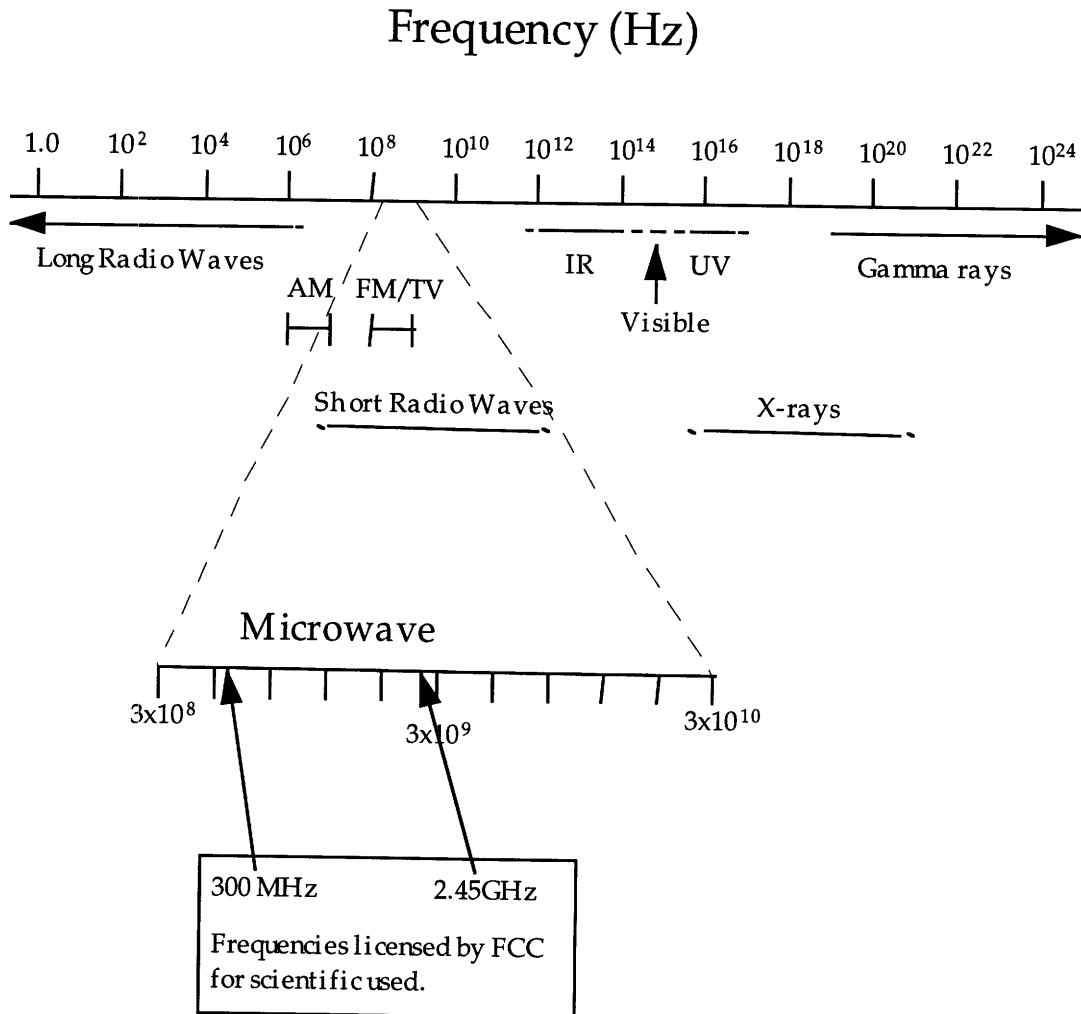
Figure 4.1.1: The electromagnetic spectrum

4.2 MICROWAVE HEATING

4.2.1 Microwave Dielectric Heating

One source of microwave heating comes from the ability of microwaves to polarize charges within a material and the inability of these charges to follow the rapid reversals of the electric field associated with the microwave radiation. As will be shown, timescales of charge reversal on the order of microwave frequency result from the necessity of overcoming potential energy barriers imposed by the surrounding medium, i.e. frictional energy losses. The lost energy is transferred to the material in the form of heat. For this treatment of dielectric heating, reviews by Caddick[1] and Mingos[2] were used extensively.

The total polarization of a material in a potential field can be described as

$$\text{Eq. 4.1} \qquad \alpha_t = \alpha_e + \alpha_a + \alpha_d + \alpha_i$$

where α_e, the electronic polarization, arises from a realignment of electrons around a nucleus (Figure 4.2.1); α_a, the atomic polarization, results from the displacement of individual nuclei (Figure 4.2.2); α_d, the dipolar polarization, results from the orientation of permanent dipoles within the material (Figure 4.2.3); and α_i, the interfacial polarization, results from the build-up of charges at the material interface. The time scales of α_e and α_a are very rapid and these components do not contribute significantly to the dielectric heating effect.

Dipolar polarization (DP) heating is not to be confused with microwave spectroscopy, the absorption of microwave energy into discrete rotational energy levels (Figure 4.2.4). DP heating arises from the ability of a microwave field to orient the dipole moments of a molecule parallel to its electric field (α_d from Eq. 4.1). In an alternating field, such as that found in microwave fields, dipole moments are forced to constantly realign with the changing

field. In the microwave frequency range, the rate with which the field changes is approximately the same as the response time for the switching of the dipole moments. At frequencies which are higher, the field changes too rapidly and the dipole moments are not able to keep up, remaining almost stationary. Since the dipoles do not rotate, no energy is absorbed and the material does not heat up. At significantly lower frequencies, insufficient energy is transferred to the material to cause significant heating.

However, for the time scales associated with microwave radiation, the moments can rotate at approximately the same frequency as the applied radiation. The moments rotate because of the torque they experience from the field, but the resulting polarization lags behind the changes in the electric field due to frictional losses from having to rotate through potential energy barriers of the surrounding medium. The lag indicates that the molecule is absorbing energy in the form of torque which is converted into heat during the rotation.

It is now instructive to introduce two parameters which are widely used to describe the phenomena of microwave DP heating. The first, ε', is the dielectric constant which describes the ability of the molecule or material to be polarized by an electric field. The second, ε'', is the dielectric loss which measures the efficiency with which the energy of electromagnetic radiation can be turned into heat. The quantity of most utility in determining whether a material will heat in an applied field is the dielectric loss tangent, $\tan\delta$, defined by:

$$\text{Eq. 4.2} \qquad \tan\delta = \varepsilon''/\varepsilon'$$

which conveniently relates the dielectric constant and the dielectric loss. $\text{Tan}\delta$ defines the ability of a material to convert electromagnetic energy into heat energy at a given frequency and temperature. Materials which have large dielectric loss tangents heat well when exposed to electromagnetic irradiation.

Both ε' and ε'' are frequency dependent, which can be described by the Debye equations:[3]

$$\text{Eq. 4.3} \qquad \varepsilon'_d = \varepsilon'_\infty + \frac{\left(\varepsilon'_0 - \varepsilon'_\infty\right)}{\left(1 + \omega^2 \tau^2\right)}$$

$$\text{Eq. 4.4} \qquad \varepsilon''_d = \frac{\left(\varepsilon'_0 - \varepsilon'_\infty\right)\omega\tau}{\left(1 + \omega^2 \tau^2\right)}$$

where ε'_∞ and ε'_0 are defined as the high frequency and static dielectric constants and ω and τ are the frequency and relaxation times which characterize the rate of build up and decay of polarization. As shown in Figure 4.2.5, the dielectric loss tangent reaches a maximum in the microwave region, which translates into high dielectric loss tangents and accounts for the utility of these waves in heating materials.

In a solid, the relative rigidity of the crystal lattice (as compared to the fluidity of a liquid matrix) creates a number of equilibrium positions which are available to a rotating dipole. These are separated by potential energy barriers which must be overcome before rotation in any direction can occur. In the simplest case only two equilibrium positions with opposite dipole directions exist and are separated by an energy barrier, U_a (Figure 4.2.6). From Boltzmann statistics, the number of transitions from one state to another is proportional to $(1 - e^{t/\tau})$ where t is the time and τ the relaxation time constant. The time constant and the dielectric constant can be related by

$$\text{Eq. 4.5} \qquad \tau = \frac{e^{u_a/kT}(\varepsilon'_o + 2)}{n(\varepsilon'_o + 2)}$$

where $1/n$ is the time for a single oscillation in the potential well. The expressions for the magnitude of the energy absorption for this model have been demonstrated to be equivalent to those followed by liquids.[4] The following form of the Onsager equation[5] has been shown to apply to many liquids and solids:

$$\text{Eq. 4.6} \qquad \varepsilon_o' - \varepsilon_\infty' = \frac{4\pi N m^2 \varepsilon_o'(\varepsilon_\infty' + 2)^2}{9kT(2\varepsilon_o' + \varepsilon_\infty')}$$

where N is the number of molecules and m their mass. It is interesting to note that in such a system, the magnitude of the dielectric absorption decreases with increasing temperature. In practice, many solid state materials are found to have very small dielectric losses. This is due primarily to the large energy differences between the equilibrium positions of the dipoles. In the majority of solid state cases, *e.g.* many long-chain esters and some ethers, there is significant dielectric absorption at room temperature which decreases with increasing temperature as expected.

The two values, ε' and ε'', can be used to describe other values of importance when designing a microwave heating system. For example, the extent to which an electromagnetic wave will penetrate into bulk materials can be determined using ε' and ε''. The penetration depth, D_p, when ε'' is small, is given by:

$$\text{Eq. 4.7} \qquad D_p \propto \lambda_0 \sqrt{(\varepsilon'/\varepsilon'')}$$

where λ_0 is the wavelength of the microwave radiation.

The equations describing ε', ε'', the dielectric loss tangent (tanδ) and the penetration depth can be applied with equal validity to both solid and liquid mediums, though dipolar losses in the solid state are rare due to the stricter energy constraints imposed on dipolar rotation by the rigidity of the surrounding crystal lattice. Some materials, such as metal powders, have no readily observable dipole yet still heat well when exposed to microwave irradiation. For these materials, it is necessary to extend our treatment of polarization to include losses from a buildup of charge at a material interface due to an electrical conduction mechanism.
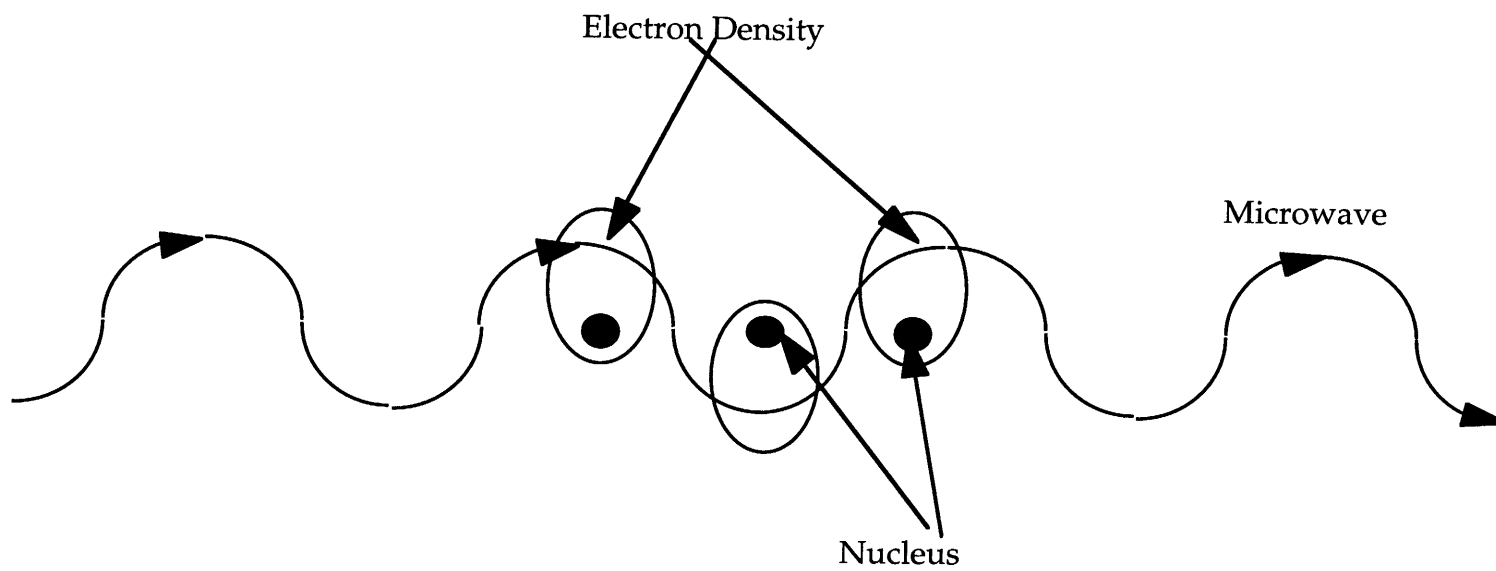
Figure 4.2.1: Electronic polarization from realignment of electrons around a nucleus.

Interaction with the electric field of the microwave causes the molecules to vibrate, thereby heating the substance.

Incoming microwave

Molecule containing a dipole moment
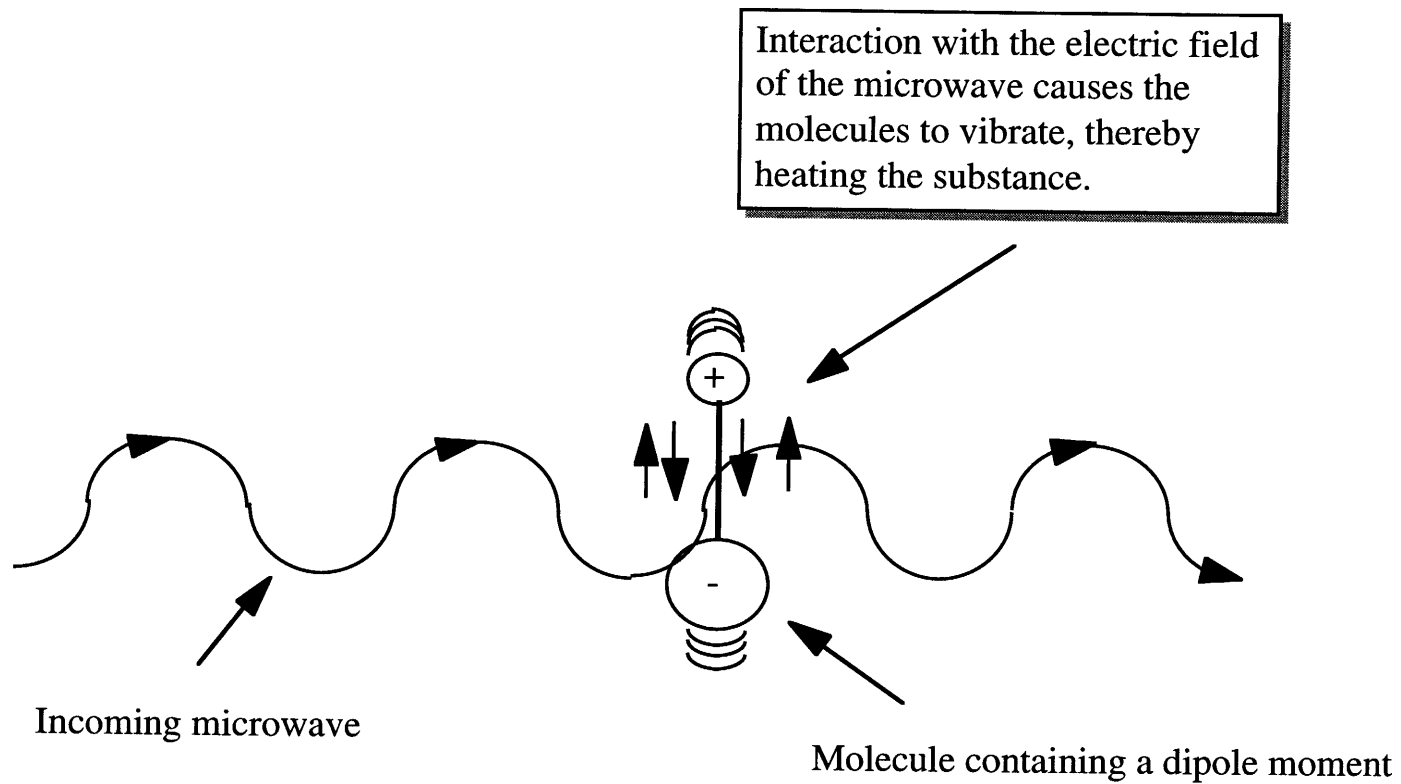
Figure 4.2.2: Atomic polarization from displacement of nuclei.

Interaction with the electric field
of the microwave causes the
molecular dipoles to rotate, thereby
heating the substance.

Incoming microwave

Molecule containing a dipole moment
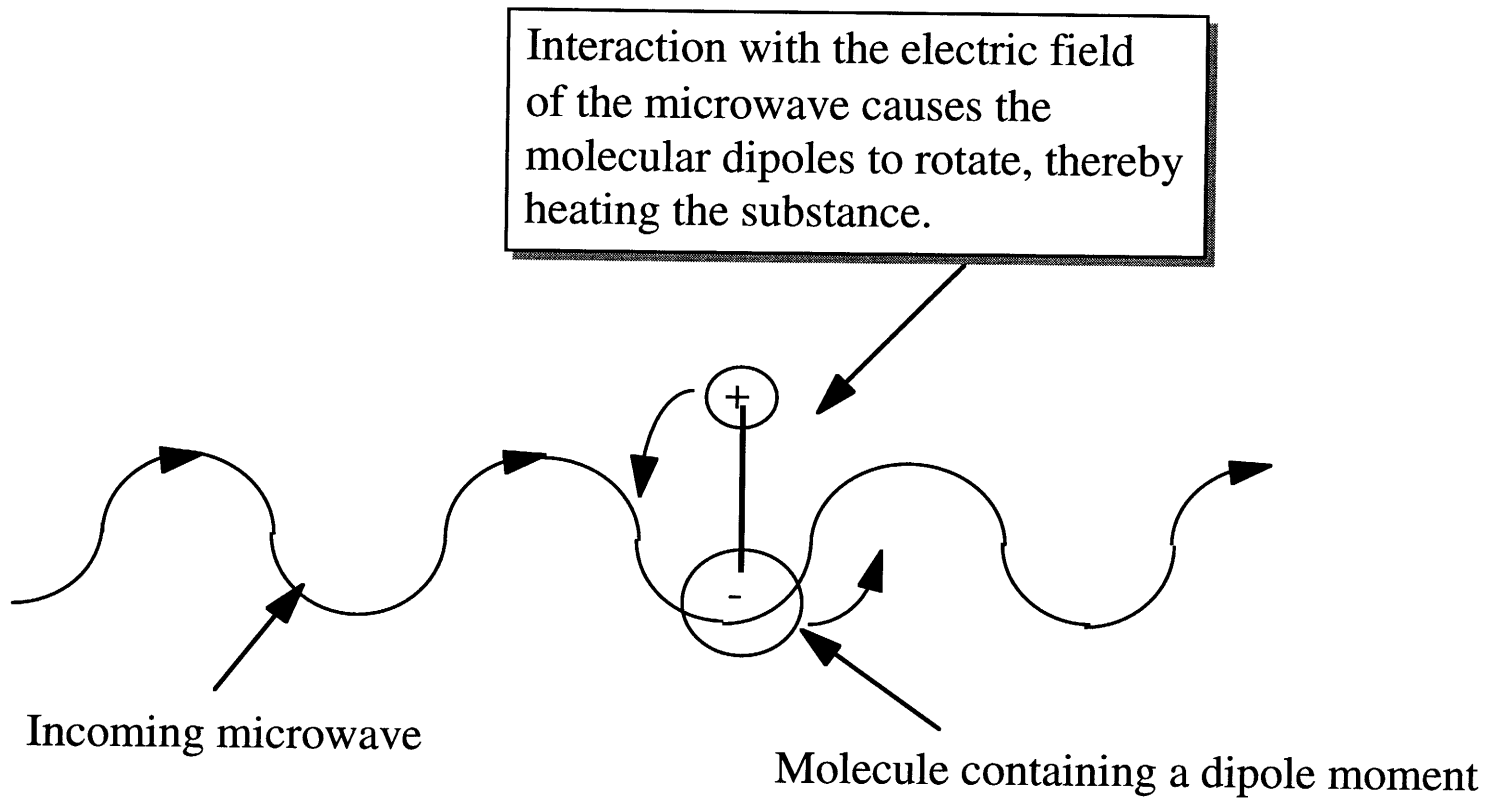
Figure 4.2.3: Dipolar polarization resulting from orientation of permanent dipoles.

Absorption of microwave energy by the molecular rotational bands.

Incoming microwave
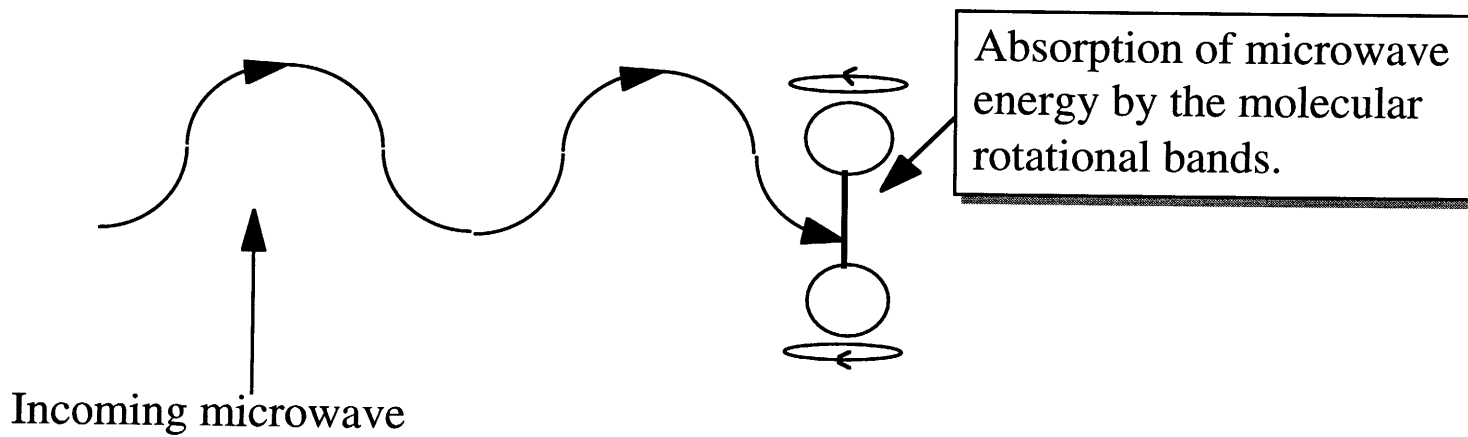
Figure 4.2.4: Microwave excitation of rotational states.
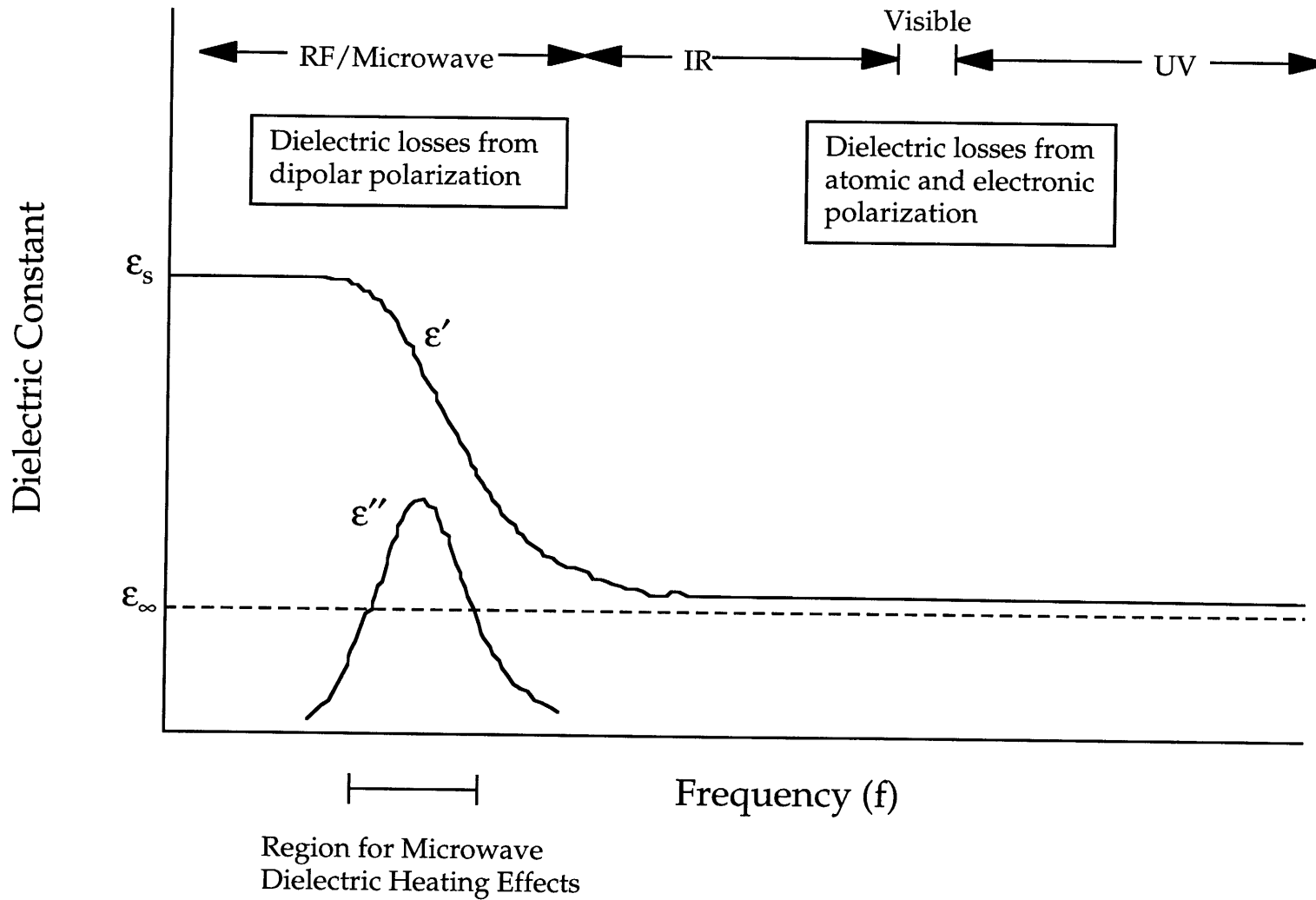
Figure 4.2.5: Frequency dependence of ε' and ε''.
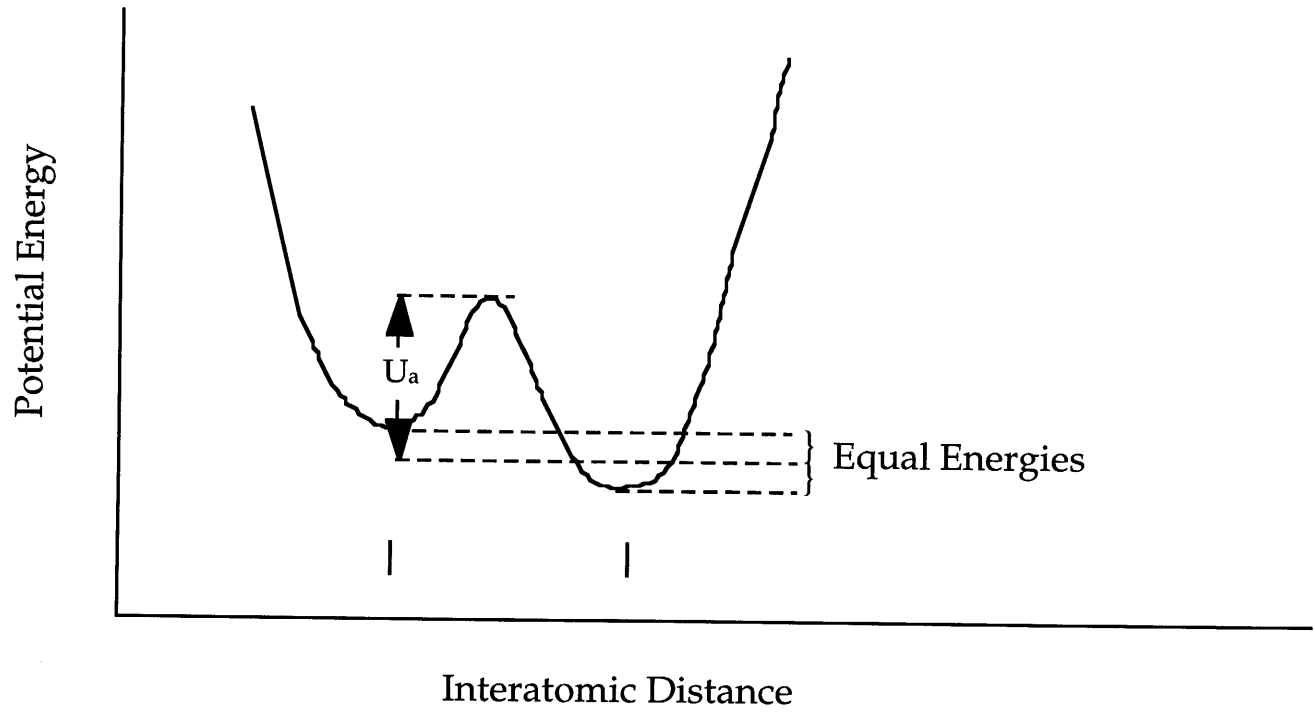
Figure 4.2.6: Potential energy diagram for two alternative positions of a dipole relative to an electric field.

4.2.2 Heating Through Conduction Losses

For highly conducting materials, either electronic or ionic, it becomes necessary to use an alternative model of polarization which takes into account the interactions between conducting areas (i.e. the sample and the surrounding air during the heating of ceramic powders). The electric current induced by an imposed electromagnetic field in a conducting medium is shown schematically in Figure 4.2.7. A general approach to interfacial polarization has been considered by Maxwell and Wagner in their two layer capacitor model as shown in Figure 4.2.8. The total Maxwell-Wagner effect, the polarization of particles due to a conduction mechanism, is seen to be a composite produced by areas of differing dielectric constants and conductivity. The complex permittivity can be described as follows:

$$\text{Eq. 4.8} \qquad \varepsilon_i^* = \varepsilon_\infty' + \frac{(\varepsilon_o' - \varepsilon_\infty')}{(1 + j\omega\tau)} - \frac{j\sigma}{\omega\varepsilon_o}$$

The real part can be reduced to give the simple Debye theory. For highly conducting materials, the conductive loss effects, $\left(\frac{j\sigma}{\omega\varepsilon_o}\right)$, can dominate the total polarization. Heating from conduction losses can be, and indeed usually is, more important than that resulting from dipolar relaxation effects in solid-state extended structures. In a material where conduction processes dominate the heating mechanism, Eq. 4.2 can be written as[6]

$$\text{Eq. 4.9} \qquad \tan\delta = \frac{\varepsilon'}{\varepsilon''} = \frac{\sigma}{2\pi f \varepsilon_o \varepsilon'}$$

where σ is the total conductivity (S/m) and f is the frequency (Ghz) of the applied radiation.

The dependence of the dielectric loss factor on the conduction mechanism has important ramifications for the synthesis of solid state materials. Some materials, i.e. alumina, do not absorb microwave energy well at room temperature and heat very poorly. The poor heating behavior can be easily explained by the lack of permanent dipole moments within the

crystal microstructure and by the insulating behavior of a material with a filled valence shell and significant bandgap. However, once the temperature of these materials is raised by a few hundred degrees, thermally activated conduction processes become important. For example, TiO_2 (anatase form) heats slowly to ~300°C, at which point it transforms into the rutile phase and heats rapidly to ~1000°C.[7] However, rutile exhibits only moderate heating, with a maximum temperature of less than 200°C.[7] The advent of extremely rapid heating, such as that exhibited by anatase, is a byproduct of the dependence of the dielectric heating on conduction processes.

The rate of rise of temperature due to exposure to the electric field of microwave radiation is determined by the following equation:[8]

$$\textbf{Eq. 4.10} \qquad \frac{\delta T}{\delta t} = \frac{constant \cdot \varepsilon'' f E_{rms}^2}{\rho C_p}$$

where E_{rms}^2 is the root mean square field intensity, ρ the density, and C_p the specific heat capacity. The heat losses due to thermal radiation[9] are governed by:

$$\textbf{Eq. 4.11} \qquad \frac{\delta T}{\delta t} = \frac{-e\alpha}{\rho C_p}\left(\frac{area}{volume}\right)_{sample} T^4$$

where e is the sample emissivity, and α is the Stefan-Boltzman constant. The resulting temperature rise is determined by such physical properties as the dielectric loss, the specific heat capacity and the emissivity of the sample as well as the strength of the applied microwave field. Since all these physical properties are temperature dependent, theoretical modeling of dielectric heating can be very complex.

However, in a highly conducting material, in which conduction losses dominate the heating mechanism, exceptionally high heating rates have been observed. As a material is heated, the conduction processes become more favorable. The higher conduction enhances the complex permittivity causing the sample to heat even faster. This catastrophic correlation between the temperature dependence of the conduction, the conduction dependence of

the complex permittivity and the complex permittivity dependence of the temperature can lead to very rapid increases in temperature of $>100°C/sec$, a phenomena known as thermal runaway. The maximum temperature achievable through thermal runaway is limited by the temperature dependence of the thermal radiation (Eq. 4.11). At some temperature, an equilibrium is established between the rate of heating from the microwave radiation and the rate of cooling from thermal losses. However, appreciable temperatures ($>1300°C$) can be easily and routinely obtained in a conventional home-use 1kW microwave oven. Table 4.1 lists several solid state materials and the maximum temperature they obtain using a conventional microwave oven as a heating source.

Thermal runaway can be used to achieve extremely fast heating rates to the final dwelling temperature of the reaction. However, in the absence of thermal runaway, many materials heat only slowly when exposed to microwave radiation. Reactions containing materials which do not heat well under microwave irradiation can be accelerated by using a non-reactive in-situ heating medium (commonly graphite) or by preheating the reaction mixture in a conventional furnace to a temperature at which heating processes become more favorable. Successful implementation of microwave radiation as a heating source can be experimentally tricky. In the following section, a detailed review of some recent applications of microwave heating to solid state materials synthesis is presented.

Microwaves
2.45 GHz

Resistance to induced
current produces heat

Conducting Solid
(Ionic or electronic)

Induced current
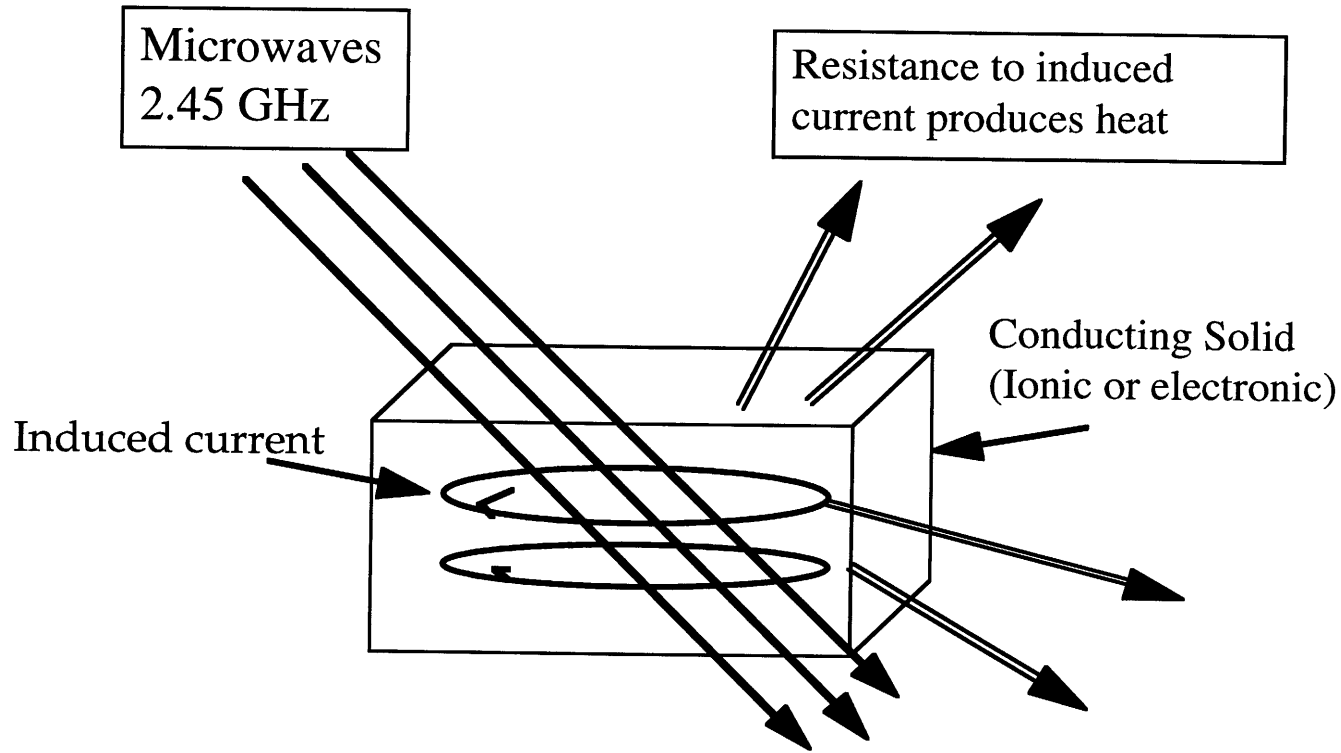
Figure 4.2.7: Microwave induction heating.
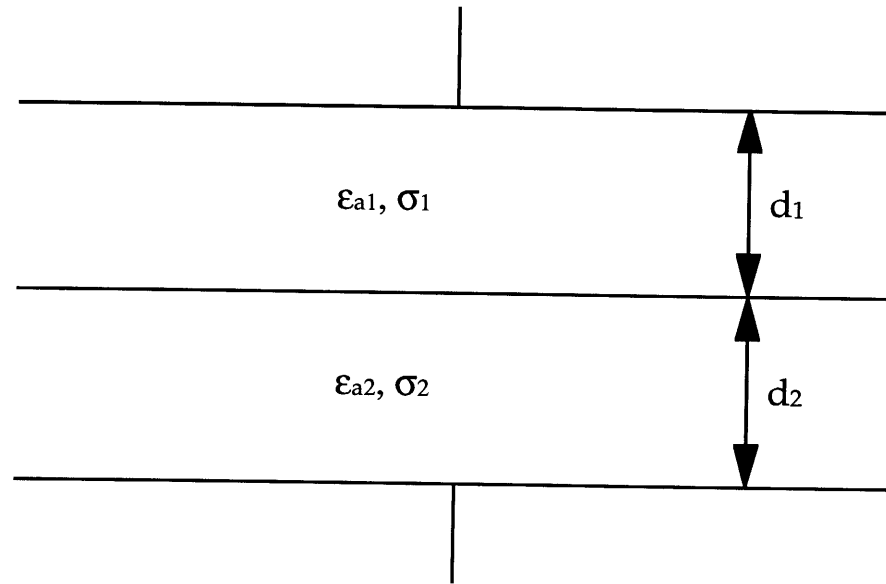
Figure 4.2.8: The Maxwell-Wagner two layer capacitor.
ε_{ax} and σ_x refer to the dielectric constant and conductivity, d_x is the distance.

Table 4.1: Effect of microwave heating on the temperatures of solids.
Column A: 25 g samples in a 1kW oven (2.45GHz) with a 1000 ml vented water load
Column B: 5-6 g samples in a 500W oven
Adapted from Mingos and Baghurst[2]

A

Chemical	T/°C	t/min
Al	577	6
C	1283	1
Co_2O_3	1290	3
CuCl	619	13
$FeCl_3$	41	4
$MnCl_2$	53	1.75
NaCl	83	7
Ni	384	1
NiO	1305	6.25
$SbCl_3$	224	1.75
$SnCl_2$	476	2
$SnCl_4$	49	8
$ZnCl_2$	609	7

B

Chemical	T/°C	t/min
CaO	83	30
CeO_2	99	30
CuO	701	0.5
Fe_2O_3	88	30
Fe_3O_4	510	2
La_2O_3	107	30
MnO_2	321	30
PbO_2	182	7
Pb_3O_4	122	30
SnO	102	30
TiO_2	122	30
V_2O_5	701	9
WO_3	532	0.5

4.3 LABORATORY USES OF MICROWAVES

4.3.1 Introduction

Ever since the early days of microwave technology development during World War II, it was recognized that microwaves could be used to efficiently heat water. Since then, the amount of research into the synthetic and processing applications of microwaves in the fields of chemistry, chemical engineering and materials science has grown exponentially. The most widely used application of microwaves on both the academic and industrial scale has been in the field of materials processing to obtain desired densities through sintering, which can improve the mechanical and electronic properties of a material.

4.3.2 Materials Processing

The processing of materials has been most widely studied for ceramic oxide materials, where the higher temperatures necessary for synthesis can be efficiently achieved using microwaves. In addition, ceramic materials synthesized using microwave heating exhibit higher experimental densities and improved mechanical properties over materials that are synthesized in traditional convection furnaces. Microwave radiation heats ceramic bodies uniformly. However, because heat is lost due to thermal radiation from the surfaces of the body, heat gradients are established from the inside (hot) to the exterior of the bodies. These gradients are opposite those obtained during conventional convection heating, which heats from the outside into the center of a particle, and may reduce the agglomeration of impurities on the surfaces of the material grains,[10] leading to the improved mechanical and electrical properties. The inverse temperature gradient also leads to improved sintering behavior of the ceramic[10] and therefore the higher measured density.

A number of studies have concentrated on whether microwaves could be a more efficient and cost effective method of heating than gas or electric heating elements. Due to the nature of microwave heating, namely the energy coupling directly to the body being heated, little or no energy is required to heat a furnace and its insulation. Second, there is some evidence that microwaves can result in enhanced reaction rates over conventional heating methods, thus lower overall reaction times.[11] Such enhancement could be the result of the inverse thermal gradients present in microwave heated materials, but some evidence points to an enhancement of ionic motion in materials exposed to microwave fields as well.[12,13] Whether the technology currently associated with microwave generation and propagation can be used to lower energy consumption and costs for bulk ceramic production is debatable.[14,15] However, as microwave technology progresses and the price of fossil fuels increases, the viability of microwaves as a processing tool will only increase.

4.3.3 Solid State Synthesis Using Microwaves

4.3.3.1 Introduction

Several studies have been made into the viability of microwaves as a synthetic heating source for a wide range of compounds. Several reviews of this chemistry have appeared recently.[2,10,16,17] The experiments conducted in a microwave oven range from organic reactions[1] and fulleride synthesis[18,19] to organometallic compounds and ceramic materials. A number of claims have been made about the enhancement of the rate of these reactions and the economical benefits of this enhancement.[14,15] Whether the actual rate of the reactions in enhanced is unclear and obviously depends on the specific reaction being studied. One fact is readily apparent though, the rate of heating of the reactants up to the final reaction temperature is very fast (in some ceramic mixtures the rate can be 100°C/sec or faster). Cooling rates are also enhanced, since the furnace is not directly heated and does not need to be

cooled. Together, these rates of heating and cooling lead to overall shorter reaction times as less time is required to ramp samples to and from the reaction temperature. In the following sections, a brief review of recent synthetic work involving a microwave heating source will be reviewed. For convenience, the materials will be presented in order chalcogenides, oxides and nitrides.

4.3.3.2 Chalcogenides

A large variety of techniques are used for the synthesis of solid-state/ceramic compounds. For reactions in which microwaves are to be used as the heating source, the simplest synthetic approach involves the direct reaction of the elements, one of which couples strongly with the microwave field to provide the heat. For example, Cu, In and S powders can be sealed into a quartz reaction tube in a 1:1:2 ratio and exposed to microwave radiation in a domestic microwave for as little as 3 min. to produce the chalcopyrite semiconductor $CuInS_2$.[20] This reaction takes advantage of the ability of copper to couple strongly with microwave radiation to produce the impressively short reaction times. The rate of reaction is also enhanced by the creation of a chalcogenide flux during the heating. The flux helps to speed the diffusion of the reactant and shorten the overall reaction time. The chalcogenides of a number of elements,[17,21] including several well studied dichalcogenides, as well as other ternary chalcogenides[20,22,23] can be prepared using similar techniques.

4.3.3.3 Oxides

Metal oxides constitute by far the largest class of compounds synthesized using microwave radiation, presumably due to the many highly evolved techniques for oxide synthesis under conventional heating which can be readily transferred to microwave applications. Metal oxide powders can be reacted directly under microwave irradiation to yield complex oxide materials such as $Bi_2VO_{5.5}$[23] and other ternary oxides.[11] Direct reaction of

metal oxides relies critically on the ability of one or more of the components to couple with microwave radiation and heat the reaction mixture. As is shown in Table 4.1, many oxide materials heat well when exposed to microwave radiation, achieving both fast heating rates and high temperatures. Several groups have synthesized $YBa_2Cu_3O_{7-x}$,[24] as well as other copper-based superconductors[25] both because of the potential technological usefulness of this material and the ability of CuO, one of the reagents, to couple with microwave radiation. Even when using solid state reactants, the reaction times for the synthesis of these complex oxide compounds are shorter then similar synthetic routes using gas or electric heaters.

Another method which has been used to synthesize ternary and higher oxides, including the copper based high-temperature superconductors, is the decomposition of aqueous metal nitrates[26,27] or hydroxides.[28] In this method, a slurry of the nitrates or hydroxides of the product's constituent metals is evaporated to near dryness and pyrolyzed in a microwave. This process can be used to synthesize bulk quantities of ceramic powders and, when coupled with an atomizing sprayer, can yield extremely small particles with a narrow particle size distribution[29] similar to that found using convection pyrolysis heating techniques. Superconductors prepared using the nitrate decomposition reaction demonstrate T_c's comparable to or even slightly higher than those made using conventional heating sources.

Some work has also been performed taking advantage of the well-known ability of microwaves to heat water. Microwave-hydrothermal reactions have been used to prepare several layered and network phosphates,[30] a number of electroceramic powders including $BaTiO_3$,[31] finely divided metal powders[32] as well several other binary and ternary oxide systems.[33] The treatment of the reactants is similar to that for conventional hydrothermal synthesis. The constituent metal hydroxides are placed in a bomb (Teflon bombs are used for microwave heating application to prevent electric arcing to the magnetron) along with some water and heated. Again

the reaction times are comparable to or shorter than those exhibited for similar syntheses using gas or electric heaters.

4.3.3.4 Nitrides and Carbides and Halides

Several other classes of solid state materials have been synthesized using microwaves as a heating source. Some work has been carried out synthesizing carbide materials through a reaction of the metal with graphite. For example, the reaction of silicon with graphite has been found to be an efficient and very fast (10 min.) route to the synthesis of β-SiC.[34] Graphite is known to couple efficiently with microwave radiation and has been used as a pro-heating medium in the synthesis of chalcogenide materials.[21] Carbide type materials have also been synthesized by carbo-thermal reduction of TiO_2 with methane to form TiC.[35]

The reaction of a metal powder with a gas has been used to synthesize a number of solid state compounds. For example, the reaction of a metal powder with a halogen gas in a fluidized bed reactor efficiently forms the metal halide[36] in good yield and impressive volume (50g in a domestic microwave). Several halide materials have been synthesized[36] including $CrCl_3$, WCl_6, $InCl_3$,$TeCl_4$, $TiBr_4$ and CuBr. Likewise, the reaction of a metal with nitrogen gas leads to the formation of binary nitrides. The synthesis of TiN[36], Cr_2N[36], and AlN[37] have all been reported.

The number of compounds which have been synthesized using microwave heating, though not large, is growing. However, the number of pure bulk phase nitrides which have been synthesized by this technique is limited to the three examples listed above, due predominately to the difficulty in obtaining reactive species of nitrogen. Elemental sulfur can be purchased and oxygen is readily incorporated into materials by heating in air. However, the reaction of a metal species with elemental nitrogen usually requires high temperatures and can be easily poisoned by the presence of trace amount of oxygen or water in the gas stream. For the synthesis of nitride materials, it would be nice to find a more reactive nitrogen source which could, under

certain application techniques, strip out residual oxygen to create a more phase pure product. Low pressure nitrogen plasmas could meet both these requirements.

4.4 PLASMAS

4.4.1 Introduction

Plasmas, loosely defined, are ionized gases. As such, plasmas have been studied for many years and have been applied successfully in many applications. Depending on the degree of ionization, plasmas can exhibit properties similar to those found in metals, semiconductors, strong electrolytes or ordinary gases. The unusual variety of the properties of plasmas, as well as their disparity compared to the properties found in the more traditional states of matter (i.e. solid, liquid and gas), lead to the classification of plasmas as a fourth state of matter. While plasmas may seem exotic (to the average person), they constitute a far larger percentage of the universe than the combination of solid and liquid matter, which are relegated to a few relatively cool planets and asteroids. Plasmas, on the other hand, constitute the bulk of most stars and nebula and therefore play a significant role in the function of the universe.

Even on earth, naturally occurring plasmas play important roles and are technologically useful. The ionosphere, the region of the atmosphere located at 60 km and higher, exists predominately in a plasma state. Radio signals broadcast from the surface reflect off the highly ionized and conducting ionosphere, which enables signals to be broadcast over much longer distances since they are constrained to follow the curvature of the earth's surface. However, despite the abundance of plasmas in the universe, they have not been harnessed by man until relatively recently.

Plasmas can be generated in a number of ways. The most complete (and destructive) ionization of a gas to form a plasma comes from the huge

amount of energy released in a fusion (or fission) process. The usefulness of plasmas generated by this method is debatable. A simpler method of plasma generation, which has found significant use in the laboratory, generates ionized gas particles by interaction of a gas with an electromagnetic field. The field can be intense visible/UV (ionization in the ionosphere results from interaction with sunlight) or longer wavelengths of light (microwaves or radio-frequency (RF) waves). Of these, microwave and RF radiation enjoy the largest commercial use because of the ease of single frequency generation and subsequent control of the waves.

The physics behind generating and sustaining plasma discharges is quite involved. The advent of the nuclear age, and the high energy plasmas generated therein, brought the generation and control of plasmas to the forefront of theoretical and applied physics. Many man-hours were put into this problem and more understanding about plasmas was obtained than is useful or prudent to discuss at this time. However, a rudimentary discussion of plasmas is helpful in understanding methods and approaches to using plasmas as a synthetic tool. The body of literature on plasma physics is quite large and includes numerous well-written and informative volumes. For this treatment of plasmas, several sources were used extensively, including Hellund[38], Delcroix[39] and Franklin[40].

4.4.2 The Physics of Plasmas

The generation of a plasma always starts with a seemingly benign event, the ionization of a gaseous atom (or molecule) by electromagnetic radiation (or intense heat). However, implied by this statement is one of the most important principles of plasmas, that they maintain charge neutrality. Every ionization event produces one electron and ionizes one atom (or molecule). After ionization, the electron and ion are free to interact with the electric field of the incident radiation and are accelerated along the electric field gradient. This process is illustrated in Figure 4.4.1. For simplicity, the motion of the ion will be ignored, as its significantly greater mass hinders

significant movement. Electrons within an electromagnetic field are accelerated by the electric component of the EM field according to Eq. 4.12.

$$\text{Eq. 4.12} \qquad m_e\left(\frac{dv}{dt}\right) = -eE(t) - m_e v v$$

In this equation, m_e is the mass of the electron, v is the collision frequency between the electron and a neutral particle and eE is the force on the electron by the electric field. Solving for v, the velocity of the electron, yields Eq. 4.13.

$$\text{Eq. 4.13} \qquad v = -\left(\frac{eE}{m_e}\right)\left(\frac{1}{(v+j\omega)}\right)$$

In this equation, ω is the frequency of the applied field. The average kinetic energy associated with this velocity is given in Eq. 4.14, where E_p^2 is the sum of the squared field intensities.

$$\text{Eq. 4.14} \qquad u(\text{avg}) = \frac{e^2 E_p^2}{4m_e\left(v^2 + \omega^2\right)}$$

The path along which an electron is accelerated by this force can be disrupted by any one of a number of events. The electron could collide with the wall of the containment vessel, usually resulting in a reduction of the container and removal of the electron from the plasma. The electron could also collide with an atom or ion within the plasma, resulting in further ionization or recombination depending on the energy of the electron. Collisions between particles in a plasma can result in elastic or inelastic interactions. Elastic interactions result in no net change in the energy configuration of either of the particles and, as such, are uninteresting to our discussion of generating and maintaining plasmas. Three kinds of inelastic process must be considered.

1) The electron can impart translational energy to the particle.

2) The energy from the electron can excite a atom to a higher energy state.

3) The energy from the electron can ionize the particle.

Of these processes, the first can usually be approximated to result only in the loss of translational energy from the electron, since momentum is conserved and the mass of the particle is significantly larger than the mass of the electron. The second results in an excited state within the atom, which will then relax through emissions corresponding to allowed transitions between excited states of the gas atom, the spectra being characteristic of the gas used. Ionization processes, the third possibility, is a special case of excitation. Through ionization, the number density of charged particles, and therefore the plasma, is maintained. In order for a plasma to be sustained, it is critical that the free electron be able to achieve sufficient kinetic energy to ionize neutral particles. A plasma is generated when equilibrium is reached between the ionization events (determined by the energy imparted to an electron by the electric field) and inelastic collisions with other particles or the reaction vessel. In order to achieve sufficient energy to cause ionization, the electron must travel, uninterrupted, in one direction, accelerated by the imposed electric field until it reaches sufficient velocity (kinetic energy) that ionization is achieved upon collision with a neutral body (a process which warrants further explanation).

Collisional processes depend critically on the cross-sectional area of the target atom, q_a, the effective area of the atom which the electron "sees" and with which it can interact. Thus the ionization rate, Z, for a collision between an electron and an atom is given by Eq. 4.15:

$$\text{Eq. 4.15} \qquad Z = n_a q_a \bar{c}_e$$

Here, n_a is the density of gas atoms and $\bar{c}_e$ is the mean thermal speed of an electron which is proportional to the average kinetic energy. At a pressure of 1 mTorr and an electron temperature of 1 eV, this gives a typical Z of 2×10^5 s^{-1}.

As is apparent from Eq. 4.14, the average energy of an electron in a plasma is not completely accurate method for determining ionization events, since all interacting particles have an energy distribution. Eq. 4.14 can be generalized to include a distribution in the energies of the electrons in a plasma. The electron must have an energy ε greater that the threshold value for the process, namely ionization ε_r. If the cross-sectional area that a particular target atom presents is $Q(\varepsilon)$ and the electron distribution function is $g(\varepsilon)$, the rate of ionization is given in Eq. 4.16:

$$\textbf{Eq. 4.16} \qquad Z=\int_{\varepsilon_I}^{\infty} g(\varepsilon)Q(\varepsilon)\left(\frac{2\varepsilon}{m}\right)^{\frac{1}{2}} d\varepsilon$$

The threshold for ionization is the ionization potential E_i, and for electron impact, $Q = a_0 p(\varepsilon-\varepsilon_i)$ can be used to approximate the cross-sectional area, where a_0 is a constant and p is the gas pressure. If one assumes a standard Maxwellian energy distribution, then the ionization collision events can be described as:

$$\textbf{Eq. 4.17} \qquad \frac{Z}{p}=\int_{\varepsilon_i}^{\infty} \frac{2}{\sqrt{\pi}}a_0\left(\varepsilon-\varepsilon_i\right)\left(\frac{2\varepsilon}{m}\right)^{\frac{1}{2}}\left(\frac{\varepsilon}{k_B T_e}\right)^{\frac{1}{2}}\exp\left(\frac{-\varepsilon}{k_B T_e}\right)\frac{d\varepsilon}{k_B T_e}$$

When integrated, this yields:

$$\textbf{Eq. 4.18} \qquad \frac{Z}{p}=\frac{4a_0}{(2\pi m)1/2}(k_B T_e)^{3/2}\left(2+\frac{eE_i}{k_B T_e}\right)\exp\left(-\frac{eE_i}{k_B T_e}\right)$$

The critical values in the ignition and maintenance of a plasma are the average kinetic energy that an electron within the plasma can obtain and the rate of the subsequent ionization events that this kinetic energy can cause. From the equations listed above, it is evident that the average kinetic energy is influenced by three variables, over which almost total control can be exerted. E_p^2, the sum of the squares of the field intensity, can be controlled by increasing or decreasing the amount of power applied to the magnetron. v,

the electron-neutral collision frequency can be controlled by varying the pressure and thus number density of neutral atoms per unit space. As the pressure is raised, the electron-neutral collision frequency will be raised due to a shortening of the electron's mean free path. This lowers the average kinetic energy, making ionization events upon collision less likely. Finally, ω, the frequency of the applied electromagnetic field, can affect the average kinetic energy of the free electrons within the gas. As the frequency is raised, the electrons are exposed to increasingly rapid fluctuations in the direction of the local electric field. As a result, the electrons are not linearly accelerated for as long, decreasing their total kinetic energy.

Clearly, by careful control of the reaction conditions, the rate of ionization within a plasma and thus the plasma temperature can be accurately controlled. For the work conducted in this project, the synthesis of bulk nitride materials by reaction of a metal powder with a nitrogen plasma, the applied microwave power and gas pressure are controlled and optimized to efficiently generate a plasma for nitriding at a fixed frequency. Plasmas have been used for years to enhanced the nitrogen content in steels in order to create harder and more durable alloys.[41,42] It is hoped that a nitrogen plasma, which contains highly excited nitrogen atoms, could enhance the rate of nitrogen uptake and, therefore, bulk nitride formation.

If energy of electron is above ionization energy of neutral, ionization can result.

Oscillating electron collides with neutral

Successive ionizations result in plasma formation.

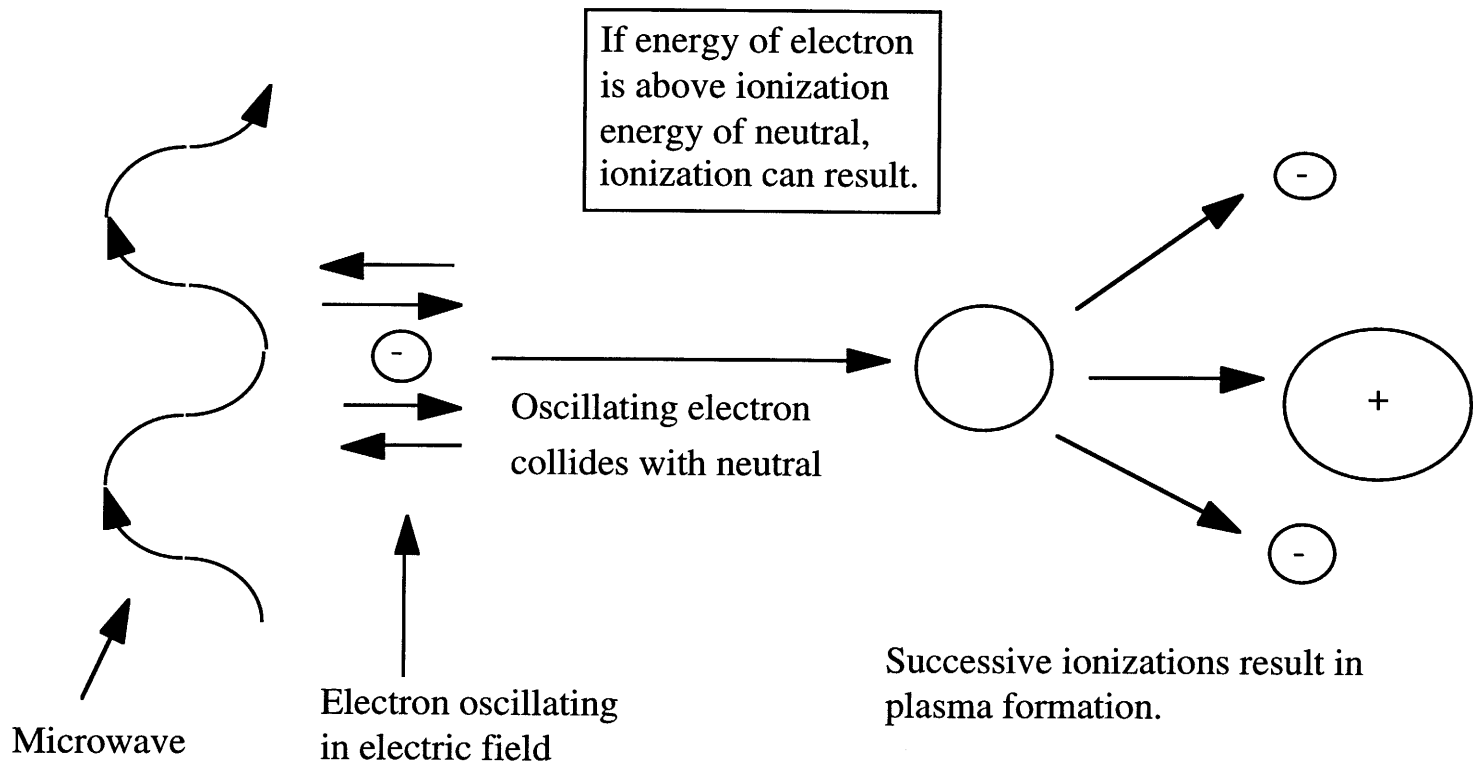Microwave

Electron oscillating in electric field

Figure 4.4.1: Microwave plasma generation__

4.5 CONCLUSION

Despite the significant amount of research into the implementation of microwaves as a viable heating source for solid-state materials syntheses, the number of compounds synthesized is quite limited due to the dearth of techniques which have been extended into a microwave oven environment. For several years, research in this group has centered around the intriguing synthetic problems associated with the synthesis of ternary and higher nitride materials (Chapters 1-3). Microwave heating can offer several unique advantages that can be utilized for the synthesis of nitride materials. The shorter reaction times often observed for solid-state materials would be a welcome addition to the field of nitride synthesis, where slow diffusion through nitride coatings can lead to very long reaction times. Also, the ability of microwaves to sustain plasmas allows the formation of extremely reactive species which could react with metal or other precursor powders to produce nitride materials. In the following chapter, both of these approaches are explored in more detail.

4.6 REFERENCES

(1) Caddick, S. *Tetrahedron* **1995**, *51*, 10403-10432.

(2) Mingos, D. M. P.; Baghurst, D. R. *Chem. Soc. Rev.* **1991**, *20*, 1-47.

(3) Debye, P. *Phys. Z.* **1935**, *36*, 100.

(4) Frohlich, H. *Theory of Dielectrics*; 2nd ed.; Oxford University Press: London, 1958.

(5) Bottcher, C. J. F. *Theory of Electric Polarisation*; Elsevier: Amsterdam, 1952.

(6) Sutton, W. H. *Ceram. Bull.* **1989**, *68*, 376-386.

(7) Gasgnier, M.; Loupy, A.; Petit, A.; Jullien, H. *J. Alloys Compd.* **1994**, *204*, 165-172.

(8) Meek, T. T. *J. Mat. Sci. Lett.* **1987**, *6*, 638.

(9) Alberty, K. A. *Physical Chemistry*; Wiley: New York, 1987; Vol. 7th, pp 326.

(10) Mingos, D. M. P. *Adv. Mater.* **1993**, *5*, 857-859.

(11) Baghurst, D. R.; Mingos, D. M. P. *J. Chem. Soc., Chem. Commun.* **1988**, 829-830.

(12) Freeman, S. A.; Booske, J. H.; Cooper, R. F.; Meng, B.; Kieffer, J.; Reardon, B. J. In *"Microwaves: Theory and Applications in Materials Processing II*; D. E. Clark, W. R. Tinga and J. R. Laia Jr., Ed.; American Ceramic Society: Westerville, OH, 1993; Vol. Ceramic Transactions 36; pp 213.

(13) Freeman, S.; Booske, J.; Cooper, R.; Meng, D. In Materials Research Society, Pittsburgh, PA: 1994; pp 479.

(14) Das, S.; Curlee, T. R. *Ceram. Bull.* **1987**, *66*, 1093-1094.

(15) Sheppard, L. M. *Ceram. Bull.* **1988**, *67*, 1656.

(16) Mingos, D. M. P. *Res. Chem. Intermed.* **1994**, *20*, 85-91.

(17) Whittaker, A. G.; Mingos, D. M. P. *J. Chem. Soc. Dalton Trans.* **1992**, 2751-2752.

(18) Ikeda, T.; Kamo, T.; Danno, M. *Appl. Phys. Lett.* **1995**, *67*, 900-902.

(19) Douthwaite, R. E.; Green, M. L. H.; Rosseinsky, M. J. *Chem. Mater.* **1996**, *8*, 394-400.

(20) Landry, C. C.; Barron, A. R. *Science* **1993**, *260*, 1653-5.

(21) Xu, Y.; Xiao, X. *J. Mater. Res.* **1995**, *10*, 334-338.

(22) Kniep, R. *Angew. Chem. Int. Ed. Engl.* **1993**, *32*, 1411-1412.

(23) Vaidhyanathan, B.; Ganguli, M.; Rao, K. *J. Mat. Res. Bull.* **1995**, *30*, 1173-7.

(24) Baghurst, D. R.; Chippindale, A. M.; Mingos, D. M. P. *Nature* **1988**, *332*, 311.

(25) Takahashi, N.; Koukitu, A.; Seki, H. *J. Crystal Growth* **1995**, *151*, 300-304.

(26) Warrier, K. G. K.; Varma, H. K.; Mani, T. V.; Damodaran, A. D. *J. Am. Ceram. Soc.* **1992**, *75*, 1990.

(27) Feldstein, H.; Ben-Dor, L.; Beilin, V. *Physica C* **1994**, *235-240*, 929-930.

(28) Sugiyama, K.; Nakano, Y.; Souri, H.; Konuma, E.; Matsuda, T. *J. Mater. Chem.* **1994**, *4*, 1897-1901.

(29) Kladnig, W. F.; Horn, J. E. *Ceram. Inter.* **1990**, *16*, 99-106.

(30) Komarneni, S.; Li, Q. H.; Roy, R. *J. Mater. Chem.* **1994**, *4*, 1903-1906.

(31) Komarneni, S.; Li, Q.; Stefansson, K. M.; R., R. *J. Mater. Res.* **1993**, *8*, 3176-3183.

(32) Komarneni, S.; Pidugu, R.; Li, Q. H.; Roy, R. *J. Mater. Res.* **1995**, *10*, 1687-1692.

(33) Komarneni, S.; Roy, R.; Li, Q. H. *Mat. Res. Bull.* **1992**, *27*, 1393-1405.

(34) Ramesh, P. D.; Vaidhyanathan, B.; Ganguli, M.; Rao, K. J. *J. Mater. Res.* **1994**, *9*, 3025-3027.

(35) Binner, J. G. P.; Hassine, N. A.; Cross, T. E. *J. Mater. Sci.* **1995**, *30*, 5389-5393.

(36) Whittaker, A. G.; Mingos, D. M. P. *J. Chem. Soc . Dalton Trans.* **1993**, 2541-3.

(37) Ramesh, P. D.; Rao, K. J. *Adv. Mater.* **1995**, *7*, 177-179.

(38) Hellund, E. J. *The Plasma State;* 1st ed.; Chapman and Hall, Ltd.: London, 1961, pp 197.

(39) Delcroix, J. L. *Plasma Physics;* 1st ed.; John Wiley and Sons, Ltd.: London, 1965, pp 266.

(40) Franklin, R. N. *Plasma Phenomena in Gas Discharges;* 1 ed.; Oxford University Press: Oxford, 1976, pp 249.

(41) Konuma, M.; Kanzaki, Y.; Matsumoto, O. *Denki Kagaku* **1979**, *47*, 597.

(42) Hudis, M. *J. Appl. Phys.* **1973**, *44*, 1489-1496.

5. Microwave Synthesis of Nitrides

5.1 INTRODUCTION

5.1.1 Microwaves as a Solid State Synthesis Tool

The solid state chemist is often plagued by extremely long reaction times cause by slow diffusion rates in solids. Consequently, the use of alternative synthesis techniques (solid state precursors, molecular precursors, fluxes, etc.) have been explored in order to achieve faster reaction rates. Interest has also been shown in alternative heating techniques, for example induction heating, arc furnaces and microwave heating. As mentioned in the previous chapter, several research groups have recently demonstrated the utility of microwaves as a heating source in the synthesis of a number of solid-state materials, such as chalcopyrite semiconductors[1], metal dichalcogenides[2], oxide superconductors[3], and metal halides.[4] All these microwave techniques take advantage of the rapid resistive heating of fine metal particles caused by electrical currents induced in them by the microwave field. Using relatively low power microwave generators, such as those found in standard for home use microwave ovens, many metal powders will heat rapidly and without noticeable electrical discharges. Such heating techniques have been extended to include the synthesis of binary nitrides such as TiN^2, Cr_2N^2, and AlN^5 by heating the metal powder under nitrogen gas in a microwave, where the use of the microwave heating source can lower the synthesis time from days to hours or minutes.

One problem with more traditional synthesis routes to nitrides is the high temperatures and long synthesis times that can make the synthesis experimentally tedious. In addition, as was seen in chapters 2 and 3, the use of precursors can lead to the incorporation of unwanted impurities into the product. For synthesizing ternary and higher nitrides, microwave heating offers several advantages over conventional heating methods, including greatly shortened reaction times. In addition, because microwaves heat the

reactants directly, they offer a more economical heating method compared to conventional heating sources, which also heat the insulation and the air within the furnace. Finally, using microwaves, the rate of heating and subsequent cooling rate are both extremely rapid. Such high heating and cooling rates could potentially lead to the formation of kinetic phases that could not be easily obtained by other routes, but will definitely lead to shorter overall reaction times due to shorter ramp times to and from the reaction temperature. In this section, we report on the synthesis of several binary and ternary nitride materials using only a microwave heating source.

5.1.2 Background on Nitride Synthesis Using Nitrogen Plasmas

Reactions using a microwave or radio frequency (RF) generated plasma as a synthetic tool have been known for a number of years. Numerous studies have been conducted on the rates of nitrogen uptake in the reaction of steel with nitrogen plasmas in order to enhance the hardness of the steel.[6,7] There have also been several studies using RF generated nitrogen plasma to nitride the surface of metal blocks. In particular, it was found that thin films of ZrN[8] and TiN[9,10] could be effectively grown on the surface of blocks of Zr and Ti, respectively, when these materials were exposed to a RF discharge that was generated using an impedance-matching network.

In the nitriding experiments of Ti, the sample turned golden colored in under 1 hr.[9] However, X-ray diffraction analysis demonstrated that the surface of the sample is a mixture of TiN and Ti_2N. The incomplete nitridation can be followed through SEM experiments, which reveal a layer of TiN at the surface and Ti_2N on the interior of the blocks. The surface of the sample can be completely converted to TiN, but only after exposure to a N_2 plasma for more than 8 hours. Measurements of weight change as a function of nitriding time indicate a critical dependence of nitrogen uptake on applied power and nitrogen pressure, as would be expected from **Eq. 4.18** and **Eq. 4.14**. In general, the rate of nitrogen uptake increases as the pressure of nitrogen and the applied RF power increases.[10] The rate of nitrogen uptake is rapid

upon initial expose to the plasma, but falls off exponentially with nitriding time. Exposure of the solid sample to the nitrogen plasma for a period of 49 hours under a pressure of 10 Torr and 200W of applied RF power results in the formation of a TiN coating about 10μm thick.[10]

Subsequent studies of the rate of nitrogen uptake from a nitrogen plasma and a nitrogen-hydrogen plasma show much higher nitrogen uptake for N_2-H_2 plasmas than for N_2 plasmas. The weight gain of the metal block can be represented by the linear law:[10]

$$\textbf{Eq. 5.1} \qquad \Delta w = \frac{B}{A}(t+\tau)$$

for reaction times up to 1 h, after which the weight change is more accurately represented by a parabolic law (Eq. 5.2).[10]

$$\textbf{Eq. 5.2} \qquad \Delta w^2 = Bt$$

In these equations, A and B are experimentally determined constants, t is time and τ is a time offset value. For a nitrogen plasma, B = 2.5×10^{-11} and B/A = 2.3×10^{-7} (g cm^{-4} s^{-1}) and for a nitrogen-hydrogen plasma, B = 1.0×10^{-10} and B/A 4.0x10^{-7} (g cm^{-4} s^{-1}), indicating the substantially higher weight gain for the nitrogen-hydrogen mixture over a solely nitrogen plasma.

Several other differences were observed between a N_2 and a N_2-H_2 plasma. The surface temperature of a metal block heated under an RF discharge was ~100°C higher under a N_2-H_2 plasma then under a N_2 plasma for both zirconium[8] and titanium[9] substrates. Also, mass spectroscopy measurements on the outflow gas from a nitridation of titanium reflect the changes in elemental composition of the plasma.[10] In a N_2 plasma, the primary ionized species are H^+, H_2^+, N^+, N_2^+ and NO^+ (the oxygen containing species presumably resulting from reactions with the quartz reaction vessel). For a N_2-H_2 plasma, the primary ionized species are H^+, H_2^+, N^+, NH^+, NH_2^+, NH_3^+, NH_4^+, and N_2^+. The presence of hydrogen in the plasma decreases the amount of reactive N_2^+. It also suppresses reaction of this molecule with the

reaction vessel and the subsequent formation of oxygen containing species in the plasma.

Several attempts have been made outside this lab to react a metal powder directly with nitrogen gas. These include the synthesis of TiN from titanium powder[2] and AlN from aluminum powder.[5] In both of these reports, no plasma formation is reported in an ambient nitrogen atmosphere. The rate of nitrogen uptake appears rapid with the reaction going to completion in under 2 hours, although Al_2O_3 is observed as an impurity phase in AlN. No impurities are reported in the formation of TiN. Despite the observed uptake of nitrogen in a plasma free environment, the presence of a nitrogen plasma should speed the rate of nitrogen uptake and subsequent nitride formation due to the presence of highly reactive nitrogen cationic species.

5.2 EXPERIMENTAL

5.2.1 Synthesis of MN (M = Ti, Al, V, Si, B, Nb)

The synthesis of metal nitrides using microwaves as the heating source was carried out by placing approximately 2 grams of the metal powder (Ti: Alfa, 99.4%, -100 mesh; Al: Cerac, 99.97%, +325 mesh; Si: Aesar, 99.5%, -325 mesh; V: Alfa, 99.5%, -325 mesh; B: Cerac, 99.5%, -100 mesh; Nb: Cerac, 99.8%, -100+325 mesh) in a microwave cavity (Sanyo model EM-604TW, 600W, 2.450 GHz, Figure 5.2.1) under nitrogen at atmospheric pressure. The metal powder was exposed to microwave radiation for 20 minutes, ground and reheated for an additional 20 minutes.

Alternatively, the powdered metal sample was placed in a plasma applicator attached to a low ripple microwave source (Cober Electronics model 9338/S1.2M, 1200 W, 2.45Ghz, Figure 5.2.2). The quartz sample container was evacuated and purged with nitrogen. A final nitrogen pressure of ~5 torr was used to maintain a steady plasma. The sample was then heated

under a nitrogen plasma for 3 hours, ground and reheated under a nitrogen plasma for an additional 3 hours. For samples which did not readily ignite a plasma, Ti powder in an adjacent alumina boat was used to spark a plasma. Once the plasma was sparked, it could be sustained by the microwave field and the boat containing the reactant was moved into it. Powder X-ray diffraction analysis of all the products was performed on a Siemens D5000 diffractometer.

5.2.2 Synthesis of $Li_{2x-3}M^{+x}N_{x-1}$ from Li_3N and a Metal (M = Fe, Al, Si, Ti)

The synthesis of ternary nitrides containing lithium ($Li_{2x-3}M^{+x}N_{x-1}$) was carried out by grinding together the metal powder (Fe(Aldrich, 99.9+%), Al(Cerac, 99.97%, +325), Si(Aesar, 99.5%, -325 mesh), Ti(Alfa/Aesar, 99.4%, -100mesh)) with a slight molar excess of Li_3N (Cerac, 99.5%, -60 mesh) in an argon filled glove box. The reaction mixture was placed in an alumina boat, which was then placed inside a quartz reaction chamber. The reaction chamber was inserted into the microwave cavity along with a beaker of water which was used as a dummy load to protect the magnetron from reflected power. Figure 5.2.1 shows a schematic diagram of the sample holder for use in the microwave cavity. The chamber was purged with N_2 before heating the reaction mixture in one minute cycles through microwave irradiation. After 8-10 one minute cycles, additional Li_3N was added to the sample and the mixture reheated in the microwave under N_2 for 8-10 one minute cycles. Powder X-ray diffraction analysis of the product mixture was performed on a Siemens D5000 diffractometer.

5.2.3 Sealed Tube Synthesis of $Li_{2x-3}M^{+x}N_{x-1}$ from Li_3N and Metal Nitride (M = AlN, Ta_3N_5, BN)

$Li_{2x-3}M^{+x}N_{x-1}$ was synthesized by grinding together the metal nitride (AlN: Cerac, 99.5%; Ta_3N_5: synthesized by reacting Ta_2O_5 with flowing

ammonia for 2 days at 900°C; BN, Alfa, 99.5%) with a slight molar excess of Li_3N (Cerac, 99.5%, -60 mesh) to yield a total sample mass of approximately 1.5 grams. The mixture was placed inside a quartz tube which was closed on one end and connected to a valve via an ultra-torr connector on the other end. The sample container was evacuated slightly and placed in the cavity of a Sanyo model EM-604TW microwave (600W, 2.450 Ghz, Figure 5.2.1). A beaker of water was used as a dummy load to protect the magnetron head from reflected energy. The sample was heated in 10 minute cycles until a reaction was started (typically 20 minutes total time). Microwave power was applied for an additional 10 minutes after visible signs of the reaction had ceased to ensure completion. Powder X-ray diffraction analysis of the product was performed on a Siemens D5000 diffractometer.

To Exhaust

To Vacuum

Alumina sample
container

Gas In
(N$_2$ or NH$_3$)

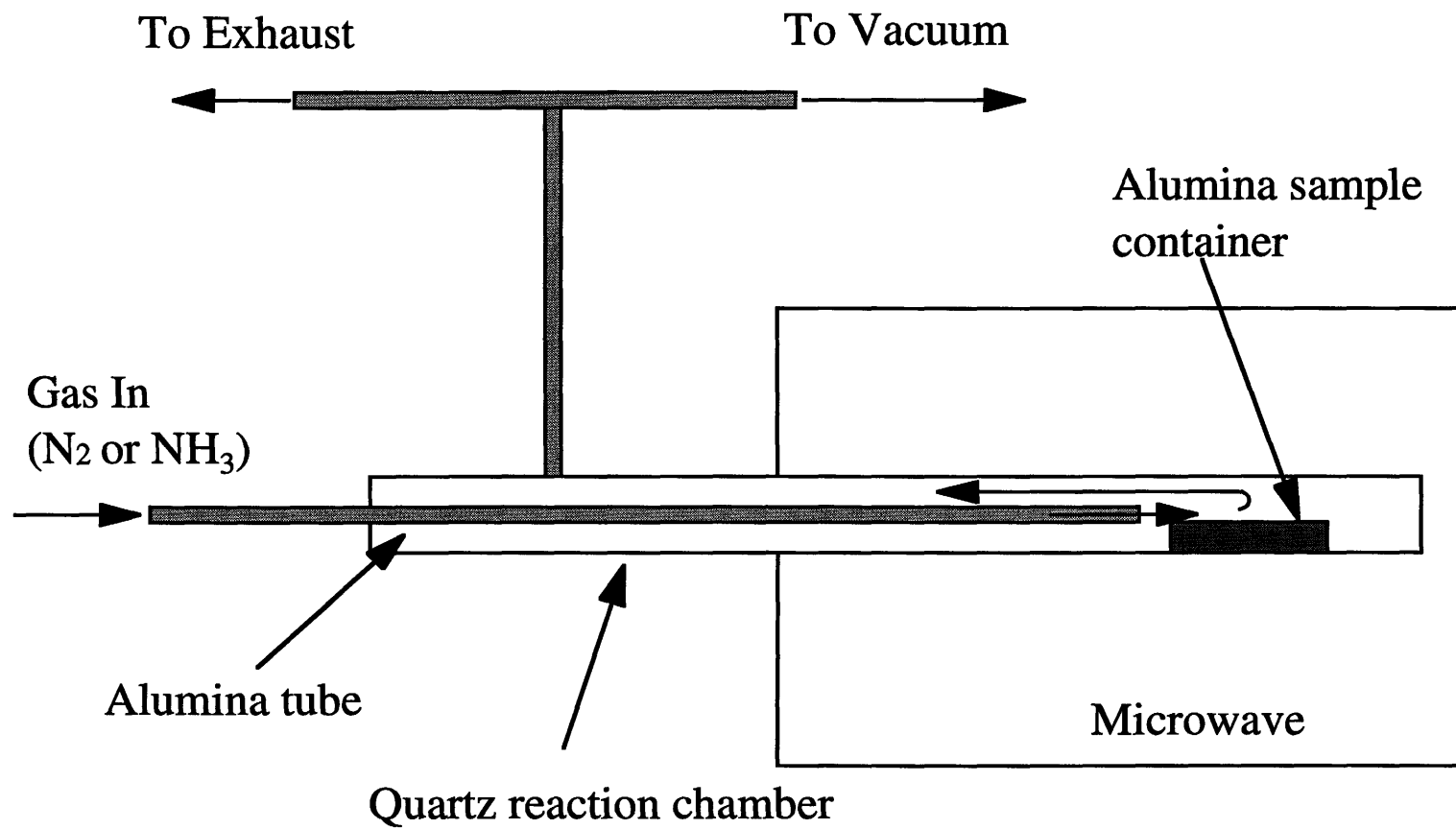Alumina tube

Quartz reaction chamber

Microwave

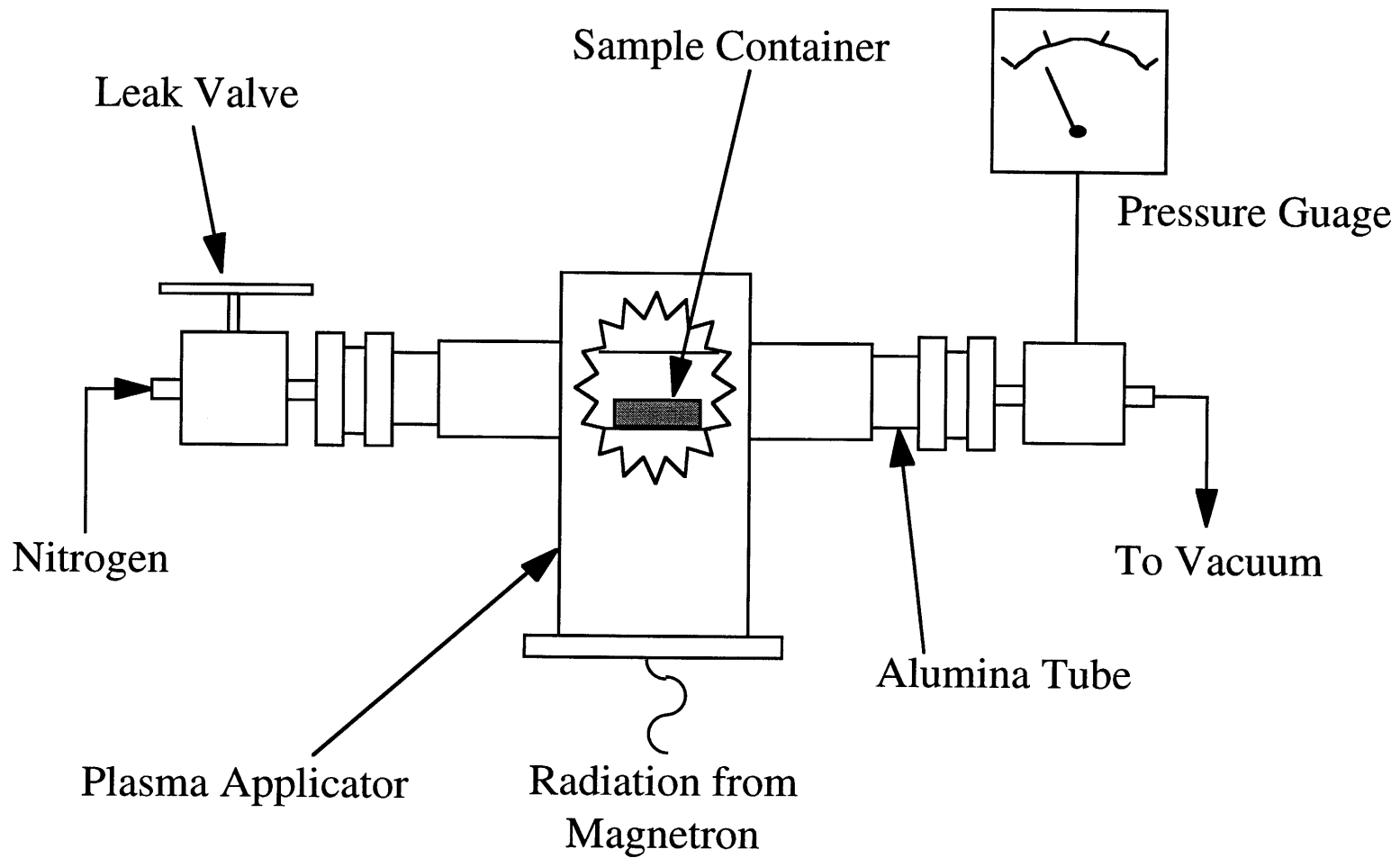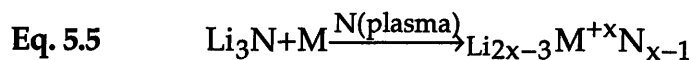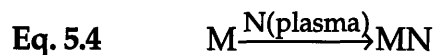**Figure 5.2.1: Schematic diagram of Sanyo microwave system used in the synthesis of nitride materials.**

Figure 5.2.2: Schematic diagram of Cober microwave system used in the synthesis of binary nitride materials by reaction with a nitrogen plasma.

5.3 RESULTS AND DISCUSSION

Two general reaction schemes were used to prepare the nitrides discussed in this paper and listed in Table 5.1 and 5.2. Ternary materials, for which nitride reactants of sufficiently high nitrogen content were available, were synthesized as per Eq. 5.3:

$$\textbf{Eq. 5.3} \qquad Li_3N + AlN \rightarrow Li_3AlN_2$$

The reactants were "sealed" into a quartz tube under vacuum and exposed to microwave radiation. Alternatively, for the synthesis of materials for which nitrogen uptake is required, for example the reactions listed in Eq. 5.4 and 5.5, the reactants can be heated under a nitrogen plasma.

$$\textbf{Eq. 5.4} \qquad M \xrightarrow{N(plasma)} MN$$

$$\textbf{Eq. 5.5} \qquad Li_3N + M \xrightarrow{N(plasma)} Li_{2x-3}M^{+x}N_{x-1}$$

In the following sections, both reaction pathways are discussed.

5.3.1 Synthesis of Binary Nitrides

Preliminary experiments to determine the viability of microwaves for the bulk synthesis of binary nitride powders consisted of the reaction between a metal powder and nitrogen. While several metal powders were found to heat well in a conventional home-use microwave, most did not demonstrate appreciable nitride formation. The most notable exception was titanium powder, over which a nitrogen plasma was readily sparked, resulting in the formation of a TiN coating on the titanium particles.

After ~20 minutes of microwave heating, the color of the titanium powder had changed to the characteristic gold color of TiN, confirming the report by Whittaker and Mingos.[2] However, powder X-ray diffraction analysis of the product revealed the presence of unreacted titanium metal in the product. Incomplete reaction has been observed in other microwave reactions between a metal powder and N_2. In the formation of AlN from Al, residual Al is seen in the product as well as an Al_2O_3 impurity, presumably

from water or oxygen in the gas stream.[5] The incomplete conversion of aluminum powder to aluminum nitride was attributed to the formation of a layer of aluminum nitride at the surface of the metal particles, which slows nitrogen diffusion into the interior of the particles.[5] This is consistent with our observation of unreacted Ti and with the notoriously slow diffusion of nitrogen through TiN.

The formation of a nitrogen plasma over the reactant metal powder was found to greatly enhance the rate of nitride formation. However, in a domestic microwave, it was not possible to sustain a plasma discharge over the titanium sample and the non-uniform nature of the microwave field led to uneven heating. In addition, the titanium samples heat rapidly to glowing yellow heat after which no plasma discharges are observed. Therefore, the synthesis of TiN was attempted in a plasma applicator attached to a 1.2 kW low-ripple microwave source. In this instrument, it was possible to generate and sustain a nitrogen plasma under reduced nitrogen pressure (~5 torr). Heating titanium metal in this nitrogen plasma for 3 hours leads to a powder with a golden color, indicative of TiN. However, powder X-ray diffraction reveals the product to be a mixture of TiN and Ti_2N. Grinding the sample briefly and heating it for an additional 3 hours results in complete conversion to TiN as evidenced by powder X-ray diffraction (Figure 5.3.1).

Elemental powders over which a plasma did not ignite (B, Si) did not form a nitride product. However, a plasma could be ignited for these compounds by placing a small amount of titanium powder in one end of the reaction vessel or in an adjacent alumina boat. Nitrogen plasmas are readily sparked over titanium powder and, in the plasma applicator, once formed are easily sustained. The reaction vessel is positioned to place the desired reactant within the plasma. Table 5.1 lists several binary nitrides which were synthesized by reaction of the metal powder with a nitrogen plasma. AlN is readily formed in the nitrogen plasma (Figure 5.3.2), even without an intermediate grinding step with a total reaction time of ~3 hours. VN required one intermediate grinding after about 3 hours of treatment with the

nitrogen plasma, followed by another 3 hour microwave treatment (Figure 5.3.3). Reactions with Nb, Si and B were less successful, yielding incomplete reactions and multi-phasic products even after repeated intermediate grindings. The reaction of niobium metal with a nitrogen plasma yields a mixture of NbN, Nb_2N and Nb_3N_4 as well as NbO_2 formed from residual oxygen in the nitrogen feed gas. Reaction of the nitrogen plasma with silicon yields small amounts of both α and β-Si_3N_4, with the predominant phase being unreacted Si (Figure 5.3.4). The reaction of the plasma with boron is also incomplete and even after several intermediate grindings, only half the boron powder can be converted into poorly crystalline turbostractic BN.

Despite the presence of small amounts of oxide impurities present in several products, the total amount of these impurity phases is very small. In the case of titanium, trace amounts of TiO can be removed by treatment with a 95% nitrogen/5% hydrogen plasma, which appears to scavenge oxygen from the substrate. Indeed, as will be reported in Section 5.4, the oxides of several transition and main group metals can be completely converted to nitride product under treatment with a nitrogen/hydrogen plasma.

Table 5.1: Nitridation reactions of metal powders using a nitrogen plasma.

Reactants	Conditions	Products
Ti	N_2 with grinding	TiN
B	N_2 with grinding	BN + B
Al	N_2	AlN
Si	N_2 with grinding	α, β-Si_3N_4 + Si
V	N_2 with grinding	V N
Nb	N_2 with grinding	NbN, Nb_2N, Nb_3N_4
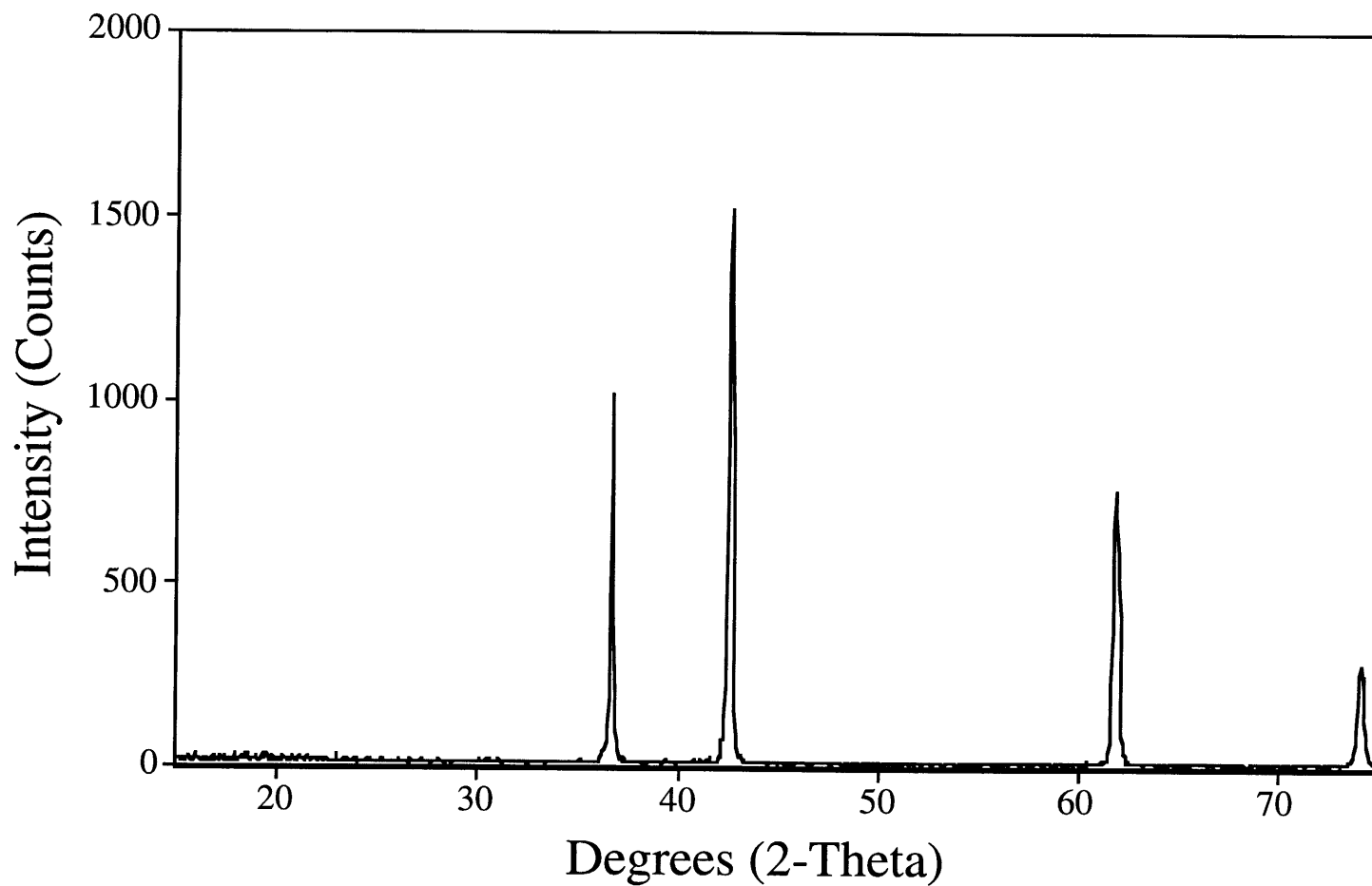
Figure 5.3.1: Powder X-ray diffraction pattern of TiN synthesized from the reaction of Ti powder with N_2 gas in a plasma applicator.
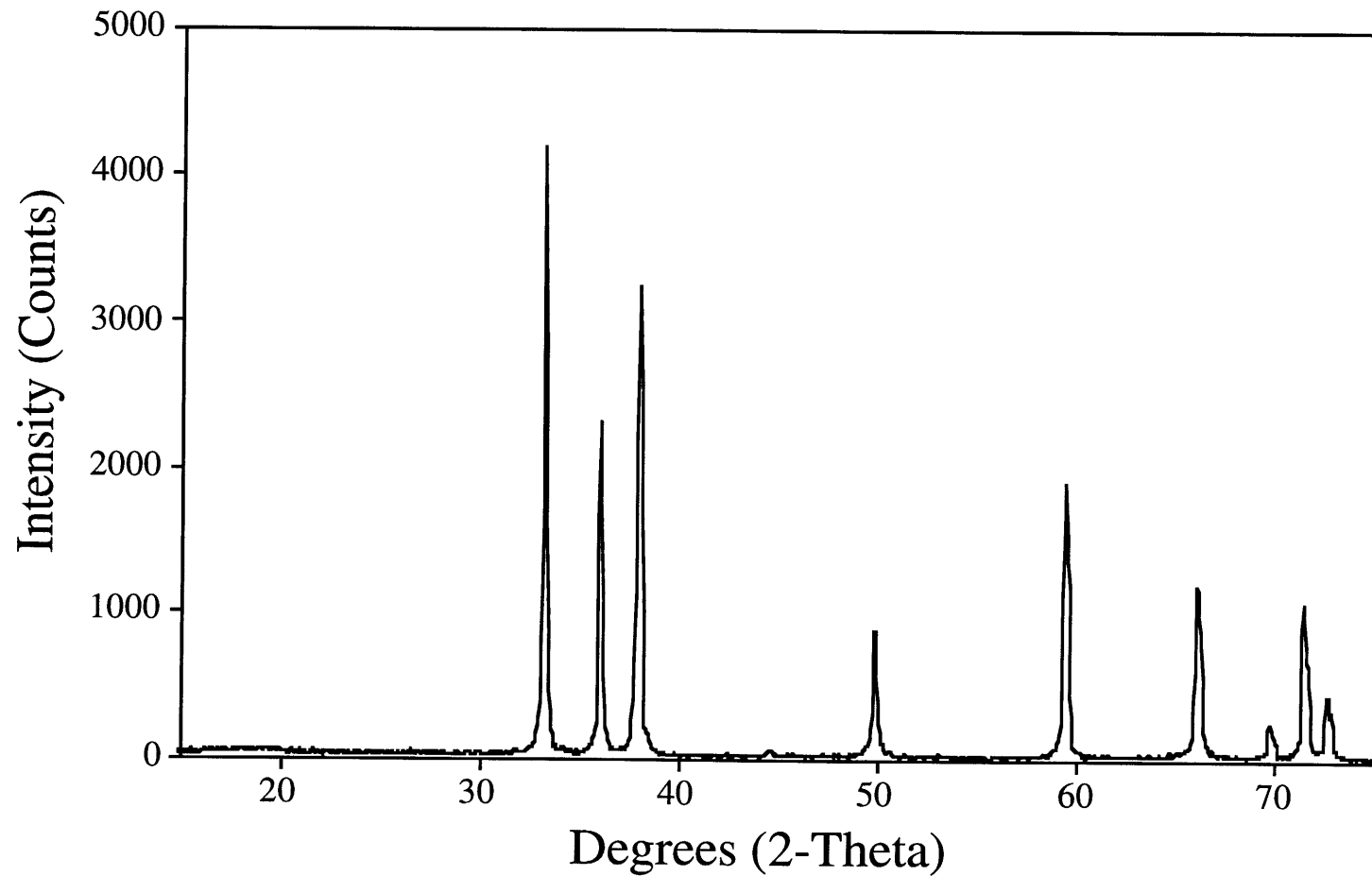
Figure 5.3.2: Powder X-ray diffraction pattern of AlN synthesized from the reaction of Al powder with N_2 gas in a plasma applicator.
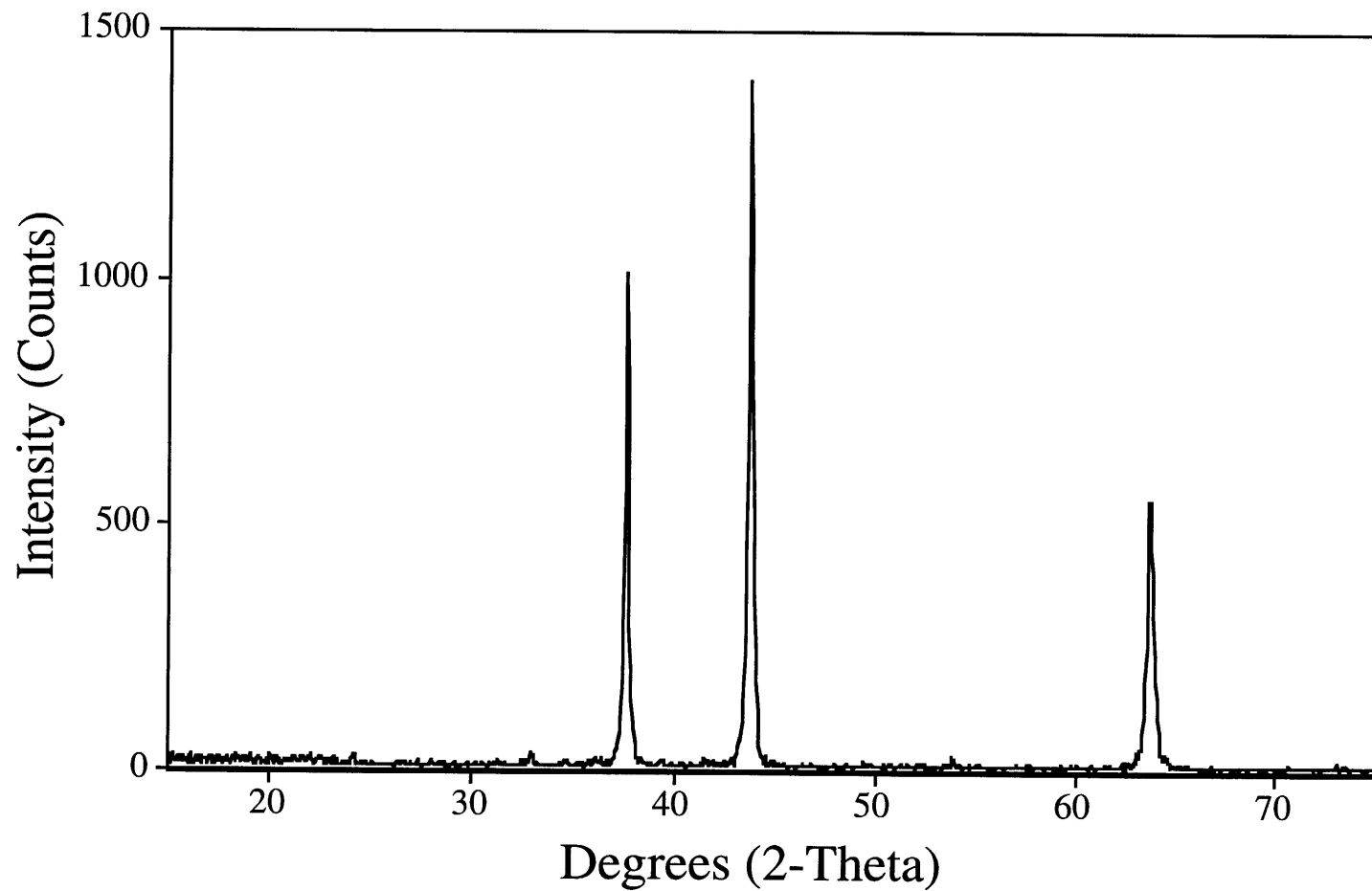
Figure 5.3.3: Powder X-ray diffraction pattern of VN synthesized from the reaction of V powder with N_2 gas in a plasma applicator.
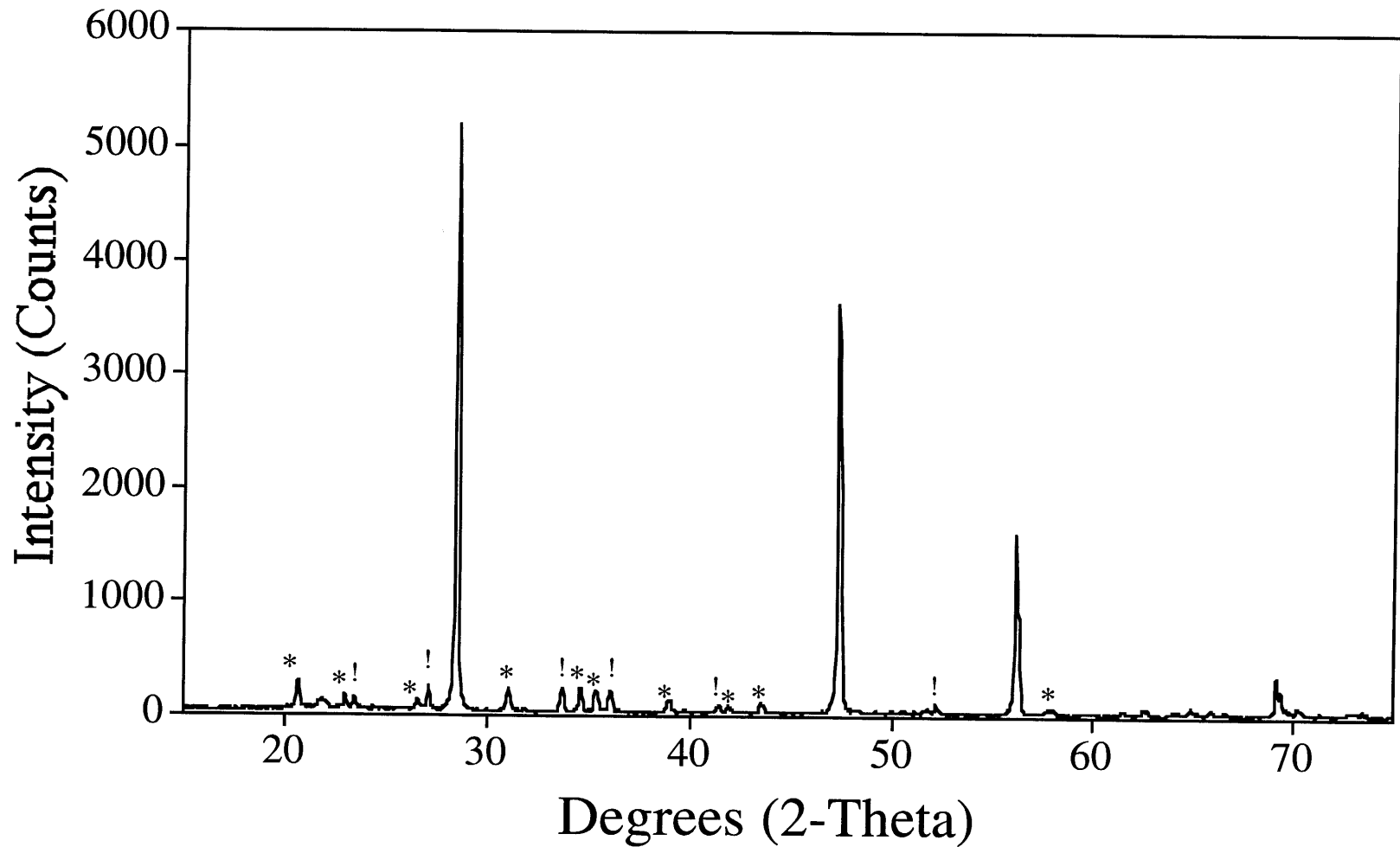
Figure 5.3.4: Powder X-ray diffraction pattern of α, β-Si₃N₄ and Si synthesized from the reaction of Si powder with N_2 gas in a plasma applicator. * = α-phase; ! = β-phase.

5.3.2 Synthesis of Ternary Nitrides

Lithium and lithium nitride are attractive starting materials for the synthesis of ternary nitrides for a number of reasons. Lithium is an electronic conductor and lithium nitride is an ionic conductor and, as such, both heat well when exposed to microwave radiation. Both materials melt at moderate temperatures and can be used as reactive fluxes. Many ternary nitrides containing lithium are known, greatly simplifying the task of product characterization. Finally, there has been some interest in lithium containing nitride for use as lithium solid electrolytes[11,12] and as cathode materials[13] for lithium ion batteries.

Attempts were made to synthesize several lithium containing ternary nitride materials starting from lithium nitride and the metal as shown in Eq. 5.5. Early experiments revealed that the extremely rapid heating of the metal particles can lead to evaporation of Li_3N from the reaction mixture and incomplete product formation. For example, the reaction of iron powder with Li_3N leads to the formation of Li_3FeN_2 and Fe (Figure 5.3.5) due to the loss of Li_3N from the reaction. The rate of lithium nitride evaporation can be slowed by observing several precautions. For example, if the reaction is stopped when the sample mixture begins to glow yellow-hot, the time that the reaction mixture spends at very high temperatures is limited and the evaporation of Li and Li_3N is slowed. Once all the lithium has either evaporated or reacted, the reaction can be driven closer to completion by the addition of more lithium followed by additional one minute heating cycles. For example, the reaction of Li_3N and Al with N_2 leads to the formation of Li_3AlN_2 and AlN in ~1:2 ratio as evidenced by powder X-ray diffraction. Addition of lithium metal to this mixture results in a Li_3AlN_2:AlN ratio of ~3:1 after further heating cycles (Figure 5.3.6), though the crystallinity of the product is not good. In Table 5.2, several other reactions between Li_3N and a metal, which also yield incomplete reactions, are shown.

The reaction between Li_3N and a metal did not yield clean products, even after three successive addition of Li_3N to account for lithium lost during heating. To restrict the loss of lithium nitride further, the amount of free volume in the reaction vessel was limited, yielding less space to which the lithium could diffuse. Also, the final reaction temperature and thermal runaway was limited by using two nitride reactants, one of which is an electrical insulator. The theoretical reaction is shown in Eq. 5.6:

Eq. 5.6 $\quad (2x-3)Li_3N + M^{+x}N_{x/3} \rightarrow Li_{2x-3}M^{+x}N_{2x-1}$

However, such a reaction pathway limits the final nitrogen content to the amount of nitrogen present in the reactants. In order to synthesize high nitrogen content products using lithium nitride as a starting material, transition or main group metal nitrides with a metal to nitrogen ratio of at least a 1:1 must be used, eliminating most if not all of the late transition metals.

Starting with two nitride reactants resulted in greatly improved yield and product crystallinity. The reaction of a 1:1 molar mixture of Li_3N and AlN heats only slowly initially. The sample must be exposed to 15-20 minutes of microwave radiation before the onset of thermal run-away, after which the reaction mixture melts. Such behavior has been observed in other solid-state materials.[14] The reaction of Li_3N and AlN is quite rapid, proceeding to completion in a couple of minutes after onset of thermal runaway. The sample was heated for several minutes after all visible signs of the reaction had subsided to assure complete reaction. After a total heating time of 40 minutes, a small amount of AlN is still present as demonstrated by powder X-ray diffraction (Figure 5.3.7). However, this impurity can be virtually eliminated by addition of more Li_3N and further heat treatment as shown in Figure 5.3.8. Several small impurity peaks are observed in the powder X-ray diffraction data; $LiAlO_2$, resulting from reaction with the walls of the quartz vessel, and a very small amount of AlN, residual starting material.

Other ternary nitride materials can be made using lithium nitride and the group XIII nitrides. For example, heating a 2:1 molar ratio of Li_3N and BN in the plasma applicator results in the formation of Li_3BN_2 and residual Li_3N (Figure 5.3.9). Excess Li_3N is needed in order for the sample to heat, since BN does not heat when exposed to a microwave field. Furthermore, microwave heating is a volumetric effect and the presence of a material in the reactant mixture which does not heat well significantly limits the ability of the sample to heat. The low density of BN further exacerbates the volumetric heating problem over other systems which include electrically insulating reactant, most notably Li_3N and AlN.

The reaction of a 5.1:1 molar mixture of Li_3N and Si_3N_4 leads to the formation of a mixture of products (Li_2SiN_2, Li_5SiN_3 and $Li_{18}Si_3N_{10}$) due to the lack of thermal control in our microwave setup. A large number of lithium silicon nitrides are known with lithium:silicon ratios ranging between 2:1 and 8:1, all of which are readily interconvertable. Without the ability to maintain the sample temperature slightly below the melting point of lithium nitride, it is lost from the reaction mixture during the course of the experiment, resulting in a mixture of several phases.

When a 7:1 molar mixture of Li_3N and Ta_3N_5 is heated in a microwave cavity under vacuum for less than 20 min., the cubic phase Li_7TaN_4[15] can be obtained. Again the reaction is slow to initiate, but proceeds rapidly once thermal runaway begins. The product is black polycrystalline Li_7TaN_4 along with residual Li_3N and TaN (Figure 5.3.10). If the reaction is allowed to proceed for longer than 20 min., a previously unknown phase is obtained. This unknown phase (Figure 5.3.11) can be indexed as orthorhombic (a = 5.171(1)Å, b = 8.462(2)Å, c = 12.765(3)Å). At this time, no further characterization of this phase has been done.

Table 5.2: Synthesis of lithium metal nitrides.

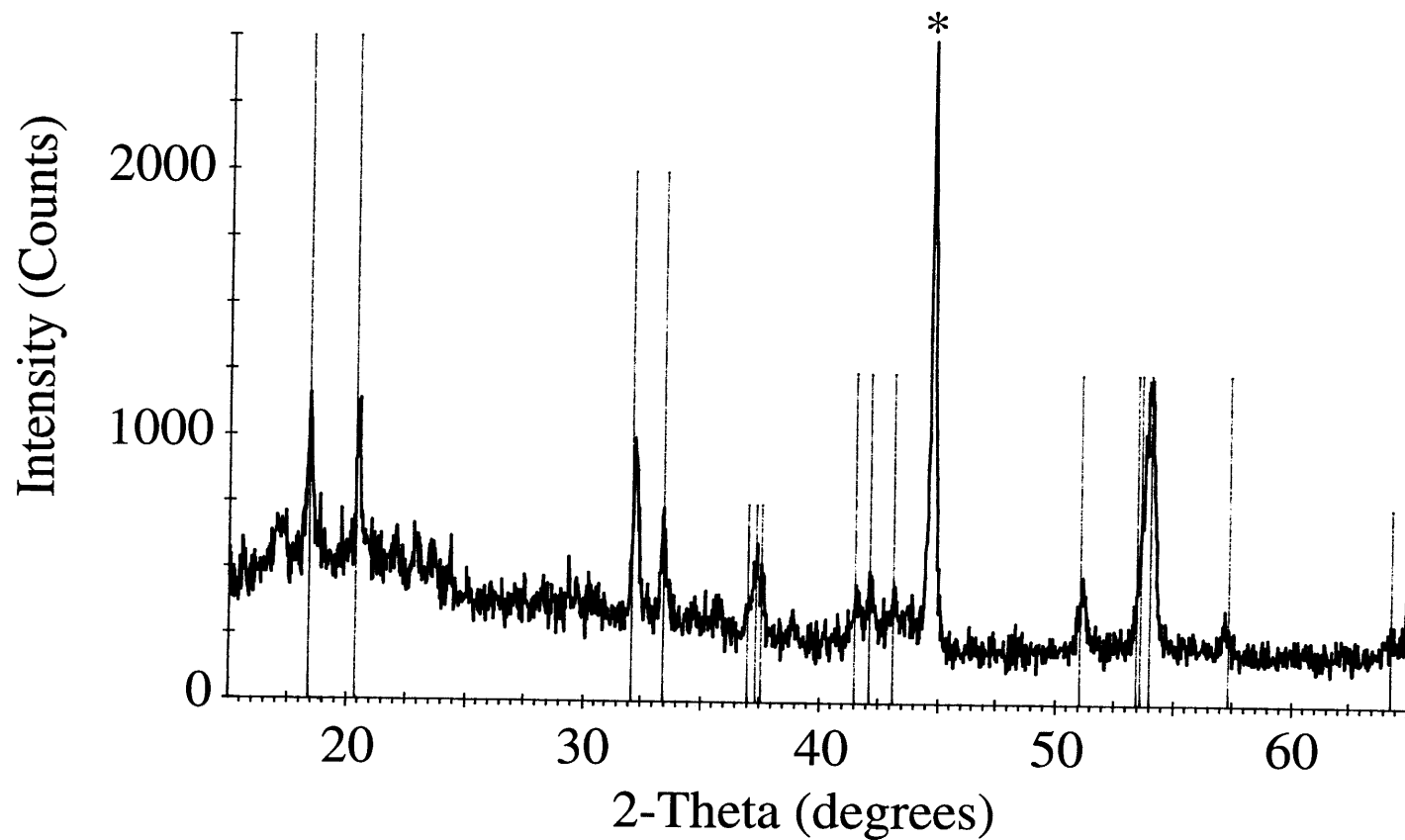| Reactants	Conditions	Products
Li_3N + Al	N_2 + additional Li_3N	Li_3AlN_2 + AlN
Li_3N + AlN	vacuum	Li_3AlN_2
$Li_3N(xs)$ + BN	vacuum	Li_3BN_2 + Li_3N
Li_3N + Fe	N_2	Li_3FeN_2 + Fe
Li_3N + Si	N_2	$LiSi_2N_3$ + Si
Li_3N + Si_3N_4	vacuum	Li_2SiN_2 + Li_5SiN_3 + $Li_{18}Si_3N_{10}$
Li_3N + Ti	N_2	Li_5TiN_3 + Ti + TiN
Li_3N + Ta_3N_5	quartz tube under vacuum	Li_7TaN_4 + Li_3N + TaN
Li_3N + TaN	vacuum	unknown new phase + Li_7TaN_4 + Li_3N

Figure 5.3.5: Powder X-ray diffraction pattern of Li_3FeN_2 synthesized from the reaction of Fe powder and Li_3N under N_2 gas in the microwave. * = Fe. Lines indicate peak positions of Li_3FeN_2 (JCPDS = 20-626).
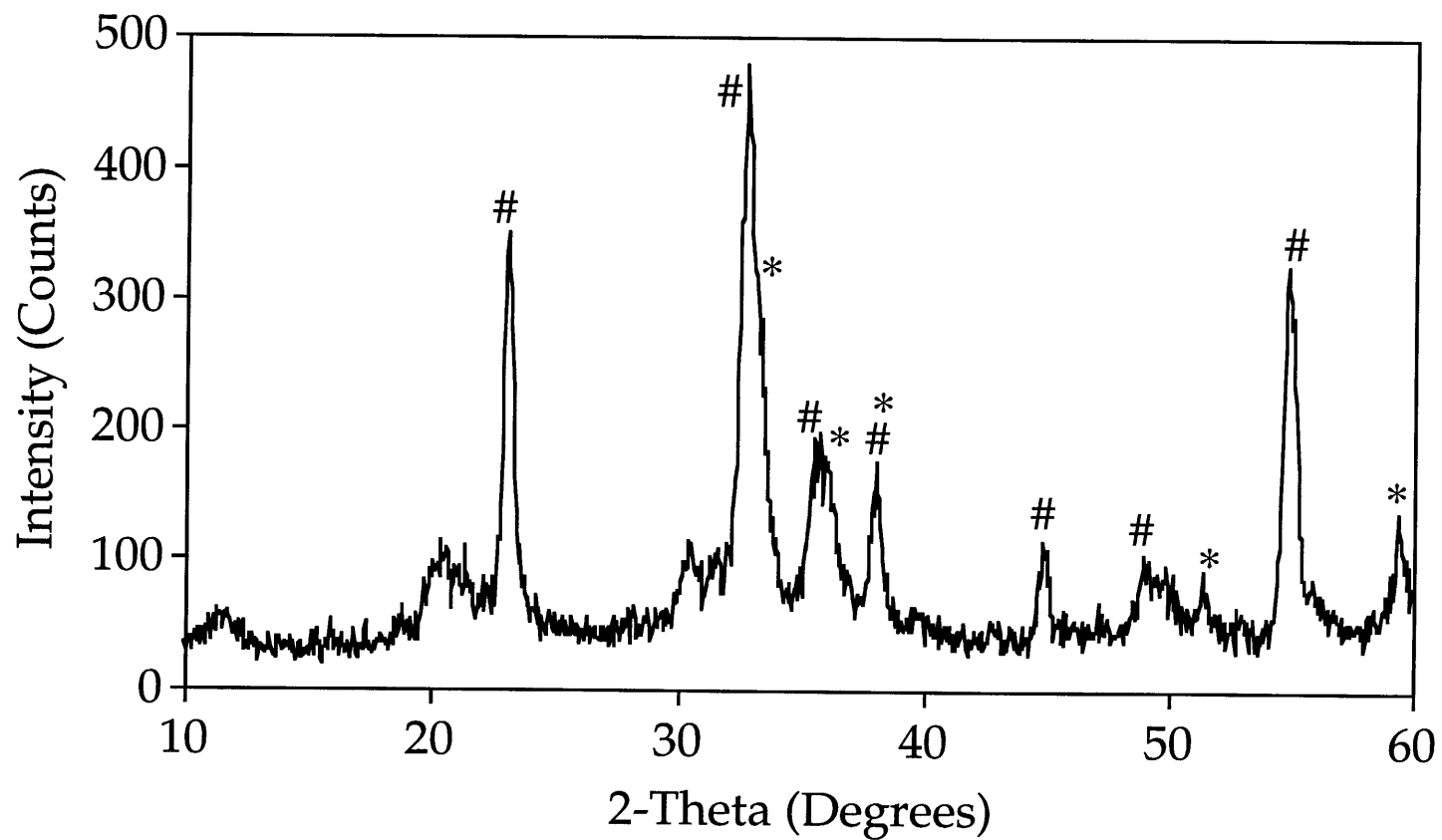
Figure 5.3.6: Powder X-ray diffraction pattern of Li_3AlN_2 synthesized from the reaction of Al powder and Li_3N under N_2 gas in the microwave. * = AlN; # = Li_3AlN_2.
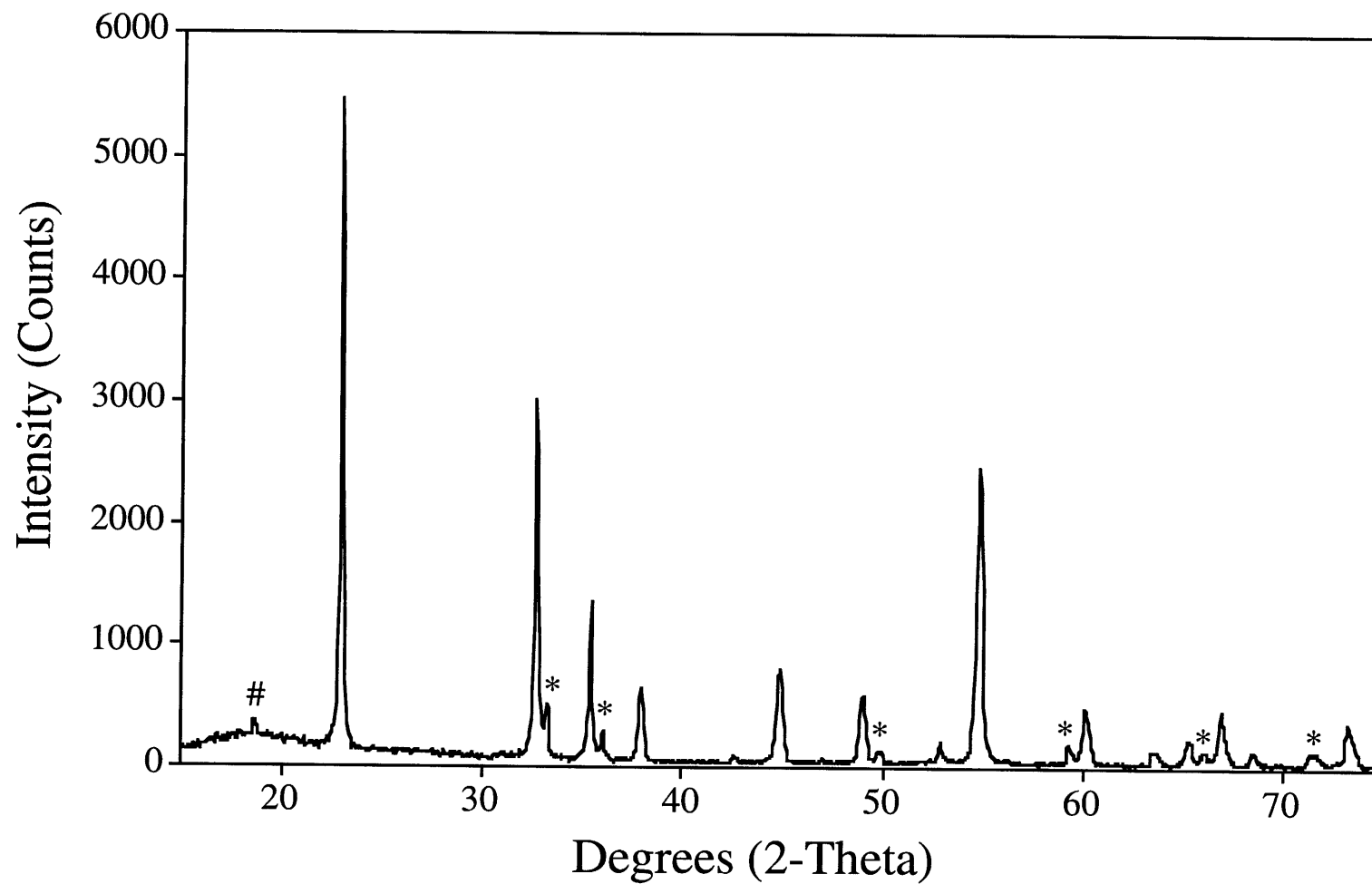
Figure 5.3.7: Powder X-ray diffraction pattern of Li_3AlN_2 synthesized from the reaction of AlN and Li_3N in a microwave. * = AlN; # = $LiTaO_2$.
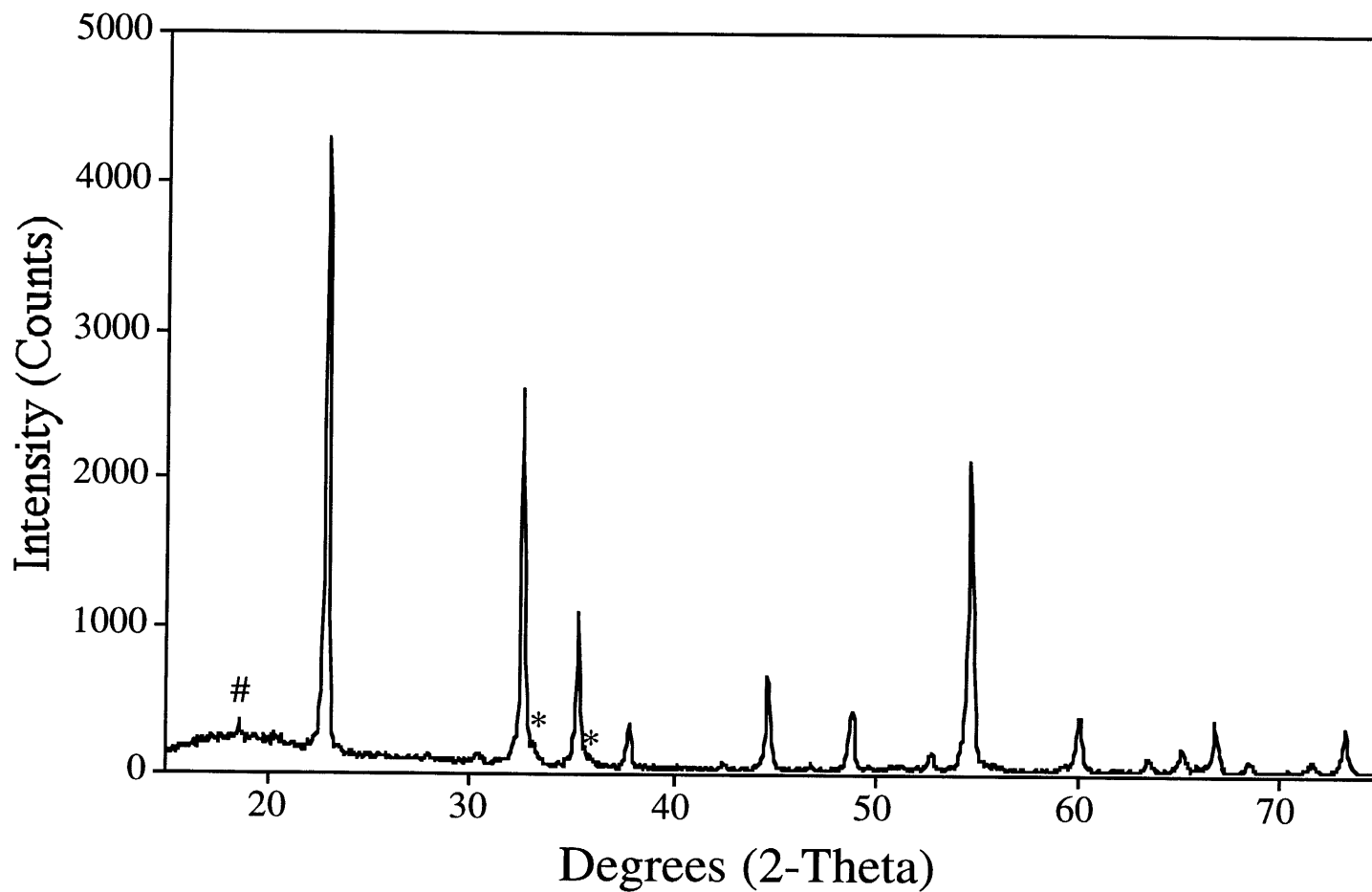
Figure 5.3.8: Powder X-ray diffraction pattern of Li_3AlN_2 with second addition of Li_3N in a microwave. * = AlN; # = $LiTaO_2$.
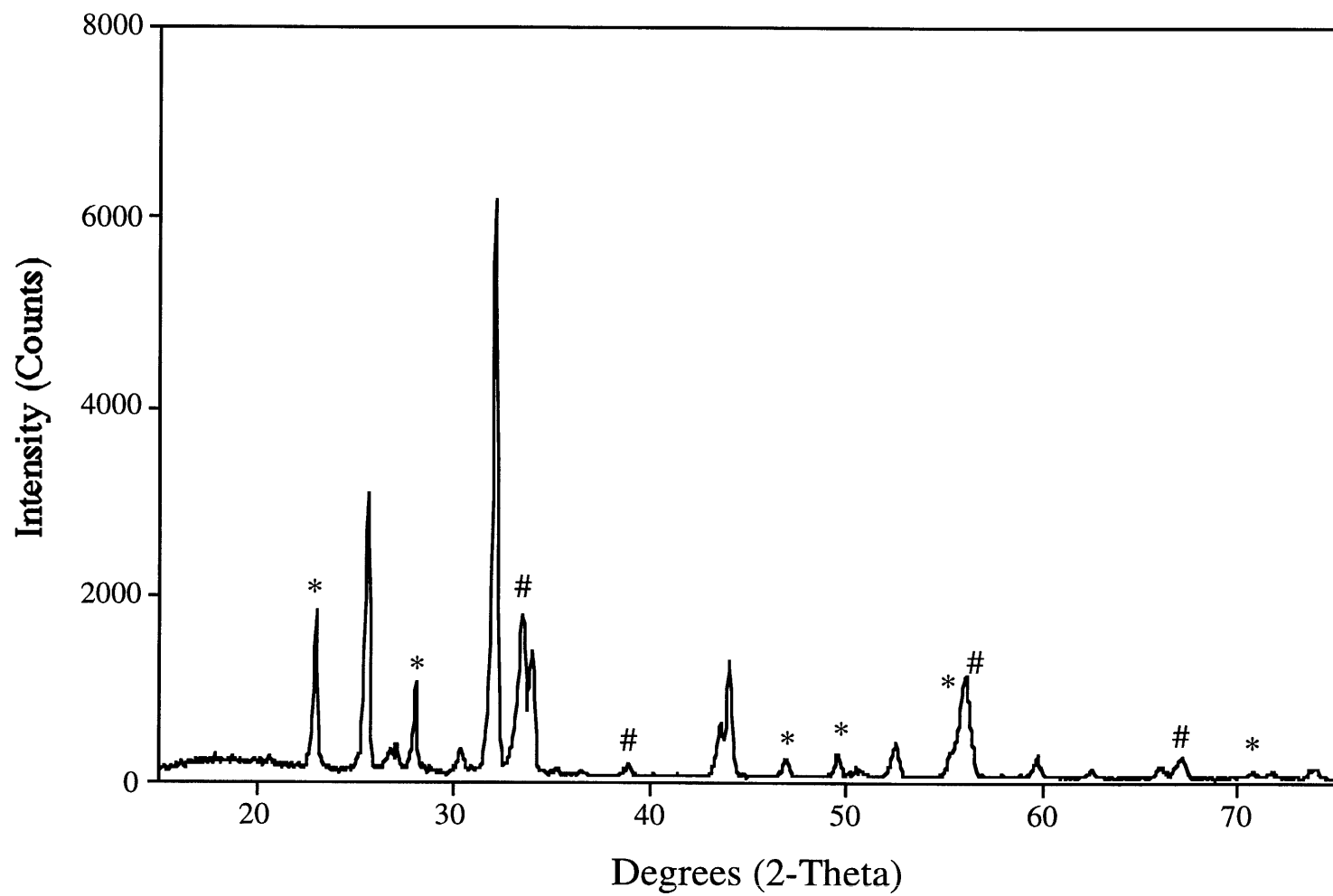
Figure 5.3.9: Powder X-ray diffraction pattern of Li_3BN_2 synthesized from Li_3N and BN. * = Li_3N; # = BN.
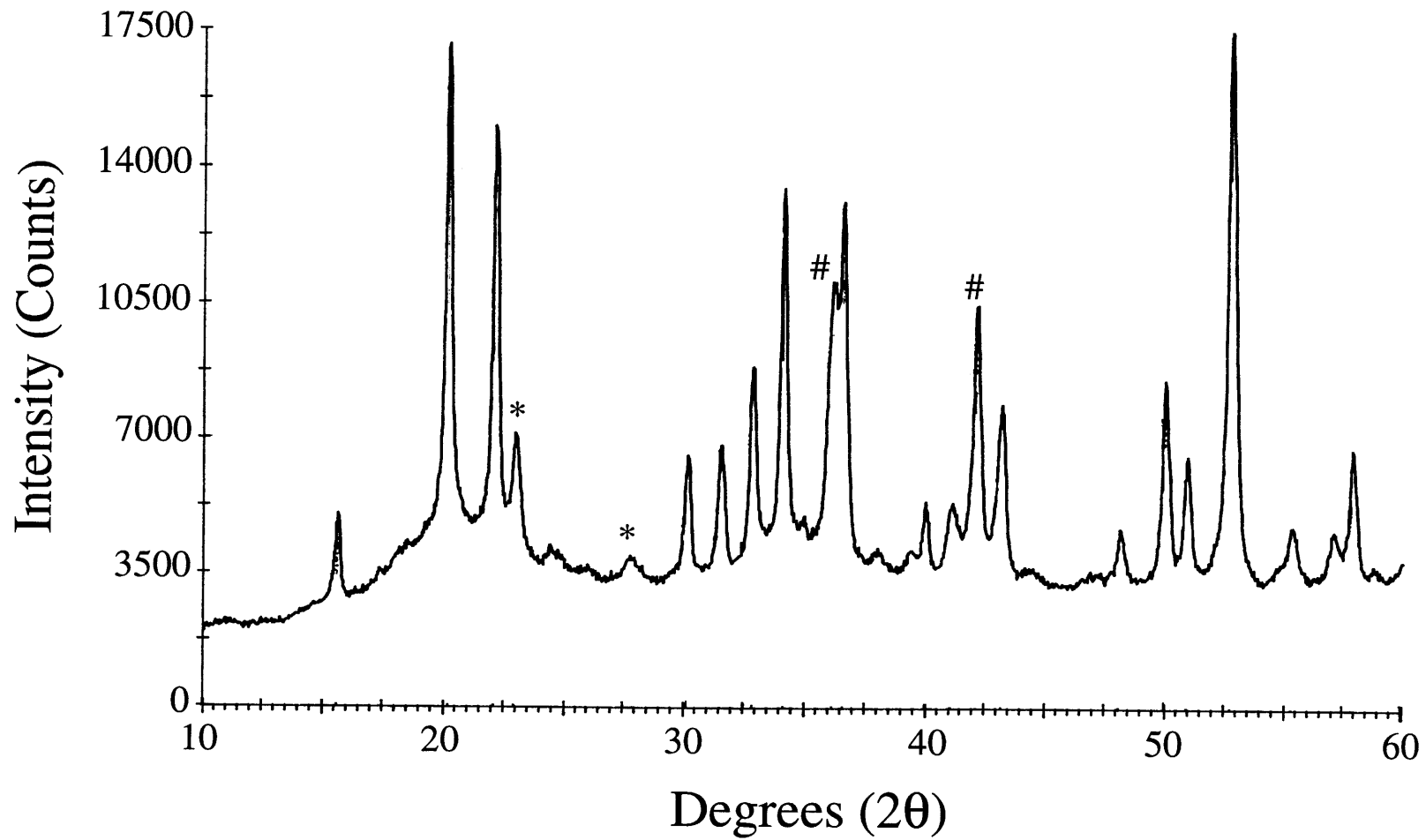
Figure 5.3.10: Powder X-ray diffraction pattern of Li_7TaN_4 synthesized by reaction of Li_3N and Ta_3N_5 in a microwave. * = Li_3N; # = TaN.
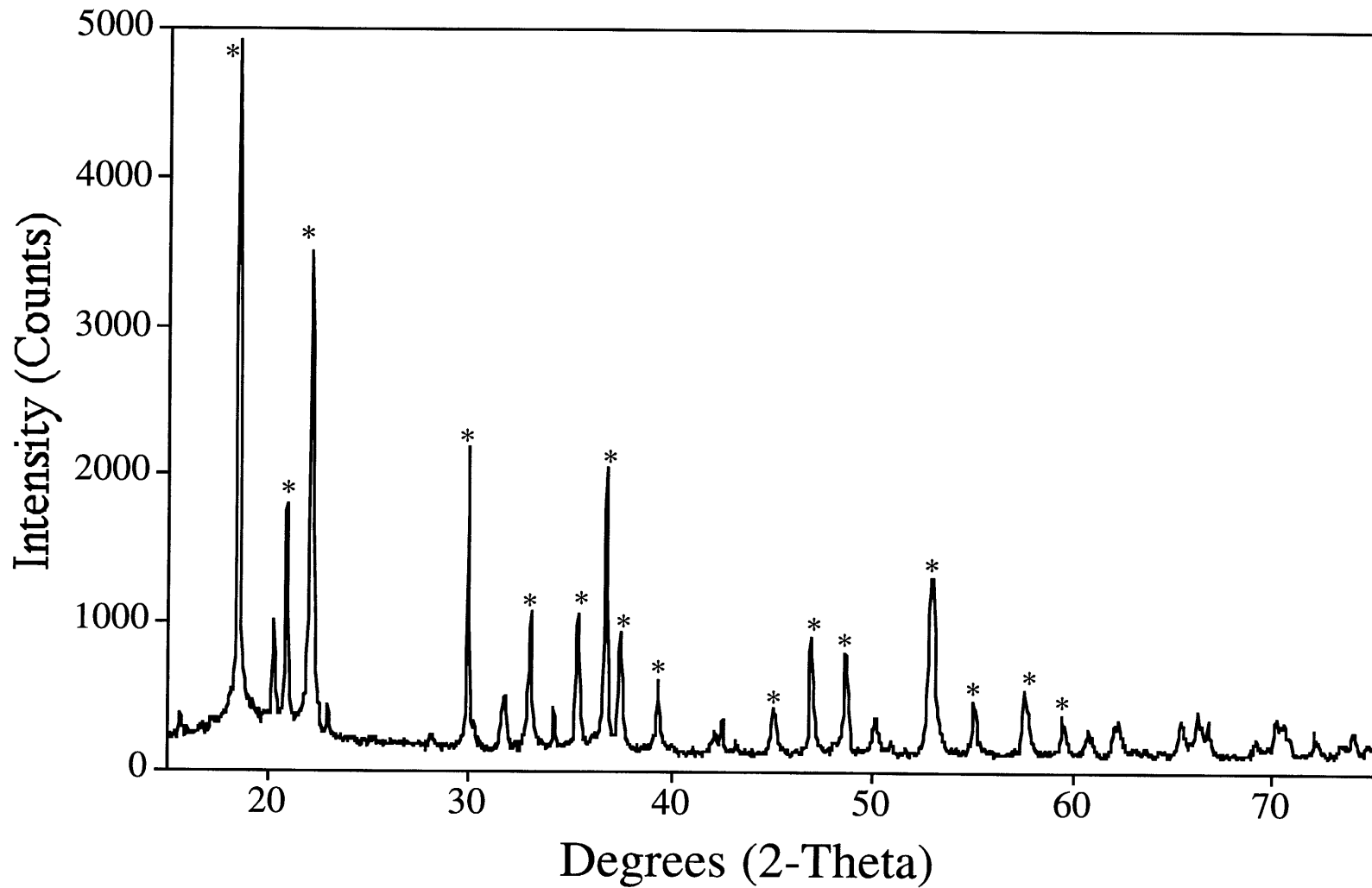
Figure 5.3.11: Unknown material synthesized from Li₃N and Ta₃N₅ under a nitrogen plasma. * = unknown phase.

5.4 Plasma Nitridation of Metal Oxides

5.4.1 Introduction

In the past, much of our work has centered on the use of non-equilibrium ammonolysis reactions of ternary transition metal oxide precursors to form ternary transition metal nitrides, which are unattainable by other routes. This approach has lead to the synthesis of a number of new ternary nitride materials, such as $(Fe_{0.8}W_{0.2})WN_2$[16], $FeWN_2$[17], $MnMoN_2$[17], Fe_3Mo_3N[18], α- and β-$MnWN_2$[19] and $M_5N_{6-8}O_y$ (M = Ta, Nb)[20], as have been discussed in detail in earlier chapters. However, many potentially interesting reactions have been precluded by a large positive free energy of reaction. For example, for the reaction

$$\text{Eq. 5.7} \qquad Al_2O_3 + 2NH_3 \rightarrow 2AlN + 3H_2O$$
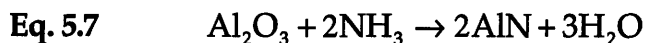
ΔG_{rxn} has been calculated to be +223 KJ/mol at 1000 K.[21] In addition, kinetic barriers further limit the number of binary nitrides which can be synthesized through ammonolysis of the oxide. ΔG_{rxn} for the reaction

$$\text{Eq. 5.8} \qquad 3TiO_2 + 4NH_3 \rightarrow 3TiN + 6H_2O + 1/2N_2$$
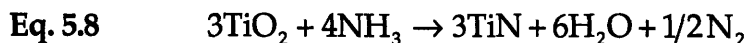
has been calculated to be only +24.1 kJ/mol at 1000K and becomes negative at higher temperatures.[21] However, despite the negative free energy of formation, kinetic limitations imposed by the formation of a nitride coating on the surface of the TiO_2 particles make this ammonolysis reaction too slow to be practical except for very high surface area precursors. As a result, only a small portion of the periodic table contains elements whose oxides are viable candidates for conversion into nitrides by ammonolysis reactions.

In previous sections, the use of microwave generated nitrogen plasmas has been demonstrated to provide an exceptionally active form of nitrogen which can be used as a reagent and heating source to form nitride materials. An extension of this work is the reaction of a metal oxide in a microwave

generated N_2/H_2 plasma. If the N_2/H_2 plasma is allowed to flow across the reactant, oxygen containing species which are evolved can be swept away by the plasma and could provide additional driving force for the reaction. In addition, in a plasma there exists a high concentration of H^+ and N^+,[10] which are rapidly accelerated by the electric component of the microwave field. These cations would bombard the metal oxide surface, roughing the surface and causing the release of oxygen from the precursor material. Together with the highly reactive nitrogen and hydrogen species and the high concentration of free electrons in the plasma, pseudo-ammonolysis reactions can be achieved which could effect reactions that would be difficult at best under ordinary ammonolysis conditions.

5.4.2 Results

To test this hypothesis, TiO_2 (Alfa, 99.9%) was placed in an alumina boat under 5 torr of flowing forming gas (5% H_2/95% N_2). The sample was heated under a N_2/H_2 plasma which is formed using a 1.2 kW microwave source (Cober Electronics, Figure 5.2.2) equipped with a plasma applicator. Since TiO_2 is insulating, nitrogen plasmas are not readily ignited over the sample. However, once the plasma is ignited using a small amount of titanium metal powder located in an adjacent reaction vessel, it can be sustained in the plasma applicator and the titania sample can be moved into the plasma. After 12 hours of heating under the N_2/H_2 plasma, the sample appears golden in color. However, powder X-ray diffraction reveals that it is a mixture of TiN, Ti_2N and TiO. The sample can be completely converted into TiN by grinding followed by an additional 12 hours heating under the N_2/H_2 plasma. The product is a golden colored powder identified as TiN by powder X-ray diffraction (Figure 5.4.1). Although the free energy of formation of TiN from TiO_2 can be forced less than zero through higher reaction temperatures and low partial-pressures of water, kinetic barriers for the diffusion of nitrogen atoms through the TiN skin formed on the surface of the TiO_2

particles make conventional ammonolysis routes nearly impossible. However, by using a N_2/H_2 plasma, complete conversion of the oxide precursor into TiN can be obtained, even using low surface area powders. Interestingly, the lattice parameters of TiN made by the reaction of TiO_2 with a N_2/H_2 plasma (a=4.241(1)Å) are nearly identical to those reported for TiN (a=4.241(1)Å[22]), indicating a low residual oxygen content.

Aluminum oxide (Aesar, alpha phase, 99.99%) can be reacted under similar conditions to yield a mixture of Al_2O_3 and AlN. As with the reaction with TiO_2, a plasma must be sparked with a small amount of titanium located in an adjacent alumina boat. ΔG_{rxn} for the ammonolysis reaction of Al_2O_3 at 1000 K is substantially higher (223 KJ/mol K[21]) than for the conversion of TiO_2 to TiN. Even after 6 heatings of 24 hours with intermediate grinding, Al_2O_3 is only partially converted into AlN by powder X-ray diffraction (Figure 5.4.2). However, if $Al(OH)_3$ is used as the starting material, complete conversion to AlN can be obtained in less than 24 hours (Figure 5.4.3). (The unusual background in Figure 5.4.3 arises from clay used in the mounting of the sample.) We believe that the loss of H_2O from the materials disrupts the Al-O lattice, allowing greater access of the nitrogen plasma species into the interior of the alumina particles. In effect, the faster conversion of $Al(OH)_3$ into AlN arises from the greater surface area of the starting material.

Gallium oxide (Johnson-Matthey, 99.999%) can be reacted under similar conditions to yield GaN (Figure 5.4.4). Powder X-ray diffraction analysis of the GaN product confirms the presence of the GaN structure type. However, the product is light yellow suggesting the presence of a small amounts oxygen. A further plasma treatment of ~12 hours results yields a product which is gray in color and with a similar powder x-ray diffraction pattern. Using the method of Elder and DiSalvo[21], ΔG_{rxn} for the ammonolysis reaction of Ga_2O_3 at 1000 K (227.9 kJ/mol) is found to be comparable to that for the conversion of Al_2O_3 to AlN (223 kJ/mol). The crystallinity of the GaN produced from plasma nitridation of Ga_2O_3 is exceptional. Currently, GaN is

synthesized by reaction of gallium metal with ammonia at 625°C. However, poor crystallinity and incorporation of oxygen make the synthesis of phase-pure GaN difficult and, therefore, costly. In addition, GaN loses N_2 above 700°C, even when heated under 1 atm N_2, which highlights another advantage of microwave generated plasmas for the synthesis on nitride materials. Unlike in conventional heating methods, two temperatures are necessary to describe the synthetic conditions. The sample temperature described the thermal energy contained within the sample material and is analogous to temperature measurements from conventional heating methods. The plasma temperature describes the kinetic energy of the plasma particles. By controlling the reaction conditions, a high plasma temperature can be obtained with only a moderate sample temperature. In the case of the nitridation of Ga_2O_3, sufficient energy is present in the plasma particles to nitride the oxide precursor. Yet the sample temperature remains below 700°C, allowing the formation of GaN. Clearly, microwave plasma nitridation offers a fast and extremely method for the synthesis of GaN from inexpensive starting materials.
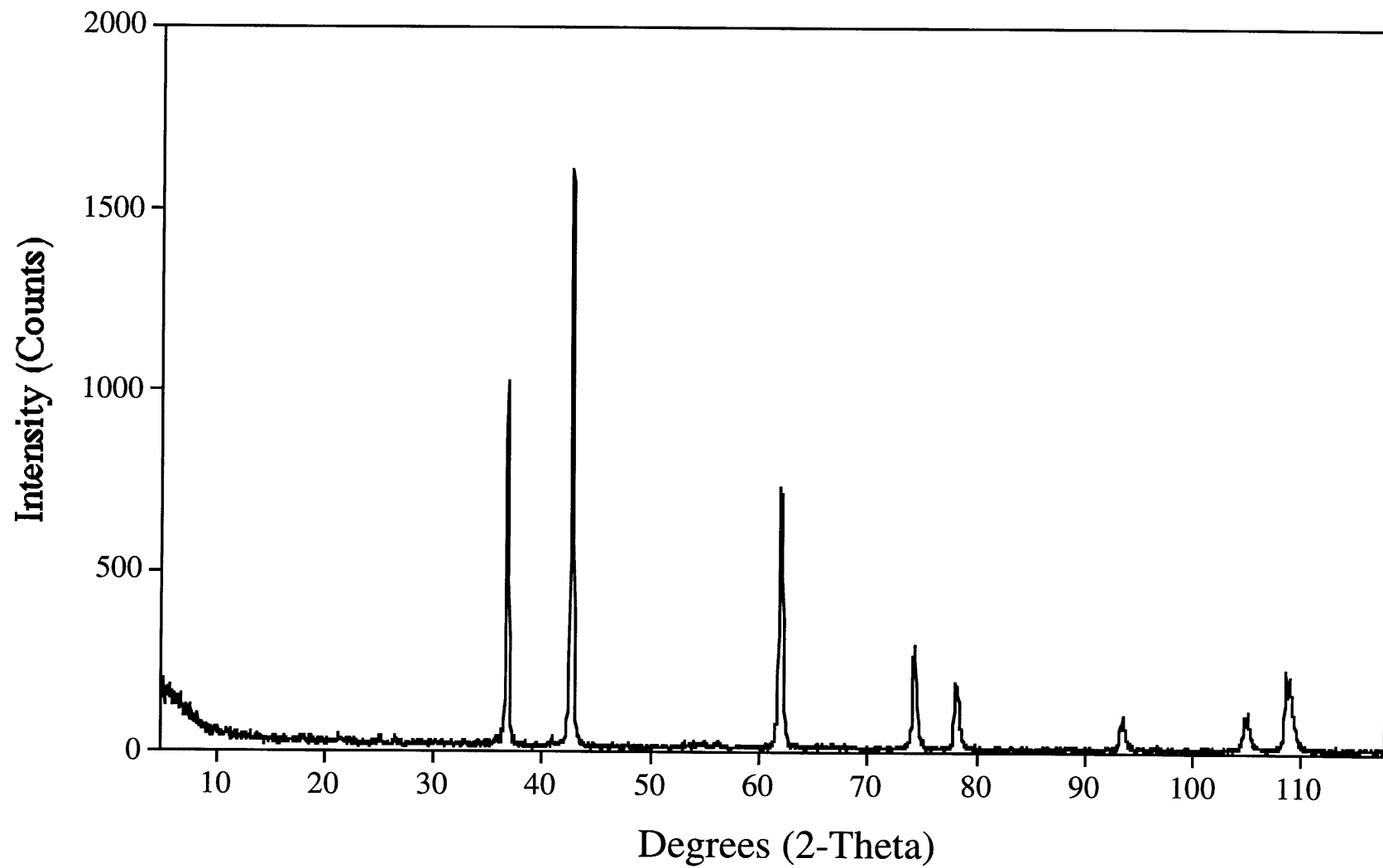
Figure 5.4.1: Powder X-ray diffraction pattern of TiN made by plasma nitridation of TiO_2.

Figure 5.4.2: Powder X-ray diffraction pattern of AlN and Al_2O_3 made by plasma nitridation of Al_2O_3. $*$ = AlN

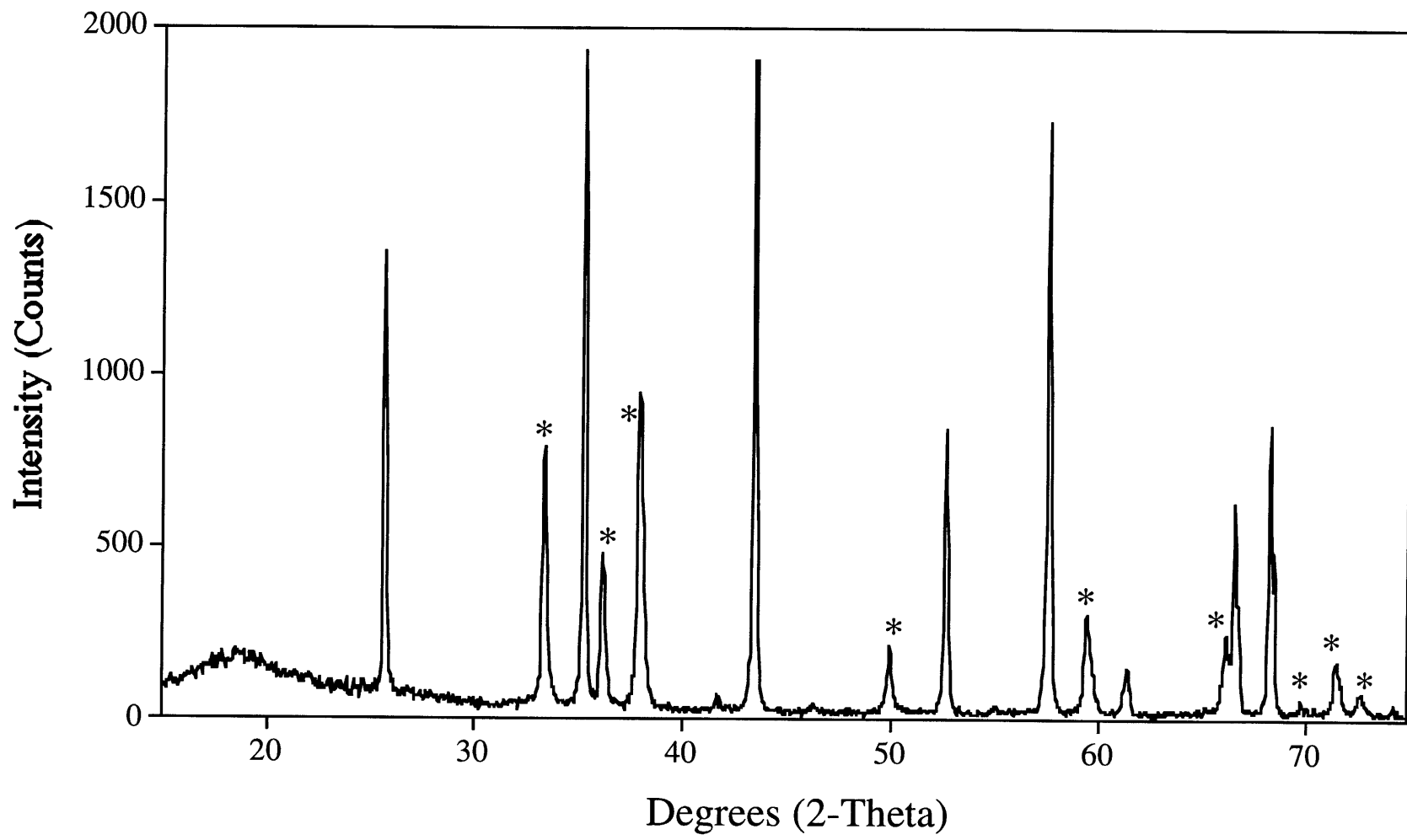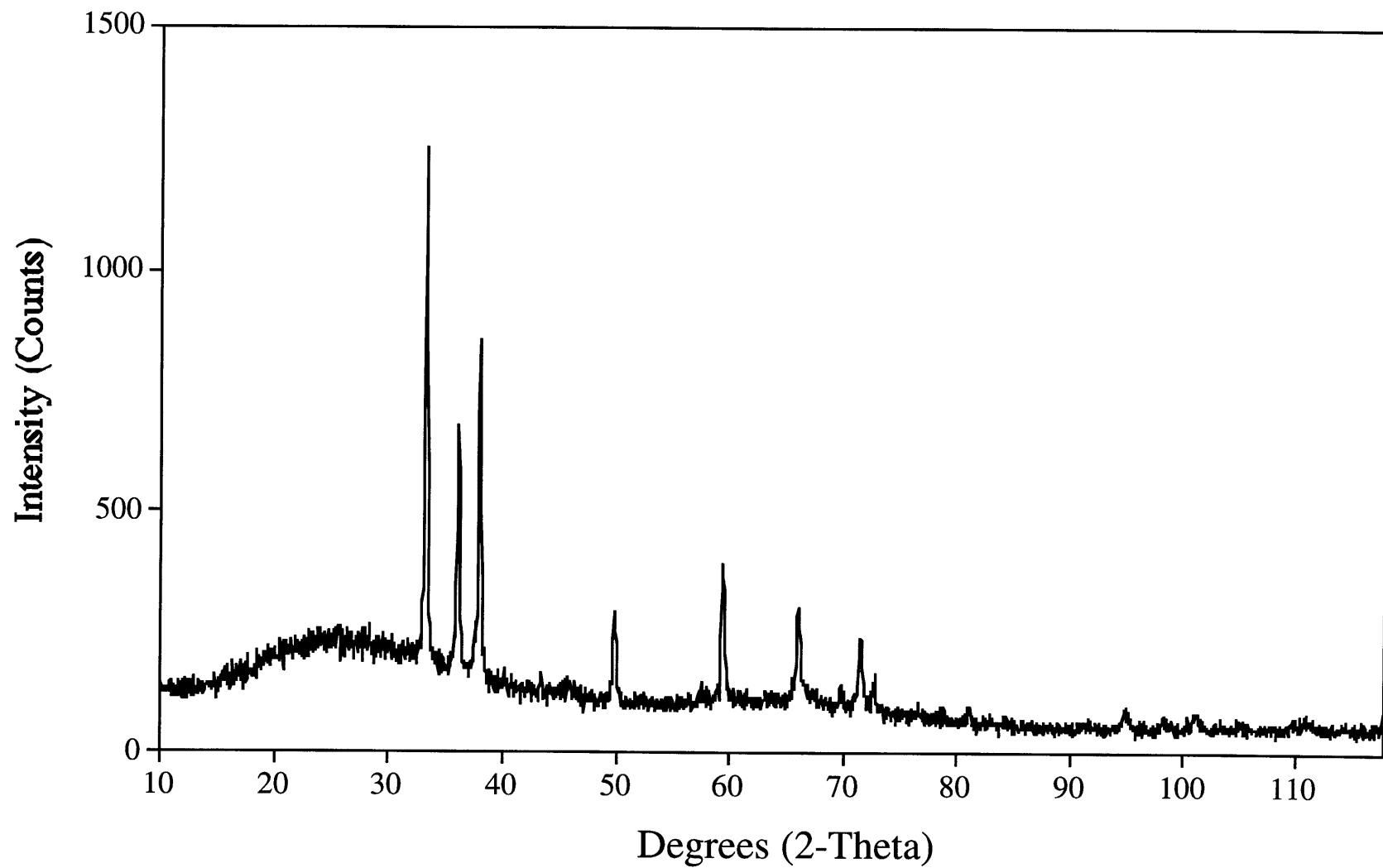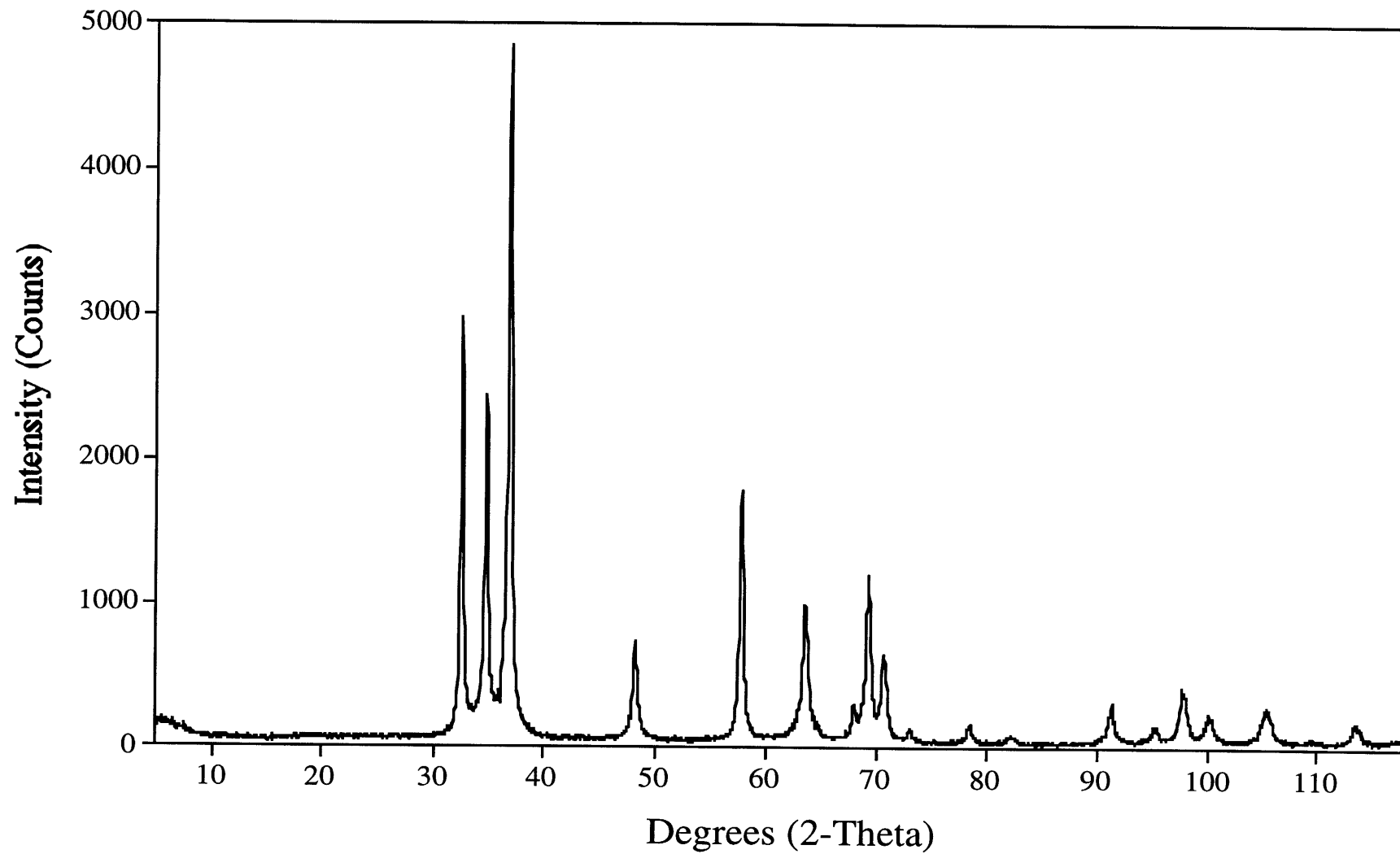Figure 5.4.3: Powder X-ray diffraction pattern of AlN made by plasma nitridation of Al(OH)₃.

Figure 5.4.4: Powder X-ray diffraction pattern of GaN made by plasma nitridation of Ga_2O_3.
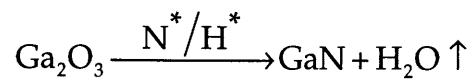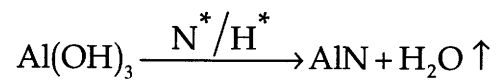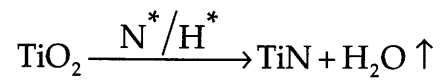
5.4.3 Discussion

Despite our successes in synthesizing binary nitrides (Figure 5.4.5) from binary oxides using a forming gas plasma, several systems were tried which did not display any significant nitrogen uptake. No reaction is observed between La_2O_3 and a N_2/H_2 plasma after treatment for 2 days. Likewise, the reaction of $SrCO_3$ with a N_2 plasma results in decomposition to SrO but no nitrogen uptake. The lack of significant reaction with the plasma is not surprising. The equivalent ammonolysis reactions of the binary oxides of lanthanum and strontium have ΔG_{rxn} of +485 and +715 kJ/mol, respectively, due to the very high crystal lattice stabilization energy of the oxides.

Our estimates of the reaction temperatures are rather approximate, consisting primarily of estimates derived from experience with materials which heat sufficiently to melt in the microwave. The uncertainty in temperature determination leads to the question as to whether a microwave nitrogen plasma actually aids in nitride formation or if plasma heating merely allows access to temperatures at which nitride formation becomes thermodynamically favorable. Based on thermodynamic data reported by Elder, et al.[21], the ammonolysis reaction of Al_2O_3 to form AlN becomes thermodynamically favorable at 2686 K, an unlikely temperature for an insulating or semi-conducting material to achieve through microwave heating. Therefore, the presence of the nitrogen/hydrogen plasma undoubtedly helps to overcome the large thermodynamic barrier for the formation of AlN. In addition, GaN above 700°C under nitrogen. Since the GaN formed by this synthetic technique is highly crystalline and with impurities, the temperature inside the reaction vessel is probably not significantly greater than 700°C. The enhanced nitridation in a nitrogen/hydrogen plasma is not unexpected. Although the conversion of the above mentioned oxide materials into the corresponding nitrides through ammonolysis is thermodynamically unfavorable, by using a nitrogen

hydrogen plasma, the reaction pathway is changed. In a nitrogen-hydrogen plasma, the oxide reactant is exposed to energetic electrons and cationic species. The energy contained in these species appears to be enough to disrupt the Al-O bonds in the material and make nitridation possible.

Besides the obvious application of these techniques to the synthesis of bulk nitrides from inexpensive oxide starting materials, the results presented in this section have important implications for the processing of nitride materials. One common contaminant in all nitride materials is oxygen, especially as oxide coatings on nitride films. Our results indicate that residual oxygen can be removed from refractory nitrides using a nitrogen/hydrogen plasma under flow through conditions. Even oxides, for which conversion to the nitride using ammonia is difficult, can be easily and quickly converted to a nitride product.

$$TiO_2 \xrightarrow{\text{N}^*/\text{H}^*} TiN + H_2O \uparrow$$

$$Al(OH)_3 \xrightarrow{\text{N}^*/\text{H}^*} AlN + H_2O \uparrow$$

$$Ga_2O_3 \xrightarrow{\text{N}^*/\text{H}^*} GaN + H_2O \uparrow$$

N*/H* = Nitrogen/Hydrogen Plasma

Figure 5.4.5: Reactions of metal oxides and hydroxides with N_2/H_2 plasma.

5.5 CONCLUSION

Clearly, the effectiveness of microwave heating and microwave induced plasmas as synthetic tools for the synthesis of nitride materials has been demonstrated. Through the use of microwave generated N_2 or N_2/H_2 plasmas, a number of binary nitride materials can be synthesized starting from either the metal or the metal oxide. Ternary nitride materials can be synthesized by taking advantage of the ability of Li_3N to heat rapidly in an applied microwave field. The reaction of Li_3N with group XIII nitrides to form Li_3MN_2 (M = B and Al) proceeds rapidly after the onset of thermal runaway. Obviously, the successes of using microwave heating and microwave induced plasmas in the synthesis of nitride materials warrants further study.

5.6 REFERENCES

(1) Landry, C. C.; Barron, A. R. *Science* **1993**, *260*, 1653-5.

(2) Whittaker, A. G.; Mingos, D. M. P. *J. Chem. Soc . Dalton Trans.* **1993**, 2541-3.

(3) Baghurst, D. R.; Chippindale, A. M.; Mingos, D. M. P. *Nature* **1988**, *332*, 311.

(4) Whittaker, A. G.; Mingos, D. M. P. *J. Chem. Soc. Dalton Trans.* **1992**, 2751-2752.

(5) Ramesh, P. D.; Rao, K. J. *Adv. Mater.* **1995**, *7*, 177-179.

(6) Konuma, M.; Kanzaki, Y.; Matsumoto, O. *Denki Kagaku* **1979**, *47*, 597.

(7) Hudis, M. *J. Appl. Phys.* **1973**, *44*, 1489-1496.

(8) Konuma, M.; Matsumoto, O. *J. Less-Common Met.* **1977**, *55*, 97-102.

(9) Konuma, M.; Matsumoto, O. *J. Less-Common Met.* **1977**, *52*, 145-152.

(10) Matsumoto, O.; Konuma, M.; Kanzaki, Y. *J. Less-Common Met.* **1982**, *84*, 157-163.

(11) Yamane, H.; Kikkawa, S.; Koizumi, M. *Solid State Ionics* **1985**, *15*, 51-54.

(12) Yamane, H.; Kikkawa, S.; Koizumi, M. *Solid State Ionics* **1987**, *25*, 183-191.

(13) Elder, S. H.; DiSalvo, F. J.; Doerrer, L. H. *Chem. Mater.* **1992**, *4*, 928-937.

(14) Gasgnier, M.; Loupy, A.; Petit, A.; Jullien, H. *J. Alloys Compd.* **1994**, *204*, 165-172.

(15) Juza, V.; Gieren, W.; Haug, J. *Z. Anorg. u. Allge. Chemie* **1959**, *300*, 61-71.

(16) Bem, D. S.; Olsen, H. P.; zur Loye, H. C. *Chem. Mater.* **1995**, *7*, 1824-1828.

(17) Bem, D. S.; Lampe-Önnerud, C. M.; H.P., O.; zur Loye, H. C. *Inorg. Chem.* **1996**, *35*, 581-585.

(18) Bem, D. S.; Gibson, C. P.; zur Loye, H.-C. *Chem. Mater.* **1993**, *5*, 397-399.

(19) Houmes, J.; Bem, D.; zur Loye, H. *Mat. Res. Soc. Symp. Proc. Vol. 327* **1994**, 153-64.

(20) Houmes, J. D.; zur Loye, H. C. *Chem. Mater.* **1996**, Submitted.

(21) Elder, S. H.; Disalvo, F. J.; Topor, L.; Navrotsky, A. *Chem. Mater.* **1993**, *5*, 1545-53.

(22) Wong-Ng, W.; McMurdie, H. F.; Paretzkin, B.; Zhang, Y.; Davis, K. L.; Hubbard, C. R.; Dragoo, A. L.; Stewart, J. M. *Powder Diffract.* **1987**, *2*, 200.

6. Conclusion and Future Directions

6.1 CONCLUDING SUMMARY

It order to evaluate the success of our research into new routes toward the preparation of nitrides, it is useful to first review the problems associated with the synthesis of this class of materials. As was detailed in Chapter 1, two problems dominate the synthesis of all nitride materials. The first is the large bond energy of N_2, which yields all nitrides unstable with respect to disproportionation at sufficiently high temperature. The second is the ease with which nitrides form coatings on the surface of the reactant particles which greatly slows diffusion into the interior of the particles. Our approaches have been to attack these problems separately. First, we used oxide precursors to lower the temperature at which nitrides are formed in an effort to form new phases that contain two transition metals and a high nitrogen content. By using low temperature routes, disproportionation of the reactant materials can be lessened. Indeed, by using oxide precursors a number of new ternary transition metal nitrides $((Fe_{0.8}W_{0.2})WN_2)$ and structurally related binary oxynitrides $((Ta_{0.67}\square_{0.33})TaN_{2-\delta}$ and $(Nb_{0.67}\square_{0.33})NbN_{2-\delta}$, $\square$ = vacancy) were formed, which exhibit a significant degree of covalent bonding and chemical stability. However, we also found that complete removal of oxygen from the product can be extremely difficult if not impossible.

Through the use of microwave heating and microwave generated plasmas, we have shown that the slow diffusion rate of nitrogen through a nitride coating on the surface of reactant metal particles can be overcome. By using microwave generated nitrogen plasmas, bulk synthesis of binary nitride materials such as TiN, VN and AlN can be accomplished in under 12 hours. In addition, by using a flux-assisted route, a number of lithium metal nitrides (such as Li_3AlN_2 and Li_3BN_2) can be made in only minutes starting from a mixture of binary nitrides. However, perhaps the most interesting result obtained is the complete nitridation of oxide precursors by a microwave

generated N_2/H_2 plasma. Even materials whose equivalent ammonolysis reactions are thermodynamically and kinetically difficult, can be easily and surprisingly quickly converted into fully nitrided materials. Though more work needs to be done to refine the synthetic conditions, plasma nitridation appears to be a simple and effective way of obtaining binary nitride materials.

6.2 FUTURE DIRECTIONS

As one looks toward the future of nitride research, several facts immediately present themselves. First, the use of precursors has not fulfilled the promise of its initial results. The use of oxide precursors has fallen upon severe compositional limitations and the number precursors which can be reasonably expected to produce fully nitrided materials has been nearly exhausted. Other precursor routes, such as metal amides, have been attempted, however, the expertise needed to synthesize molecular and polymer based materials which could potentially lead to new and interesting materials has not yet been fully brought to bear on the problem. In general, a lack of communication and cooperation between the solid state and molecular communities has limited the potential contributions from both sides in the quest for new precursor materials to solid state materials.

Second, the use of flux based systems for the synthesis of new ternary and higher nitrides, though successful, also has not lived up to initial expectations. Certainly, a number of new materials have been synthesized using Li_3N, MNH_2 (M = Li, Na, K, Rb), MN_3 and alkali metal fluxes. However, all these routes are again compositionally limited, experimentally complex (due to the highly corrosive nature of the fluxes), and tend to yield materials which are not stable to atmospheric conditions. Several newer and higher temperature precursor routes have been studied, including silicon amides. However, the applicability of these techniques to other systems has not yet been explored.

For reasons discussed in earlier chapters of this thesis, precursors are still an attractive avenue toward the synthesis of nitride materials. However, significant works remains to be done to explore new precursor systems. In particular, the pyrolysis of metal amides or amines could provide a fruitful methodology toward the synthesis of nitride materials. Perhaps the easiest method to produce large quantities of such precursors would be to create mixed-metal amide gels in liquid ammonia in a fashion similar to that used for the synthesis of alkoxide gels. This approach could create a highly cross-linked precursor with metal nitrogen bonds already formed. Pyrolysis of such mixed-metal materials could be expected to yield ternary nitride products. Through careful precursor design and pyrolysis control carbon contamination could be limited and metal stoichiometry could be controlled.

In Chapter 1, several difficulties in the synthesis of nitride materials were listed, including the thermodynamic stability of N_2 and slow diffusion through nitride coatings. Despite a tendency for disproportionation, a number of nitride materials have been synthesized which demonstrate appreciable temperature stability. A combination of crystal lattice stabilization energy and the inductive effect can greatly increase the temperature stability of nitride materials and open new classes of materials to investigation. In addition, recent work has found that some materials can form highly covalent M-N networks, even at high temperatures, which lend additional stability to the material. However, in order to rationally synthesize new nitride materials which contain high nitrogen contents and are stable to high temperatures, a more fundamental understanding of bonding and structure in nitride materials will be needed. In particular, a greater understanding of the ability of the inductive effect to stabilize nitride structures is needed in order to broaden both compositional and structural limits.

The second difficulty associated with the synthesis of nitride materials, the formation of nitride coatings on the surface of the reactant particles, is an easier problem to tackle. Here again, the use of precursors can be helpful in overcoming kinetic barriers. One method to counteract the slow diffusion

rate of nitrogen through these coatings is to create a precursor in which the metal(s) and nitrogen are mixed on an atomic level. Such an approach reduces the diffusion distance and lessens the impact on diffusion rates of nitride coatings. However, to this date, work on nitrogen containing precursors for the synthesis of ternary and higher nitrides has been extremely limited.

A second method to overcome the slow rate of nitrogen diffusion through nitride coatings is to use a flux which can partially dissolve the reactant and speed diffusion. Again, to this date, the number of materials which can be used as fluxes is extremely limited. Most current fluxes are exceptionally corrosive (alkali metals, amides and azides) and often result in incorporation of the flux metal into the nitride product, a property which often is not desirable. Here again high temperatures could hold a key to the formation of more successful fluxes. For reactions run in the 1200-1500°C range, a wider variety of materials may be considered as fluxes, including materials which are not as corrosive as those containing alkali metals. Several ternary nitride materials have been synthesized using silicon as a reactive flux at these temperatures. It is likely that other high temperature fluxes, particularly those of main group elements, could be used in similar reactions.

Recently, a number of new systems have been synthesized which utilize higher reaction temperatures and/or higher temperature fluxes to synthesize new materials. Our preliminary work on the use of microwave heating as a synthesis technique for ternary and higher nitrides falls into this class of reactions. Our success using microwave induced plasma nitridation leads to several possible avenues of further research. More work needs to be done to determine the limitations of the synthetic routes presented in this thesis. In particular, several other metal powders and metal oxide powders should be reacted with a nitrogen plasma in order to determine the scope of these approaches. In addition, many other lithium containing ternary nitrides are known and further research into this reaction could yield several

successful syntheses. Also, the reaction of an alkaline earth nitride with a transition metal nitride should be explored.

Our goal in the synthesis of nitride materials has always been the synthesis of new nitride materials. The use of a microwave as a heating technique for the synthesis of nitride materials still holds promise for the synthesis of new materials, both through existing pathways and several other avenues. By creating alloys (through melting in an arc furnace), ternary nitride materials could be synthesized by reaction with a N_2 or N_2-H_2 plasma. In addition, the ability of a N_2-H_2 plasma to convert oxide precursors into fully nitrided products could be exploited to synthesize ternary nitride materials from ternary oxide precursors.

From a more conventional solid state synthetic background, several other systems could be used for the synthesis of ternary nitrides through reaction with N_2 or N_2/H_2 plasmas. Alkaline earth nitrides are attractive starting materials for the synthesis of ternary materials because 1) they exist (no nitrides are known for the heavier alkali metals) and 2) because they exhibit some temperature stability. However, preliminary experiments into the use were unsuccessful due to some volatility of the alkaline earth nitride, which attacked the reaction vessel and caused structural failure. However, with some fine-tuning of reaction conditions, Sr_3N_2 could be used as a reactant for the synthesis of ternary nitride materials in a reaction such as that listed in Eq. 6.9:

$$Eq.\ 6.9 \qquad Sr_3N_2 + Si_3N_4 \rightarrow 3SrSiN_2$$
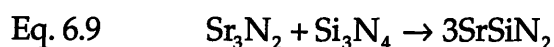
One additional problem was encountered when using Sr_3N_2 as a starting material for the synthesis of ternary nitrides, the purity of commercially available Sr_3N_2 is poor. X-ray analysis on the materials as received reveals it to be a mixture of Sr_3N_2, Sr_2N and SrO. The presence of these impurities could probably be reduced by in-house synthesis of Sr_3N_2 from Sr metal under ammonia. However, this procedure was not attempted.

Work in this group on the use of microwave heating and microwave generated nitrogen plasmas will continue. It is hoped that advances in this

field will lead to the synthesis of a number of new nitride materials. In addition, work will continue on the use of precursors in nitride synthesis. Although the use of oxides as precursors has been nearly exhausted, other precursor systems will be tried. The main thrust of this work will be the use of moderate-pressure thermal synthesis of molecular precursors which will be decomposed under ammonia to yield nitride products.